VOLUME XLIII

GEMS & GEMOLOGY

WINTER 2007

CVD Synthetic Diamonds
Canary Tourmaline
Fluorescence Spectroscopy
Napoleon Necklace

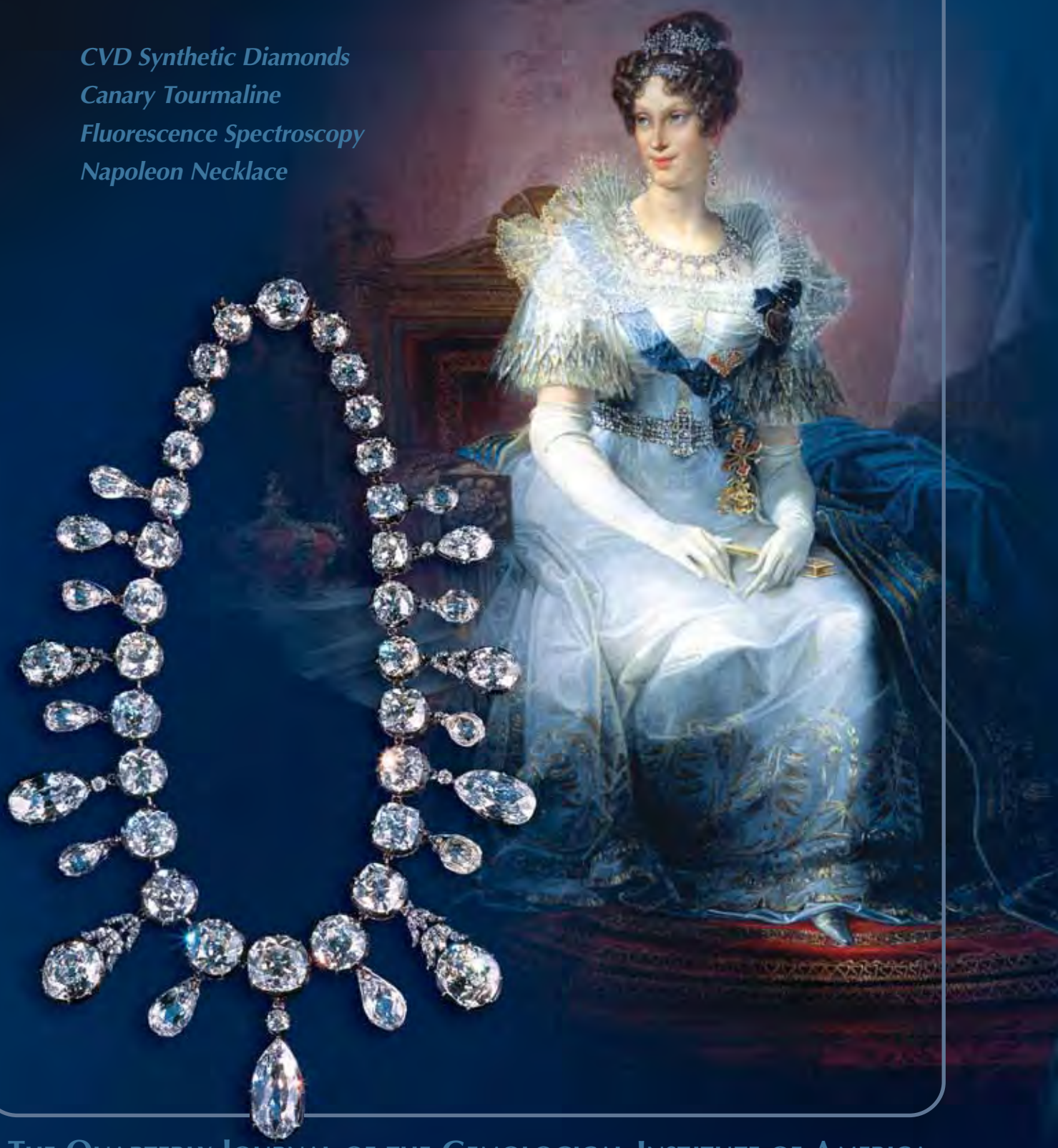

THE QUARTERLY JOURNAL OF THE GEMOLOGICAL INSTITUTE OF AMERICA

GEMS & GEMOLOGY®

Winter 2007

VOLUME 43, NO. 4

pg. 295

pg. 329

pg. 360

pg. 383

GEMS & GEMOLOGY

SUBSCRIPTIONS

Subscriptions to addresses in the U.S. are priced as follows: **$74.95** for one year (4 issues), **$194.95** for three years (12 issues). Subscriptions sent elsewhere are **$85.00** for one year, **$225.00** for three years. Canadian subscribers should add GST.

Special rates are available for GIA alumni and current GIA students. One year: **$64.95** to addresses in the U.S., **$75.00** elsewhere; three years: **$179.95** to addresses in the U.S., **$210.00** elsewhere. Please have your student or Alumni number ready when ordering. Go to www.gia.edu or contact the Circulation Coordinator (see above).

Single copies of this issue (print or PDF) may be purchased for **$19.00** in the U.S., **$22.00** elsewhere. Discounts are given for bulk orders of 10 or more copies of any one issue. A limited number of back issues are also available for purchase. Please address all inquiries regarding subscriptions and single copy or back issue purchases to the Circulation Coordinator or visit www.gia.edu.

To obtain a Japanese translation of *Gems & Gemology*, contact GIA Japan, Okachimachi Cy Bldg., 5-15-14 Ueno, Taitoku, Tokyo 110, Japan. Our Canadian goods and service registration number is 126142892RT.

DATABASE COVERAGE

Gems & Gemology's impact factor is 1.381 (ranking 11th out of the 26 journals in the Mineralogy category), according to Thomson Scientific's 2006 Journal Citation Reports (issued July 2007). Full-text electronic (PDF) versions of *Gems & Gemology* issues from Spring 2005 to the present are available through EBSCO. *Gems & Gemology* is abstracted in Thomson Scientific products (*Current Contents: Physical, Chemical & Earth Sciences* and Science Citation Index—Expanded, including the Web of Knowledge) and other databases. For a complete list, see www.gia.edu/gemsandgemology.

MANUSCRIPT SUBMISSIONS

Gems & Gemology welcomes the submission of articles on all aspects of the field. Please see the Guidelines for Authors on our Website, or contact the Managing Editor. Letters on articles published in *Gems & Gemology* are also welcome.

Gems & Gemology is published quarterly by the Gemological Institute of America, a nonprofit educational organization for the gem and jewelry industry, The Robert Mouawad Campus, 5345 Armada Drive, Carlsbad, CA 92008.

Postmaster: Return undeliverable copies of *Gems & Gemology* to GIA, The Robert Mouawad Campus, 5345 Armada Drive, Carlsbad, CA 92008.

ABOUT THE COVER

The Napoleon Necklace was presented by Napoleon Bonaparte to his second wife, Empress Marie-Louise, in 1811 to celebrate the birth of their son. In this issue, the article by Drs. Eloïse Gaillou and Jeffrey Post presents gemological data on a selection of diamonds from this notable jewel. Necklace courtesy of the Smithsonian Institution, Washington, DC; photo © Harold & Erica Van Pelt. Painting of Marie-Louise by Giovan Battista Borghesi, courtesy of Scala/Art Resource, New York.

Color separations for Gems & Gemology *are by Pacific Plus, Carlsbad, California.*
Printing is by Allen Press, Lawrence, Kansas.

 ISSN 0016-626X

Letters

G&G IN THE BUSH

So there I am, out in the middle of the Tanzanian bush at Tunduru, spitting distance from Mozambique, on the Muhuwesi River. I'm haggling over a parcel of sapphire with a miner named Joseph. He reaches into his bag and pulls out one of the most dog-eared documents I've ever laid eyes on (figure 1). It's one of his most treasured possessions.

I thought you and your readers might get a kick out of this photo.

Richard W. Hughes
Fallbrook, CA

Figure 1. Tanzanian miner Joseph Mayunga, who lives along the eastern side of the Muhuwesi River near Mining Area number 8, displays a weathered copy of the Winter 1996 Gems & Gemology. *He was given the issue by a Sri Lankan gem dealer in thanks after closing a large deal for chrysoberyl rough. Photo by R. W. Hughes.*

REPLY

The *G&G* editors indeed enjoyed the photo, and we would dearly like to replace Mr. Mayunga's tattered issue. Any *G&G* readers who plan to travel to the area in the near future should contact us so that we can send a replacement (and a copy of this issue) for him.

MORE ON COATED COLORED DIAMONDS

Although the Spring 2007 article by A. H. Shen et al., "Serenity coated colored diamonds: Detection and durability," imparted a vast amount of technical information, I believe it also omitted important elements and warnings that would be of use to *G&G* readers lacking technical backgrounds.

I note that the authors did not show pre- and post-treatment spectra of the same diamond, but rather chose to compare arbitrary treated diamonds with their natural counterparts, a comparison that may be misleading for the vast majority of readers, as it discounts the inevitability that natural very light fancy-colored diamonds will be, and probably have been, color enhanced by this or similar treatments. This important fact was not stressed enough.

In the case of the yellow color treatment, the authors noted the presence of the N2 center in natural yellows and the implied absence in treated yellows (see figure 7). I sincerely doubt that this is the general case, as it would depend strongly on the starting material. I consider this element of the figure somewhat misleading.

In addition, I do not think that the authors stressed and warned strongly enough that treated melee of this type will surely show up in mounted goods without disclosure, and that few if any jewelers and appraisers will have a realistic chance of discriminating them from untreated goods. This is a legal liability problem for all in the trade and one that requires attention from industry authorities, and perhaps the authors would

have some suggestions on how the trade could appropriately, and simply, handle that.

Finally, GIA has the data to present ratios of treated spectra normalized to the untreated spectra such that the relative effects of a particular treatment can be predicted. It would be in the best interest of education that these data be made available on the *G&G* web site. In fact, I would suggest that in the future ASCII text spectral information (wavelength vs. absorbance) files for *all* spectra presented in *G&G* be made so available.

Martin D. Haske
Brookline, Massachusetts

REPLY

We appreciate Mr. Haske's thoughtful comments. We did, in fact, collect pre- and post-treatment spectra of the same stones. However, we felt that the vast majority of readers would be more interested in seeing the difference between a treated diamond and a natural diamond with similar color. Such information, in our opinion, is more useful in gem identification than simply comparing pre- and post-treatment spectra.

Indeed, not every yellow diamond shows the N2 absorption feature in its spectra. However, the apparent color of these treated yellow diamonds is quite close to that of the "cape" diamonds known to the trade, and these natural stones typically *do* display the N2, N3, and cape absorption lines. Therefore, we tried to show the difference in spectral features between these treated stones and natural-color diamonds of similar hue. However, we do agree that we should have pointed this out in the figure caption.

We agree wholeheartedly that the issue of treated melee is an important one. In fact, this is a problem with any gemstone treatment. We know that there are irradiated and HPHT-treated melee diamonds in the market, but there is no easy or simple solution to this dilemma. Once the coated stones are mounted, especially in a bezel setting, it can be very difficult to correctly identify them. We feel the best approach to this problem is to educate the trade and the public to the existence of such treatments, and to promote vigilance in the trade by providing identification information. These were the main purposes of this article.

With respect to the raw spectral data, the *G&G* editors have informed us that they will be happy to collect and post such data files in the *Gems & Gemology* Data Depository, at the discretion of the authors involved.

Andy H. Shen, Shane F. McClure, and James E. Shigley
Carlsbad, California

Wuyi Wang, Matthew S. Hall, and Thomas M. Moses
New York, New York

Steven Novak
East Windsor, New Jersey

IN MEMORIAM
MASASHI FURUYA (1948–2007)

Gems & Gemology author Masashi Furuya passed away suddenly on October 23 at the age of 59. Mr. Furuya, the founder and director of the Japan Germany Gemmological Laboratory in Kofu, Japan, had recently completed an article titled "Copper-bearing Tourmalines from New Deposits in Paraíba State, Brazil" for the journal's Fall 2007 issue (pp. 236–239). He was also a co-author of "Paraíba-type Copper-bearing Tourmaline from Brazil, Nigeria, and Mozambique: Chemical Fingerprinting by LA-ICP-MS" (Spring 2006), which received third place in last year's Edward J. Gübelin Most Valuable Article Awards.

After studying German at Reitaku University, Mr. Furuya traveled to Idar-Oberstein and received a Diploma in Gemmology from the German Gemmological Association in 1972. Four years later, he was awarded a Diploma in Gemmology from the Gemmological Association of Great Britain. Throughout his career, Mr. Furuya visited many new gem-producing localities and introduced those goods to the Japanese market. He established the Japan Germany Gemmological Laboratory in 1994 and had served as a delegate to the International Gemmological Conference since 1999. Mr. Furuya is survived by his wife, Kimiko, and son and daughter, Masaki and Rena. His son will continue the work of the Japan Germany Gemmological Laboratory.

LATEST-GENERATION CVD-GROWN SYNTHETIC DIAMONDS FROM APOLLO DIAMOND INC.

Wuyi Wang, Matthew S. Hall, Kyaw Soe Moe, Joshua Tower, and Thomas M. Moses

Gemological and spectroscopic properties of 43 CVD synthetic diamonds from Apollo Diamond Inc. were examined to characterize the latest generation of their CVD products. These samples, which included both faceted gems and partially polished crystals, were provided as representative examples of Apollo's 2006–2007 production. Relative to the Apollo CVD products examined in 2003, the new samples showed significant improvements in size, color, and clarity. In addition to colorless and near-colorless material, fancy orange-to-pink colors are now produced. These high-quality CVD-grown diamonds, comparable in color and clarity to natural diamonds, can be identified using a combination of gemological and spectroscopic properties.

The ability to grow high-quality diamond in the laboratory has been aggressively pursued for several decades, due to the value that diamond holds in the semiconductor, optics, and gem industries. While the growth of gem-quality single-crystal diamonds under high-pressure, high-temperature (HPHT) conditions has been intensely studied and well documented, the synthesis of single-crystal diamond by the chemical vapor deposition (CVD) technique is relatively new and has evolved rapidly over the past few years. Before 2003, the CVD technique was primarily used to grow polycrystalline diamonds of micrometer size. Badzian and Badzian (1993) reported the growth of CVD single-crystal synthetic diamond as thick as 1.2 mm; subsequently, several other groups (e.g., Doering et al., 1999; Linares and Doering, 1999) reported the CVD growth of undoped and boron-doped single-crystal diamond of approximately 1 mm thickness. Yan et al. (2004) reported the successful synthesis of "thick" nitrogen-doped free-standing single-crystal diamond using the microwave plasma CVD technique, a discovery that led to numerous new applications for this material. Since then, significant improvements in growth technique and, consequently, crystal quality have been reported (Martineau et al., 2004; Yan et al., 2004; Tallaire et al., 2005; Wang et al., 2005; Miyatake et al., 2007).

Apollo Diamond Inc. of Boston, Massachusetts, demonstrated its ability to grow single-crystal CVD synthetic diamonds of moderate gem quality several years ago (Wang et al., 2003). For the most part, the samples examined in 2003 were relatively small and of limited thickness for faceting purposes. Nearly all of these early crystals were predominantly brown with varying degrees of saturation. Colorless CVD-grown diamonds, both nitrogen doped and high purity, were also synthesized by LIMHP-CNRS in France (Achard et al., 2005; Wang et al., 2005), but the reported crystals were usually

See end of article for About the Authors and Acknowledgments.
GEMS & GEMOLOGY, Vol. 43, No. 4, pp. 294–312.

Figure 1. The latest-generation CVD synthetic diamonds produced by Apollo Diamond Inc., which are now available in the gem market, showed significant improvement in quality compared to those reported by Wang et al. in 2003. These representative samples weigh 0.24–0.67 ct. Photo by Robert Weldon.

less than 1.6 mm thick. More recent CVD products from Apollo, however, have shown substantial improvements in quality.

Apollo Diamond began to formally introduce its CVD-grown diamonds to the general public in 2007. They are currently available through Bostonian Jewelers, a Boston retailer, and via inquiries directed through the company's website at www.apollodiamond.com. Due to the potential impact that gem-quality CVD synthetic diamonds might have in the consumer market, the jewelry industry has shown great interest in developing a better understanding of these products, improvements in their quality, and their potential use in jewelry applications, as well as the ability of gem-testing laboratories to identify this material and separate it from natural diamonds. In this report, we characterize the properties of CVD synthetic diamonds produced by Apollo from 2006 to 2007 that are representative of their current generation of products (figure 1).

CVD GROWTH

The CVD method of growing diamond is very different from the well-known HPHT technique. The CVD method involves gaseous reagents—typically a small amount of methane (CH_4 as the source of carbon) in hydrogen (H_2)—in a chamber with a single-crystal diamond substrate usually with {100} orientation. More than one substrate can be placed in the reaction chamber to grow several synthetic diamond crystals simultaneously. A reaction among these components is initiated with a plasma, hot filament, or combustion flame. Carbon atoms, products of a series of chemical reactions, deposit as diamond on a substrate at relatively low temperatures (~1000°C) and low pressures (between 10 and 200 torr). The reactants, products, and reactive species are transported throughout the chamber by diffusion and convection. On the substrate surface, various reactions (adsorption, diffusion, and desorption) occur among the chemical species, leading to the deposition of synthetic diamond and, ultimately, the growth of a continuous layer of synthetic diamond. Goodwin and Butler (1997) reviewed the important features of the growth environment and critical aspects of the growth process.

MATERIALS AND METHODS

CVD Samples. For this study, Apollo Diamond provided a total of 43 CVD synthetic diamonds to the GIA Laboratory for examination; 31 were faceted, and the remainder were fashioned into cylinders or partially polished plates. The samples were segregated into three color groups: colorless to near colorless (29), fancy orange to pink (11), and dark brown (3). The entire suite ranged from 0.13 to 1.20 ct. See

TABLE 1. The three groups of latest-generation Apollo CVD-grown synthetic diamonds examined for this study.

Sample number	Shape	Cut grade[a]	Weight (ct)	Color	Clarity	Fluorescence to long-wave UV	Fluorescence to short-wave UV
Near colorless							
AP-01	Round brilliant	Very good	0.15	E	VVS_2	Inert	Inert
AP-02	Princess	na	0.30	F	VS_1	Very weak orange	Very weak orange
AP-03	Round brilliant	Very good	0.19	F	VVS_2	Inert	Inert
AP-04	Round brilliant	Very good	0.14	G	VS_1	Inert	Inert
AP-05	Round brilliant	Excellent	0.21	F	VS_1	Inert	Inert
AP-06	Round brilliant	Very good	0.16	G	VS_1	Inert	Inert
AP-07	Round brilliant	Good	0.20	I	SI_2	Inert	Very weak orange
AP-08	Round brilliant	Very good	0.27	H	VS_2	Inert	Inert
AP-09	Round brilliant	Very good	0.23	H	VVS_2	Inert	Very weak orange
AP-10	Round brilliant	Excellent	0.27	J	SI_2	Inert	Very weak orange
AP-12	Round brilliant	Very good	0.20	H	VVS_2	Inert	Inert
AP-13	Round brilliant	Good	0.21	L	VS_2	Inert	Inert
AP-14	Round brilliant	Very good	0.25	I	VS_2	Inert	Inert
AP-15	Round brilliant	Very good	0.30	I	SI_1	Inert	Inert
AP-16	Round brilliant	Good	0.25	M	VS_1	Inert	Inert
AP-17	Round brilliant	Very good	0.20	J	VVS_1	Inert	Inert
AP-18	Round brilliant	Excellent	0.62	K	I_1	Inert	Very weak orange
AP-19	Round brilliant	Good	0.28	H	VS_2	Very weak orange	Inert
AP-20	Round brilliant	Excellent	0.26	I	SI_2	Very weak orange	Very weak orange
AP-21	Cylinder	na	0.36	na	na	Inert	Inert
AP-22	Cylinder	na	0.24	na	na	Inert	Inert
AP-23	Cylinder	na	0.19	na	na	Inert	Inert
AP-24	Cylinder	na	0.31	na	na	Inert	Inert
AP-25	Cylinder	na	0.37	na	na	Inert	Inert
AP-26	Cylinder	na	0.52	na	na	Inert	Very weak orange
AP-27	Cylinder	na	0.13	na	na	Inert	Inert
AP-28	Cylinder	na	0.52	na	na	Inert	Inert
AP-29	Cylinder	na	0.32	na	na	Inert	Inert
AP-30	Cylinder	na	0.25	na	na	Inert	Inert
Orange to pink							
AP-31	Tabular	na	1.05	Brownish orangy pink	na	Weak orange, chalky	Very weak orange
AP-32	Tabular	na	1.20	Pinkish brown	na	Very weak orange	Very weak orange
AP-33	Rectangular	na	0.71	Fancy Dark brownish pinkish orange	SI_1	Weak orange, chalky	Very weak orange
AP-34	Princess	na	0.28	Fancy Dark pink-brown	VS_2	Weak orange, chalky	Very weak orange
AP-37	Round brilliant	na	0.34	Fancy brown-pink	VVS_2	Weak-to-moderate orange, chalky	Very weak orange
AP-38	Round brilliant	na	0.40	Fancy orange-brown	SI_2	Moderate orangy yellow	Weak orangy yellow
AP-39	Round brilliant	na	0.62	Fancy brown-orange	SI_2	Moderate orangy yellow	Weak orangy yellow
AP-40	Round brilliant	na	0.18	Fancy brown-pink	VVS_2	Weak orange, chalky	Weak orange
AP-41	Round brilliant	na	0.16	Fancy brown-pink	VVS_1	Weak orange, chalky	Very weak orange
AP-42	Round brilliant	na	0.58	Fancy brownish orangy pink	VVS_1	Moderate orange, chalky	Weak orange, chalky
AP-49	Round brilliant	na	0.19	Fancy brownish pink	VS_2	Weak orange, chalky	Weak orange, chalky
Dark brown							
AP-35	Round brilliant	na	0.33	Fancy Dark yellowish brown	SI_1	Inert	Inert
AP-50	Round brilliant	na	0.46	Fancy Dark orangy brown	VS_1	Inert	Inert
AP-51	Round brilliant	na	0.29	Fancy Dark orangy brown	SI_2	Inert	Inert

[a]*GIA's cut grading system applies only to colorless or near-colorless round brilliant cut diamonds. For other shapes and fancy colors, "na" (not applicable) is indicated.*

table 1 for a full description of the individual samples. These CVD-grown diamonds are representative of current Apollo Diamond production processes.

Gemological Examination. For the purpose of this study, experienced GIA diamond grading staff determined color and clarity grades on all faceted samples using the standard conditions and methodology of GIA's clarity and color grading systems (see, e.g., King et al., 1994). We examined the internal features of all the samples using both a standard gemological binocular microscope and a research microscope with a variety of lighting techniques. Reactions to ultraviolet radiation (again, see table 1) were checked in a darkened room with a conventional four-watt combination long-wave (365 nm) and short-wave (254 nm) UV lamp. We also examined all samples for their fluorescence and phosphorescence properties, as well as growth characteristics, using the Diamond Trading Company (DTC) DiamondView deep-ultraviolet (<230 nm) luminescence imaging system (Welbourn et al., 1996).

Spectroscopic Analysis. All samples were tested by all of the following methods. To avoid surface contamination in the spectroscopic analysis, we cleaned the samples thoroughly in acetone using an ultrasonic bath. Infrared absorption spectra were recorded in the mid-infrared (6000–400 cm^{-1}, 1 cm^{-1} resolution) and near-infrared (up to 11000 cm^{-1}, 4 cm^{-1} resolution) ranges at room temperature with a Thermo-Nicolet Nexus 670 Fourier-transform infrared (FTIR) spectrometer equipped with KBr and quartz beam splitters. We used a diffuse reflectance apparatus to focus the incident beam on the sample, and collected a total of 512 scans (per spectrum) to improve the signal-to-noise ratio. Spectra in the mid-infrared and near-infrared regions were normalized based on the two-phonon and three-phonon absorptions of diamond, respectively. Absorption spectra in the ultraviolet to visible to near-infrared (UV-Vis-NIR) range (250–850 nm) were recorded with a Thermo-Spectronic Unicam UV500 spectrophotometer that used a sampling interval of 0.1 nm for all samples. The synthetic diamonds were mounted in a cryogenic cell and cooled to liquid nitrogen temperature (~77 K).

Raman and photoluminescence (PL) spectra were recorded using a Renishaw InVia Raman confocal microspectrometer with an Ar-ion laser operating at two excitation wavelengths: 488 nm (for the 490–950 nm range) and 514.5 nm (for the 517–950 nm range). We collected PL spectra in the 640–850 nm range using a He-Ne laser (633 nm), and in the 835–1000 nm range using a NIR laser (830 nm). For PL analysis, all samples were cooled by direct immersion in liquid nitrogen. Three scans were accumulated to achieve a better signal-to-noise ratio.

GEMOLOGICAL OBSERVATIONS

Shapes. Most of the 31 faceted samples were round brilliants (two were princess cuts and one was a rectangular cut); they ranged in size from 0.14 to 0.71 ct. All the faceted gems exhibited standard cut dimensions. Based on the GIA cut grading system for round brilliant diamonds (Moses et al., 2004), most (14 of 18) of the colorless/near-colorless round brilliants were graded as excellent or very good.

Both ends of the 10 near-colorless cylinders were polished for quantitative spectroscopic analysis and better examination of internal features. These cylinders varied in diameter from 2.40 to 3.75 mm and in thickness from 1.51 to 2.56 mm. All displayed distinctive groove patterns on their edges, indicating that each was laser cut from a larger crystal; similar grooves were seen on the girdles of many of the faceted samples (figure 2). The two partially polished plates (1.05 and 1.20 ct) exhibited a tabular morphology (figure 3), which is characteristic of as-grown CVD synthetic diamonds.

Color. An outstanding feature of the 43 CVD-grown diamonds were the colors represented (again, see table 1). Twenty-nine samples were colorless, near colorless (figure 4), or only very slightly colored, and these are collectively referred to as the "near-colorless" group in this article. Of the 19 samples in this group given color grades (table 1; the cylinders were not color graded), four were colorless (E to F), 12 were near colorless (G to J), and three displayed very slight coloration (K to M). All the faceted Apollo samples in this group, except for the colorless ones, had a slightly brown component with no yellow apparent. Of the 14 fancy-color CVD products, 11 had significant orange or pink (or both) components with moderate-to-strong saturation (e.g., figure 5, a–c), and the other three samples were dark brown (e.g., figure 5d). Although the hue descriptions are similar between some of the samples in the "orange-to-pink" group and the three in the "dark brown" group (again, see table 1), these latter three specimens showed distinctly darker tone than the other 11 fancy-color samples and the predominant

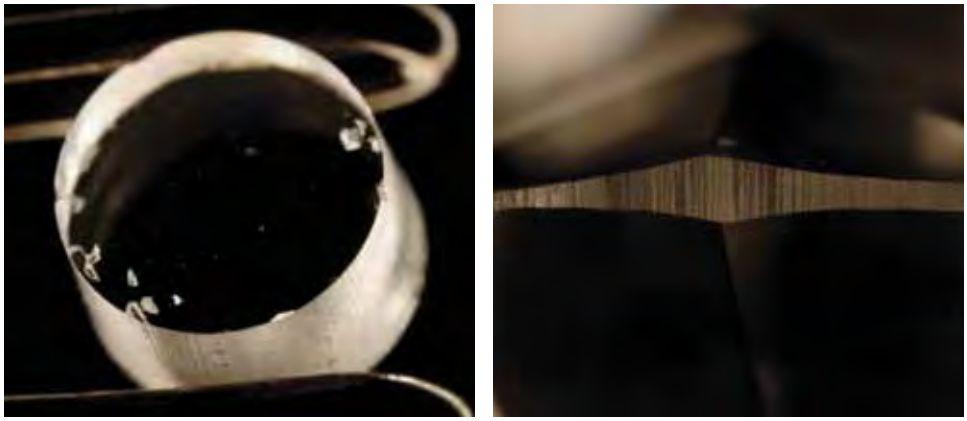

Figure 2. Most of the partially polished CVD-grown crystals examined were cylindrical with distinctive laser grooves along the outer rims. The diameter of this cylinder (left, sample AP-21) is 3.46 mm. The laser grooves were still visible on the girdles of many of the faceted round brilliants (right, sample AP-10, field of view 1.0 mm). Photomicrographs by W. Wang.

hue in all three was brown. Two samples in the "orange-to-pink" group were graded Fancy Dark, but both displayed a distinct orange-to-pink hue. Throughout this article, gemological and spectroscopic features will be presented and discussed in terms of these three color groups.

Clarity. GIA lab staff also determined clarity grades for the 31 faceted CVD-grown diamonds. Nine were given VVS grades (29%), 12 were VS (39%), and nine were SI (29%). One sample fell into the I ("included") category. Cavities, fractures, small inclusions, and pinpoints (figure 6) were the most common clarity grade–setting internal features. The fractures and cavities varied from micrometer to millimeter scale, and most were surface reaching. Unlike what is typically seen in natural diamonds, the fractures in the CVD samples were usually not connected to inclusions. In general, the small inclusions and pinpoints were randomly distributed. In rare cases, numerous pinpoints and small inclusions occurred together in cloud-like groups (figure 6c). Internal features were typically light in color with only a few small dark inclusions observed.

Reactions to UV Radiation. Observation of the samples while they were exposed to conventional short- and long-wave UV lamps revealed a close correlation between fluorescence and bodycolor (table 1). For the near-colorless group, only eight of the 29 samples showed very weak orange fluorescence to short- and/or long-wave UV radiation; the remaining samples were inert to both wavelengths. In contrast, all the samples in the orange-to-pink group showed orange fluorescence of very weak to moderate intensity to long-wave UV, with obvious turbidity ("chalkiness") in eight of the 11 samples. When exposed to short-wave UV, all of these CVD samples displayed very weak to weak orange to orangy yellow fluorescence. No UV fluorescence was observed in the three diamonds in the dark brown group. None of the samples in the present study showed phosphorescence to conventional long- or short-wave UV radiation.

When exposed to the high-intensity ultra-short wavelengths of the DTC DiamondView, most of the near-colorless group of synthetic diamonds displayed strong pinkish orange fluorescence (figure 7a and 7c), and a few fluoresced strong orange or

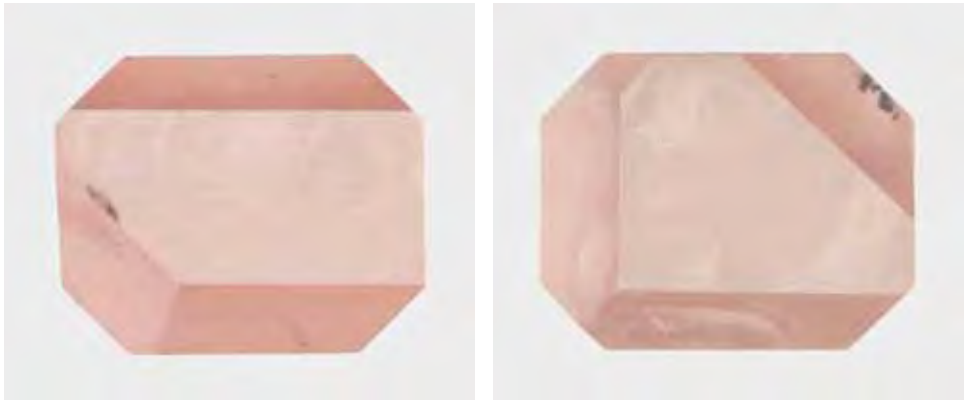

Figure 3. These two partially polished CVD crystals (1.05 and 1.20 ct) had a tabular morphology that is characteristic of CVD synthetic diamonds. Photos by Jian Xin (Jae) Liao.

Figure 4. These faceted CVD samples from Apollo Diamond (0.15–0.30 ct) range from E to H on the GIA color grading scale. Photos by Jian Xin (Jae) Liao.

orangy red (figure 7b). An interesting feature was the occurrence of regions with irregularly patterned strong blue fluorescence. The size of these regions varied significantly between samples. In some of the samples, the blue fluorescence was concentrated near the culet (figure 7c), and in others it was on the table facet. In the latter case, a violetish blue fluorescence was typically observed as well (figure 7d). All samples were also checked for phosphorescence in the DiamondView (all under the same conditions). Weak-to-moderate blue phosphorescence was seen in 15 of the 29 samples in the near-color-

Figure 5. Some of the CVD samples showed attractive fancy colors: (a) 0.71 ct, Fancy Dark brownish pinkish orange; (b) 0.34 ct, Fancy brown-pink; (c) 0.28 ct, Fancy Dark pink-brown; (d) 0.33 ct, Fancy Dark yellowish brown. Photos by Jian Xin (Jae) Liao.

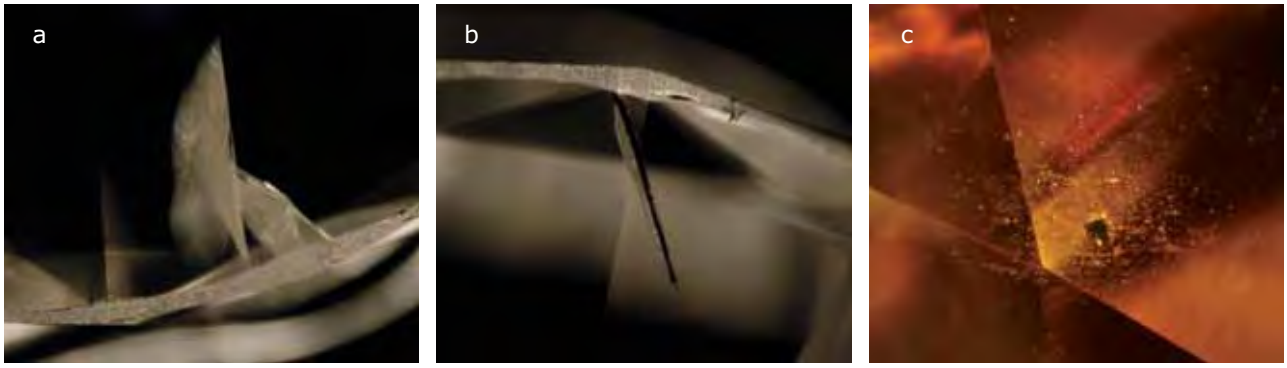

Figure 6. Most of the faceted CVD synthetic diamonds studied had high clarity grades, in the VVS and VS ranges. The internal features that most affected the clarity grades were: (a) surface-reaching fractures (field of view 2.5 mm); (b) surface-reaching cavities (field of view 1.4 mm); and (c) pinpoints and clouds (field of view 0.9 mm). Photomicrographs by W. Wang and K. S. Moe.

less group (figure 8). Within this group, we did not observe any systematic changes in fluorescence/phosphorescence in the DiamondView as the color grade increased from E to M. In general, the phosphorescence colors appeared evenly distributed throughout the CVD-grown diamonds, with no variations visible even in samples showing the distinct zonations of blue and orange-to-pink fluorescence.

The orange-to-pink CVD synthetic diamonds showed stronger reddish orange fluorescence in the DiamondView (figure 9a-d) than was seen in the near-colorless samples; none showed the irregularly patterned blue fluorescence. In general, the fluorescence in the orange-to-pink samples was evenly distributed, with only three of the 11 samples showing bands of weaker orange color. These bands were uniform in thickness, oriented parallel to the table facet, and had sharp, well-defined boundaries (figure

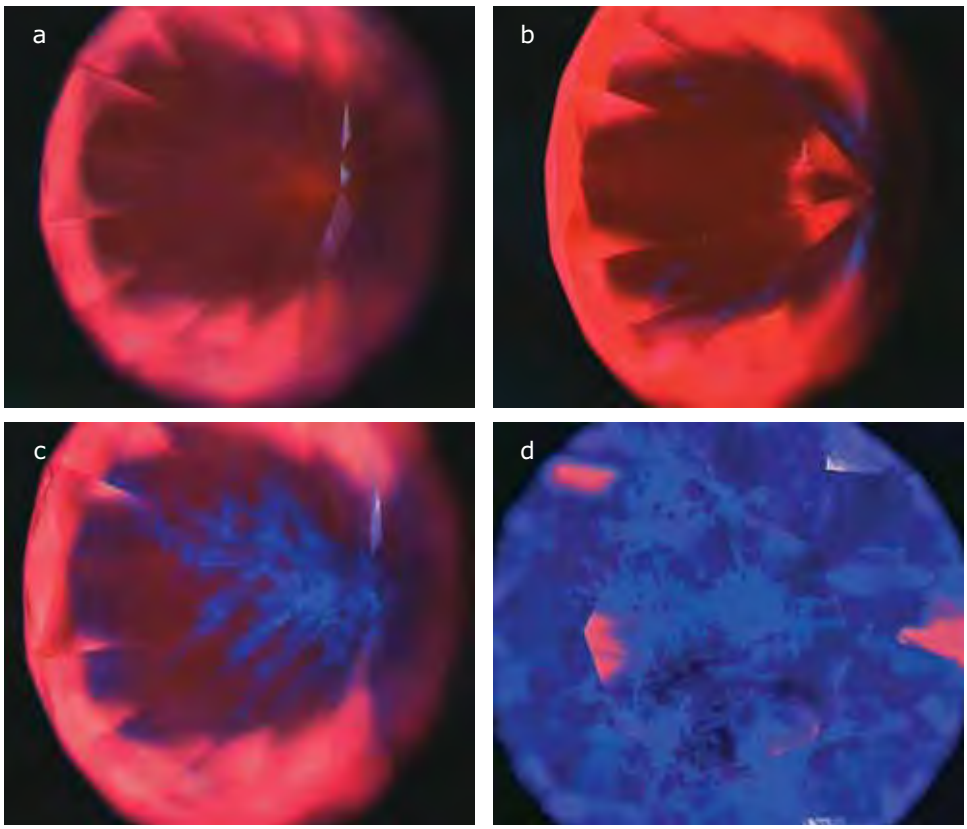

Figure 7. In the DTC DiamondView, most of the near-colorless group of CVD synthetic diamonds displayed strong pinkish orange fluorescence (a and c), and some fluoresced strong orange or orangy red (b). Several had very irregular regions with strong blue (c) or violetish blue (d) fluorescence. Photos by W. Wang.

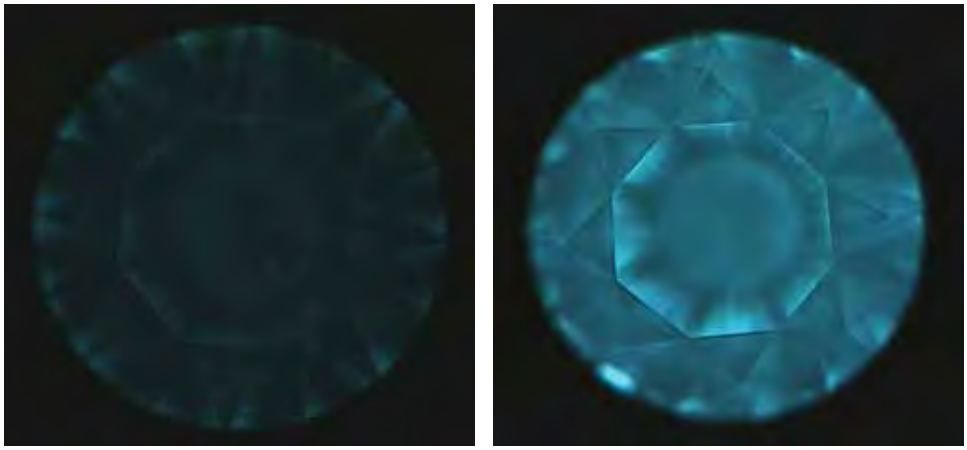

Figure 8. The DiamondView revealed blue phosphorescence of weak (left) to moderate (right) intensity in about half of the CVD-grown diamonds in the near-colorless group. All the phosphorescence images were collected under the same conditions. Photos by W. Wang and K. S. Moe.

9b). Narrow growth striations were visible in many of the samples due to variations in fluorescence intensity, and evenly distributed weak green fluorescence (figure 9c) was also observed in five of the 11 orange-to-pink samples. Of all the fancy-color CVD synthetic diamonds studied, only one of the orange-to-pink samples (AP-34) showed weak blue plus some small areas of green phosphorescence (figure 10) in the DiamondView.

The three dark brown CVD synthetic diamonds showed orangy red fluorescence in the DiamondView, but with much weaker intensity than that of the other two groups. The irregularly patterned blue fluorescence observed in the near-colorless group also occurred in the brown samples, but was very limited in distribution.

Graining and Birefringence. Graining was a common feature in all the CVD synthetic diamonds studied. In contrast to that observed in natural dia-

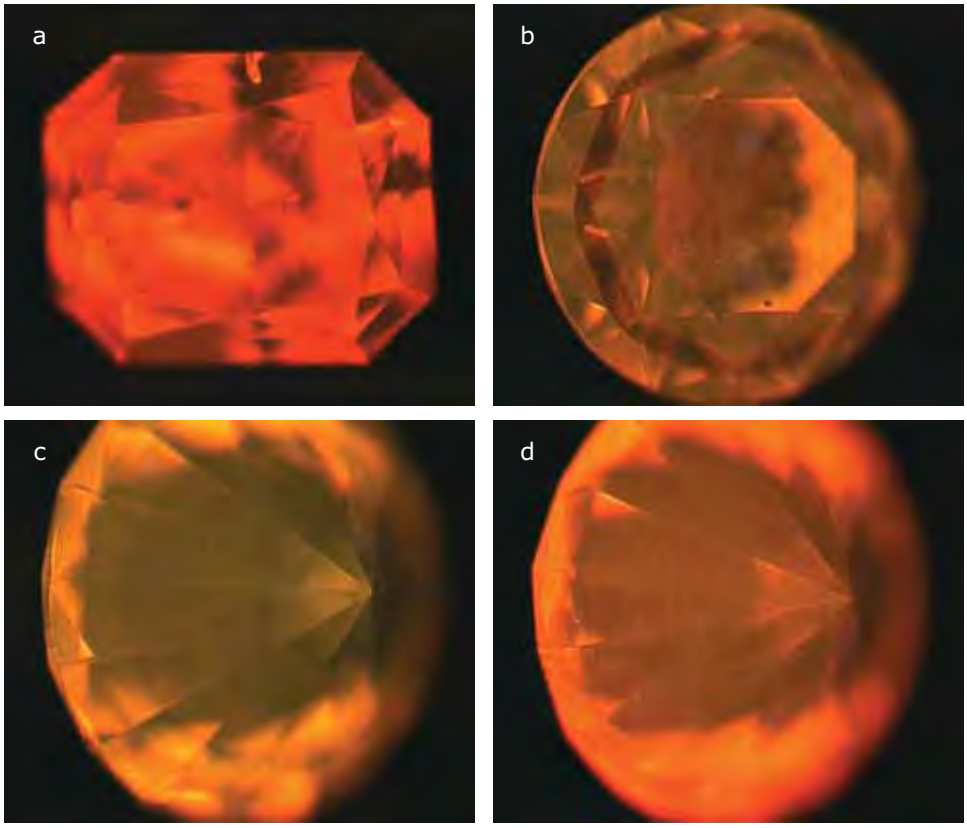

Figure 9. The fancy-color CVD synthetic diamonds with distinct orange-to-pink colors showed a more intense reddish orange fluorescence (a–d) than the near-colorless group when examined with the DiamondView. Three of the 11 samples in this group showed bands of weaker orange fluorescence (b), possibly due to variations in crystal growth conditions. Five also displayed distinct green fluorescence (c). Photos by W. Wang and K. S. Moe.

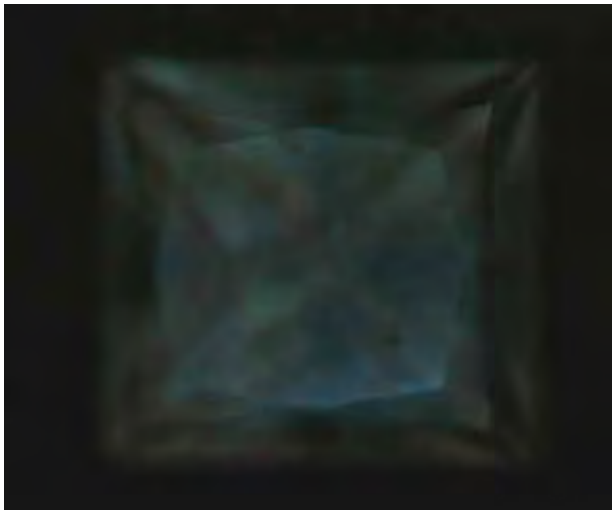

Figure 10. Only one (AP-34) of the 14 fancy-color CVD-grown diamonds phosphoresced in the DiamondView, showing weak blue with minor amounts of green luminescence. Photo by W. Wang.

Figure 11. Internal graining was well developed but "fuzzy" in most of the CVD synthetic diamonds studied. Graining with clearly observable outlines, as seen here in sample AP-18, was rare. Photomicrograph by W. Wang; field of view 2.4 mm.

monds, the internal graining in most of the CVD samples showed indistinct boundaries that appeared fuzzy. Only three samples showed graining with relatively well-defined edges (see, e.g., figure 11).

Strong birefringence was another important feature of these CVD samples. Under magnification with crossed polarizers, all the samples displayed very high-order interference colors (figure 12). The CVD products commonly showed red, blue, green, and even white interference colors that were in sharp contrast to the gray colors that are typical of natural type IIa diamonds. While bands of interference colors occurred in a few samples, most displayed irregular patterns. No correlation was observed between bodycolor and interference color or pattern; comparable interference features occurred in both the near-colorless and fancy-color CVD groups.

RESULTS OF SPECTROSCOPIC ANALYSIS

Infrared Absorption Spectroscopy. Several distinct features in the IR spectra correlated directly with the bodycolors of the CVD synthetic diamonds. In the mid-infrared region, samples in the near-colorless group showed no detectable absorptions related to nitrogen or boron impurities, indicating they

Figure 12. When examined with crossed polarizers, type IIa CVD synthetic diamonds usually show much higher-order interference colors than natural type IIa diamonds, as illustrated by the samples shown here: (a) type IIa faceted CVD-grown diamond; (b) type IIa cylindrical CVD-grown crystal; and (c) interference pattern of a typical natural type IIa diamond. Photomicrographs (fields of view 1.8, 3.8, and 1.4 mm, respectively) by W. Wang and K. S. Moe.

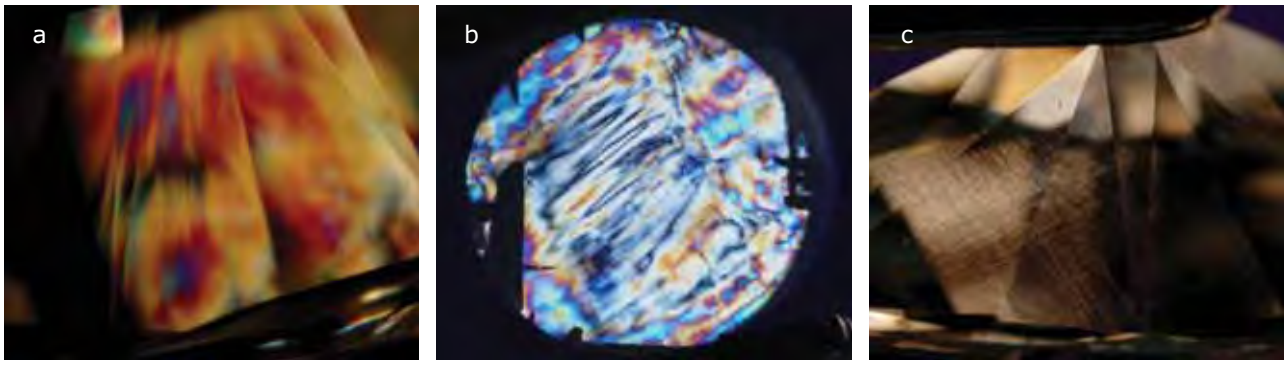

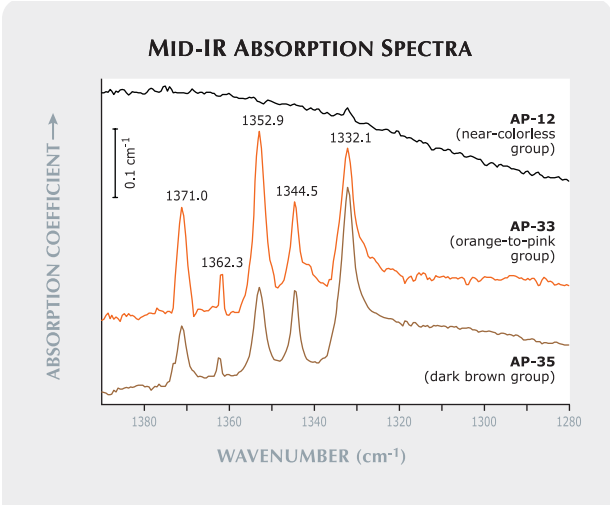

Figure 13. CVD synthetic diamonds from the near-colorless group (e.g., AP-12) showed only a weak absorption at 1332.1 cm^{-1}. In the fancy-color CVD diamonds (e.g., AP-33, AP-35), more intense peaks were observed. Spectra shifted vertically for clarity.

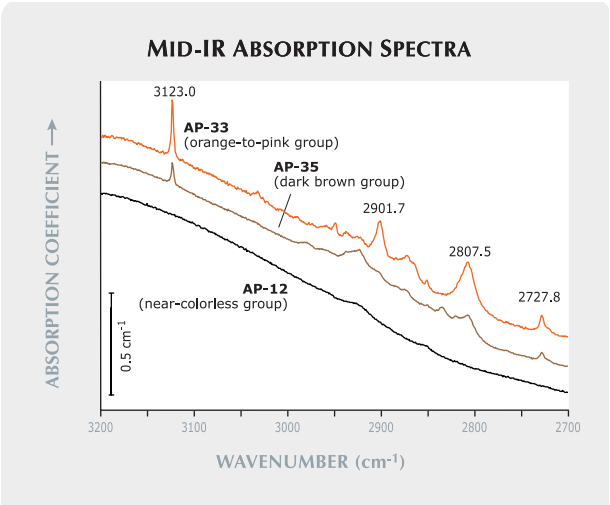

Figure 14. In the near-colorless group of CVD synthetic diamonds (e.g., AP-12), no absorption at 3123.0 cm^{-1} was recorded. In contrast, that H-related absorption is very strong in the fancy-color CVD diamonds (e.g., AP-33, AP-35). Spectra shifted vertically for clarity.

were all type IIa, and exhibited only a weak peak at 1332.1 cm^{-1} (figure 13). All the fancy-color samples showed stronger absorption at 1332.1 cm^{-1}. Additionally, all were classified as type IIa; however, they showed a weak absorption at 1344.5 cm^{-1} (~0.1 cm^{-1} in intensity) that was due to the presence of ~5 ppm of isolated nitrogen. In addition, weak but distinct absorptions at 1371.0, 1362.3, and 1352.9 cm^{-1} were consistently recorded in the fancy-color CVD-grown diamonds, but did not occur in the near-colorless group.

Differences between the near-colorless and fancy-color samples were also noted in the region of 3200–2700 cm^{-1} (figure 14). In this range, CVD samples in the near-colorless group showed only the gradual increase in absorption that is intrinsic to diamond. In contrast, all the fancy-color samples exhibited a sharp absorption at 3123.0 cm^{-1} with significant intensity caused by a hydrogen-related lattice defect (Fuchs et al., 1995a,b). Many other weak and broad features also occurred in this region, including peaks at 2901.7, 2807.5, and 2727.8 cm^{-1}.

The integrated intensities of the absorptions (i.e., the areas under the peaks) at 1371.0 and 1352.9 cm^{-1}, as represented in figure 13, displayed positive linear correlations with each other (figure 15, left; a similar correlation for the 1362.3 peak is not shown) and with the H-related peak at 3123.0 cm^{-1} (figure 15, right), but no correlation was observed with the concentration of isolated nitrogen (i.e., the 1344.5 cm^{-1} peak).

We also observed significant variations in the near-infrared range (figure 16). For the near-colorless CVD group, the samples ranging in color from F to J showed only two very weak absorptions at 6855 and 5562 cm^{-1}, whereas the E-color sample (AP-01) had no detectable absorptions in the entire NIR region. The K-to-M CVD synthetic diamonds generally showed two additional weak absorptions at 7353 and 6425 cm^{-1}. While all of these absorptions were <1.0 cm^{-2} in integrated intensity, NIR features in the K-to-M samples appeared slightly stronger than those in samples from the rest of the near-colorless group.

The orange-to-pink CVD samples exhibited much stronger absorptions at 7353 (average integrated intensity 2.12 cm^{-2}) and 6425 cm^{-1}. However, they did not show the peaks at 6855 and 5562 cm^{-1}; instead, many sharp peaks occurred in the range 9000–4200 cm^{-1}, including the strong absorptions at 7917 and 7804 cm^{-1} reported by Twitchen et al. (2007) as the 1263 and 1281 nm lines. This group of samples showed other major NIR peaks at 7533, 6963, 6828, 6425, 6064, 5219, 4888, 4672, and 4337 cm^{-1} (again, see figure 16, left). All the lines were sharp and relatively strong in intensity.

The three dark brown CVD synthetic diamonds showed absorption features that were very similar to those of the K-to-M colors, with two additional sharp and strong peaks at 8752 and 7837 cm^{-1}, and two sharp peaks at 7225 and 7189 cm^{-1} (figure 16, right). In these three dark brown diamonds, all the peaks were very strong and linearly correlated with

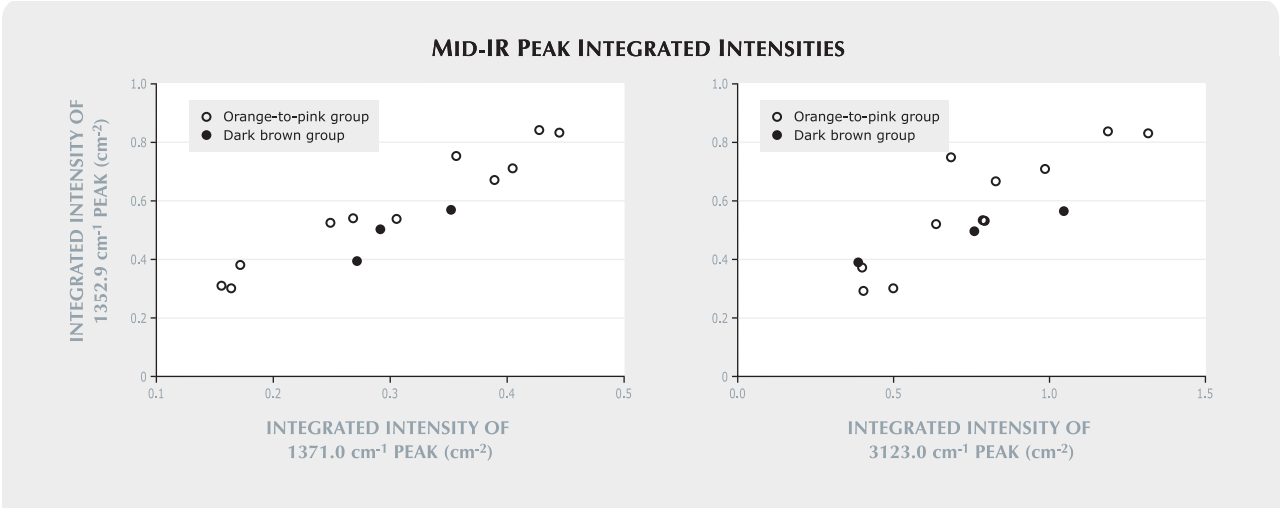

Figure 15. In the fancy-color CVD synthetic diamonds, the integrated intensities displayed positive linear correlations between (left) absorptions at 1352.9 cm^{-1} and 1371.0 cm^{-1}, and (right) those absorptions (represented here by the peak at 1352.9 cm^{-1}) and the H-related absorption at 3123.0 cm^{-1}.

one another in integrated intensity (figure 17). For example, the average integrated intensity of the 7353 cm^{-1} peak in the dark brown samples was 89.2 cm^{-2}.

UV-Vis-NIR Absorption Spectroscopy. The E-to-J CVD-grown diamonds in the near-colorless group showed no specific features in the UV-Vis region except for a very slight increase in absorption from ~500 nm to the high-energy (low-wavelength) side (e.g., sample AP-22 in figure 18). An extremely weak and broad band at ~270 nm was recorded in the slightly brown samples. Sample AP-16, which had the most brown ("M") in the near-colorless group, also had the highest-intensity absorption at ~270 nm of the near-colorless samples. The broad ~270 nm band is caused by trace amounts of isolated nitrogen.

Analysis of the samples in the orange-to-pink group revealed some consistent absorption features, including broad bands at ~270 nm and ~520 nm, a gradual increase in absorption from ~450 nm to the

Figure 16. Some distinct correlations were observed between absorptions in the near-infrared region and the body-colors of the CVD samples. Generally, the orange-to-pink samples (e.g., AP-33) showed stronger peaks than those in the near-colorless group (e.g., AP-04 and AP-13; left). In dark brown CVD diamonds (e.g., AP-51; right), very strong absorptions were consistently observed. Note the difference in scale between the spectra on the left and right; also, spectra on the left have been shifted vertically for clarity.

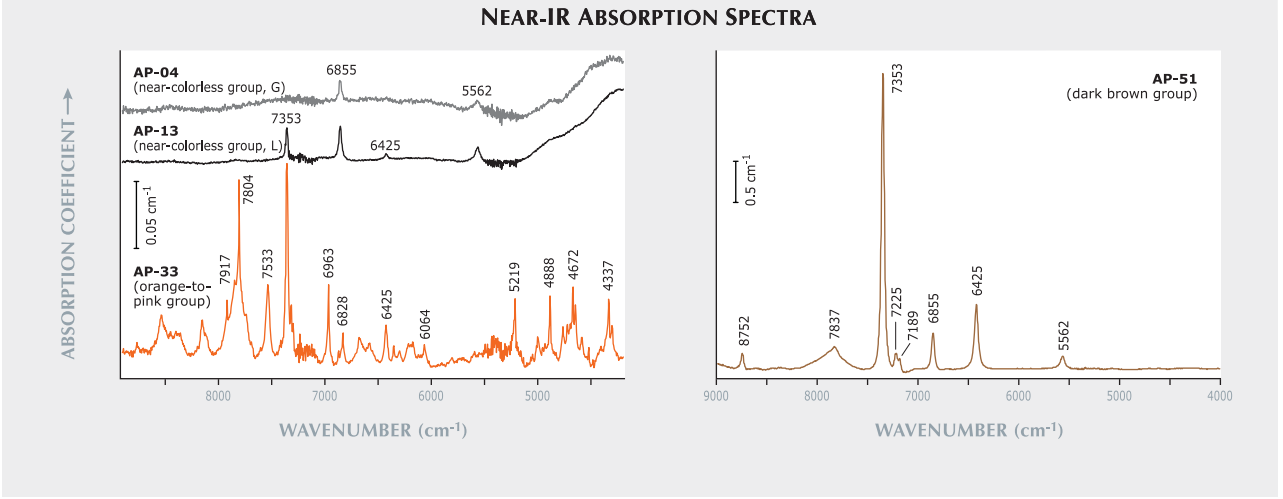

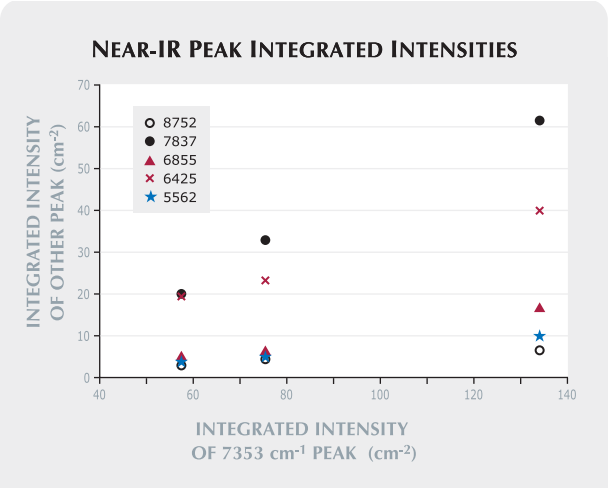

Figure 17. Six absorption peaks in the near-infrared region of the dark brown CVD synthetic diamonds displayed positive linear correlations.

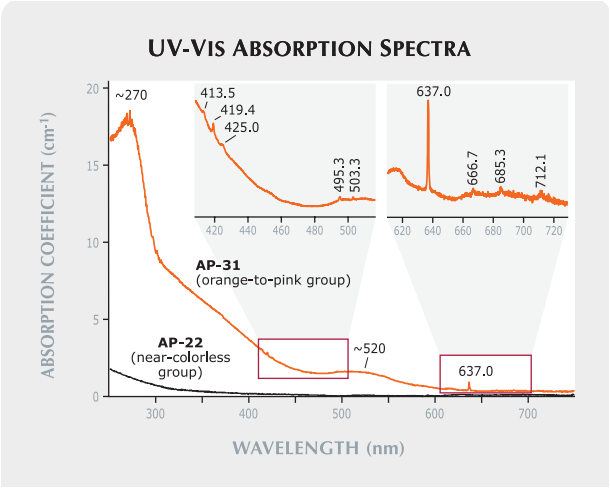

Figure 18. In the UV-Vis region, absorption spectra from CVD samples of the near-colorless group (e.g., AP-22) are generally flat. Broad bands at ~270 nm and ~520 nm and some sharp peaks including a ZPL at 637.0 nm were consistently recorded in CVD samples with orange-to-pink coloration (e.g., AP-31).

high-energy (low-wavelength) side, and sharp peaks at 413.5, 419.4, 425.0, 495.3, 503.3, 637.0, 666.7, 685.3, and 712.1 nm (see spectrum of sample AP-31 in figure 18). Among the sharp absorptions, the 637.0 nm peak, the zero phonon line (ZPL) of the nitrogen-vacancy $[N\text{-}V]^-$ center, was the strongest. In the three dark brown samples, absorption increased gradually from ~600 nm to the high-energy (low-wavelength) side with a broad band centered at ~520 nm (figure 19). Only two sharp, but weak, absorptions at 624.5 and 637.6 nm were recorded. A broad shoulder centered at ~370 nm appeared in samples AP-35 and AP-50; however, the feature is difficult to discern in sample AP-51 due to very strong absorption in this region. All these broad features are similar to those reported in as-grown brown CVD synthetic diamond by, for example, Martineau et al. (2004, figure 11), Twitchen et al. (2004, 2007), and Hounsome et al. (2005).

Photoluminescence and Raman Spectroscopy. Numerous emission lines were recorded with four different lasers, some of which were observed with multiple excitation wavelengths. The major PL features are summarized below on the basis of individual laser excitation in the defect's most sensitive region.

When blue laser (488 nm) excitation was employed (figure 20), all the CVD synthetic diamonds in the near-colorless group displayed weak and sharp peaks at 543.3 and 546.1 nm. Weak peaks at 501.2, 534.0, 534.4, and 540.0 nm also occurred in over 70% of the samples in this group (not shown); in general, these weak peaks were either all present or all absent. A weak emission at 512.2 nm (not shown) was also observed in about half the samples tested. An outstanding feature in the near-colorless group was the occurrence of a weak 3H emission (ZPL at 503.5 nm) in about 70% of the samples. Only one sample (AP-14) showed a very weak H3 emission (ZPL at 503.1 nm). All the orange-to-pink CVD samples showed extremely strong H3 emissions as well as a cluster of weak emissions at 493.7–500.9 nm with major lines at 494.6, 498.1 (not shown), and 546.1 nm. Moderate H3 emissions

Figure 19. This absorption spectrum is typical of the dark brown CVD synthetic diamonds.

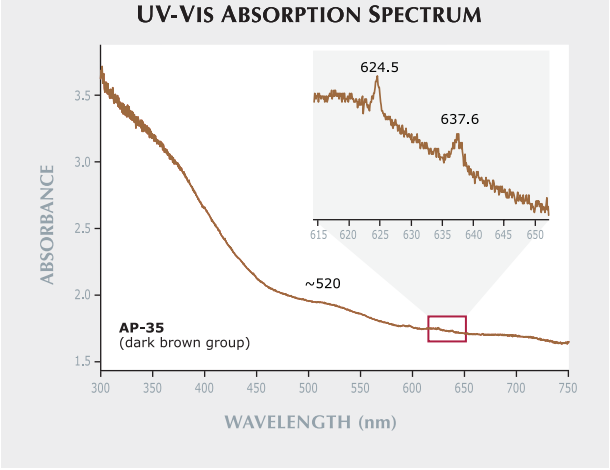

were also recorded in all three dark brown CVD samples, together with a 512.2 nm peak (not shown). Additional weak emissions at 540.0 (not shown), 543.3, and 546.1 nm were present in some of the samples of this group.

Green laser (514.5 nm) excitation revealed strong emission systems of N-V centers in the CVD samples of all colors (575 and 637.0 nm [not shown]; figure 21). Doublet emissions at 596.5 and 597.0 nm occurred in all samples of the near-colorless group. The same doublet appeared in all three dark brown samples, but with an additional weak peak at 595.3 nm. In contrast, these features were absent in the orange-to-pink CVD synthetic diamonds. In addition, all three dark brown samples exhibited weak peaks, as shown in the inset to figure 21, at 555.0, 557.1, and 559.1 nm, with the strongest intensity at 559.1 nm. These correspond to Raman shifts at 1418, 1486, and 1550 cm^{-1}, respectively. The last of these is due to the presence of non-diamond carbon (Zaitsev, 2001). The Raman shifts of these three peaks were confirmed based on the same energy shift (i.e., these features appeared at different wavelengths, but with the same Raman shift, when excited by the two different lasers) using 488 nm laser excitation but with weaker intensity than those obtained from 514.5 nm laser excitation.

When excited by a red laser (633 nm), all the samples in the near-colorless group showed weak silicon-related emission (figure 22), which is usually composed of two very sharp peaks at 736.6 and 736.9 nm (generally referred to as the 737 nm defect; Vavilov et al., 1980; Clark et al., 1995; Iakoubovskii et al., 2001). We should point out that this emission also was present in 75% of the samples of this group when 488 or 514.5 nm laser excitation was used. In addition, weak emissions at 664.0, 665.8, and 833.8 nm (not shown) were recorded with the red laser in about half the samples in the near-colorless group. In all the orange-to-pink samples, a weak emission occurred at 823.4 nm. However, the Si-related 737 nm emission was observed in eight of the 11 samples. While most Si-related emissions were very weak in this group, two samples (AP-38 [figure 22] and AP-39) displayed extremely strong peaks. None of the orange-to-pink samples showed Si-related emission peaks when 488 or 514.5 nm laser excitation was used. Of the three dark brown CVD synthetic diamonds, only one (AP-50) showed a very weak emission at the Si-related 737 nm defect (again, see figure 22). No emission at 737 nm was observed in the other two dark brown samples with any laser excitation.

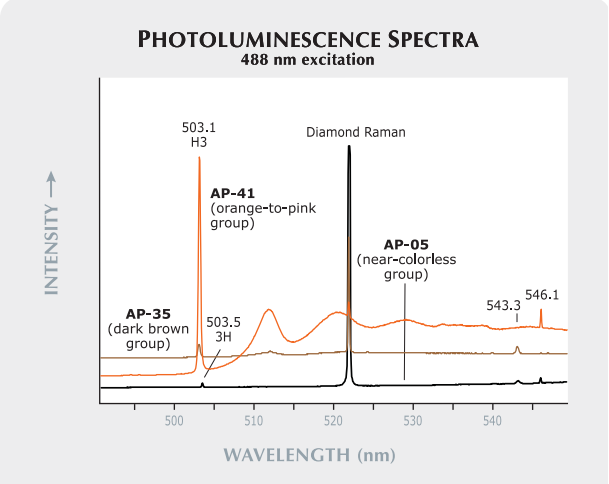

Figure 20. When blue laser (488 nm) excitation was used, the PL spectra showed H3 emission in the orange-to-pink (e.g., AP-41) and dark brown (e.g., AP-35) CVD samples. A weak 3H emission occurred in most of the CVD samples in the near-colorless group (e.g., AP-05). Other peaks, such as at 543.3 and 546.1 nm, were also observed among the various color groups.

Infrared laser excitation at 830 nm produced many weak and sharp emission features in the

Figure 21. The PL spectra of all CVD synthetic diamonds examined in this study were dominated by N-V center emission systems at 575 nm (the 637 nm peak is not shown) when green laser (514.5 nm) excitation was employed. In addition, Raman scattering peaks at 1418, 1486, and 1550 cm^{-1} (555.0, 557.1, and 559.1 nm) were observed in all three dark brown CVD synthetic diamonds (inset) but not in any sample of other colors.

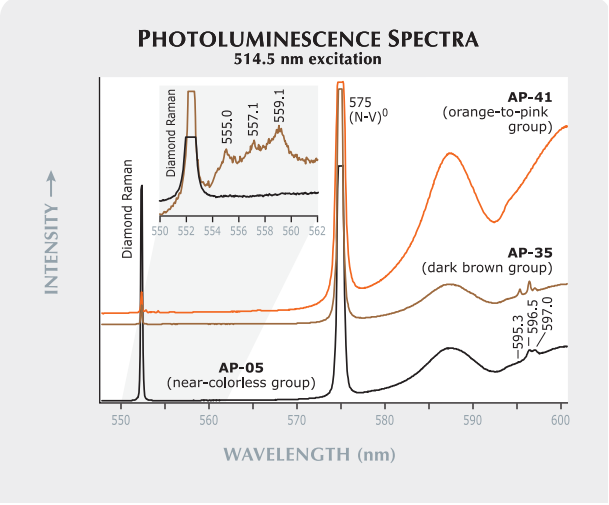

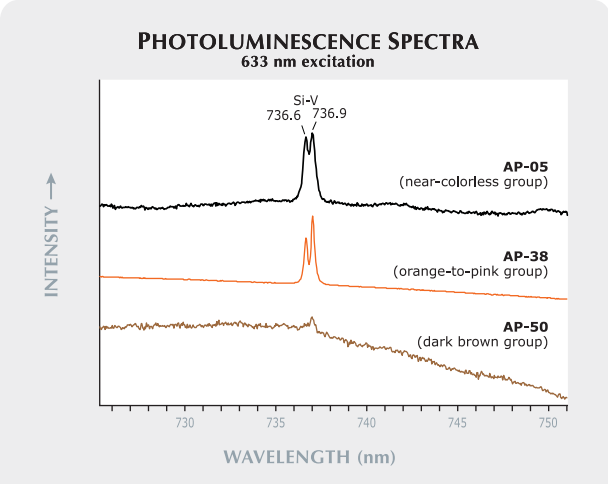

Figure 22. Si-related emission peaks at 736.6 and 736.9 nm were recorded with varying intensities in the PL spectra of most CVD synthetic diamonds. These features were best seen when red laser excitation at 633 nm was used.

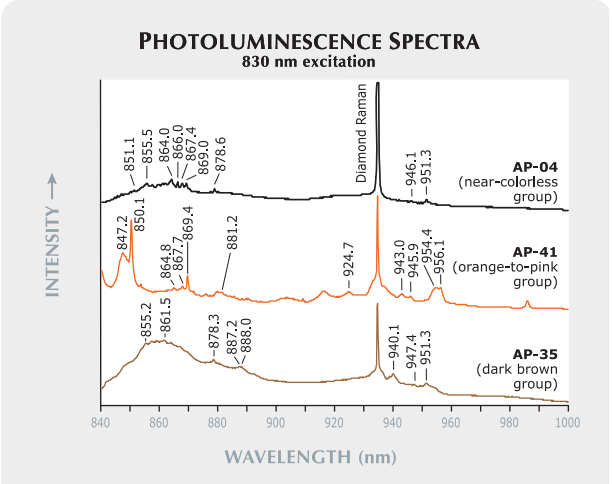

Figure 23. Many weak emission lines were detected in the infrared region of the PL spectra when 830 nm laser excitation was used. Clear differences were observed among the near-colorless, orange-to-pink, and dark brown CVD samples.

850–880 nm region for the near-colorless group of CVD-grown diamonds, including peaks at 851.1, 855.5, 864.0, 866.0, 867.4, 869.0, and 878.6 nm (figure 23). We also observed weak peaks at 946.1 and 951.3 nm in all samples of this group. In the orange-to-pink CVD-grown diamonds, we recorded even more weak emissions, including those at 847.2, 850.1, 864.8, 867.7, 869.4, 881.2, 924.7, 943.0, 945.9, 954.4, and 956.1 nm. The dark brown CVD samples exhibited fewer emissions, among them weak peaks at 855.2, 861.5, 878.3, 887.2, 888.0, 940.1, 947.4, and 951.3 nm.

DISCUSSION

Improvements in Gem Quality. As previously reported (Wang et al., 2003), gem-quality synthetic diamonds grown by Apollo Diamond Inc. represented some of the first examples of single-crystal material grown by the CVD process that were intended for the jewelry trade. Most of the samples produced at the time that article was published showed limited thickness due to the tabular morphology of the CVD crystal. For the most part, the few faceted synthetic diamonds studied were a very strong brown, relatively small (<0.30 ct), and received moderate-to-low clarity grades (VS_1–SI_2). In comparison, the 2006–2007 Apollo Diamond products showed substantial improvements in color, with colorless, near-colorless, and fancy orange-to-pink material representative of the gem-quality CVD-grown diamonds that are now commercially available.

In addition to the previously documented near-colorless and brown CVD material, Martineau et al. (2004) reported on high-quality single-crystal CVD synthetic diamond with blue color produced by boron doping during crystal growth and on a 0.85 ct round-cut as-grown fancy brownish pink CVD synthetic diamond (see sample N8 in table 3 of that reference). Until the present article, little was known about the gemological and spectroscopic features of orange-to-pink CVD synthetic diamonds produced by Apollo Diamond. These very attractive colors, as shown in figures 1 and 5, are comparable to some top-quality fancy-color natural diamonds.

Improvements in clarity were also observed. The clarity grades of over 67% of the samples provided from Apollo's recent production fell in the range VVS_1–VS_2. Only a few were in the SI–I range. Improved clarity was mainly achieved by reducing the amount of larger inclusions and pinpoints. While most of the samples examined for this study contained some pinpoints, very few contained other inclusions that could be resolved even under magnification up to 100×. However, several fractures were observed, particularly in the samples fashioned as cylinders. Significant internal stress was indicated by strong birefringence in many specimens (figure 12). As with natural diamonds, internal stress in these CVD synthetic diamonds—or the stress of the cutting process—is likely to contribute to cracking. Improvements in the CVD growth process have led to larger faceted gems. Even though most of the faceted gems in the current study were still under

0.30 ct, the fact that many samples over half a carat were available and that those cut as round brilliants were well proportioned (table 1) indicates that thicker crystals are used to create the latest-generation Apollo products. In brief, the overall color and clarity of the CVD synthetic diamonds examined in this study is similar to that of the Element Six CVD products reported by Martineau et al. (2004).

It should be noted, though, that the CVD synthetic diamonds examined by Martineau et al. are not commercially available. Apollo products similar in quality to those described in this report have been introduced to the gem trade. All of these CVD-grown products carry a distinctive inscription that identifies them as Apollo Diamonds.

Causes of Improved Clarity and Color. Production of top-quality CVD synthetic diamonds using a relatively high growth rate continues to be a challenge, leading to extensive testing of various combinations of growth parameters. Achard et al. (2005) reported that incorporating as little as 10 ppm of nitrogen in the total gas phase could increase the crystal growth rate by a factor of 2.5 with no degradation of the surface morphology or color. However, Achard et al.'s samples were not of gem thickness, so the color could not be graded using accepted gemological techniques.

According to Martineau et al. (2004), based on growth conditions and additional treatment after growth, CVD synthetic diamonds may be divided into four groups, including high purity and nitrogen doped. The nitrogen-doped product contains a detectable amount of N-bearing lattice defects in UV-Vis absorption and/or photoluminescence spectroscopy, whereas high-purity samples do not. The occurrence of N-V centers, observed as very strong emission systems in the PL spectra of all the Apollo CVD samples tested for the present study (figure 21), indicated that all the samples contained nitrogen. Even in the colorless (E and F) CVD samples, emission from the N-V centers was readily detectable. However, there is a strong correlation between increasing color and greater N-V emission (normalized to the Raman peak height). This is further evidence that nitrogen plays a leading role in the determination of color in the CVD-grown diamonds.

The reasons for nitrogen doping in these CVD samples were different for each color group. For the near-colorless group, nitrogen was controlled at relatively low levels to achieve high growth rates while maintaining crystal quality (Linares and Doering, 2003). IR absorption spectroscopy did not detect any nitrogen impurities in samples of this group. However, the extremely weak, broad band seen at ~270 nm in the UV-Vis-NIR absorption spectra of the samples with a slightly brownish hue is due to isolated nitrogen in concentrations at the ppm (parts per million) level. Non-diamond carbon, deposited during CVD diamond growth, is known to cause brown color in CVD synthetic diamonds; however, the absence of non-diamond carbon (figure 21), and the weak correlation between the concentration of isolated nitrogen and the color grades, suggests that the slight brownish hue in near-colorless samples could be caused by a combination of the detected defects such as isolated nitrogen and N-V centers; additionally, non-diamond carbon could be present, but in concentrations too low to be detected with Raman spectroscopy.

The impact of nitrogen doping in the fancy-color CVD synthetic diamonds is more complicated. Higher concentrations of nitrogen were added into the gas phase and, as a result, more nitrogen was incorporated into the diamond lattice during growth. Relatively high concentrations of isolated nitrogen were revealed in the IR and UV-Vis-NIR absorption spectra (figures 13 and 18). Only 5 ppm of isolated nitrogen is needed to produce yellow-to-orange color in diamond. Moderately strong absorption from the $[N\text{-}V]^-$ defect (ZPL at 637.0 nm; figure 18) in combination with the broad ~520 nm band likely resulted in selective absorption of orange light, and produced a pink color. Assignment of the ~520 nm broad band is unclear, but in these samples it functioned very similarly to the ~550 nm broad absorption band known to cause the color in many natural pink diamonds by selectively absorbing green-to-orange light. The ~520 nm broad band could have been the main color contributor for this group of diamonds.

The dark brown diamonds are distinctive due to the presence of non-diamond carbon (figure 21), which was not detected in either of the other two CVD groups studied. The combination of relatively high concentrations of isolated nitrogen, a weak-to-moderate absorption band at ~520 nm, and the presence of non-diamond carbon resulted in a gradual increase in absorption from the low-energy to high-energy (high-wavelength to low-wavelength) side of the UV-Vis-NIR absorption spectra. Consequently, brown coloration was produced in these samples.

Defect Interrelations and Their Implications. Absorptions with varying intensities at 3123.0,

1371.0, 1362.3, and 1352.9 cm^{-1} occurred in the fancy-color CVD samples (again, see figures 13 and 14). The 3123.0 cm^{-1} absorption is routinely observed in nitrogen-doped single-crystal CVD synthetic diamonds (Wang et al., 2003; Martineau et al., 2004). The absorption was studied via isotopic substitution with ^2D (i.e., deuterium, isotope of hydrogen with mass 2 amu) and determined to be a vibration involving a single hydrogen atom (Fuchs et al., 1995b). Recent investigation of the 3123.0 cm^{-1} absorption using a combination of annealing and uniaxial-stress experiments suggested that the NVH^- defect is responsible (Cruddace et al., 2007a).

The negative nitrogen-vacancy-hydrogen complex, NVH^-, was first identified in single-crystal CVD synthetic diamond using electron paramagnetic resonance (EPR) spectroscopy (Glover et al., 2003). Hydrogen is a common IR-active impurity in natural type Ia and occasionally type IIa diamonds, often showing a sharp absorption at 3107 cm^{-1}. Chrenko et al. (1967) first found this absorption, and Woods and Collins (1983) proposed that it originated from a C-H stretching vibration mode.

The variation in peak positions of hydrogen-related absorption is one of the most important spectroscopic differences between natural and CVD synthetic diamonds. Positive correlations in intensity among all these four peaks (figure 15) indicated that the other three peaks (1371.0, 1362.3, and 1352.9 cm^{-1}) could also be related to or caused by the NVH^- defect. Meanwhile, recent studies (Cruddace et al., 2007a,b) using uniaxial-stress experiments revealed different symmetries of these centers. These discrepancies are not fully understood. Based on the relationship Cruddace et al. (2007a) established, we calculated that the concentrations of NVH^- defect varied from 1.3 to 4.3 ppb in these fancy-color CVD synthetic diamonds.

Many of the peaks in the near-infrared region (8752, 7353, 6855, 6425, and 5562 cm^{-1}; figure 16) were reported in Wang et al. (2003). These peaks were present in the near-colorless and dark brown samples, but with an additional one at 7837 cm^{-1}. Interstitial hydrogen and hydrogen trapped at vacancies are potential candidates for the absorption at 7353 cm^{-1} (Goss, 2003). In the dark brown samples, these absorptions were extremely strong, which permitted accurate determination of their integrated intensities and thus allowed us to investigate their correlations. Similar positive linear correlations also occurred among six absorption peaks (8752, 7837, 7353, 6855, 6425, and 5562 cm^{-1}) in the near-infrared region (figure 17), but none of these peaks showed any observable correlation with the 3123.0 cm^{-1} absorption in intensity. All these observations indicate that the six absorption peaks in the near-IR region of the dark brown samples are very likely related to or caused by the same defect, but not the NVH^- defect.

An outstanding feature of the PL spectrum of the orange-to-pink CVD-grown diamonds is the strong H3 center (figure 20). The occurrence of H3 is reinforced by the green fluorescence (figure 9c). The H3 defect is in the neutral charge state $(N\text{-}V\text{-}N)^0$. This defect forms in nitrogen-bearing diamonds through combination of the nitrogen A aggregate and a vacancy. Formation of this defect usually involves irradiation and annealing at relatively high temperatures (e.g., Collins, 1982, 2001) or is associated with distinct plastic deformation features. While very common in irradiated/annealed type Ia diamonds, varying concentrations of the H3 defect also occur in some natural-color type Ia diamonds. The H3 defect can be a major contributor to the yellow color in some natural diamonds (King et al., 2005). In natural type IIa diamonds, though, the H3 defect is observed in extremely low concentrations or is not detectable even when very sensitive PL spectroscopy is employed. Strong H3 emissions, as observed in the PL spectra of the orange-to-pink CVD samples in this study, are extremely rare in natural type IIa diamonds, as well as in CVD synthetic diamonds of other colors. The occurrence of relatively high concentrations of the H3 defect in this specific group indicates a possible link to the production of orange-to-pink hues.

The 3H defect that was observed in most diamonds in the near-colorless group is widely believed to be introduced by radiation and has a complicated annealing behavior. Heating to 300–400°C may increase the 3H center intensity considerably depending on the concentration of nitrogen in the diamond (Zaitsev, 2001). This defect can be stable at temperature as high as 1000°C (Steeds et al., 1999). Most CVD diamond growth occurs at ≥800°C and it is more likely that the 3H center was introduced during the crystal growth process.

Twitchen et al. (2007) first reported the development of 7917 and 7804 cm^{-1} absorptions in the near-infrared region (corresponding to the 1263 and 1281 nm peaks in the reference) in CVD synthetic diamonds when annealed to 1400–1500°C at ambient pressure. In a recent uniaxial stress and annealing study, Cruddace et al. (2007c) further found that

the 7354 cm^{-1} system annealed out in the temperature range of 1300–1600°C at ambient pressure, and two lines at 7917 and 7804 cm^{-1} appeared. These two peaks, as well as many others, were observed in all the Apollo fancy orange-to-pink samples with varying intensities (figure 16).

In addition, features similar to those seen in prior research were observed in the UV-Vis-NIR absorption spectra. Weak absorption peaks at 503.3 (due to H3 defects) and 666.7 nm (figure 18) in their orange-to-pink CVD synthetic diamonds developed when brown CVD synthetic diamond was annealed (Twitchen et al., 2007). The absorption feature at approximately 624 nm disappeared when their sample was heated in the range of 1200–1400°C (Twitchen et al., 2007). In the present study, a feature at 624.5 nm was seen in the spectra of the dark brown samples (figure 19) but not in those of the orange-to-pink group. The mechanism for the occurrence of the spectroscopic features observed with IR/UV-Vis-NIR absorption and PL spectroscopy in the orange-to-pink CVD synthetic diamonds studied for the present report is not well understood, and further investigation is ongoing.

Identification Features. The progress made over the past few years toward the efficient growth of single-crystal CVD synthetic diamond has opened a range of possible industrial and jewelry applications (figure 24). Several other organizations and institutes (e.g., Element Six, Carnegie Institute, LIMHP-CNRS in France, and the National Institute for Material Sciences in Japan) have demonstrated the capability to grow single-crystal CVD diamond with products of varying sizes and quality. In addition, Apollo Diamond Inc. has begun producing and marketing CVD-grown gems to the jewelry industry.

Identification and separation of CVD synthetic diamonds from natural diamonds can be achieved through careful attention to the gemological and spectroscopic properties. While not conclusive, several gemological observations serve as good indications of CVD material: strong internal graining with an indistinct "fuzzy" appearance, high-order interference colors (figure 12a), occurrence of pinpoints and occasional clouds (figure 6), and remnant laser grooves on the girdles (figure 2b). These gemological features do, however, appear in some natural diamonds (Moses et al., 1999). Crystal inclusions are not commonly present in either CVD or natural type IIa diamonds, but when they are present, their appearance can be diagnostic of natural origin.

Early products from Apollo with varying saturations of brown color displayed a weak orange fluorescence to UV radiation that was considered a useful indication of CVD synthesis (Wang et al., 2003; Martineau et al., 2004). However, this feature is absent from most of the new products due to improvements in the growth technique and crystal quality. Most of the samples in the near-colorless and dark brown groups were inert, and only a few near-colorless samples showed very weak orange fluorescence under the UV lamp. The very weak to moderate orange fluorescence observed in the orange-to-pink samples, on the other hand, was similar to that seen in some natural pink diamonds (King et al., 2002), which also makes this property problematic as an identification criterion.

Fluorescence and phosphorescence images obtained from the DTC DiamondView continue to be very useful for identification of CVD synthetic diamonds. Orange fluorescence with irregularly patterned areas of blue fluorescence, narrow growth bands, and blue phosphorescence (figures 7–9) appear to be characteristic features of CVD-grown diamonds, if present. Most natural type IIa diamonds show relatively uniform blue fluorescence and rarely show phosphorescence in the DiamondView. Although a few natural type IIa diamonds show orange fluorescence, the co-existence of orange and irregular blue fluorescent regions has not been observed in natural stones. In addition, natural type IIa diamonds often show characteristic internal features (e.g., "mosaic" networks of polygonized dislocations) that likely would not occur in CVD synthetic diamonds. Natural diamonds with trace amounts of isolated nitrogen rarely show any pink hue, or dominant red-orange fluorescence in the DiamondView.

Spectroscopic features are very important for CVD identification. For near-colorless samples, the occurrence of weak absorptions in the near-infrared region (7353, 6855, 6425, 5562 cm^{-1}; figure 16) and/or a very weak absorption band at ~270 nm in the UV-Vis-NIR region are indicative of CVD growth. Occurrence of a 3123.0 cm^{-1} absorption in the mid-infrared region was considered to be an important feature of the early CVD synthetic diamonds (Wang et al., 2003), but this absorption was absent in all of the near-colorless group tested. Important identification features from photoluminescence spectroscopy (figures 20–23) include strong emissions from N-V centers, the 596/597 doublet, and emissions at 534.0, 543.3, 546.1, 736.6,

Figure 24. CVD lab-grown diamonds are now available in fine jewelry, such as these stackable rings set in yellow and white gold. Courtesy of Apollo Diamond Inc.

736.9, 946.1, and 951.3 nm. These luminescence features can be activated by lasers of various wavelengths. Occurrence of the 3H defect in most of the near-colorless group of CVD samples (figure 20) is not well understood, and this feature has also been reported in CVD synthetic diamonds from another producer (Wang et al., 2005).

Many of the previously listed emissions (596/597 doublet, and emissions at 534.0, 543.3, 546.1, 736.6, 736.9, 946.1, and 951.3 nm) are specific to CVD synthetic diamonds and have not been detected in natural diamonds (Martineau et al., 2004; Wang et al., 2005). However, it should be pointed out that the Si-related 737 nm emission was recently found in natural type IIa and low-nitrogen diamonds (Breeding et al., 2007). Since the Si-related 737 nm emission is extremely rare in natural diamonds, its occurrence in photoluminescence spectroscopy is still a very useful indicator of a CVD synthetic diamond.

For those CVD synthetic diamonds with orange-to-pink and dark brown colors, IR absorption spectroscopy proved more useful for identification than photoluminescence. Occurrence of a sharp 3123.0 cm^{-1} absorption (figure 14) from an H-related defect and the combination of absorptions at 1371.0, 1362.3, 1352.9, and 1344.5 (due to isolated nitrogen) are specific to these fancy-color CVD synthetic diamonds (figure 13). Very strong absorptions at 8752, 7837, 7353, 6855, 6425, and 5562 cm^{-1} in dark brown samples and numerous (7917, 7804, 7533, 7353, 6963, 6828, 6425, 6064, 5219, 4888, 4672, and 4337 cm^{-1}) sharp absorption peaks in the near-infrared region of orange-to-pink samples (figure 16) are characteristic identification features for these two groups. The ~520 nm broad absorption band in UV-Vis-NIR spectra (figures 18 and 19) is slightly lower in position than the 550 nm band in natural diamonds. The well-known 596/597 photoluminescence doublet emissions were entirely absent in the orange-to-pink CVD synthetic diamonds, and the Si-related 737 nm emission occurred in few of the fancy-color CVD-grown diamonds.

The identification of CVD synthetic diamonds from natural stones may be achieved based on a combination of various gemological and spectroscopic features. There is no single feature that will ensure proper identification of all CVD synthetic diamonds, and testing in a properly equipped gemological laboratory is needed to guarantee confident identification.

CONCLUSIONS

Compared to earlier-generation products, the CVD synthetic diamonds submitted by Apollo Diamond Inc. as representative of their 2006–2007 production showed significant improvements in color and clarity. Relatively larger, well-proportioned, faceted CVD products have also become more common. Colorless, near-colorless, and attractive fancy-color material is now being produced. The new products are comparable in quality to many natural diamonds in the marketplace. The gem sizes (0.14–0.71 ct) reflect the highest-volume segment of the natural diamond market. These CVD synthetic diamonds exhibited unusual internal graining, high birefringence, complex fluorescence zoning, and several distinct spectroscopic features. All of these CVD synthetic diamonds can be identified, but a combination of various gemological and, especially, spectroscopic features is required to do so consistently and accurately. We anticipate that CVD diamond growth techniques will continue to improve and CVD products with even better quality will eventually be introduced to the gem market.

ABOUT THE AUTHORS
Dr. Wang (wuyi.wang@gia.edu) is manager of research projects, Mr. Hall is manager of identification services, Mr. Moe is research technician, and Mr. Moses is senior vice president, at the GIA Laboratory, New York. Mr. Tower is senior scientist at Apollo Diamond Inc., Boston, Massachusetts.

ACKNOWLEDGMENTS
The authors thank Ivana Balov, Thomas Gelb, Joshua Cohn, Paul Johnson, Dino DeGhionno, Shane McClure, Dr. James Shigley, Dr. Andy H. Shen, and Dr. Christopher M. Breeding of the GIA Laboratory for their many suggestions and assistance in this study. Dr. Robert Linares, Patrick Doering, and their team at Apollo Diamond are specially thanked for their continued cooperation with GIA and for their efforts to cooperate with the jewelry industry to develop a better understanding of CVD diamond growth technology. Constructive reviews by Dr. John Angus, Dr. James Butler, Dr. Philip Martineau, and Dr. Christopher Welbourn helped improve this article substantially.

REFERENCES

Achard J., Tallaire A., Sussmann R., Silva F., Gicquel A. (2005) The control of growth parameters in the synthesis of high-quality single crystalline diamond by CVD. *Journal of Crystal Growth*, Vol. 284, No. 3/4, pp. 396–405.

Badzian A., Badzian T. (1993) Diamond homoepitaxy by chemical vapor deposition. *Diamond and Related Materials*, Vol. 2, No. 2/4, pp. 147–157.

Breeding C.M., Wang W. (2007) Occurrence of the Si-V (737 nm) center in a natural type IIa colorless gem diamond. *Abstract of 18th European Conference on Diamond, Diamond-like Materials, Carbon Nanotubes, and Nitride.* Berlin, Germany, September 9–14 , p. P1.04.04.

Chrenko R.M., McDonald R.S., Darrow K.A. (1967) Infrared spectra of diamond coat. *Nature*, Vol. 213, No. 5075, pp. 474–476.

Clark C.D., Kanda H., Kiflawi I., Sittas G. (1995) Silicon defects in diamond. *Physical Review B*, Vol. 51, No. 23, pp. 16681–16688.

Collins A.T. (1982) Colour centers in diamond. *Journal of Gemmology*, Vol. 18, No. 1, pp. 35–75.

Collins A.T. (2001) Colour of diamond and how it may be changed. *Journal of Gemmology*, Vol. 27, No. 6, pp. 341–359.

Cruddace R.C., Newton M.E., Smith H.E., Davies G., Martineau P.M., Twitchen D.J. (2007a) Identification of the 3123 cm^{-1} absorption line in SC-CVD diamond as the NVH^- defect. *Proceedings of the 58th De Beers Diamond Conference*, Coventry, England, pp. 15.1–15.3.

Cruddace R.C., Newton M.E., Smith H.E., Davies G., Fisher D., Martineau P.M., Twitchen D.J. (2007b) Uniaxial stress and annealing measurements on C-H bands in diamond. *Proceedings of the 58th De Beers Diamond Conference*, Coventry, England, pp. P19.1–P19.3.

Cruddace R.C., Newton M.E., Davies G., Martineau P.M., Twitchen D.J. (2007c) Uniaxial stress and annealing studies of the NIR 913 meV system in SC-CVD diamond. *Proceedings of the 58th De Beers Diamond Conference*, Coventry, England, pp. P20.1–P20.2.

Doering P.J., Linares R.C. (1999) Large area single crystal CVD diamond: Properties and applications. *Proceedings of Applied Diamond Conference / Frontier Carbon Technology Joint Conference 1999*, Tsukuba, Japan, pp. 32–35.

Fuchs F., Wild C., Schwarz K., Muller-Sebert W., Koidl P. (1995a) Hydrogen induced vibrational and electronic transitions in chemical vapor deposited diamond, identified by isotopic substitution. *Applied Physics Letters*, Vol. 66, No. 2, pp. 177–179.

Fuchs F., Wild C., Schwarz K., Koidl P. (1995b) Hydrogen-related IR absorption in chemical vapour deposited diamond. *Diamond and Related Materials*, Vol. 4, No. 5/6, pp. 652–656.

Goss J.P. (2003) Theory of hydrogen in diamond. *Journal of Physics: Condensed Matter*, Vol. 15, No. 17, pp. R551–R580.

Glover C., Newton M.E., Martineau P.M., Twitchen D.J., Baker L.M. (2003) Hydrogen incorporation in diamond: The nitrogen-vacancy-hydrogen complex. *Physical Review Letters*, Vol. 90, No. 18, pp. 185507–185510.

Goodwin D.G., Butler J.E. (1997) Theory of diamond chemical vapor deposition. In M.A. Prelas, G. Popovici, and L.K. Bigelow, Eds., *Handbook of Industrial Diamonds and Diamond Films*, Marcel Dekker, New York, pp. 527–581.

Hounsome L.S., Jones R., Martineau P.M., Shaw M.J., Briddon P.R., Öberg S., Blumenau A.T., Fujita N. (2005) Optical properties of vacancy related defects in diamond. *Physica Status Solidi (a)*, Vol. 202, No. 11, pp. 2182–2187.

Iakoubovskii K., Adriaenssens G.J., Dogadkin N.N., Shiryaev A.A. (2001) Optical characterization of some irradiation-induced centers in diamond. *Diamond and Related Materials*, Vol. 10, No. 1, pp. 18–26.

King J.M., Moses T.M., Shigley J.E., Liu Y. (1994) Color grading of colored diamonds at the GIA Gem Trade Laboratory. *Gems & Gemology*, Vol. 30, No. 4, pp. 220–242.

King J.M., Shigley J.E., Guhin S.S., Gelb T.H., Hall M. (2002) Characterization and grading of natural-color pink diamonds. *Gems & Gemology*, Vol. 38, No. 2, pp. 128–147.

King J.M., Shigley J.E., Gelb T.H., Guhin S.S., Hall M., Wang W. (2005) Characterization and grading of natural-color yellow diamonds. *Gems & Gemology*, Vol. 41, No. 2, pp. 88–115.

Linares R.C., Doering P.J. (1999) Properties of large single crystal diamond. *Diamond and Related Materials*, Vol. 8, No. 2/5, pp. 909–915.

Linares R.C., Doering P.J. (2003) *System and method for producing synthetic diamond.* US Patent 6,582,513.

Martineau P.M., Lawson S.C., Taylor A.J., Quinn S.J., Evans D.J.F., Crowder M.J. (2004) Identification of synthetic diamond grown using chemical vapor deposition (CVD). *Gems & Gemology*, Vol. 40, No. 1, pp. 2–25.

Miyatake H., Arima K., Maida O., Teraji T., Ito Y. (2007) Further improvement in high crystalline quality of homoepitaxial CVD diamond. *Diamond and Related Materials*, Vol. 16, No. 4/7, pp. 679–684.

Moses T.M., Shigley J.E., McClure S.F., Koivula J.I., Van Daele M. (1999) Observations on GE-processed diamonds: A photographic record. *Gems & Gemology*, Vol. 35, No. 3, pp. 14–22.

Moses T.M., Johnson M.L., Green B., Blodgett T., Cino K., Geurts R.H., Gilbertson A.M., Hemphill T.S., King J.M., Komylak L., Reinitz I.M., Shigley J.E. (2004) A foundation for grading the overall cut quality of round brilliant cut diamonds. *Gems & Gemology*, Vol. 40, No. 3, pp. 202–228.

Steeds J.W., Davis T.J., Charles S.J., Hayes J.M., Butler J.E. (1999) 3H luminescence in electron-radiated diamond samples and its relationship to self-interstitials. *Diamond and Related Materials*, Vol. 8, No. 10, pp. 1847–1852.

Tallaire A., Achard J., Sussmann R.S., Silva F., Gicquel A. (2005) Homoepitaxial deposition of high-quality thick diamond films: Effect of growth parameters. *Diamond and Related Materials*, Vol. 14, No. 3/7, pp. 249–254.

Twitchen D.J., Martineau P.M., Scarsbrook G.A., Dorn S.C., Cooper M.A. (2004) *Coloured diamond.* Patent publication number US2004194690.

Twitchen D.J., Martineau P.M., Scarsbrook G.A. (2007) *Coloured diamond.* Patent publication number US2007079752.

Vavilov V.S., Gippius A.A., Zaitsev A.M., Deryagin B.V., Spitsyn B.V., Aleksenko A.E. (1980) Investigation of the cathodoluminescence of epitaxial diamond films. *Soviet Physics-Semiconductors*, Vol. 14, pp. 1078–1079.

Wang W., Moses T., Linares R., Shigley J.E., Hall M., Butler J.E. (2003) Gem-quality synthetic diamonds grown by the chemical vapor deposition method. *Gems & Gemology*, Vol. 39, No. 4, pp. 268–283.

Wang W., Tallarie A., Hall M.S., Moses T.M., Achard J., Sussmann R.S., Gicquel A. (2005) Experimental CVD synthetic diamonds from LIMHP-CNRS, France. *Gems & Gemology*, Vol. 41, No. 3, pp. 234–244.

Welbourn C.M., Cooper M., Spear P.M. (1996) De Beers natural versus synthetic diamond verification instruments. *Gems & Gemology*, Vol. 32, No. 3, pp. 156–169.

Woods G.S., Collins A.T. (1983) Infrared absorption spectra of hydrogen complexes in type I diamonds. *Journal of Physics and Chemistry of Solids*, Vol. 44, No. 5, pp. 471–475.

Yan C.-S., Mao H.-K., Li W., Qian J., Zhao Y.S., Hemley R.J. (2004) Ultrahard diamond single crystals from chemical vapor deposition. *Physica Status Solidi, Rapid Research Note*, Vol. 201, No. 4, pp. R25–R27.

Zaitsev A.M. (2001) *Optical Properties of Diamond*. Springer-Verlag, Berlin, 502 pp.

YELLOW MN-RICH TOURMALINE FROM THE CANARY MINING AREA, ZAMBIA

Brendan M. Laurs, William B. (Skip) Simmons, George R. Rossman, Eric A. Fritz,
John I. Koivula, Björn Anckar, and Alexander U. Falster

The most important source of yellow gem elbaite is the Canary mining area in the Lundazi District of eastern Zambia. The tourmaline has been mined since 1983 from both pegmatite and eluvial/alluvial deposits, in colors typically ranging from yellow-green to yellow to orange and brown; much of the orange-to-brown material is heated to attain a "golden" or "canary" yellow color. The tourmaline is Mn-rich (up to 9.18 wt.% MnO documented in the literature) and contains traces of Ti and little or no Fe. The distinctive composition of this tourmaline is probably the result of the crystallization of abundant schorl from an unusual B-rich, Li-poor pegmatite magma, which depleted Fe while conserving Mn until the late-stage crystallization of gem pockets.

Since the early 1980s, gem-quality yellow elbaite has been intermittently mined from a small area in eastern Zambia. Marketed as Canary tourmaline since 2001, this material is notable for its vivid yellow color and high Mn content—among the highest ever recorded in any tourmaline (e.g., Shigley et al., 1986). Starting in 2002, organized purchasing and mining initiatives brought greater quantities of this elusive tourmaline to the market, particularly in Japan, where it has gained popularity and commanded high prices (Federman, 2002; "Supplier to vertically integrate…," 2004). Although most of the cut tourmaline available is in melee sizes (<0.20 ct), exceptional faceted stones up to 50 ct have been cut (figure 1).

Due to its unusual color and composition, this tourmaline attracted considerable attention in the mineralogical literature when it first entered the marketplace (see Nuber and Schmetzer, 1984; Schmetzer and Bank, 1984a; Rossman and Mattson, 1986; Shigley et al., 1986). While some of these articles did not specify the locality within Zambia, others stated "near Chipada," which refers to the largest town (Chipata) in eastern Zambia, located near the border with Malawi. However, there are no gem-bearing pegmatites in the Chipata area, and the actual locality is the Lundazi District, located ~160 km to the north (as indicated by Rossman and Mattson, 1986). Since the location was kept secret for many years, some more recent reports have named the source locality as Mozambique (Wong, 2001) or Malawi (e.g., Boehm, 2001; Federman, 2002). The enriched manganese content of this Zambian elbaite has led some authors to refer to it as *tsilaisite* (Schmetzer and Bank, 1983, 1984b; Kane, 1986).[a]

While in Zambia in August 2004, three of the authors (BML, WBS, and BA) visited the most important deposit for yellow elbaite, known as the Canary mining area, to gather information on the geology and production of this unusual material, and to obtain samples for gemological characterization and chemical analysis. Two days were spent at

See end of article for About the Authors and Acknowledgments.
GEMS & GEMOLOGY, Vol. 43, No. 4, pp. 314–331.

Figure 1. Commercial quantities of Mn-rich "canary" yellow elbaite come from just one deposit, the Canary mining area in eastern Zambia. Although the material is typically cut in melee sizes, this exceptional stone weighs 50.26 ct. Courtesy of Shire Trading Ltd.; photo © Harold & Erica Van Pelt.

the deposit with Tommy Wu (Shire Trading Ltd., Hong Kong), who was leasing the mine in partnership with a Zambian company. Since then, Mr. Wu has updated information on the mining and production, and supplied additional samples for our research.

LOCATION AND ACCESS

The Canary mining area is located at coordinates 12°23.764′ S, 32°53.471′ E, and ~1,440 m elevation. This position lies 32 km west-southwest of Lundazi (figure 2 inset), from which the deposit can be reached in about one hour by car on moderately well-maintained dirt roads. Two small villages are located near the mining area: Muchapansala and Chanyalubwe. The mining camp (figure 3) is powered by a generator and obtains drinking water from a well. The deposit can be worked roughly 10 months of the year, excluding the rainy season from late December to early February. In the past, the deposit also has been referred to as the Kaombeka or Doost-Chiwele mine (Njamu, 2003).

HISTORY AND PRODUCTION

Initial gem discoveries in the Lundazi District probably occurred in the late 1970s through activities of local villagers (Patney and Tether, 1988). The Canary mining area was originally worked for electronic-grade quartz (ca. 1982), and the brown tourmaline was tossed into the mine dumps (Njamu, 2003). Yellow tourmaline from eastern Zambia was first documented by Schmetzer and Bank (1983). It is likely that the material came from the Canary mining area (known as Kaombeka at the time), which is the most important source of this tourmaline in the area. A survey of the literature revealed only one other yellow tourmaline–producing site in the Lundazi District, which was mapped by O'Connor (1998) as the Chamunjili mine, located 18 km northeast of the Canary mining area. To the authors' knowledge, this locality has not been active for several years.

The first organized search for tourmaline in the Canary mining area occurred in 1987 (when it was still known as Kaombeka). At that time, the main pegmatite was worked by the Small Mines Unit of Zambian Consolidated Copper Mines (ZCCM). Although Zgambo (1995) reported that ZCCM removed 540 m^3 of material from two pits, yielding 242 kg of gem rough, the total production of tour-

[a] *Tsilaisite* is the name proposed by Kunitz (1929) for a hypothetical Mn-rich tourmaline end member, after the first locality where high-Mn tourmaline was documented (Tsilaisina, Madagascar). The term appeared in a list of new mineral names published by Dunn et al. (1985), although it had not been approved by the Commission on New Minerals and Mineral Names of the International Mineralogical Association. Tsilaisite was recently included in a list of discredited minerals (Burke, 2006), because no samples have been documented with sufficient Mn to attain the end-member composition. Therefore, we have placed the term in quotes when referring to the Mn-rich end-member composition in this article.

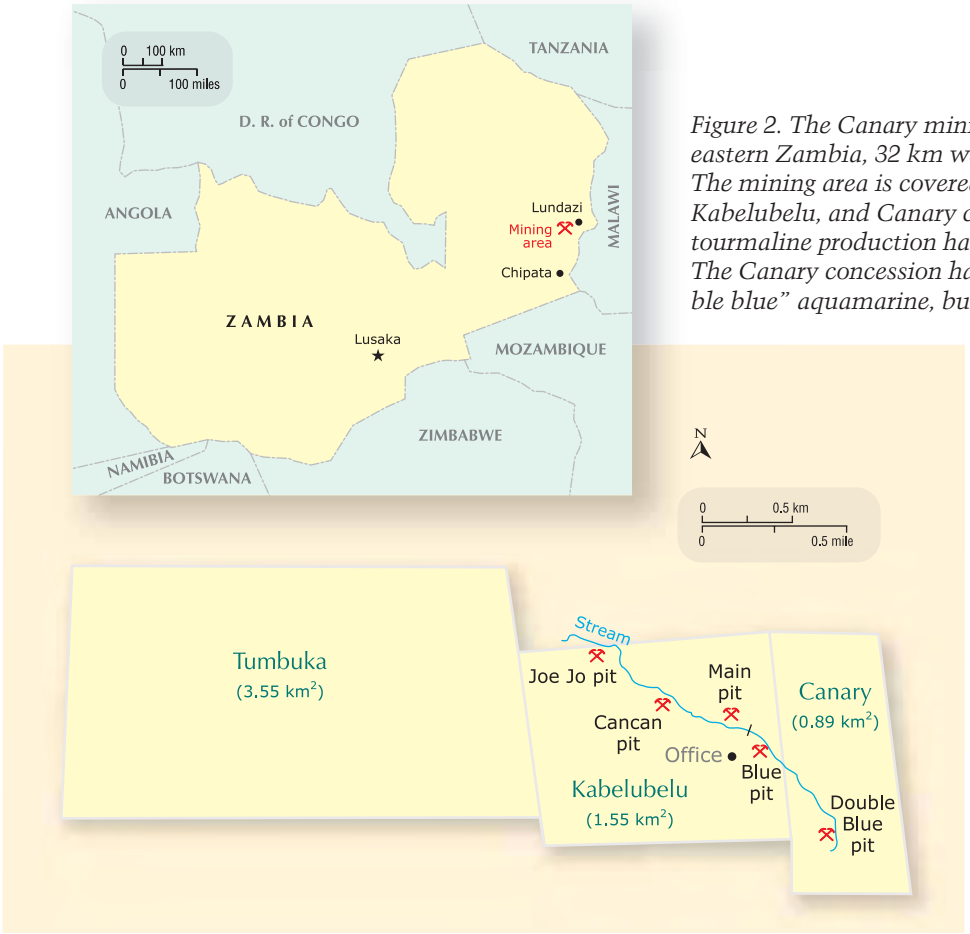

Figure 2. The Canary mining area is located in eastern Zambia, 32 km west-southwest of Lundazi. The mining area is covered by the Tumbuka, Kabelubelu, and Canary concessions. Most Canary tourmaline production has come from Kabelubelu. The Canary concession has been a source of "double blue" aquamarine, but not tourmaline.

maline (of all qualities) obtained by ZCCM was probably several tonnes (T. Wu, pers. comm., 2004). The largest single gem pocket was reportedly discovered in the mid-1990s by a subsequent owner; it produced approximately 3 tonnes of tourmaline, of which 0.5 tonne was of good gem quality (T. Wu, pers. comm., 2004). This pocket was found at a depth of about 4 m, and two smaller cavities—which yielded up to 100 kg of tourmaline—were encountered at approximately the same depth as mining proceeded to the east. As of November 1997, the deposit lay idle and the pit was filled with water (O'Connor, 1998).

In 2001, Mr. Wu together with Rita and Arun Mittal entered a purchasing agreement with as many as 60 local miners working the eluvial and alluvial deposits. They began creating a market for yellow tourmaline in Japan (and, to a lesser extent, in the U.S. and Europe) with gems cut from 3–4 kg of good-quality rough material. In late 2002, Mr. Wu and the Mittals formed a partnership to lease the area under the name Canary Mining Ltd. By the end of 2002, Canary Mining had amassed ~800 kg of rough tourmaline. Most of this would cut small stones of 3 mm or less, but a few large gems (e.g., 30, 14, and 11 ct) also were faceted.

In February 2003, Canary Mining began working secondary deposits near the original pegmatite, with modest results over the next five months. From December 2003 to August 2004, they used an excavator to explore primary deposits on the property (figure 4). However, they did not recover any tourmaline from the new areas tested, and the main pit appeared to be exhausted. Subsequent work has focused on intermittently mining the secondary deposits, typically producing 30–40 kg per month (or ~2 kg of tourmaline per day, consisting of 500–800 g of good gem rough). The 50 ct tourmaline in figure 1 was cut from this material (T. Wu, pers. comm., 2006).

In July 2007, Canary Mining Ltd. was acquired by Canary Gemstone International DMCC, a holding company formed in Dubai, with Mr. Wu and Mrs. Mittal as major shareholders. The influx of capital obtained through this venture will allow for the expansion of mining activities in 2008.

Figure 3. The mining camp for Canary tourmaline, shown here in the dry season (August), is located in a remote part of the Lundazi District. Photo by W. B. Simmons.

GEOLOGY

Pegmatites in the Lundazi area are known for producing mica and gem-quality aquamarine, spessartine, tourmaline (green, pink, or yellow), and rose quartz. These pegmatites and their gems have been described by Thomas (1982), Patney and Tether (1988), Zgambo (1995), Johnson et al. (1997), Milisenda et al. (2000), and Njamu (2003). Patney and Tether (1988) defined two belts of gem-bearing pegmatites in the Lundazi District, and indicated that they are broadly synchronous with the late Pan-African Sinda Batholith (~489 million years old [Ma]). Snelling et al. (1972) dated an undeformed pegmatite near Lundazi at 485 Ma.

The Canary mining area is underlain by Precambrian metamorphic rocks of the Irumide Foldbelt (e.g., Johns et al., 1989). O'Connor (1998) mapped the deposit within leucocratic gneiss (containing biotite, garnet, and sillimanite) of the Lumezi Gneiss Group. Deep soils cover the area, and the best exposures of the basement rocks are found in some mining pits and along the stream that crosses the mining claims.

The main pegmatite in the Canary mining area

Figure 4. Canary Mining Ltd. used a large excavator to explore primary deposits from December 2003 to August 2004. The main pegmatite is being mined down-dip from the area that produced large amounts of tourmaline in the mid-1990s; Asok Napa (in the foreground) was the mine's general manager during that time. Photo by Tommy Wu.

Figure 5. The contact between the footwall of the main pegmatite and the weathered host rock is marked by the sharp boundary to the right of the hammer (see yellow line). The hammer is sitting on the medium-grained border zone, which is separated from the coarse-grained feldspar-rich intermediate zone by a vein of black tourmaline + K-feldspar. Photo by B. M. Laurs.

is a lens-shaped body that discordantly intrudes biotite gneiss; it strikes east-west (~100°) and dips moderately south. At the time of the authors' 2004 visit, a large open pit (~16 m deep) partially filled with water marked the site where most of the pegmatite had been removed. Based on the extent of the workings, the pegmatite is believed to have been at least 60 m long and perhaps 18 m at its widest point (Njamu, 2003). Exposures of the footwall showed a medium-grained border zone (~15 cm wide) and in places a discontinuous aplitic zone that abruptly transitioned into a coarse-grained intermediate zone consisting mainly of K-feldspar and subordinate sodic plagioclase (figure 5). The hydrothermal leaching of quartz had resulted in vugs that contained euhedral overgrowths of albite and black tourmaline needles. We also observed conspicuous veins (up to 10 cm thick) of black tourmaline ± K-feldspar + albite cross-cutting the pegmatite. The host gneiss adjacent to the pegmatite was locally biotized and tourmalinized near the contact, but the minimal alteration overall indicated that the pegmatite had little interaction with the wallrock.

The large cavity found in the mid-1990s was in the central-northwestern part of the pit, in or near the core of the pegmatite. This pocket also contained abundant quartz crystals and "cleavelandite" feldspar. Although remains of these minerals were found on the mine dump, there was no evidence of any micas, such as the lepidolite that is commonly associated with gem tourmaline in granitic pegmatites.

The Canary deposit is distinctly different from other gem-bearing pegmatites in the area in that it lacks micas and is not a source of aquamarine. Zgambo (1995) indicated that rose quartz, mica, beryl, and gem-quality pink tourmaline were encountered during mining in 1987, but no evidence of these minerals was seen during our visit. There was also no evidence of the allanite, magnetite, and blue/pink/green tourmaline that were reported by Njamu (2003). One of the present authors (BA) noted some spessartine in the mine dumps in 2003, but no garnet was seen in the pegmatite itself.

A reconnaissance survey of past workings in the surrounding area during the authors' visit revealed two additional pegmatites with similar mineralogy, but they were much smaller than the main pegmatite and reportedly did not yield any gem tourmaline *in situ* (T. Wu, pers. comm., 2004). In addition, pegmatites with a distinctively different mineralogy were seen in the area. These quartz-rich pegmatites contained biotite (in sparse amounts, and typically no schorl) as the mafic mineral, and formed segregations in a granitoid rock or cross-cutting dikes in biotite gneiss. They were mined for dark blue (or "double blue") aquamarine (Laurs, 2004), which is frozen within the pegmatites rather than forming in cavities; therefore, the beryl rarely yields cut stones larger than 0.5 ct. Ductile deformation (the presence of bent and deformed crystals) of the beryl-bearing pegmatites indicated that they are older than the undeformed feldspar- and black tourmaline–rich type of pegmatite that contains Canary tourmaline. In places the deformed pegmatites underlie the eluvial deposits mined for tourmaline,


Figure 6. Secondary deposits downslope from the main Canary pegmatite are typically mined to a depth of 1–1.5 m (left). The miners recovered the gem rough by wet-screening the excavated material using water from a flooded mining pit (right). Photos by B. Anckar, June 2003.

which has created confusion about the original source of this gem material. O'Connor (1998) also documented at least two phases of pegmatites in this part of the Lundazi District, and indicated that the magnetic signature of the area suggests it may be underlain by a large granitic body.

According to Mr. Wu, other pegmatites located within a few kilometers of the Canary mining area have produced spessartine and chrysoberyl.

MINING AND PROCESSING

The Canary mining area consists of three mining concessions, covering a total of 600 ha (6 km^2). From west to east, these are the Tumbuka, Kabelubelu, and Canary licenses (again, see figure 2). During the authors' visit in 2004, 13 workings were seen, most of which were located on the Kabelubelu concession. These ranged from large open pits to small exploration trenches, in both primary and secondary (alluvial and eluvial) deposits.

Most of the Canary tourmaline produced since 2000 has come from the Kabelubelu concession, from secondary deposits located downslope of the main pegmatite. Mining was done by hand (figure 6, left) or with a small excavator to a depth of ~1–1.5 m (exceptionally, down to 5 m). The most favorable soil horizon for tourmaline was marked by a concentration of quartz fragments or pebbles. Miners wet-screened the material using 4 × 4 mm mesh (figure 6, right) or processed it through a simple washing plant (figure 7) consisting of a cement mixer, vibrating screens with mesh from 5 cm to 1 cm, and a sorting table (Njamu, 2003). Using water from a seasonal stream that flows through the mining area, the washing plant can process about 10–12 tonnes of material per day.

Mining of the primary deposits (for both tourmaline and aquamarine) was done using a large excavator (again, see figure 4), a pneumatic hammer, and by hand with picks, shovels, pry bars, hammers, and chisels. To avoid breaking the gem material, Canary

Figure 7. The washing plant that is also used to process material from the secondary deposits consists of a cement mixer followed by a series of vibrating screens. The water tank is filled from a small reservoir made in a seasonal stream that flows through the mining area. Photo by B. M. Laurs.

Figure 8. The yellow tourmaline in this slab (2.2 cm wide) is cut by veins and masses of black and brown tourmaline and brownish pink K-feldspar. A brecciated texture resulted from the late-stage influx of the tourmaline + K-feldspar. Photo by W. B. Simmons.

Mining Ltd. has limited the use of explosives. Since 2003, the mine has employed up to 20 workers from local villages, who are paid a salary and provided three meals a day (T. Wu, pers. comm., 2004).

The rough is sorted in Lusaka, and the material suitable for faceting (about 5–10% of the production) is cut in Bangkok. As mined, the tourmaline ranges from yellowish green to yellow, orange, and brown. Large pieces (up to 40 kg) have been recovered, but these typically consist of a brecciated assemblage of yellow to brownish yellow tourmaline that has been fractured and intruded by black/brown tourmaline ± K-feldspar (figure 8), requiring extensive processing to obtain small pieces of gem rough. However, some high-quality transparent yellow areas have been found within such material (figure 9). The veinlets of black tourmaline may show a scalloped texture along their planes of contact with the yellow tourmaline (figure 10), which suggests that the fractures were etched by hydrothermal fluids before being intruded by the schorl.

About 30% of the tourmaline is vivid yellow as mined. After being pre-formed, most of the other colors are heat treated to 500°C (and again to 550°C, as needed) in air to reduce the brown/orange component (see figure 19 of Kane, 1986). Heating does not always completely remove the brown hue (even after the second treatment), and it has no effect on the green component (T. Wu., pers. comm., 2006). The resulting hues range from bright yellow to brownish yellow to yellowish green (figures 11 and 12). Preliminary experiments at higher temperatures have succeeded in creating a pinkish red color from brownish yellow material (see box A).

According to Mr. Wu, most of the Canary tourmaline is faceted as calibrated stones in a variety of common shapes, in sizes ranging from 2 mm to 10 × 8 mm. About 5% of the production consists of larger stones that are faceted in free sizes, typically around 1 ct, with a very few stones in the 1–5 ct range. Briolettes have been cut from material containing minute fluid inclusions (figure 13). As of November 2007, enough rough material had been stockpiled to produce an estimated 20,000 carats of small (2–3 mm) cut stones.

Figure 9. These two views show a sample (6.5 cm in maximum dimension) containing a central core of gem-quality yellow tourmaline that is surrounded and partially cross-cut by black tourmaline (schorl). Courtesy of Shire Trading Ltd.; photos by Robert Weldon.

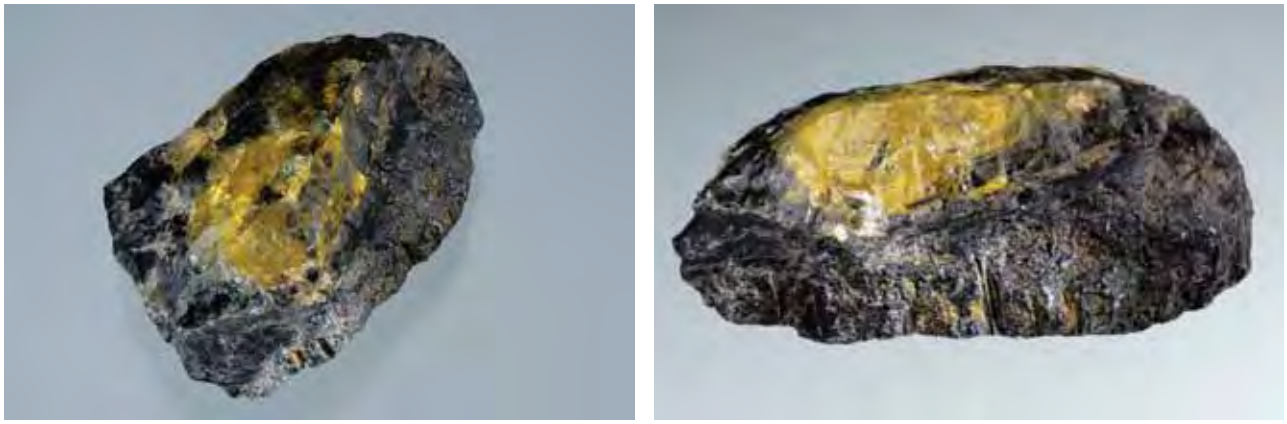

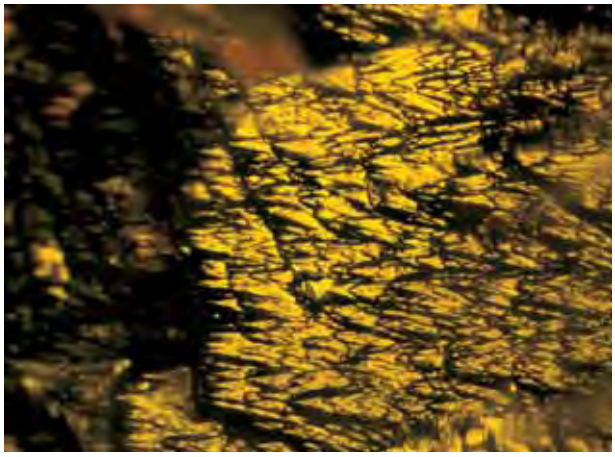

Figure 10. A distinctive scalloped pattern is visible at the interface between a cross-cutting veinlet of schorl and the surrounding tourmaline. Photomicrograph by J. I. Koivula; field of view is 2.5 mm.

Figure 11. These unusually large (7.32–12.60 ct) heated Canary tourmalines show the yellow to "golden" yellow color range that is typical of this material. Courtesy of Shire Trading Ltd.; photo by C. D. Mengason.

Canary tourmaline publicly debuted in the gem trade at the International Jewellery Tokyo show in January 2001 ("Capturing the Canary…," 2003). Until the middle of this decade, most of the production was sold in Japan, but then demand shifted toward manufacturers in Thailand and Hong Kong that produce mass-market jewelry for U.S. customers ("Substantial increase in sales…," 2005).

In addition to the yellow elbaite, black tourmaline from the Canary mining area has been polished into beads and cabochons for the Japanese market. This schorl also has been powdered for use in the cosmetics industry in Japan.

MATERIALS AND METHODS

Thirty-one Canary tourmalines were gemologically characterized at GIA: five unheated cabochons (5.38–18.02 ct) and 26 heat-treated faceted stones (0.38–2.16 ct). We measured refractive indices with a Duplex II refractometer. Specific gravity was calculated by the hydrostatic method with a Mettler CM1200 electronic balance. Fluorescence to UV radiation was documented in a darkened room using a standard 4-watt long-wave (365 nm) and short-wave (254 nm) UV lamp. We also examined the samples with a Chelsea filter and a desk-model spectroscope. Internal features were observed using a standard binocular gemological microscope.

The chemical composition of 21 grain mounts of unheated yellow-to-orange-to-brown and yellow-green tourmaline (from one to six analyses per sample) was measured by electron microprobe at the

Figure 12. These unheated cabochons (10.45–18.02 ct) and heated cut stones (1.92 and 2.16 ct; GIA Collection nos. 37339 and 37340) have a distinctive yellowish green color that is less common in Canary tourmaline than the yellow to "golden" yellow. All of these samples were gemologically characterized for this report. Courtesy/gift of Shire Trading Ltd.; photo by Robert Weldon.

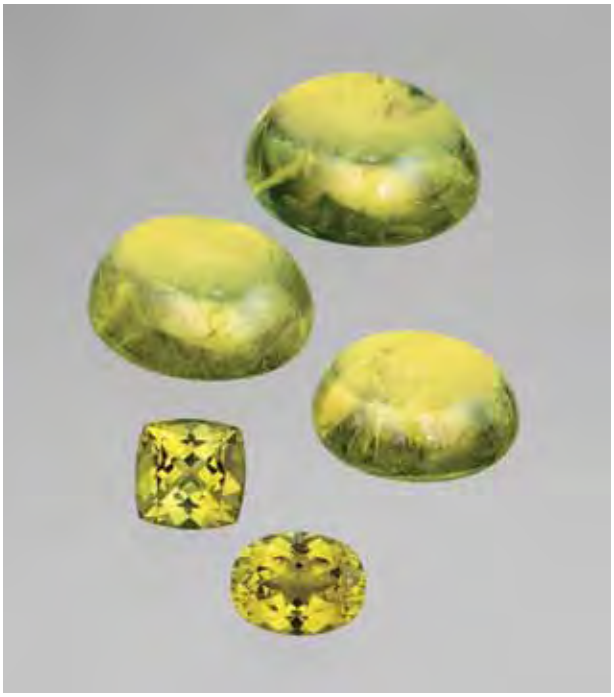

BOX A: PRELIMINARY STUDY OF HIGHER-TEMPERATURE HEAT TREATMENT OF CANARY TOURMALINE

Andreas Ertl (andreas.ertl@A1.net)
Institut für Mineralogie und Kristallographie, Universität Wien, Austria
George R. Rossman

Most Canary tourmaline is heat treated to 500–550°C to reduce the brown/orange component and produce the characteristic bright yellow coloration. Pieczka and Kraczka (2004) pointed out that heating of Mn^{2+}-bearing tourmalines above ~550°C initiates oxidation. Therefore, the yellow coloration would be expected to change to pink-red when Mn^{2+} is oxidized to Mn^{3+}. To investigate the effect of treating Canary tourmaline at higher temperatures, a faceted brownish yellow sample was heated to 700°C for 20 hours in air, using a Nabertherm furnace. The sample had been previously heated to 500–550°C to bring out the yellow color (figure A-1). This elbaite was Mn-rich (~6.5 wt.% MnO) and poor in Fe, Ti, Mg, Cr, and V, which were below the detection limits of X-ray energy-dispersive spectral (EDS) analysis. (However, the instrument used, a JEOL-EDAX analytic system, had relatively high detection limits for iron and titanium, at ~0.3 wt.% FeO and TiO_2.) A slow heating/cooling rate was employed (50°C/hour) to reduce the possibility of fracturing.

After heating, the brownish yellow sample was brownish red (figure A-1), as expected for the oxidation of Mn^{2+} to Mn^{3+} (the visible-NIR absorption spectrum [figure A-2] showed a broad band near 532 nm, which is due to Mn^{3+}). The brown component of the red color probably resulted from traces of Fe in the sample (below the detection limit of the EDS analysis), as indicated by weak Fe bands in the absorption spectrum. Therefore, the heat treatment of very-low iron material would be expected to yield a purer pink-red coloration.

In addition, two slabs of yellow-green tourmaline that were heated for seven days at 700°C or for five days at 750°C also showed distinct changes. These slabs turned nearly opaque, but were dark orangy red when viewed through very thin edges. Both of those samples experienced a total loss of hydroxide, as observed in their Raman spectra.

After heating, we observed pervasive tiny cracks in all samples, which most likely were caused by the release of water during the oxidation process. It is possible that such cracking could be minimized by heating the tourmaline to lower temperatures (>600°C but <700°C) and/or a shorter time, but additional experiments would be needed to test this.

Gamma-irradiation experiments on brownish yellow Zambian Mn-bearing elbaite by Reinitz and Rossman (1988) also generated a pink-red color. In their sample, they documented a decrease in the intensity of the Mn^{2+} absorption bands and a corresponding increase in the Mn^{3+} band. This irradiation mechanism does not remove hydroxide from the crystal and is a fundamentally different way of generating Mn^{3+} than the high-temperature oxidation.

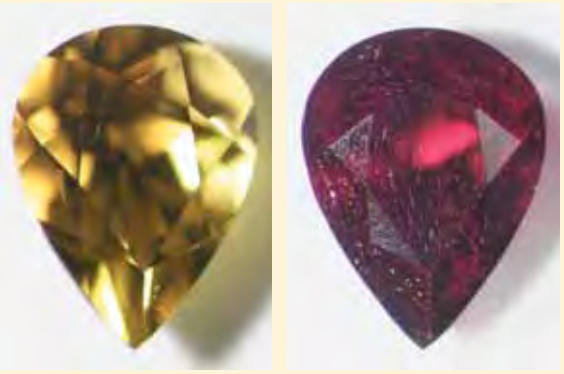

Figure A-1. This 0.18 ct Mn-rich tourmaline from the Canary mining area turned brownish yellow after conventional heating to 550°C (left) and brownish red after higher-temperature treatment to 700°C (right). Photos by A. Wagner.

Figure A-2. The visible-NIR absorption spectrum of the heated brownish red tourmaline in figure A-1 shows features related to Mn^{3+}, Fe^{2+}, and OH.

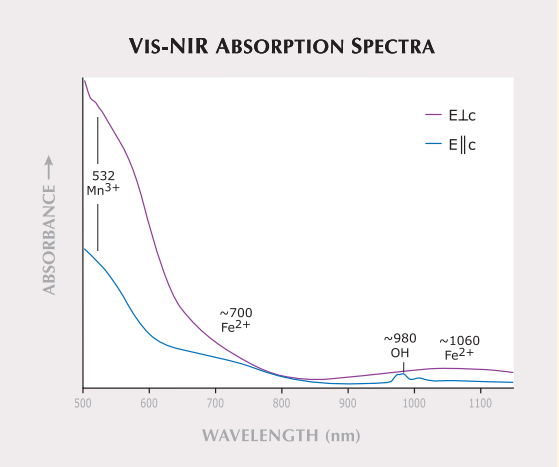

University of New Orleans. Also analyzed were eight of the faceted stones that were gemologically characterized for this study: four yellow to orangy yellow and four yellowish green. Data were collected using an ARL-SEMQ electron microprobe with 15 kV (for sodium) and 25 kV accelerating voltages, 15 nA beam current, and 3 μm beam diameter. The measurements were calibrated with natural mineral and synthetic compound standards, and a ZAF correction procedure was applied to the data.

To investigate the origin of color before and after heating, we first oriented a brownish orange sample using the optical interference pattern and then sliced and polished it so that the c-axis lay in the plane of the slices. We prepared one slice for spectra in the visible and near-infrared region (2.59 mm thick; 350–1100 nm) and another for spectroscopy in the UV–near Vis region (0.59 mm thick; 250–450 nm). We retained a portion of each slice in its unheated state and then heated the remaining portions (packed in sand) at a rate of 10°C/minute to 550°C, where they were held for two hours before they were cooled at 20°C/minute. We obtained spectra on transparent 340 × 340 μm areas of the heated and unheated samples using a custom-made microspectrometer with a silicon diode-array for the visible region, an indium-gallium-arsenide diode-array for the near-infrared region, and a silicon CCD detector for the UV–near Vis region.

We also prepared and treated a yellow-green sample using the same procedure as for the brownish orange sample, but it did not change color on heating to 600°C for two hours in air, so no further testing was done on it. One faceted brownish yellow Canary tourmaline that had previously been heated to 500–550°C was subjected to further heating to 700°C (again, see box A). In addition, two yellow-green slabs (0.9 and 1.7 mm thick) were heated in air to 500°C (two hours), 600°C (two hours), 700°C (seven days, one sample), and 750°C (five days, the other sample). Results for the latter two experiments are also described in box A (no changes in coloration were seen after the first two heating sessions).

RESULTS

Gemological Properties. The gemological properties of these Zambian samples are summarized (and compared to yellow tourmalines from Kenya; see Discussion) in table 1. Of the 31 Canary tourmalines, 11 were yellowish green (e.g., figure 12) and 20 were yellow to orangy yellow (figure 14). Microscopic

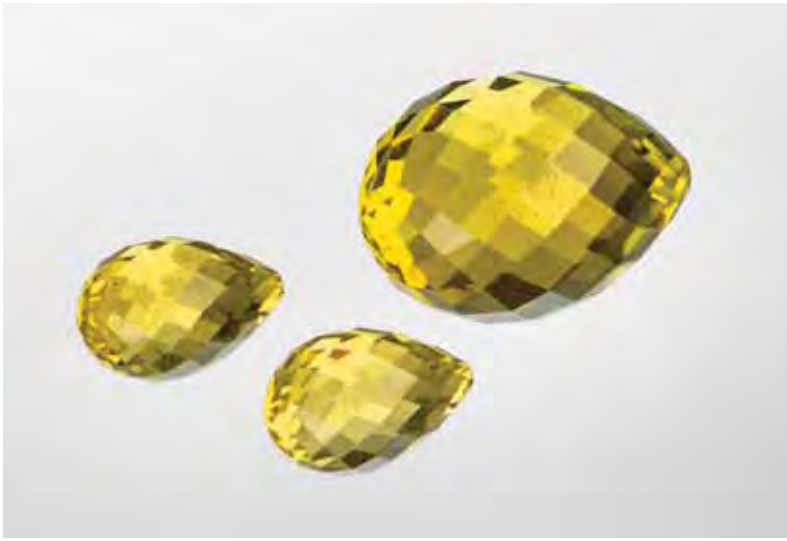

Figure 13. These briolettes of Canary tourmaline are notable for their large size. The largest stone is 65.74 ct, and the combined weight of the matched pair is 26.70 ct. Due to the presence of fluid inclusions, which can cause the material to fracture, none of the stones have been heated. Courtesy of Joeb Enterprises, Solana Beach, California; photo by C. D. Mengason.

Figure 14. Gemological properties were collected on these yellow to orangy yellow heated Canary tourmalines (0.38–1.79 ct). Gift of Shire Trading Ltd., GIA Collection nos. 37333–37338; photo by Robert Weldon.

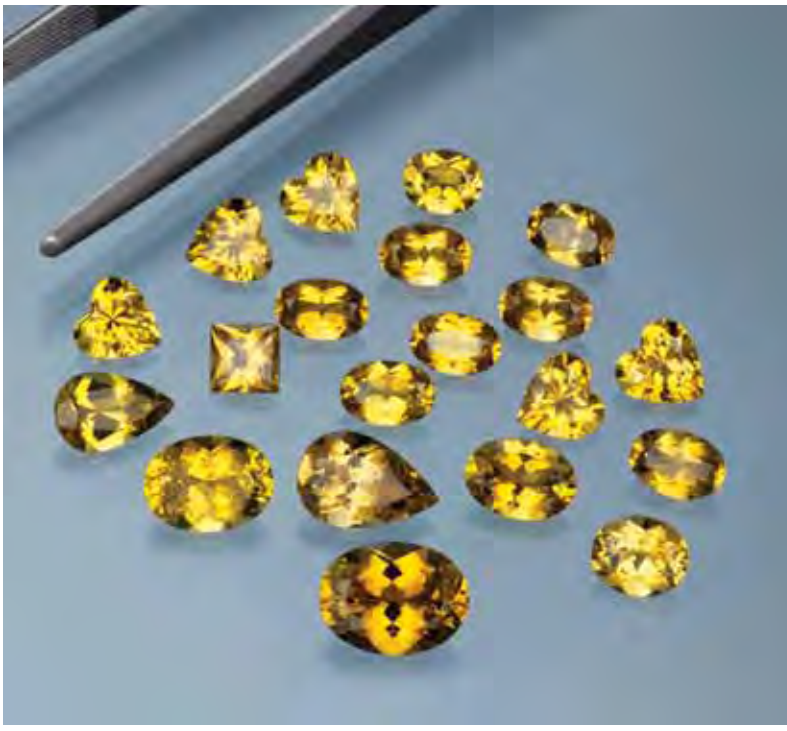

TABLE 1. Gemological properties of yellow tourmaline from Zambia and Kenya.

Properties	Zambia[a] Elbaite	Kenya[b] Dravite-uvite
Color range	Yellowish green or yellow to orangy yellow	Greenish yellow or yellow to brownish yellow
Pleochroism	Yellowish green, yellow, or orangy yellow to pale yellowish green, yellow, or orangy yellow	Yellow or orangy yellow to pale yellow or greenish yellow
RI (spot)	1.62	
n_o	1.645–1.649	1.642–1.650
n_e	1.623–1.625	1.619–1.630
Birefringence	0.020–0.025	0.020–0.023
SG	3.11–3.17	3.04–3.05
UV fluorescence		
Long-wave	Inert	Inert
Short-wave	Inert	Inert to moderate yellow
Chelsea filter	No reaction	No reaction
Absorption spectrum	General absorption to ~460 nm	Wide 440 nm band or general absorption to 480 nm
Internal features	Growth tubes, groups of two-phase (liquid-gas) fluid inclusions, and planar fluid inclusions	Small growth tubes, fluid inclusions, and two-phase (liquid-gas) inclusions

[a]*Data from this study. Slightly lower RI and SG values were reported for two samples by Boehm (2001): 1.620–1.641 and 3.10, respectively. Milisenda et al. (2000) give a lower SG value (3.05) for yellow tourmaline from Zambia.*

[b]*Data from Hänni et al. (1981), Johnson and Koivula (1996), and Simonet (2000).*

observation revealed internal features that are typical of tourmaline (figure 15), such as growth tubes, groups of two-phase (liquid and gas) inclusions along healed fractures, planar fluid inclusions, and a few angular primary three-phase fluid inclusions. The majority of the stones also contained transparent linear growth zoning. In general, the yellow to orangy yellow samples were small (<1.80 ct) and of high clarity; two were devoid of any internal features and showed only minor abrasions. The yellowish green stones ranged from slightly included (faceted stones) to moderately included (cabochons).

The physical properties of all samples were remarkably similar, regardless of color or heat treatment, except that the unheated stones contained more two-phase inclusions. This is consistent with the fact that (to reduce the risk of breakage) only very clean material is heat treated. There were no differences in the RI and SG values, or reaction to UV radiation, between the two color groups or the heated/unheated stones.

Chemical Composition. The electron-microprobe analyses showed that all samples were elbaite (e.g., figure 16), with 1.14–7.59 wt.% MnO and 0.04–0.54 wt.% TiO_2; iron was typically below the detection limit (0.016 wt.% FeO), but in rare cases it ranged up to 0.21 wt.% FeO (see table 2 and the *G&G* Data Depository). The faceted stones had compositions similar to those of the rough stones, except for a narrower range of Mn contents (~4–6.5 wt.% MnO) and no Fe was detected. The enriched Mn and low Fe content of Canary tourmaline is evident in figure 17.

UV-Vis-NIR Spectroscopy. Absorption spectra were collected on two sets of slices cut from a brownish orange sample that was heated to yellow (e.g., figure 18). The UV–near Vis spectra of both slices showed a

Figure 15. Inclusions seen in Canary tourmaline (particularly in unheated samples) include a group of secondary two-phase (liquid-gas) fluid inclusions that appear to have developed as the result of fracture healing (left, magnified 45×); growth tubes oriented parallel to the optic axis (or c-axis) direction (center, magnified 30×); and angular primary three-phase fluid inclusions (right, magnified 30×). Photomicrographs by J. I. Koivula.

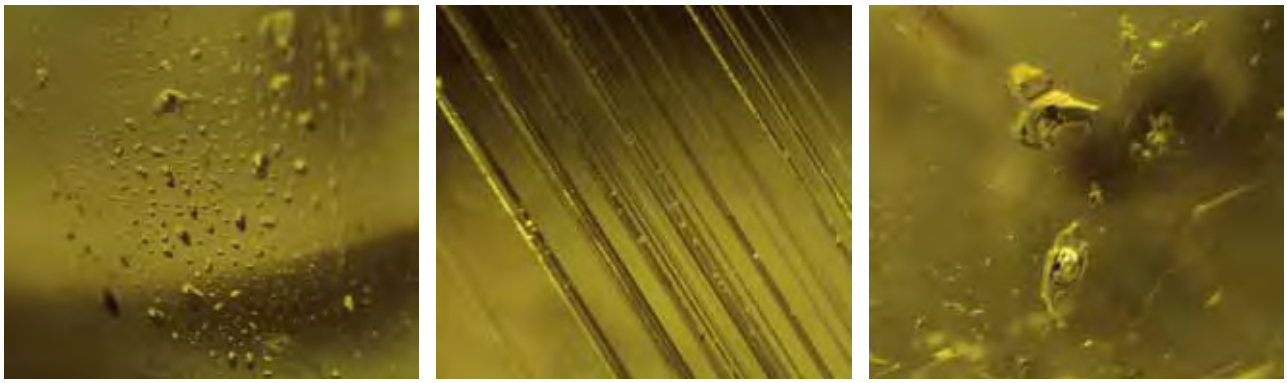

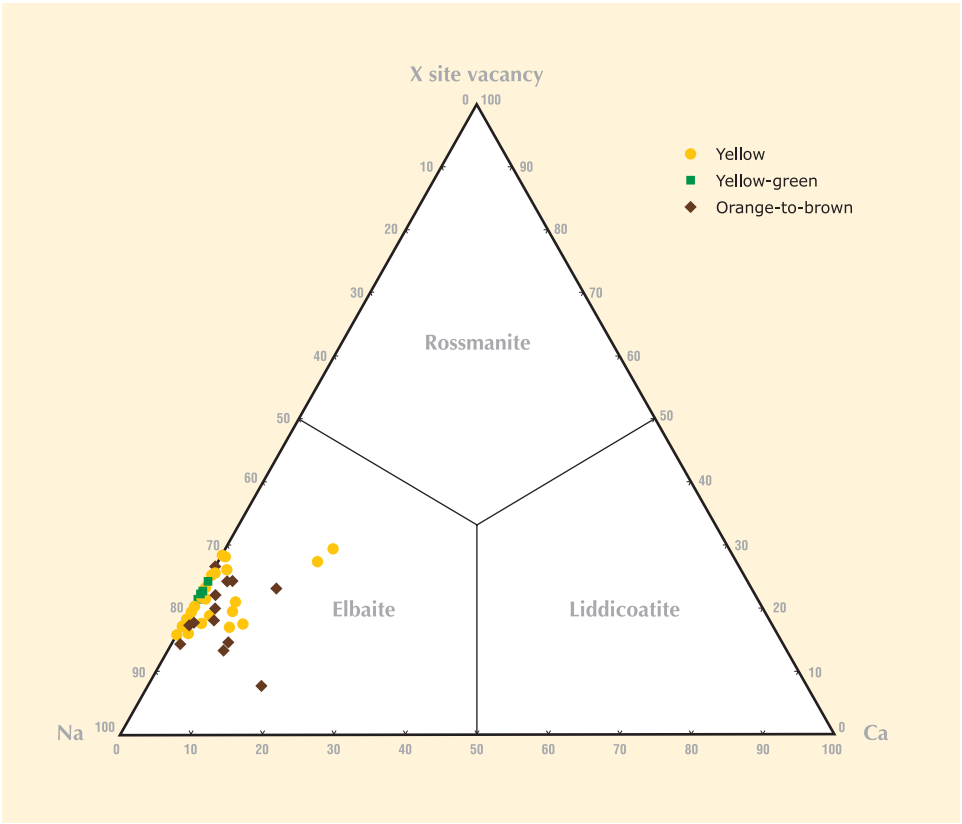

Figure 16. All the tourmaline samples analyzed by electron microprobe were elbaite. Shown here are the data for the rough samples; the compositions of the faceted stones overlapped the area occupied by these samples.

Figure 17. The Mn-rich, Fe-poor composition of Canary tourmaline is clearly illustrated by this plot, which shows the atoms per formula unit (apfu) of these elements. Also indicated for comparison is the Mn content required to attain the hypothetical Mn tourmaline end member "tsilaisite."

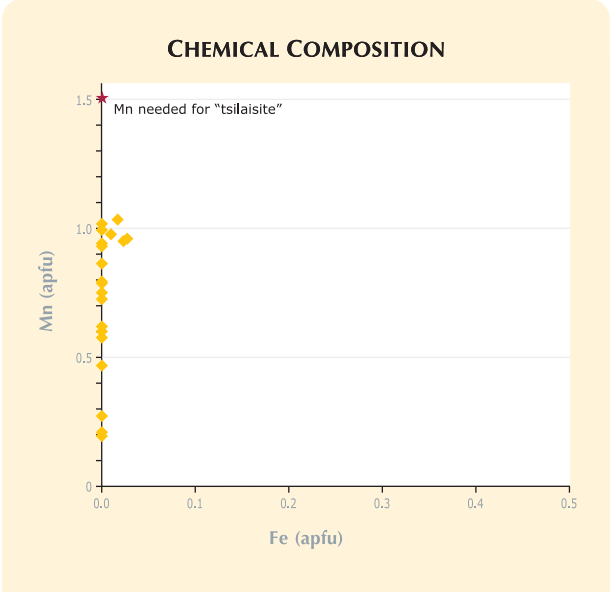

broad band at ~320 nm due to Mn^{2+}-Ti^{4+} intervalence charge transfer (IVCT), which was only slightly more pronounced in the heated sample (figure 19). The tail of this feature extended into the visible region, causing absorption of the violet-to-blue wavelengths (figure 20). The unheated sample showed both Mn^{2+}

Figure 18. These two slabs (~8 mm tall) were cut from the same piece of rough, and oriented with the c-axis in the plane of the slices. The brownish orange slab is unheated, while the yellow slice was heated for two hours at 550°C.

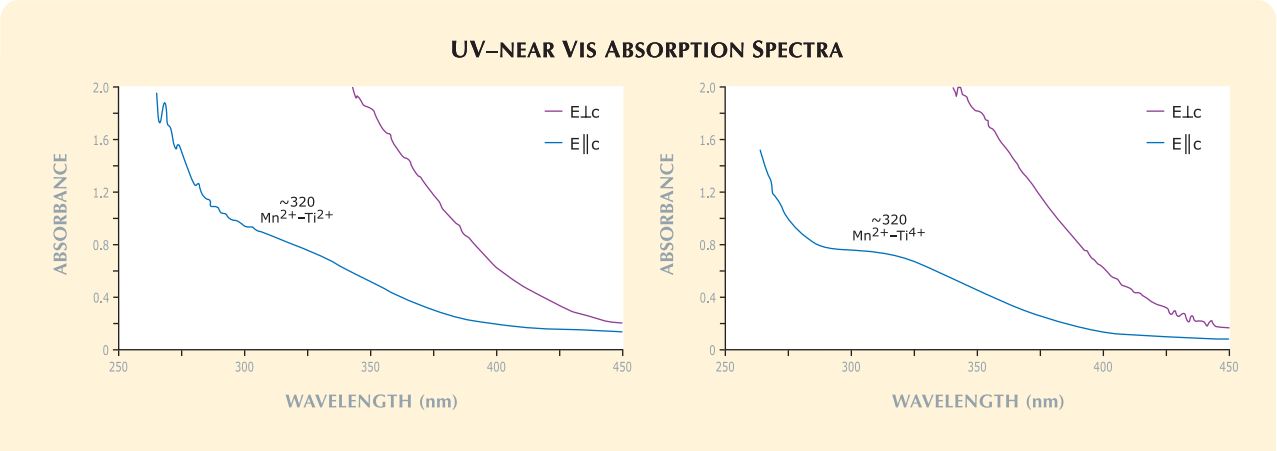

Figure 19. These UV–near Vis absorption spectra were collected on unheated brownish orange (left) and heat-treated yellow (to 550°C; right) slices of tourmaline (each 0.59 mm thick). No significant differences are seen after heating.

(sharp band at ~412 nm) and Mn^{3+} (band centered at 532 nm) features in the Vis-NIR spectra (Rossman and Mattson, 1986; Reinitz and Rossman, 1988). The Mn^{3+} band was absent from the heated sample, but that was the only change observed. Weak broad bands near 700 and 1060 nm are associated with Fe^{2+} (Mattson and Rossman, 1987). An Fe^{2+} band near 700 nm overlaps a Mn^{3+} band in the same region (Reinitz and Rossman, 1988). Features near 980 nm are overtones of the OH-stretching vibrations (Rossman and Mattson, 1986).

DISCUSSION

Gemological Properties. The gemological properties of the Canary tourmalines are typical for Mn-rich elbaite, and are comparable to those given in previous reports on yellow Zambian tourmaline (see Schmetzer and Bank, 1984b; Kane, 1986; Shigley et al., 1986; Milisenda et al., 2000; Boehm, 2001). Note, though, that none of our rough or cut samples exhibited the black needle-like inclusions mentioned in the literature (e.g., Boehm, 2001; Genis, 2001). According to Mr. Wu, such needles typically occur in the greenish yellow material but are usually removed during the cutting process.

For comparison, table 1 summarizes the properties of yellow tourmaline from Kenya, the only other known commercial source of yellow gem tourmaline. Whereas the Zambian material is elbaite, the Kenyan tourmaline is dravite-uvite (Mg-rich; see Simonet, 2000). Nevertheless, most of their physical properties overlap with two exceptions: (1) the Kenyan tourmalines have lower SG

Figure 20. These Vis-NIR absorption spectra were collected on the unheated (left) and heat-treated (right) tourmaline slices shown in figure 18 (2.59 mm thick). The Mn^{3+} absorption at 532 nm disappeared after heating to 550°C.

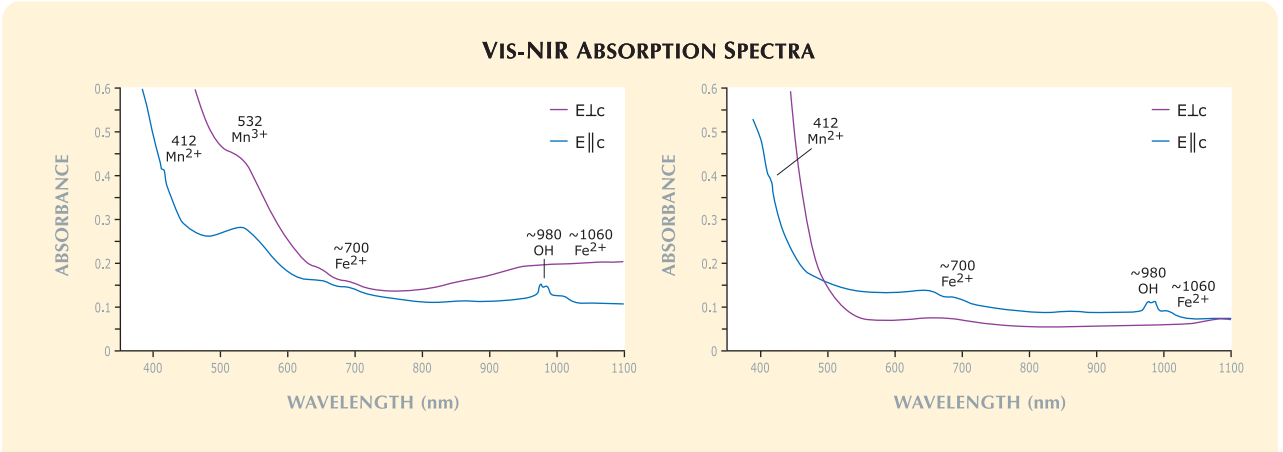

TABLE 2. Electron-microprobe analyses of tourmaline of various colors from the Canary mining area.[a]

Chemical composition	Grain mounts[b]									Faceted stones[b]	
	Greenish yellow	Yellow-brown	Pinkish brown	Bright yellow	Light brown	Light yellow	Yellow-green	Dk. brownish orange	Brownish orange[c]	Yellow	Yellowish green
Oxide (wt.%)											
SiO_2	36.26	36.22	36.33	36.34	36.32	36.56	36.58	36.58	36.59	36.64	36.54
TiO_2	0.31	0.33	0.24	0.41	0.44	0.17	0.14	0.15	0.13	0.43	0.10
B_2O_3 calc.	10.71	10.80	10.73	10.82	10.75	10.84	11.00	10.96	10.98	10.90	10.85
Al_2O_3	37.56	38.58	37.90	38.54	37.85	39.68	41.54	41.79	41.86	38.87	40.02
V_2O_3	0.15	nd	0.03	nd	0.02	nd	nd	nd	nd	nd	nd
FeO	nd	0.08	nd	nd	nd	nd	nd	nd	nd	nd	nd
MnO	7.39	7.16	6.61	6.34	6.33	4.41	2.68	1.52	1.31	6.21	4.00
MgO	nd	nd	nd	nd	nd	nd	nd	nd	0.05	nd	nd
CaO	0.03	0.06	0.08	0.40	0.46	0.03	0.02	nd	0.05	nd	nd
ZnO	nd	nd	nd	nd	nd	nd	nd	0.02	0.02	nd	nd
Li_2O calc.	1.32	1.29	1.44	1.48	1.54	1.59	1.75	1.82	1.88	1.51	1.60
Na_2O	2.48	2.47	2.65	2.43	2.50	2.44	2.54	2.34	2.47	2.40	2.36
K_2O	0.11	0.03	0.06	0.02	0.02	0.02	0.03	nd	0.02	0.02	0.01
H_2O calc.	3.20	3.19	3.24	3.28	3.46	3.26	3.25	3.21	3.27	3.22	3.19
F	1.05	1.13	0.98	0.97	0.53	1.01	1.16	1.21	1.10	1.15	1.17
Subtotal	100.56	101.33	100.30	101.05	100.22	100.01	100.68	99.58	99.72	101.36	99.85
-O=F	0.44	0.47	0.41	0.41	0.22	0.42	0.49	0.51	0.46	0.48	0.49
Total	100.12	100.86	99.89	100.64	100.00	99.58	100.20	99.07	99.26	100.88	99.36
Ions per 31 (O,OH,F)											
Si	5.884	5.825	5.885	5.834	5.869	5.860	5.779	5.802	5.790	5.840	5.856
T Al	0.116	0.175	0.115	0.166	0.131	0.140	0.221	0.198	0.210	0.160	0.144
Tet. sum	6.000	6.000	6.000	6.000	6.000	6.000	6.000	6.000	6.000	6.000	6.000
B calc.	2.999	2.999	2.999	2.999	2.999	2.999	2.999	2.999	2.999	3.000	3.000
Al Z	6.000	6.000	6.000	6.000	6.000	6.000	6.000	6.000	6.000	6.000	6.000
Al Y	1.067	1.138	1.121	1.127	1.078	1.355	1.514	1.613	1.598	1.142	1.414
V^{3+}	0.019	nd	0.003	nd	0.003	nd	nd	nd	nd	nd	nd
Ti	0.038	0.039	0.030	0.050	0.053	0.021	0.016	0.017	0.016	0.052	0.013
Fe^{2+}	nd	0.010	nd	nd	nd	nd	nd	nd	nd	nd	nd
Mn	1.015	0.975	0.907	0.863	0.866	0.598	0.359	0.204	0.176	0.838	0.543
Mg	nd	nd	nd	nd	nd	nd	nd	nd	0.012	nd	nd
Li calc.	0.859	0.835	0.938	0.958	0.999	1.026	1.110	1.163	1.195	0.967	1.030
Zn	nd	nd	nd	nd	nd	nd	nd	0.002	0.002	nd	nd
Y sum	2.999	2.999	2.999	2.999	2.999	2.999	2.999	2.999	2.999	3.000	3.000
Ca	0.006	0.011	0.014	0.069	0.079	0.004	0.003	nd	0.009	nd	nd
Na	0.782	0.769	0.832	0.757	0.785	0.759	0.778	0.718	0.757	0.743	0.734
K	0.024	0.005	0.013	0.003	0.004	0.004	0.006	nd	0.004	0.005	0.002
Vacancy	0.189	0.216	0.141	0.170	0.133	0.232	0.213	0.282	0.230	0.253	0.263
X sum	1.000	1.000	1.000	1.000	1.000	1.000	1.000	1.000	1.000	1.000	1.000
F	0.539	0.572	0.502	0.490	0.269	0.510	0.578	0.608	0.549	0.577	0.594
OH calc.	3.461	3.428	3.498	3.510	3.731	3.490	3.422	3.392	3.451	3.423	3.405
Mol.% tourmaline species											
Elbaite	80.0	77.3	84.3	76.0	78.7	76.3	78.3	71.8	76.0	74.6	73.6
Rossmanite	19.4	21.7	14.3	17.0	13.3	23.3	21.4	28.2	23.1	25.4	26.4
Liddicoatite	0.6	1.1	1.4	7.0	8.0	0.4	0.3	0.0	0.9	0.0	0.0

[a] *Cr, Cu, Bi, Ba, Pb, and Cl were analyzed for but not detected. Abbreviation: nd = not detected.*
[b] *Grain mounts were prepared by mounting pieces taken from rough samples in epoxy and polishing them smooth; representative analyses are shown for the main colors analyzed, and arranged by decreasing Mn content. For the faceted stones, the average of five analyses across the table of each sample is shown for the stones with the highest and lowest Mn contents.*
[c] *This sample was also used for heat treatment (it became yellow; see figure 18) and spectroscopy.*

values; and (2) it is not uncommon for the Kenyan stones to fluoresce yellow to short-wave UV radiation, while the Zambian tourmaline is inert.

Raman spectra of a yellowish green Canary tourmaline sample are available at http://rruff.info (sample R070077). A Raman peak located at ~850

Figure 21. The vivid yellow color of Canary tourmaline is quite distinctive for gem elbaite. The relatively large examples shown here weigh 25.00 ct (pear), 18.00 ct (oval), and approximately 6 ct each (smaller pear shapes). Courtesy of Joeb Enterprises; photo by Robert Weldon.

cm^{-1} in the spectra is stronger than in any other tourmaline analyzed for the RRUFF database, with the exception of the dark green portion of a color-zoned Mn-poor sample from Brazil (R060566; R. Downs, pers. comm., 2007). The origin of this strong Raman peak is unknown.

Chemical Composition. In addition to the Lundazi District of Zambia, significant occurrences of yellow Mn-rich elbaite are known from Tsilaisina in central Madagascar (Duparc et al., 1910), Elba Island in Italy (Bosi et al., 2005), Austria (Ertl et al., 2003, 2004), Nepal (Rossman and Mattson, 1986; Burns et al., 1994), the Malkhan District in Russia (Mashkovtsev and Zagorsky, 1997), and the Pamir Mountains in Tajikistan (Mashkovtsev and Zagorsky, 1997). Recently, substantial amounts of this tourmaline have come from the Muva area in Mozambique (unpublished data of BML and WBS).

The highest Mn content found in the samples analyzed for this study was 7.59 wt.% MnO. This is considerably less than the 9.18 wt.% MnO measured by Shigley et al. (1986), which approaches "tsilaisite" composition (i.e., 10.7 wt.% MnO needed to attain a 50:50 ratio of tsilaisite:elbaite). Schmetzer and Bank (1984b) reported 6.3–6.9 wt.% MnO in a yellow Zambian tourmaline, and Rossman and Mattson (1986) measured 6.18–6.85 wt.% oxide in their yellow to yellow-green samples. These values are similar to the higher Mn contents measured in this study, but our values ranged considerably lower (1.14 wt.%) among the greenish yellow to yellow to brownish yellow samples we analyzed (see *G&G* Data Depository). The maximum Mn contents measured in our samples are only about two-thirds the amount needed to attain a "tsilaisite" composition (figure 17).

Kunitz (1929) documented a systematic decrease in RI values with lower Mn content in elbaite. The limited range of RI values obtained for the polished stones in this study (table 1) is consistent with the rather narrow range of Mn contents (~4–6.5 wt.% MnO; see *G&G* Data Depository) that was measured in eight of these stones by electron microprobe analysis.

Cause of Color. The yellow-green coloration is due to a Mn^{2+} plus Mn^{2+}-Ti^{4+} intervalence charge transfer interaction that is responsible for absorbing the violet-to-blue portion of the spectrum (Rossman and Mattson, 1986). Variations from greenish yellow to yellow to brown are due to Fe^{2+}-Ti^{4+} IVCT; in contrast, the green color of typical elbaites from granitic pegmatites is associated with much higher Fe and lower Ti contents (Rossman and Mattson, 1986).

The unheated brownish orange tourmaline (again, see figure 18) initially owed its color to a superposition of a Mn^{3+} absorption centered in the 530 nm region of the tourmaline spectra. After heating for two hours at 550°C, the sample lost the 530 nm absorption band and turned yellow. It has long been recognized that Mn^{3+} can be thermally reduced to Mn^{2+} by heating pink tourmaline at temperatures between 500°C and 600°C (Reinitz and Rossman, 1988). However, heating to higher temperatures causes the Mn^{2+} to be re-oxidized to Mn^{3+} and create pink color, as shown in box A.

The Mn^{2+} and Mn^{2+}-Ti^{4+} IVCT features in the spectra of the heated brownish orange tourmaline were not significantly altered. It follows, then, that yellow-green Canary tourmaline does not change color on heating to 500–600°C because it does not contain the Mn^{3+} component.

Formation of Canary Tourmaline. Gem tourmaline typically consists of pink, green, or blue elbaite that is mined from the lepidolite-bearing inner zones of complex LCT (lithium, cesium, tantalum) pegmatites. In contrast, Mn-rich (and Ti-bearing) yellow elbaite from the Canary mining area appears to have formed in a pegmatite with a simpler mineralogy. The enrichment of Mn in granitic pegmatites is usually associated with significant amounts of Li (Černý et al., 1985), leading to its incorporation into

Li-micas or Li-phosphates. Spessartine crystallization is an even more important mechanism for depleting Mn from the pegmatite system, and the Mn content of tourmaline has been shown to be influenced by the abundance of garnet in the pegmatite (Novák et al., 2000). Although minor amounts of spessartine were observed by one of us (BA) in a tailings pile at the Canary mine, we infer that it was not a common mineral in the pegmatite. We suggest that the rarity of Mn-rich yellow elbaite in nature is due to the need for an unusual combination of high B and Mn with low Li in pegmatite-forming magma.

The formation of Canary tourmaline required that Mn (and some Ti) was conserved until the final stage of pegmatite crystallization (in gem pockets). However, the bright yellow coloration of this tourmaline (natural or after heat treatment) will only develop in the absence of significant Fe. The most likely mechanism for conserving Mn while depleting Fe is early crystallization of abundant schorl, since Fe is much more compatible in schorl than Mn (Wolf and London, 1997; London et al., 2001). Although little primary schorl was seen in the remaining portions of the pegmatite footwall during our visit, we saw abundant black tourmaline in an earlier photo of the pegmatite.

The enriched B content of the original pegmatite magma promoted schorl crystallization, rather than the formation of micas or spessartine (which would deplete Mn). The formation of schorl also consumed some Ti, but schorl is much less efficient than biotite at scavenging Ti from the pegmatite melt (Icenhower and London, 1995). Therefore, since biotite was apparently absent from the Canary pegmatite, there was still enough Ti available during the crystallization of the gem pockets to develop the yellow color in Canary tourmaline via Mn^{2+}-Ti^{4+} intervalence charge transfer.

Following pegmatite crystallization, the influx of an unusual B-, Fe-, K- and Na-rich fluid (apparently from an external source) resulted in local tourmaline ± K-feldspar + albite veining and quartz dissolution; the same event also brecciated some of the yellow elbaite with black tourmaline ± K-feldspar + albite assemblages.

CONCLUSION

This study presents additional information on Mn-rich yellow gem tourmaline from the Lundazi District of eastern Zambia. The principal source of this elbaite is the Canary mining area, where it has been mined from eluvial/alluvial and primary (pegmatite) deposits since the early 1980s. The gemological properties are typical of elbaite, but the chemical composition is notable for high Mn and low Fe combined with relatively enriched Ti for gem tourmaline. This composition probably resulted from the evolution of a B-rich, Li-poor granitic pegmatite in which early crystallization of abundant schorl removed the Fe while conserving Mn until the late-stage formation of gem tourmaline–bearing pockets.

Most of the tourmaline is heat treated to 500–550°C to reduce the brown/orange component. Although some relatively large stones have been faceted (e.g., figure 21), most are <1 ct. Considering the amount of Canary tourmaline that has been sold into marketplace, it is still relatively uncommon to encounter it in jewelry (figure 22). Although the potential reserves of this tourmaline are unknown, abundant melee could be cut from the current stockpiles of rough, and additional mining is expected to increase the availability of larger material.

Figure 22. Canary tourmaline is set with diamonds in this ring (2.28 ct center stone) and pair of earrings. Ring courtesy of Tommy Wu, and earrings are from Henry Jewelry Inc., Los Angeles; photo by Robert Weldon.

ABOUT THE AUTHORS

Mr. Laurs (blaurs@gia.edu) is editor of Gems & Gemology *at GIA in Carlsbad. Dr. Simmons is professor of mineralogy and university research professor, and Mr. Falster is senior research technologist, at the University of New Orleans, Louisiana. Dr. Rossman is professor of mineralogy at the California Institute of Technology, Pasadena. Mr. Fritz is staff gemologist, and Mr. Koivula is chief gemologist, at the GIA Laboratory in Carlsbad. Mr. Anckar is gemologist/geologist with Mayfair Mining & Minerals Inc., Lindfield, West Sussex, England.*

ACKNOWLEDGMENTS

The authors are grateful to Tommy Wu (Shire Trading Ltd., Hong Kong) for providing logistical support in the field and access to the mining property, as well as supplying information and loaning/donating samples for research. We also thank Rita and Arun Mittal (Southstream Enterprises Ltd., Lusaka, Zambia) for providing information and samples during the authors' visit to Zambia. Useful insights on the geology were provided by mine geologist Naveen Torgalmoth, who tragically died of malaria in 2006. Robert Downs (University of Arizona, Tucson) provided assistance with interpreting the Raman spectrum of Canary tourmaline.

REFERENCES

Boehm E. (2001) Gem News International: Canary tourmaline from Malawi. *Gems & Gemology*, Vol. 27, No. 2, pp. 151–152 (see erratum in Vol. 40, No. 1, p. 86).

Bosi F., Agrosì G., Lucchesi S., Melchiorre G., Scandale E. (2005) Mn-tourmaline from island of Elba (Italy): Crystal chemistry. *American Mineralogist*, Vol. 90, pp. 1661–1668.

Burke E.A.J. (2006) A mass discreditation of GQN minerals. *Canadian Mineralogist*, Vol. 44, pp. 1557–1560.

Burns P.C., MacDonald D.J., Hawthorne F.C. (1994) The crystal chemistry of manganese-bearing elbaite. *Canadian Mineralogist*, Vol. 32, pp. 31–41.

Capturing the Canary yellow tourmaline (2003) *Idex Magazine*, Vol. 18, No. 158, pp. 89–91.

Černý P., Meintzer R.E., Anderson A.J. (1985) Extreme fractionation in rare-element granitic pegmatites: Selected examples of data and mechanisms. *Canadian Mineralogist*, Vol. 23., pp. 381–421.

Dunn P.J., Fleischer M., Langley R., Shigley J.E., Zilczer J.A. (1985) New mineral names. *American Mineralogist*, Vol. 70, pp. 871–881.

Duparc L., Wunder M., Sabot R. (1910) Les minéraux des pegmatites des environs d'Antsirabé a Madagascar. *Mémoires de la Société de physique et d'Histoire Naturalle de Genève*, Vol. 36, No. 3, pp. 283–410.

Ertl A., Hughes J.M., Prowatke S., Rossman G.R., London D., Fritz E.A. (2003) Mn-rich tourmaline from Austria: Structure, chemistry, optical spectra, and relations to synthetic solid solutions. *American Mineralogist*, Vol. 88, pp. 1369–1376.

Ertl A., Schuster R., Prowatke S., Brandstätter F., Ludwig T., Bernhardt H.-J., Koller F., Hughes J.M. (2004) Mn-rich tourmaline and fluorapatite in a Variscan pegmatite from Eibenstein an der Thaya, Bohemian massif, Lower Austria. *European Journal of Mineralogy*, Vol. 16, pp. 551–560.

Federman D. (2002) Gem Profile—Canary tourmaline: Miracle from Malawi. *Modern Jeweler*, Vol. 101, No. 1, pp. 45–46.

Genis R. (2001) Canary yellow tourmaline makes grand entrance. *Rapaport Diamond Report*, Vol. 24, No. 35, pp. 123, 125.

Hänni H.A., Frank E., Bosshart G. (1981) Golden yellow tourmaline of gem quality from Kenya. *Journal of Gemmology*, Vol. 17, No. 7, pp. 437–442.

Icenhower, J.P., London, D. (1995) An experimental study of element partitioning between biotite, muscovite and coexisting peraluminous granitic melt at 200 MPa (H_2O). *American Mineralogist*, Vol. 80, pp. 1229–1251.

Johns C.C., Liyungu K., Mabuku S., Mwale G., Sakungo F., Tembo F., Vallance G. (1989) The stratigraphic and structural framework of eastern Zambia. *Journal of Applied Earth Sciences*, Vol. 9, No. 1, pp. 123–136.

Johnson M.L., Koivula J.I., Eds. (1996) Gem News: Golden tourmaline from Kenya. *Gems & Gemology*, Vol. 32, No. 2, pp. 135–136.

Johnson M.L., Wentzell C.W., Elen S. (1997) Multicolored bismuth-bearing tourmaline from Lundazi, Zambia. *Gems & Gemology*, Vol. 33, No. 3, pp. 204–211.

Kane R.E. (1986) Gem Trade Lab Notes: Tourmaline, unusual yellowish green. *Gems & Gemology*, Vol. 22, No. 3, pp. 175–176.

Kunitz W. (1929) Betrage zur Kenntnis der magmatischen Assoziationen I. Die Mischungsreihen in der Turmalingruppe und die genetischen Beziehungen zwischen Turmalinen und Glimmern. *Chemie der Erde*, Vol. 4, pp. 208–251.

Laurs B.M. (2004) Gem News International: Update on several gem localities in Zambia and Malawi. *Gems & Gemology*, Vol. 40, No. 4, pp. 347–350.

London D., Evensen J.M., Fritz E., Icenhower J.P., Morgan G.B., IV, Wolf M.B. (2001) Enrichment and accommodation of manganese in granite-pegmatite systems. In *Eleventh Annual V. M. Goldschmidt Conference*, Abstract #3369, LPI Contribution No. 1088, Lunar and Planetary Institute, Houston (CD-ROM).

Mashkovtsev R.I., Zagorsky V.E. (1997) Spectroscopic study of Mn-bearing elbaites. *Tourmaline 1997*, June 20–25, Moravian Museum, Brno, Czech Republic, p. 54.

Mattson S.M., Rossman G.R. (1987) Fe^{2+}-Fe^{3+} interactions in tourmaline. *Physics and Chemistry of Minerals*, Vol. 14, pp. 163–171.

Milisenda C.C., Malango V., Taupitz K.C. (2000) Edelsteine aus Sambia—Teil 2: Turmalin und aquamarin. *Gemmologie: Zeitschrift der Deutschen Gemmologischen Gesellschaft*, Vol. 49, pp. 31–48.

Njamu F.M. (2003) Survey of productive mines in Nyimba, Petauke, Chadiza and Lundazi Districts, Eastern Province, Zambia. Unpublished report prepared on behalf of Lundazi Gemstone Association in cooperation with Mining Sector Diversification Programme and Zambia Trade Investment Enhancement, Lusaka, 129 pp.

Novák M., Selway J.B., Černý P., Chapman R.C., Masau M. (2000) Correlation between Mn content in tourmaline and garnet abundance in two elbaite-subtype pegmatites: Dolní Rožínka and Pikárec, Czech Republic. *Geological Association of Canada—Mineralogical Association of Canada, Joint Annual Meeting*, abstract #584.

Nuber B., Schmetzer K. (1984) Structural refinement of tsilaisite (manganese tourmaline). *Neues Jahrbuch für Mineralogie, Monatshefte*, Vol. 7, pp. 301–304.

O'Connor E.A. (1998) *Geology of the Lumezi River and Lundazi areas—Explanation of Degree Sheets 1232 NE Quarter and Parts of 1233 NW and NE Quarters*. Geological Survey Department Report No. 71, Lusaka, 29 pp., 2 maps.

Patney R.K., Tether J. (1988) The gem bearing pegmatites of eastern Zambia. *Zambian Journal of Applied Earth Sciences*, Vol. 2, No. 2, pp. 41–53.

Pieczka A., Kraczka J. (2004) Oxidized tourmalines—A combined chemical, XRD and Mössbauer study. *European Journal of Mineralogy*, Vol. 16, pp. 309–321.

Reinitz I.L., Rossman G.R. (1988) Role of natural radiation in tourmaline coloration. *American Mineralogist*, Vol. 73, pp. 822–825.

Rossman G.R., Mattson S.M. (1986) Yellow, Mn-rich elbaite with Mn-Ti intervalence charge transfer. *American Mineralogist*, Vol. 71, pp. 599–602.
Schmetzer K., Bank H. (1983) Intensiv gelb gefärbter Tsilaisite (Manganturmalin) von Edelsteinqualität aus Sambia. *Zeitschrift der Deutschen Gemmologischen Gesellschaft*, Vol. 32, No. 4, pp. 159–163.
Schmetzer K., Bank H. (1984a) Crystal chemistry of tsilaisite (manganese tourmaline) from Zambia. *Neues Jahrbuch für Mineralogie, Monatshefte*, Vol. 2, pp. 61–69.
Schmetzer K., Bank H. (1984b) Intensive yellow tsilaisite (manganese tourmaline) of gem quality from Zambia. *Journal of Gemmology*, Vol. 19, No. 3, pp. 218–223.
Shigley J.E., Kane R.E., Manson D.V. (1986) A notable Mn-rich gem elbaite tourmaline and its relationship to "tsilaisite." *American Mineralogist*, Vol. 71, pp. 1214–1216.
Simonet C. (2000) Geology of the Yellow mine (Taita-Taveta District, Kenya) and other yellow tourmaline deposits in East Africa. *Journal of Gemmology*, Vol. 27, No. 1, pp. 11–29.
Snelling N.J., Johnson R.L., Drysdall A.R. (1972) The geochronology of Zambia. *Records of the Geological Survey of Zambia*, Vol. 12, pp. 19–30.
Substantial increase in sales of Canary tourmaline: Japanese trader (2005) *Jewellery News Asia*, No. 245, pp. 66, 68.
Supplier to vertically integrate mining, polishing and wholesaling of Zambian yellow tourmaline (2004) *Jewellery News Asia*, No. 236, pp. 128, 138, 140.
Thomas A.E. (1982) Zambian tourmaline. *Journal of Gemmology*, Vol. 18, pp. 4–6.
Wolf M.B., London D. (1997) Boron in granitic magmas: Stability of tourmaline in equilibrium with biotite and cordierite. *Contributions to Mineralogy and Petrology*, Vol. 130, pp. 12–30.
Wong M. (2001) IJT 2001 reports slower traffic but similar sales. *Jewellery News Asia*, No. 199, pp. 208–210.
Zgambo N. (1995) The Lundazi aquamarine pegmatites of eastern Zambia. *International Conference on Industrial Minerals Proceedings*, Lusaka, Zambia, publ. by Council for Geosciences, Pretoria, South Africa, pp. 226–239.

FLUORESCENCE SPECTRA OF COLORED DIAMONDS USING A RAPID, MOBILE SPECTROMETER

Sally Eaton-Magaña, Jeffrey E. Post, Peter J. Heaney, Roy A. Walters,
Christopher M. Breeding, and James E. Butler

Numerous natural-color colored diamonds from the Aurora Butterfly of Peace and other collections were studied using a new type of fluorescence spectrometer that has many advantages for gemological research, including high portability, low cost, and rapid collection times. For comparison, 10 irradiated diamonds were also studied. With only two exceptions, the natural-color diamonds could be separated into three categories—based on the peak wavelength and shape of the fluorescence spectra—that *generally* corresponded to their bodycolors: (1) ~450 and ~490 nm, recorded mainly for pink, yellow, and fancy white diamonds; (2) ~525 nm, mainly for green-yellow or yellow-green and brown diamonds; and (3) ~550 nm, mainly for orange, gray-green (including chameleon), and type Ia blue-gray or gray-blue diamonds. A spectrum that is anomalous for the diamond's bodycolor may indicate that it has been treated, and in some cases, fluorescence spectroscopy can help determine diamond type.

Prior fluorescence studies performed at GIA found that about 35% of near-colorless gem diamonds fluoresce to long-wave UV radiation, with 97% of those diamonds showing blue fluorescence (Moses et al., 1997). However, colored diamonds more commonly show fluorescence, and in a wider variety of colors (e.g., figure 1). Given the methodology with which fluorescence is typically observed, it is sometimes difficult to determine the underlying mechanism of this behavior and, specifically, the influence of the natural, synthetic, or treated nature of the diamond on its fluorescence.

Becquerel (1868) and Dyer and Matthews (1958) were among the first scientists to study the fluorescence properties of diamonds. Dyer and Matthews studied the luminescence of the 415.5 and 504.0 nm systems (now identified as the N3 and H3 defects; see, e.g., Collins, 1982a) and found that these features were related to blue and green fluorescence, respectively. A review by Fritsch and Waychunas (1994) detailed the observed fluorescence and phosphorescence of diamonds according to their bodycolor.

While a large number of peaks and defect centers have been chronicled in natural diamonds using UV-Vis absorption, cathodoluminescence, and photoluminescence spectroscopy (see, e.g., Zaitsev, 2001), spectral data for fluorescence and phosphorescence are limited in the gemological literature, since luminescence is typically described by visual observations (again, see Fritsch and Waychunas, 1994). However, visual assessment of fluorescence and phosphorescence tells only part of the story. The color discerned by the unaided eye may represent a combination of two or more wavelength regions. For example, Anderson (1960) asserted that although most fluorescing diamonds appear to luminesce blue, a yellow or green component may be present but masked by the stronger blue emission. He used color filters and a spectroscope to try to identify some of the relevant

See end of article for About the Authors and Acknowledgments.
GEMS & GEMOLOGY, Vol. 43, No. 4, pp. 332–351.

Figure 1. The colored diamonds in the Aurora Butterfly of Peace were assembled over a 12-year period by Alan Bronstein and Harry Rodman of Aurora Gems Inc., New York (these photos date from 2005). The 240 stones (0.09–2.11 ct; total weight of 166.94 carats) show nearly the full spectrum of color and cut styles available in natural colored diamonds. The collection is shown here in standard daylight-equivalent illumination (left) and long-wave UV radiation (right). Photos by Robert Weldon.

peaks. Also, a spectral peak may exhibit a long tail that will cause the observed color to differ from that of other diamonds in which fluorescence is constrained to a narrower wavelength range.

The gem collection at the Smithsonian Institution's National Museum of Natural History provided an opportunity to study the fluorescence and phosphorescence characteristics of a wide variety of colored diamonds. The materials came from the permanent collection, including the DeYoung Red and the DeYoung Pink, along with a temporary exhibit of the Aurora Butterfly collection (Solotaroff, 2003; "Rodman, Bronstein…," 2005; Eaton-Magaña, 2006a; again, see figure 1), which is a suite of 240 colored diamonds that had been loaned to the museum by Alan Bronstein and Harry Rodman of Aurora Gems. Additionally, we examined some natural and treated diamonds from GIA collections. The luminescence properties of 67 natural-color blue diamonds, including the Hope Diamond and the Blue Heart, are discussed in separate publications (Eaton-Magaña et al., 2006b, 2008).

The present study also provided an opportunity to test a new-generation charge-coupled device (CCD) spectrometer for the routine measurement of fluorescence and phosphorescence spectra of gem diamonds. This spectrometer is highly mobile (it is about the size of a deck of playing cards), extremely durable, easy to set up in minutes, permissive of rapid data collection, and relatively inexpensive (see box A for more information).

MATERIALS AND METHODS

Samples. This article provides fluorescence results for 72 colored diamonds: 62 natural, untreated (as indicated on their gem laboratory reports) and 10 irradiated (table 1). Nine of the natural-color and one of the treated samples were rough; all of the others were faceted. Most of the diamonds (48) were selected from the Aurora Butterfly collection, and the remainder came from GIA collections (22) and the National Gem Collection (2). We selected the samples according to the rarity of their bodycolor (e.g., purple and red) or the presence of visual fluorescence across the range of bodycolors. Therefore, this is not a random sampling of colored diamonds, and general statistics of fluorescing vs. nonfluorescing diamonds should not be inferred from these data. Our intent was to detect trends that might be useful for colored

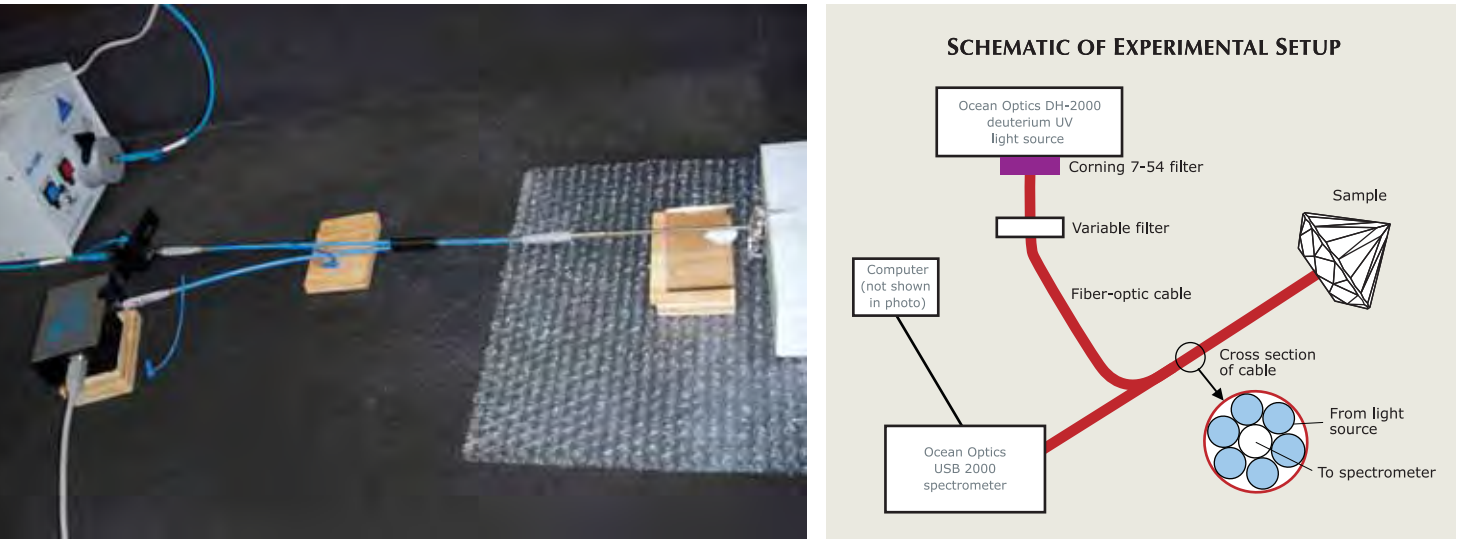

Figure 2. This photo and diagram illustrate the components of the mobile instrument (composed principally of Ocean Optics equipment) used for fluorescence and phosphorescence spectroscopy. When phosphorescence spectra were recorded, the Corning 7-54 filter and the variable filter were removed. Photo by S. Eaton-Magaña.

diamond characterization and, ultimately, identification. The very slightly yellow (G-to-I grade; Fryer and Koivula, 1986) 127 ct Portuguese Diamond was also examined to provide an example of how fluorescence intensity is related to the size of a diamond.

At GIA and the Smithsonian, all samples were tested for visible fluorescence and phosphorescence using standard 4-watt long- and short-wave UV lamps. The color descriptions in table 1 were taken from grading reports issued by gemological laboratories. For the purposes of this article, the diamonds are assigned a "key bodycolor" (see table 1) according to their dominant bodycolor, although each group may include various modifying hues. For example, within the pink color group, most were graded solely as pink, and a few were purplish pink or reddish purplish pink. Due to the variety of fluorescence results, diamonds with a green component are sorted according to their specific (dominant plus modifying hue) color description. Several diamonds graded as green-yellow to yellow-green are grouped together (key bodycolor given as yellow-green). Similarly, three diamonds graded as blue-gray or gray-blue are grouped together (key bodycolor given as blue-gray).

Fluorescence and Phosphorescence Spectroscopy. The instrumentation used to measure fluorescence and phosphorescence spectra consisted of a deuterium lamp UV source (215–400 nm), filters to control the wavelengths of incident light, a sample holder, a fiber-optic bundle to deliver incident light and collect the emitted signal, an Ocean Optics USB 2000 CCD spectrometer, and a computer (see figure 2). The UV source used for most of the fluorescence and phosphorescence spectroscopic measurements was an Ocean Optics DH-2000. The UV radiation was filtered to ~250–400 nm, and was transferred through a bundle of six optical fibers (600 µm diameter each). A seventh fiber in the core of the bundle channeled the emitted light from the diamond to the spectrometer (figure 2, right). The tip of the fiber-optic bundle was placed directly in contact with the table of each sample, which enabled us to illuminate and measure approximately equivalent volumes of each sample. Thus, we were able to compare relative intensities of signals from a wide range of sample sizes. The CCD spectrometer used in these experiments is described further in box A.

For the fluorescence measurements (again, see figure 2, right), we used a Corning 7-54 filter to block visible light (~400–650 nm) from the deuterium UV source and a variable filter (Ocean Optics LVF-HL) to deliver only a narrow band (full width at half maximum [FWHM] = 22 nm) of UV radiation to the sample. This narrow band was varied between 250 and 400 nm (e.g., figure 3). The fluorescence recorded by the spectrometer at each excitation wavelength was collected for 30 seconds. Since excitation intensity varied with wavelength (again, see figure 3), the measured fluorescence spectra were scaled uniformly over the wavelength range. Except for one sample to monitor the change, no radiometric (i.e., wavelength-dependent) calibration

BOX A: THE MOBILE CCD SPECTROMETER

The Ocean Optics USB 2000 CCD spectrometer measures wavelengths from 340 to 1020 nm and has a 200 µm slit width that provides a 10-nm FWHM resolution. This small mobile spectrometer was configured for exceptional sensitivity of broad spectral structures so that phosphorescence decay could be measured. The accuracy of the spectrometer's wavelength position was confirmed using the 435.8 and 546.1 nm lines from a mercury lamp. However, for the majority of the data, the spectrometer was not radiometrically calibrated, which would adjust the relative intensities obtained across the wavelength range. We have elected to provide the uncorrected data (i.e., the direct output from the spectrometer), as these are the spectra most likely to be produced by others using this type of instrumentation.

The CCD spectrometer was initially selected for the blue diamond study reported in Eaton-Magaña et al. (2006b, 2008), because its ability to resolve low-intensity luminescence allowed the collection of time-resolved phosphorescence spectra. In addition, the portability and ease of use enabled us to take the instrument to the gems, providing access to many more stones than would otherwise have been possible. The experimental apparatus shown in figure 2 was easily transported to and quite effectively used in the vaults of the Smithsonian Institution and in the business office of a diamantaire. When fitted with appropriate filters, the spectrometer proved effective for rapidly recording fluorescence spectra, permitting the study of a large number of colored diamonds within the limited time constraints of their availability. Nevertheless, it should be noted that this CCD spectrometer might be inappropriate for investigations that require the higher resolution of traditional research spectrofluorometers.

An important strength of the Ocean Optics spectrometer is that the fiber tip, when placed on the table of the stone, illuminates approximately similar volumes for each stone. Therefore, comparison of relative intensities is a reasonable possibility and likely more so than when luminescence is measured through a stone or from multiple facets of a stone as occurs in traditional measurements. We were able to compare the measured fluorescence intensities of the diamonds tested with this equipment since we used a consistent configuration and testing method; however, we do not feel that the *absolute* intensities we obtained could be reliably compared to data collected using similar experimental setups.

Comparison of the mobile CCD spectrometer with a standard spectrofluorometer revealed some distinct advantages and disadvantages. Speed is one advantage of the CCD instrument: The spectrofluorometer took four hours to collect the series of spectra for each sample shown in figures 7 and 11, whereas the CCD spectrometer generated its spectra in mere seconds. Additionally, a spectrofluorometer cannot record time-dependent spectra, such as phosphorescence spectra, because the instrument slowly scans across the wavelength range. The CCD spectrometer is ideal for collecting such spectra, as data for the entire wavelength range may be collected simultaneously over integration periods as short as 0.5 second.

Figure A-1. The latest CCD spectrometer from Ocean Optics, the USB 4000, is an updated version of the model used for this study. Courtesy of Ocean Optics, Inc.

The spectral resolution of the CCD spectrometer is lower than that of the spectrofluorometer and most other standard spectroscopy equipment available in a gemological laboratory, as smaller peaks typically are obscured by dominant bands, and in most cases only the general shape of the band is provided. Consequently, spectra obtained using the Ocean Optics system may need to be cross-referenced initially with other spectroscopic methods to fully analyze the defects causing the observed fluorescence.

Last, but of singular importance for small labs especially, the CCD spectrometer is quite economical. The latest model (figure A-1) currently sells for about $2,300.

TABLE 1. Summary of fluorescence results for 62 natural-color and 10 treated-color diamonds examined for this study, organized by fluorescence category.

Sample	Color	Weight (ct)	Shape	Other spectroscopy[a]	Observed long-wave UV fluorescence[b]	Key bodycolor group	Fluorescence spectra peak category	Peaks (nm) observed with 350 nm excitation (dominant peak in bold type)
Natural-Color Diamonds: Category 1								
B55[c,d]	Pink	0.48	Pear	nt	Strong blue	Pink	1	**450**, 490
B58	Pink	0.44	Pear	nt	Strong blue	Pink	1	**450**, 486
B59[d]	Purplish pink	0.36	Pear	nt	Strong blue	Pink	1	**451**, 488
B121	Deep pink	0.53	Marquise	nt	Weak blue	Pink	1	**451**, 491
B224	Reddish purplish pink	0.67	Marquise	nt	Very weak blue	Pink	1	**460**, 500
B226	Pink	0.42	Pear	nt	Moderate blue	Pink	1	**450**, 490
DeYoung Pink[d]	Fancy Light purplish pink	2.09	Pear	nt	Very strong blue	Pink	1	**460**, 485
GIA 12172-9	Faint pink	0.16	Rough	UV-Vis-NIR, FTIR	Moderate chalky blue	Pink	1	**450**, 490
GIA 21194	Pink	0.42	Rough	UV-Vis-NIR, FTIR	Moderate blue	Pink	1	**450**, 484
GIA 21232	Deep pink	0.61	Rough	UV-Vis-NIR, FTIR	Moderate greenish blue	Pink	1	**450**, 485
B1	Intense yellow	1.47	Trillion	nt	Weak blue	Yellow	1	**450**, 490
B157	Yellow	1.04	Oval	nt	Moderate blue	Yellow	1	**453**, 495
B173[d]	Yellow	1.06	Half-moon	nt	Weak blue	Yellow	1	**453**, 495
B43[d]	Fancy white	1.93	Pear	FTIR	Moderate blue	Fancy white	1	**450**, 497
B146	Fancy white	2.11	Pear	FTIR	Moderate blue	Fancy white	1	**450**, 485
B223[d]	Fancy white	1.92	Marquise	FTIR	Weak blue	Fancy white	1	**450**, 500
B190	Gray green (chameleon)	0.88	Marquise	FTIR	Moderate white	Gray-green (incl. chameleon)	1	**450**, 490
B11	Green	1.15	Cushion	nt	Moderate blue	Green	1	**450**, 490
Natural-Color Diamonds: Category 2								
B17	Yellow-green	0.55	Radiant	nt	Strong yellowish green	Yellow-green	2	441, **526**
B96[e]	Green-yellow	0.97	Oval	nt	Strong green-blue	Yellow-green	2	449, **518**
B137	Yellow-green	1.20	Pear	nt	Very strong green	Yellow-green	2	525
B194	Green-yellow	0.51	Oval	nt	Very strong green	Yellow-green	2	445, **527**
B213	Yellow-green	0.46	Marquise	nt	Strong green	Yellow-green	2	447, **523**
B236[f]	Intense green-yellow	0.91	Radiant	nt	Very strong greenish blue	Yellow-green	2	445, **523**
B239[f]	Intense green-yellow	1.03	Radiant	nt	Very strong green	Yellow-green	2	446, **524**
B98	Brown	0.54	Round	nt	Moderate red	Brown	2	510
B100	Greenish orangy brown	1.40	Pear	nt	Weak yellowish green	Brown	2	520
B167	Yellowish brown	0.76	Marquise	nt	Weak yellowish green	Brown	2	450, **520**
GIA 12172-1	Yellowish brown	0.66	Rough	UV-Vis-NIR, FTIR	Very strong orange	Brown	2	532
GIA 12172-5a	Pinkish orangy brown	0.40	Rough	UV-Vis-NIR, FTIR	Moderate orangy yellow	Brown	2	520
GIA 12172-5b	Orangy brown	0.26	Rough	UV-Vis-NIR, FTIR	Very strong yellow	Brown	2	525
B16[d]	Violet	0.31	Shield		Inert	Violet	2	445, **524**
GIA 12172-2	Faint yellow	0.58	Rough	UV-Vis-NIR, FTIR	Moderate chalky blue	Yellow	2	450, **520**
Natural-Color Diamonds: Category 3								
B13	Gray-blue	0.31	Heart	FTIR	Strong green	Blue-gray	3	530
B31	Gray-blue	0.58	Round	FTIR	Moderate blue	Blue-gray	3	450, **530**
B187[d]	Blue-gray	0.62	Marquise	FTIR	Weak blue	Blue-gray	3	532
B163	Violet	0.36	Pear		Weak green	Violet	3	535
B24[d]	Gray-green	0.34	Round	FTIR	Strong yellowish white	Gray-green (incl. chameleon)	3	450, **547**
B32	Gray-green (chameleon)	1.74	Round	FTIR	Moderate chalky yellow	Gray-green (incl. chameleon)	3	450, **545**
B70	Gray-green (chameleon)	1.01	Half-moon	FTIR	Strong orangy yellow	Gray-green (incl. chameleon)	3	555
B87	Gray-green (chameleon)	1.00	Marquise	FTIR	Strong yellowish white	Gray-green (incl. chameleon)	3	450, **542**
B127	Gray-green (chameleon)	0.31	Round	FTIR	Moderate orangy yellow	Gray-green (incl. chameleon)	3	553

Sample	Color	Weight (ct)	Shape	Other spectroscopy[a]	Observed long-wave UV fluorescence[b]	Key bodycolor group	Fluorescence spectra peak category	Peaks (nm) observed with 350 nm excitation (dominant peak in bold type)
Natural-Color Diamonds: Category 3 (cont.)								
B184	Gray-green (chameleon)	0.95	Pear	FTIR	Moderate yellow	Gray-green (incl. chameleon)	3	555
B231[e]	Chameleon	0.79	Kite	FTIR	Strong yellow	Gray-green (incl. chameleon)	3	449, **548**
B234	Chameleon	1.37	Oval	FTIR	Strong yellow	Gray-green (incl. chameleon)	3	450, **555**
GIA 12172-8b	Gray-green	0.52	Rough	UV-Vis-NIR, FTIR	Moderate orange-yellow	Gray-green (incl. chameleon)	3	540
GIA 487947202	Fancy Dark grayish yellowish green (chameleon)	0.70	Pear	UV-Vis-NIR, FTIR	Moderate yellow	Gray-green (incl. chameleon)	3	450, **548**
GIA 487988302	Fancy brownish greenish yellow (chameleon)	2.11	Heart	UV-Vis-NIR, FTIR	Very strong orangy yellow	Gray-green (incl. chameleon)	3	558
GIA 488015402	Fancy Deep brownish greenish yellow (chameleon)	0.65	Rectangle	UV-Vis-NIR, FTIR	Very strong orangy yellow	Gray-green (incl. chameleon)	3	554
B2	Brownish yellow-orange	1.02	Emerald	nt	Moderate yellowish orange	Orange	3	540
B33	Vivid yellow-orange	1.17	Pear	nt	Strong yellow-orange	Orange	3	555
B56	Vivid yellowish orange	1.67	Oval	nt	Moderate yellow-orange	Orange	3	552
B72	Yellowish orange	0.77	Round	nt	Moderate yellow	Orange	3	450, **546**
B78	Brownish yellow-orange	0.63	Round	nt	Weak orange	Orange	3	560
B166	Yellow-orange	0.81	Oval	nt	Moderate orange	Orange	3	545
B218	Orange	0.45	Pear	nt	Very strong orange	Orange	3	450, **548**
GIA 12172-8a	Yellowish orange	0.19	Rough	UV-Vis-NIR, FTIR	Moderate whitish orange	Orange	3	535
Other Natural-Color Diamonds								
B172	Yellow-orange	0.52	Round	nt	Weak brownish orange	Orange	Other	610
B181	Yellow-orange	0.58	Round	nt	Very weak brownish orange	Orange	Other	608
B39	Purple	1.60	Oval	nt	Inert	Purple	Inert	None
B232	Purple	0.17	Oval	nt	Inert	Purple	Inert	None
DeYoung Red[e]	Brownish red	5.03	Round	nt	Very weak yellow	Red	Inert	None
Treated-Color Diamonds								
GIA 21503	Green	0.31	Round	FTIR	Inert	Green	1	**450**, 490
GIA 21506	Bluish green	0.20	Round	UV-Vis-NIR, FTIR	Inert	Green	2	460, **520**
GIA 21509	Bluish green	0.42	Round	UV-Vis-NIR, FTIR	Strong blue	Green	1	**450**, 490
GIA 21510	Green	2.05	Round	FTIR	Inert	Green	1	**450**, 495
GIA 21512	Green	0.32	Round	UV-Vis-NIR, FTIR	Strong blue	Green	1	**450**, 490
GIA 21513	Greenish blue	0.26	Round	UV-Vis-NIR, FTIR	Weak bluish green	Blue	1	**450**, 487
GIA 21518	Green	0.26	Rough	FTIR	Inert		1	**450**, 490
GIA 21542	Greenish yellow	0.39	Marquise	UV-Vis-NIR, FTIR	Moderate greenish blue	Yellow-green	2	450, **525**
GIA 22020	Greenish yellow	0.44	Round	UV-Vis-NIR, FTIR	Strong greenish yellow	Yellow-green	2	444, **525**
GIA 22700	Brownish orangy yellow	0.90	Round	FTIR	Inert	Yellow	2	523

[a] For all samples tested by FTIR, the diamonds were classified as type Ia. Abbreviation: nt = not tested.

[b] Observed using standard long-wave UV lamps.

[c] A map showing the location of the diamonds in the Aurora Butterfly collection as they correspond to figure 1 is provided in the G&G Data Depository.

[d] This diamond showed blue fluorescence when examined with the DiamondView instrument.

[e] This diamond showed blue fluorescence, accompanied by areas of green, when examined with the DiamondView instrument.

[f] This diamond showed green fluorescence when examined with the DiamondView instrument.

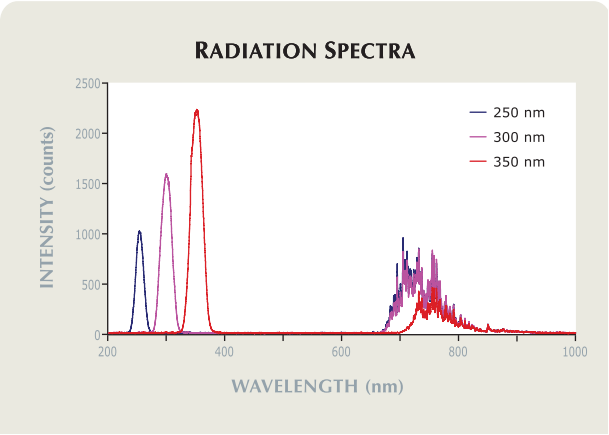

Figure 3. This plot shows the spectra of radiation used to excite the diamonds for the fluorescence spectroscopy measurements. A Corning 7-54 filter removes the light in most of the visible region of the spectrum (~400–650 nm). A variable filter further reduces the light to a narrow band in the UV region. The position of the variable filter determines the wavelength of maximum intensity of the UV radiation. Shown here are three experiments using an empty sample chamber with the variable filter positioned to give 250, 300, and 350 nm as the peak intensity. Unfiltered light is present at wavelengths higher than 650 nm.

was performed. Despite the filters, in some cases the spectra contained second-order artifacts (i.e., at twice the excitation wavelength) that were caused by the spectrometer grating.

The filters were removed for the phosphorescence measurements, because the filtered incident UV radiation necessary to perform the fluorescence measurements was insufficient to excite measurable phosphorescence in many of the diamonds. (Similarly, some samples might have exhibited fluorescence that was too weak for this system to detect.) The phosphorescence spectra were collected after an exposure period of 20 seconds; our initial testing indicated that longer exposure times did not yield significantly better results. During decay, the spectra were collected over integration times of 0.5, 1, and 2 seconds.

For the purpose of describing the fluorescence, we assigned intensity designations relative to the entire dataset. The empirical boundaries we used to describe fluorescence strength were based on the peak intensity over the 30-second collection period: *very weak* (<20 counts), *weak* (20–100 counts), *moderate* (100–600 counts), *strong* (600–1000 counts), and *very strong* (>1000 counts). These descriptors generally correspond to visual perceptions of fluorescence intensity.

At GIA in Carlsbad, we used a Thermo Aminco Bowman II Luminescence spectrofluorometer to investigate the fluorescence spectra of four diamonds (GIA nos. 12172-5b, 12172-8b, 21194, and 21542) to provide a comparison with the measurements made using the Ocean Optics equipment. Fluorescence was excited at wavelengths ranging from 220 to 400 nm (5 nm intervals), and the fluorescence spectra were recorded in the 370–750 nm range (1 nm resolution).

DiamondView Imaging. Fourteen samples were examined with the DiamondView instrument, which uses ultra-short-wave UV radiation at <230 nm, and the resulting fluorescence and phosphorescence were imaged using a CCD camera. We wished to compare the results obtained with ultra-short-wave UV to those from conventional UV lamps. Additionally, the DiamondView should illustrate any spatial differences in the observed fluorescence spectrum. The samples imaged by DiamondView were randomly selected from the Aurora Butterfly collection.

Absorption Spectroscopy. To assess the identity of the fluorescence bands, we measured ultraviolet–visible–near infrared (UV-Vis-NIR) and Fourier-transform infrared (FTIR) spectra that would better show the defects present in the diamonds.

We obtained UV-Vis-NIR spectra on most of the 22 samples from the GIA collections (see table 1) at the GIA Laboratory in Carlsbad using a Thermo-Spectronic Unicam UV500 spectrophotometer over the range of 250–850 nm with a sampling interval of 0.1 nm. The faceted samples were cooled in a cryogenic cell using liquid nitrogen and oriented with the beam passing through the girdle plane.

We recorded FTIR spectra on all 22 diamonds from the GIA collections at GIA Carlsbad and on 15 diamonds from the Aurora Butterfly collection at GIA New York (see table 1). Spectra were collected in the mid-infrared range (6000–400 cm^{-1}, at 1 cm^{-1} resolution) at room temperature with a Thermo-Nicolet Magna IR 760 FTIR spectrometer at GIA in Carlsbad and a Thermo-Nicolet Nexus 670 FTIR spectrometer at GIA in New York. We ran a total of 1,024 scans per sample to improve signal-to-noise ratios. The concentrations of A and B aggregates were calculated from these spectra using an algorithm derived from Kiflawi et al. (1994) and Boyd et al. (1995). The FTIR spectra were baseline corrected and normalized using the two-phonon region of a type IIa diamond.

RESULTS

The results of the spectroscopic measurements are described below according to three main categories of diamonds that exhibit similar fluorescence spectra at long wavelengths. In most cases, these categories corresponded well to the diamonds' bodycolors, which are discussed within each grouping. FTIR and UV-Vis-NIR spectroscopic data are also described below. Phosphorescence spectra for these samples, and for an additional 32 natural-color diamonds from the Aurora Heart and Aurora Butterfly collections, can be found in the *G&G* Data Depository at www.gia.edu/gemsandgemology. A summary of the phosphorescence results for the natural-color diamonds is reported in box B.

Category 1: Fluorescence Spectra with Dominant Peaks at ~450 and ~490 nm. All diamonds described in this section showed similar fluorescence spectra (see, e.g., figure 4). Most of the natural-color diamonds had yellow, fancy white, and pink bodycolors, but one green and one gray-green natural-color diamond also followed this fluorescence pattern. Six irradiated diamonds also showed this fluorescence pattern with weak-to-moderate intensity; they had green to greenish blue bodycolors.

All 10 pink diamonds, including the DeYoung Pink, showed moderate fluorescence with peak intensity at ~450 and ~490 nm. One pink diamond examined with the high-resolution spectrofluorometer (GIA 21194) showed the zero-phonon line (ZPL) at 415 nm related to the N3 defect and its lower-energy (higher-wavelength) sideband.

In general, most yellow diamonds show weak or no fluorescence; of those that do fluoresce, blue has been reported as the dominant color (King et al., 2005). Here, three of the four natural-color yellow diamonds without a greenish component exhibited moderate-to-strong fluorescence with peaks at ~450 and ~490 nm.

The three fancy white diamonds showed moderate fluorescence peaks at the same wavelengths. One green and one gray-green (chameleon) diamond showed moderate-to-strong fluorescence intensities that were consistent with category 1.

Absorption Spectra. The UV-Vis-NIR spectra for three natural-color diamonds and three treated samples from the GIA collections with category 1 fluorescence showed the N3-related ZPL at 415 nm. The FTIR spectra of these diamonds, as well as four diamonds from the Aurora Butterfly collection, showed them to be type Ia, generally with both A and B aggregates in various concentrations. All three fancy white diamonds tested by FTIR spectroscopy showed significant concentrations of hydrogen, as evidenced by the 3107 cm^{-1} peak.

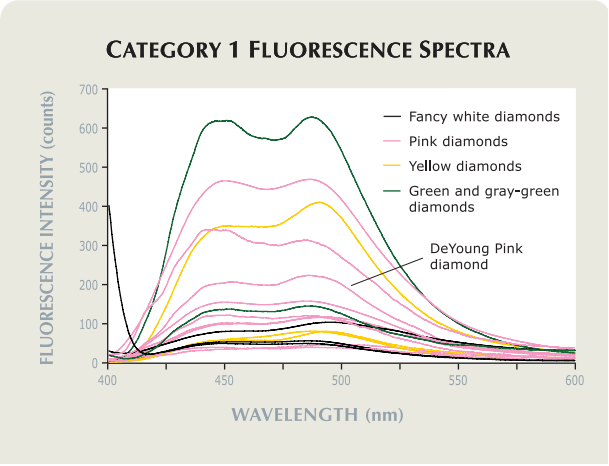

Figure 4. Category 1 fluorescence spectra (excited by 350 nm radiation) of natural-color diamonds with various bodycolors show similar peak positions and shapes due to the presence of the N3 defect.

Category 2: Fluorescence Spectra with a Dominant Peak at ~525 nm. Figure 5 shows a compilation of 350 nm–excited fluorescence spectra for the seven diamonds in the yellow-green group, six brown, and two other natural-color diamonds (violet and yel-

Figure 5. Category 2 fluorescence spectra (excited by 350 nm radiation) of natural-color diamonds with various bodycolors show similar peak locations and shapes. The responsible mechanism is the presence of H3 centers.

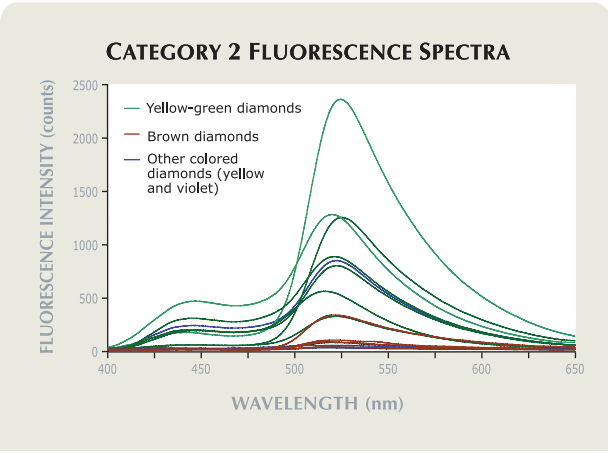

BOX B: PHOSPHORESCENCE SPECTROSCOPY OF NATURAL-COLOR DIAMONDS

Phosphorescence is quite rare in natural near-colorless diamonds, and its presence has been used to indicate a synthetic origin, as many such gems grown at high pressures and temperatures display some phosphorescence (Shigley et al., 2002). In our study, however, we recorded measurable phosphorescence on 56 of the 94 natural-color diamonds examined (see *G&G* Data Depository), with an intensity ranging from very weak to moderate, except for a few colors such as gray-green and blue that phosphoresce quite strongly (again, see Eaton-Magana et al., 2008). None of the irradiated diamonds we tested showed measurable phosphorescence. In our samples, there was a larger variety of peak shapes and positions in the phosphorescence than fluorescence spectra across all bodycolors, but general consistency within most bodycolors. Diamonds showing phosphorescence that is strong or that appears anomalous from the spectra obtained for natural stones may be suspect. Some diamonds showing strong phosphorescence (i.e., gray-green [most of which were chameleon] stones) are discussed in detail below, and the remaining bodycolors will be briefly summarized.

The empirical boundaries employed for describing phosphorescence spectra were: *very weak*, less than 5 counts; *weak*, 5–20 counts; *moderate*, 20–100 counts; *strong*, 100–300 counts; and *very strong*, >300 counts. When recording phosphorescence spectra, we evaluated its half-life instead of its duration. *Half-life* is defined as the time necessary for the initial intensity to decrease by one-half (see Watanabe et al., 1997). The more common term in gemology, *duration*, may be appropriate for visual observations, but it is actually a combination of two independent variables: initial intensity and the rate of decay. With phosphorescence spectroscopy, we are able to separate these variables to better distinguish one diamond from another. Additionally, the observed duration may be influenced not only by initial intensity, but also by the size of the stone. Therefore, *half-life* is preferable as it provides a better measure of the differences between the rates of phosphorescence decay because it is not influenced by these other factors. The longer the half-life is, the slower the rate of phosphorescence decay will be. Additionally, the shape of the decay curve (i.e., the rate at which intensity decreases with time) can indicate the mechanism causing the phosphorescence (again, see Watanabe et al., 1997).

Within most of the color groups, there were wide variations in calculated half-lives, with values between 0.2 and 4.8 seconds (for comparison, the half-life of the Hope Diamond is 8.2 seconds and the longest half-life we measured was 25.2 seconds [B234]).

The pink diamonds phosphoresced at weak-to-moderate intensity in a variety of wavelengths (half-life: 0.2–4.8 seconds). Two of the four yellow diamonds showed very weak phosphorescence centered at ~600 nm (half-life: 1.3–3.5 seconds); the other two did not show measurable phosphorescence. The three fancy white diamonds phosphoresced at moderate-to-strong intensity at ~450 and ~490 nm, identical to their fluorescence (half-life: 1.2–2.1 seconds). Six of 10 diamonds in the yellow-green group phosphoresced; they generally showed weak phosphorescence at 570–585 nm (half-life: 1.7–4.7 seconds). Seven violet and three type Ia blue-gray diamonds had weak-to-moderate phosphorescence at 565 nm (half-life: 0.25–4.2 seconds), and 4 of the 11 orange diamonds showed weak phosphorescence at a variety of wavelengths. None of the brown diamonds showed phosphorescence.

Therefore, while pink and orange diamonds showed a variety of phosphorescence patterns within their bodycolor range, we observed consistency within the color range for the other diamonds tested. Of particular interest were the gray-green (including chameleon) diamonds.

All eight gray-green (including chameleon) diamonds in the Aurora Butterfly collection and the four tested at GIA exhibited moderate phosphorescence

low) that showed distinctive asymmetry: a strong onset of fluorescence at ~500 nm, a peak maximum at ~525 nm (±7 nm), and a long tail on the high-wavelength side. Most of the spectra in figure 5 also showed a secondary peak at ~450 nm.

The yellow-green diamonds predominantly showed weak-to-moderate fluorescence intensity at ~445 nm and very strong asymmetric fluorescence centered at ~525 nm. Figure 6 shows fluorescence spectra at different excitation wavelengths for a green-yellow diamond that is representative of all seven diamonds of this color range.

The six brown diamonds showed weak-to-moderate fluorescence spectra with peaks centered at 510–532 nm. Figure 7 shows fluorescence spectra for one sample (GIA 12172-5b) obtained from the spec-

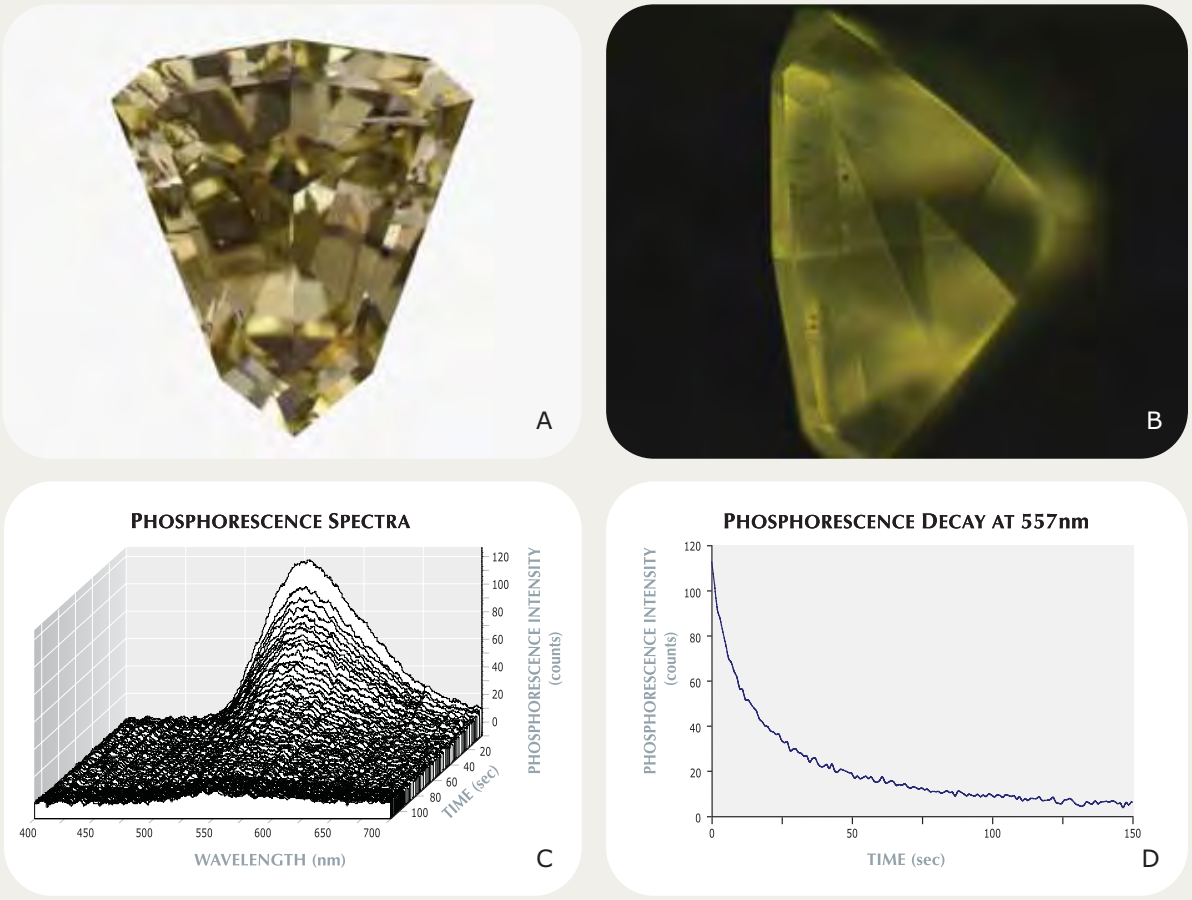

Figure B-1. Sample B231, a 0.79 ct chameleon diamond (A), shows greenish yellow phosphorescence in the DiamondView (B). Its phosphorescence spectra illustrate the decay of the diamond's phosphorescence with time (C). The phosphorescence spectrum at the back of the three-dimensional plot was taken immediately after the UV lamp was extinguished. The decay in intensity of the peak maximum (557 nm) with time is also provided (D). The calculated half-life is 13 seconds. Photos by Jian Xin (Jae) Liao (A) and S. Eaton-Magaña (B).

with peaks at 557–562 nm. These diamonds showed the greatest consistency in peak position of any of the color groups, and greater consistency in their phosphorescence than fluorescence spectra. The half-lives were long, ranging from 3.4 to 25.2 seconds. These samples had a similar rate of decay as that described by Watanabe et al. (1997) for synthetic type IIb diamonds. Figure B-1 shows a typical phosphorescence peak for the gray-green (chameleon) diamonds, and a corresponding plot of the decay of the phosphorescence maximum at 557 nm. Additional research is necessary to fully characterize the phosphorescence mechanism in these diamonds and to explain the variability in the measured half-lives.

trofluorometer compared to spectra obtained from the CCD spectrometer. The spectrofluorometer data show ZPLs for the N3 and H3 centers at 415 and 503 nm, respectively, along with their related sidebands. Due to the lower resolution of the CCD spectrometer, only the sidebands are observed in figure 7 (right).

A yellow diamond had a weak fluorescence spectrum, and a violet diamond showed a moderate fluorescence spectrum. Four irradiated diamonds also showed category 2 fluorescence: weak spectra were measured for the brownish orangy yellow and bluish green samples, and strong to very strong spectra were obtained from the greenish yellow samples.

Absorption Spectra. UV-Vis-NIR absorption spectra were collected for four natural and three treated

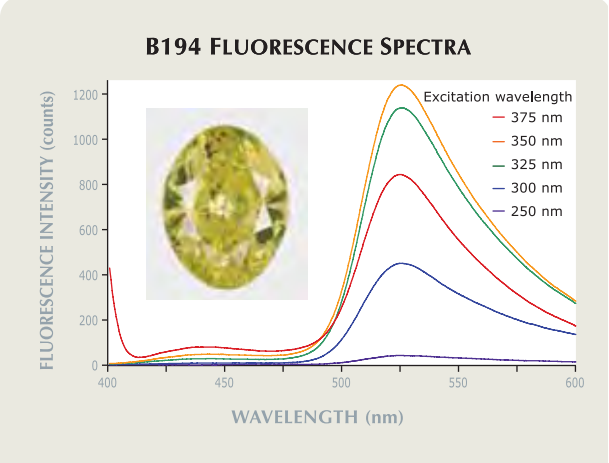

Figure 6. The fluorescence spectra of sample B194, a 0.51 ct green-yellow diamond, show a dominant peak at ~525 nm (i.e., category 2 fluorescence). The most intense fluorescence occurs when the stone is excited by UV radiation at ~350 nm. Photo by Jian Xin (Jae) Liao.

diamonds from the GIA collections that had category 2 fluorescence spectra (again, see table 1). All UV-Vis-NIR spectra showed the H3-related ZPL at ~504 nm. This peak was only observed in diamonds showing the category 2 fluorescence spectra. FTIR spectra of these diamonds along with an additional treated diamond showed they were type Ia, generally with both A and B aggregates in variable amounts.

Category 3: Fluorescence Spectra with a Dominant Peak at ~550 nm. Figure 8 shows a compilation of the category 3 fluorescence spectra, excited by 350 nm UV radiation, obtained from orange, violet, gray-green (including chameleon), and the type Ia diamonds in the blue-gray group.

One violet diamond along with three diamonds in the blue-gray group had fluorescence spectra with weak-to-moderate intensity at 525–530 nm. In a related study, 93% of the 67 gray-to-blue diamonds tested did not show measurable fluorescence, but showed phosphorescence spectra that proved to be distinctive of type IIb diamonds (Eaton-Magaña et al., 2008).

Most of the gray-green (including chameleon) diamonds indicated weak fluorescence at ~450 nm and moderate-to-strong fluorescence extending from ~450 to ~650 nm, with the center of the band ranging from 535 to 558 nm. Data obtained for a gray-green diamond using a spectrofluorometer at excitation wavelengths from 220 to 400 nm showed many interesting features (figure 9, left). The fluorescence intensity was quite low when excited at short UV wavelengths. However, as the excitation wavelength increased, the fluorescence intensity increased, with contributions from peaks centered at 495 and ~545 nm. The intensity reached a maximum when excited by UV radiation at 340–345 nm and then decreased as the wavelength of the excitation intensity increased further. At the higher excitation wave-

Figure 7. The graph on the left shows the fluorescence spectra for a 0.26 ct orangy brown diamond (GIA 12172-5b) collected at excitation wavelengths from 220 to 400 nm using the spectrofluorometer. Both N3- and H3-related luminescence may be observed, with ZPLs at 415 and 504 nm, respectively. The plot on the right shows the corresponding (lower resolution) fluorescence spectra obtained from the Ocean Optics CCD spectrometer.

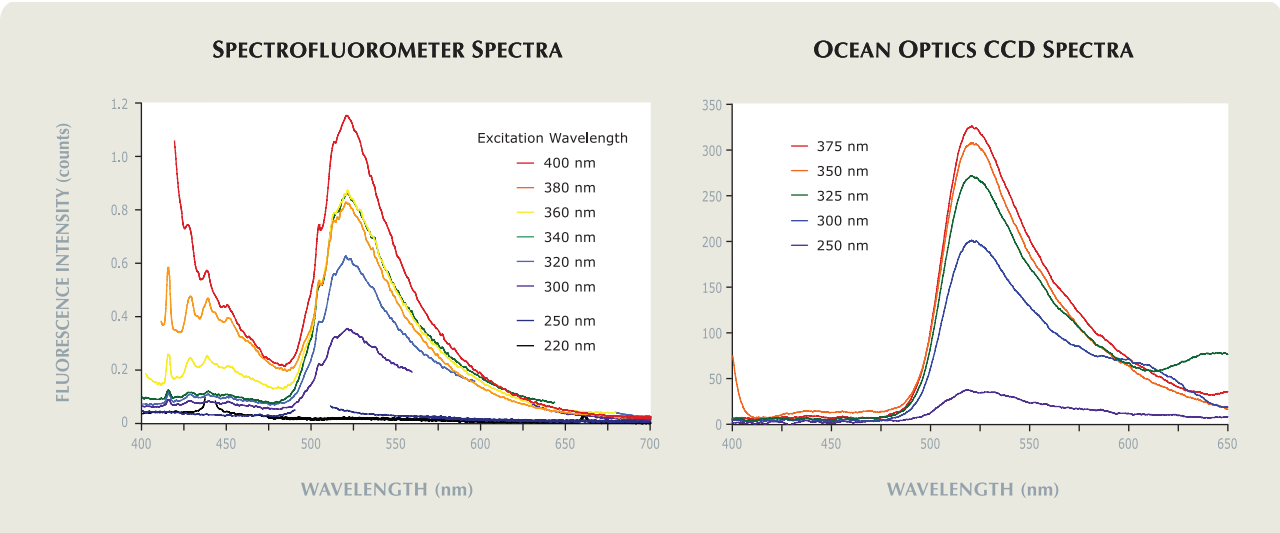

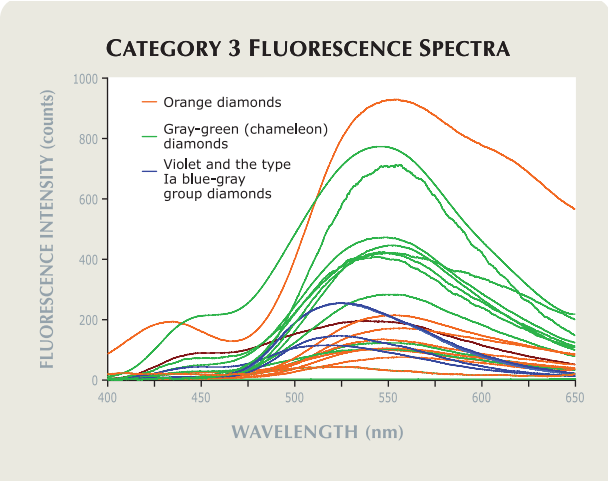

Figure 8. Category 3 fluorescence spectra (excited by 350 nm radiation) of the orange, violet, gray-green (including chameleon), and type Ia blue-gray diamonds have similar peak locations and shapes.

lengths, the two fluorescence peaks were centered at 495 and ~560 nm. The greater resolution of this instrument compared to the CCD spectrometer (figure 9, right) revealed the additional peak at 495 nm.

Of the 10 orange diamonds measured by fluorescence spectroscopy, seven showed weak-to-moderate and one showed strong category 3 fluorescence spectra with peaks ranging from 540 to 560 nm. Several of the diamonds also showed subordinate peaks at ~450 nm. The spectra at different excitation wavelengths illustrated in figure 10 for a Fancy Vivid yellowish orange diamond are representative of the other samples.

Absorption Spectra. FTIR spectra were collected for all eight gray-green (including chameleon) diamonds from the Aurora Butterfly collection with category 3 fluorescence spectra (again, see table 1), and FTIR and UV-Vis-NIR spectra were collected for the five diamonds from the GIA collections showing this fluorescence pattern. The UV-Vis-NIR spectra for these diamonds showed prominent bands centered at ~370 and ~480 nm.

The FTIR spectra of three diamonds in the blue-gray group indicated that they are type Ia instead of type IIb. Most blue diamonds receive their color from boron and are designated type IIb (see Fritsch and Scarratt, 1992, for an explanation of diamond types). The nitrogen concentrations in the category 3 diamonds generally were much lower for both the A aggregate (up to 114 ppm) and B aggregate (up to 22 ppm) compared to diamonds from categories 1 and 2: up to 415 and 890 ppm, respectively, for the A aggregate and up to 700 and 270 ppm, respectively, for the B aggregate.

Figure 9. These fluorescence spectra of a 0.52 ct gray-green diamond (GIA 12172-8b) were collected at excitation wavelengths of 220–400 nm with a spectrofluorometer (left) and at wavelengths of 250–375 nm with an Ocean Optics CCD spectrometer (right). Spectrofluorometer second-order artifacts (i.e., peaks at twice the excitation wavelength) have been removed for clarity. Also shown, at left, are the fluorescence spectra excited by wavelengths equivalent to a short-wave UV lamp (255 nm) and the DiamondView (~220 nm). The higher-resolution spectrofluorometer revealed a peak at 495 nm that was not visible with the CCD spectrometer.

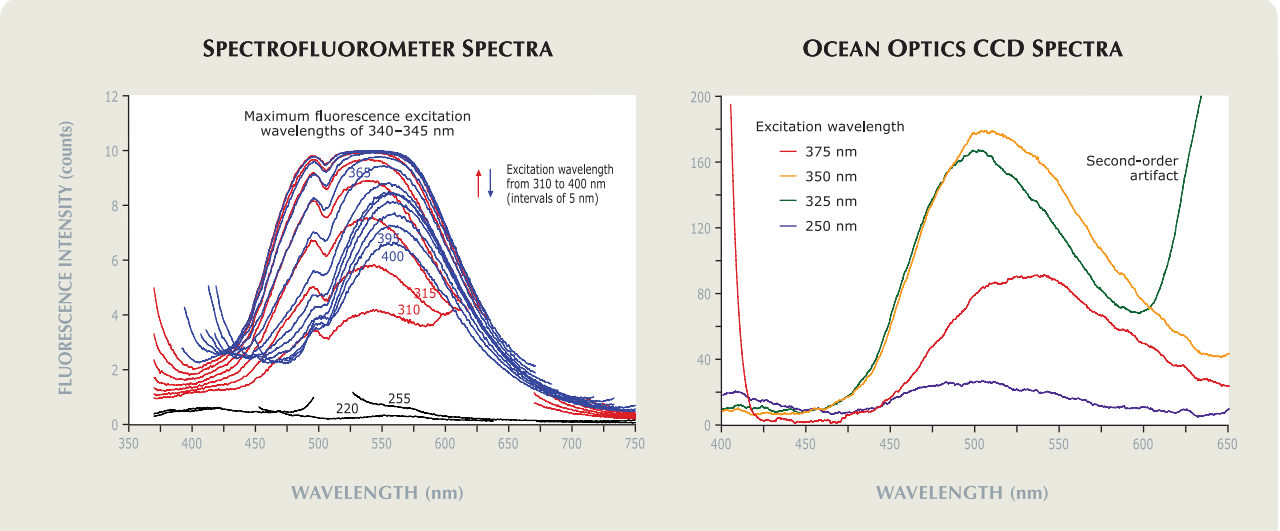

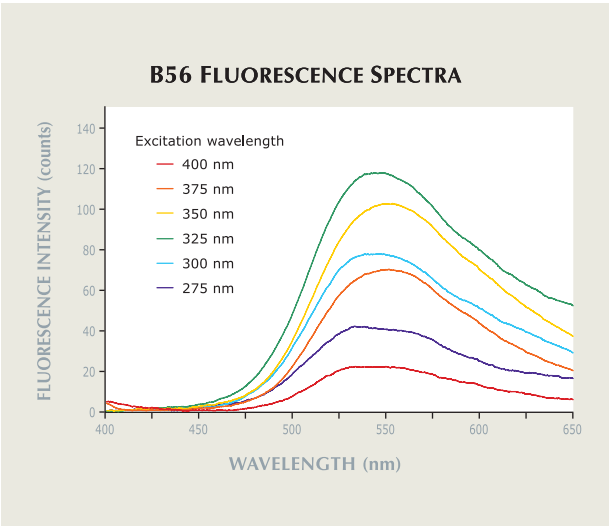

Figure 10. A 1.67 ct Fancy Vivid yellowish orange diamond, B56 (left), fluoresces moderate yellow-orange (center) with a long-wave UV lamp. The fluorescence spectra show a dominant peak at ~550 nm (i.e., category 3 fluorescence, right). The most intense fluorescence was recorded when excited by UV radiation at 325 nm. Photos by Jian Xin (Jae) Liao.

The orange, type Ia blue-gray group, and gray-green (including chameleon) diamonds that exhibited category 3 fluorescence spectra and were tested by FTIR spectroscopy all showed significant concentrations of hydrogen, as evidenced by the 3107 cm^{-1} peak.

Natural Diamonds with Other Fluorescence Behavior. Two yellow-orange natural-color diamonds (172 and 181) showed fluorescence spectra (figure 11) with a single dominant peak at ~610 nm.

The one red and two purple diamonds were inert or did not show measurable fluorescence spectra. Admittedly, the number of samples we examined was small, but these colors are among the rarest of all natural diamonds. In the DeYoung Red, we observed a barely discernible yellow fluorescence to long-wave UV (inert to short-wave), which was noted also by Shigley and Fritsch (1993), who further documented a green luminescence when excited by 425 nm light. However, we could not discern a fluorescence spectrum with the CCD instrument. In the ultra-short-wave UV wavelengths of the DiamondView, the DeYoung Red showed blue fluorescence and well-defined growth bands, as well as a few narrow green zones (figure 12).

Figure 13 provides a summary of the categories of fluorescence spectra collected for the natural-color diamonds we examined, organized by key bodycolor.

Gemological Observations. The observed colors and intensities of long-wave UV fluorescence are summarized in table 1. Note that the fluorescence spectra did not always correlate directly to the fluorescence color observed with a standard UV lamp. Some reasons for such discrepancies are detailed in the Discussion section. The short-wave fluorescence was weaker for all the natural-color diamonds, and some diamonds exhibited no apparent luminescence to either UV wavelength. While no significant inhomogeneity or turbidity in the fluorescence colors was noted, we did not look specifically for such characteristics. A few samples showed a different fluorescence color when examined by the DiamondView, which was probably due to the difference in the excitation wavelength and/or saturation of the CCD camera used in the DiamondView instrument.

Figure 11. The fluorescence spectra of these two natural-color diamonds (B172 and B181) differ from those in the three common categories, with broad peaks centered at ~610 nm.

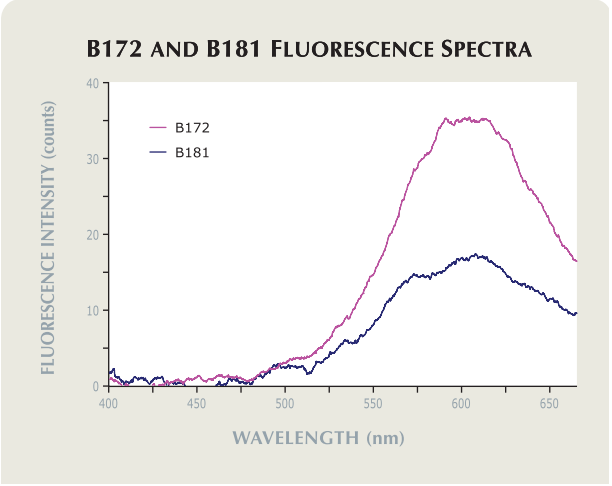

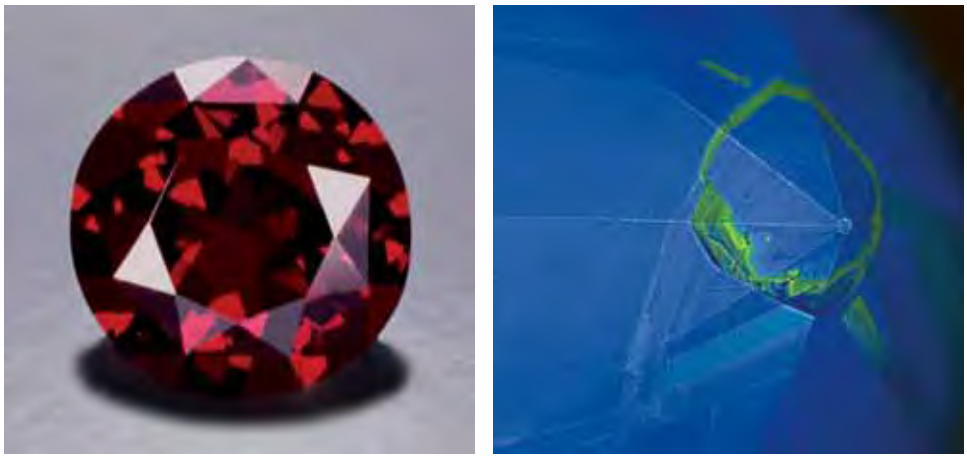

Figure 12. The DeYoung Red, at 5.03 ct, is one of the largest red diamonds in the world. Its DiamondView image shows a dominant blue fluorescence that is also typically observed in pink diamonds. Photos by Chip Clark (left) and S. Eaton-Magaña (right).

DISCUSSION

The vast majority of the fluorescence spectra for the natural-color diamonds tested fell into three categories with respect to the peak wavelengths and shapes. In fact, only two of the 62 natural-color diamonds described in this article (again, see figure 11) had peak positions other than those described in the three major categories (~450 and ~490 nm; ~525 nm; and ~550 nm). As shown in figure 13, the colored diamonds we tested are largely segregated into these three categories on the basis of their bodycolor. The information conveyed by these categories may provide clues to the origin of their color.

Category 1: Fluorescence Spectra with Dominant Peaks at ~450 and ~490 nm. For all the diamonds represented in figure 4, the fluorescence spectra show double peaks with maxima at ~450 (±12) nm and ~490 (±13) nm. This spectral pattern generally manifested itself as blue and is likely representative of fluorescence spectra for the vast majority of blue-fluorescing diamonds (e.g., Moses et al., 1997).

UV-Vis-NIR spectra of three natural and three irradiated diamonds showed the presence of the N3 center—a grouping of three nitrogen atoms in a (111) plane surrounding a vacancy—and higher-resolution spectra using the spectrofluorometer all confirmed that the ~450 and ~490 nm fluorescence peaks in the blue region of the spectrum are derived from the N3 center. The band centered at ~490 nm is artificially high in intensity, which is an artifact of the CCD spectrometer. On a spectrum for one sample obtained with the CCD spectrometer, radiometric correction of the output intensity across the wavelength range decreased the intensity of the ~490 nm peak so that it conformed better with spectra obtained from higher-resolution spectrofluorometers, thus confirming that the two observed peaks originate from the N3 center.

The category 1–fluorescing diamonds derive their bodycolors from different origins. Pink diamonds have a broad absorption band with a peak at 550 nm, which is thought to be due to plastic deformation (Fritsch, 1998). The color of most yellow diamonds is attributed to the N3 center, although some are colored by isolated nitrogen atoms (Fritsch, 1998). Fancy white diamonds are typically colored by light scattered from minute particles, some of which may be carbonates (Titkov et al., 2006), or their color may be related to the nitrogen B aggregate (Fritsch, 1998). Despite their different origins of color, all showed similar fluorescence spec-

Figure 13. Most of the 62 natural-color diamonds tested showed one of three distinct fluorescence spectra. Three diamonds included in this study were inert and two shared a different type of fluorescence spectrum.

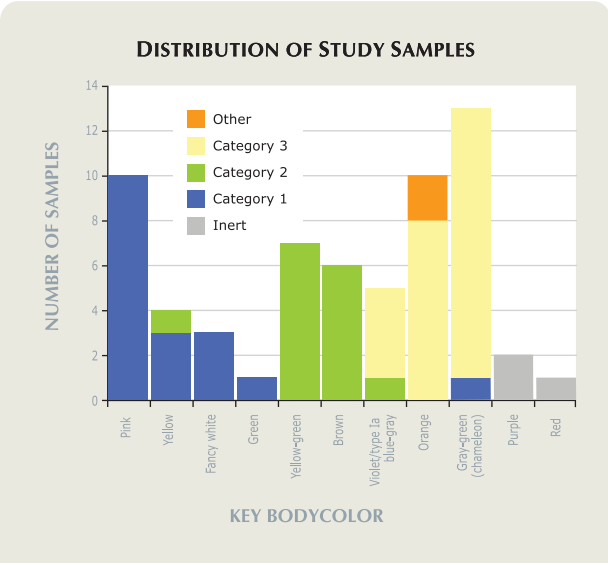

tra, indicating a common tie among them, namely the presence of the common N3 center and the lack of more dominant fluorescing defects or significant concentrations of defects that can quench fluorescence, such as the A aggregate (Davies and Crossfield, 1973; Davies et al., 1974).

The category 1 fluorescence spectrum is associated with the N3 center, as is the subordinate peak at ~450 nm in the categories 2 and 3 fluorescence spectra (i.e., figures 5 and 8). This feature was seen in most of the diamonds, both natural and treated color.

Category 2: Fluorescence Spectra with Dominant Peak at ~525 nm. The spectral pattern shown in figure 5 generally manifested itself as bluish green to yellowish green fluorescence and is likely representative of the vast majority of green-fluorescing diamonds (Fritsch and Waychunas, 1994). The category 2 spectra are nearly identical to cathodoluminescence and photoluminescence spectra of a diamond with H3 defects (Collins and Woods, 1982). All seven of the category 2 diamonds for which UV-Vis-NIR absorption spectra were recorded (see table 1) showed the H3 center at 504 nm, and higher-resolution spectra taken with the spectrofluorometer on two of these samples (e.g., figure 7) confirmed the presence of the H3 center.

The H3 center results when a vacancy is trapped at the nitrogen A aggregate (Collins, 1982a). To create an H3 center, the diamond must be exposed to radiation and heat. These conditions are known to occur naturally, and the H3 center has been observed in natural, untreated diamonds (De Weerdt and Van Royen, 2001), although the luminescence of the center is greatly increased after deliberate irradiation and annealing (Collins et al., 2000).

Although yellow-green and brown diamonds show similar fluorescence spectra, these bodycolors have different origins. The green component of diamond color typically results from radiation damage (Fritsch, 1998). However, this color appearance may also be caused by strong green luminescence (much like the Portuguese Diamond can appear bluish due to its blue fluorescence; Fryer and Koivula, 1986). The specific defect that causes the color of brown diamonds is unknown, but it is believed to be related to the plastic deformation mechanism that also causes pink coloration (Fritsch, 1998). Theoretical modeling has suggested that brown coloration may be related to large vacancy disks (Hounsome et al., 2006).

We observed an inverse correlation between the concentration of A aggregates and the intensity of the 525 nm peak (figure 14); therefore, the presence of A aggregates appears to quench H3-related luminescence. This observation was noted previously (Zaitsev, 2001), and such data confirm the usefulness of this spectrometer for a variety of applications.

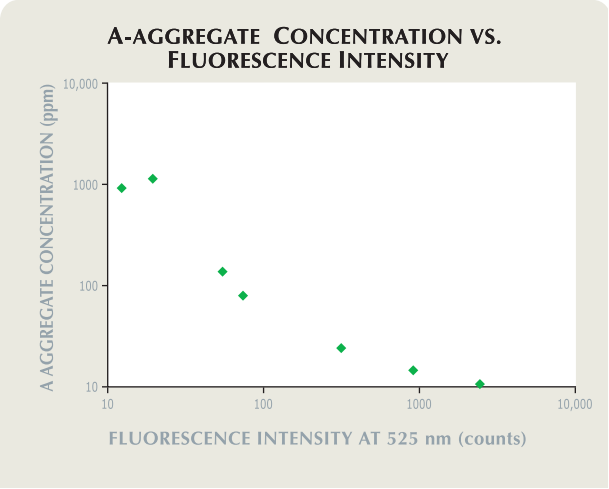

Figure 14. A comparison of the intensity of the green fluorescence at 525 nm with the concentration of A aggregates in each diamond (as calculated from the FTIR spectra) shows an inverse correlation. The fluorescence spectra were collected over 30 seconds, and both concentrations and intensities are presented here on logarithmic scales.

Category 3: Fluorescence Spectra with Dominant Peak at ~550 nm. All the diamonds represented in figure 8 showed similar fluorescence spectra. This spectral pattern generally manifested itself as yellow to orangy yellow fluorescence, and is likely representative of the fluorescence spectra for the vast majority of fluorescence observations within this color range (Fritsch and Waychunas, 1994).

Most of the spectra showed a broad (FWHM ~100 nm), rather symmetrical peak centered at 530–560 nm. They are similar to a fluorescence spectrum published for a 22 ct chameleon diamond (Fritsch et al., 1995), also excited by 350 nm radiation. Nearly all of the category 3 diamonds showed a secondary peak at ~450 nm that correlated to the N3 defect in those samples tested by UV-Vis-NIR spectroscopy. The absorption spectra also showed the presence of the 480 nm band in these diamonds. Previous researchers have observed yellow fluorescence in diamonds with a 480 nm band (Collins, 1980; Collins, 1982b; Hainschwang et al., 2005), or in those that are rich in hydrogen (Fritsch and Scarratt, 1992). The 480 nm band is a common feature in orange and chameleon diamonds (Hainschwang et

al., 2005); however, a great many issues about the origin of the 480 nm band are still unresolved.

The category 3 fluorescence spectra may be linked to the high concentration of hydrogen that was observed in chameleon, other gray-green, type Ia blue-gray, and orange diamonds by FTIR spectroscopy. Among the diamonds from other fluorescence categories that were tested by FTIR, only the fancy white diamonds had consistently measurable hydrogen-related peaks at 3107 cm^{-1}.

Although violet, type Ia blue-gray, gray-green (including chameleon), and orange diamonds may show similar fluorescence spectra, their bodycolors are derived from different origins. Hydrogen has been observed in violet and type Ia gray-to-blue diamonds (Robins et al., 1991; Fritsch and Scarratt, 1992; Fritsch and Scarratt, 1993), but the specific configuration causing the color has not yet been identified. The origin of orange color is unknown (Bosshart, 1999), but it most likely derives from nitrogen-related defects (Fritsch, 1998). The color of gray-green and chameleon diamonds has been linked to the presence of a rare nitrogen-related defect that gives rise to the 480 nm band along with hydrogen centers (Massi et al., 2006).

None of the 10 treated diamonds showed category 3 fluorescence spectra, but study of a broader group of such diamonds is needed to confirm this trend.

Fluorescence Spectra with Dominant Peak at ~610 nm. Two yellow-orange diamonds showed broadband fluorescence with peaks centered at ~610 nm (again, see figure 11). This spectral pattern, which is very different from those described above, would generally manifest itself as brownish orange fluorescence. We were unable to positively identify the defect responsible, but it is likely related to the neutral N-V center with its ZPL at 575 nm (Anderson, 1960, 1962; Martineau et al., 2004). In sample B181, a slight peak at ~575 nm is suggestive of this mechanism as well.

Comparison to Observed Fluorescence. The color of observed fluorescence is typically recorded as a response to long- or short-wave UV radiation. In actuality, many UV lamps do not provide single, isolated peak emissions at 365 nm for long wave and at 254 nm for short wave (Williams, 2007). Instead, long-wave lamps often contain peaks at 404 and 435 nm, in addition to a broad band that extends from the UV into the visible region of the spectrum; likewise, many short-wave lamps show peaks at 315 and 365 nm (i.e., long-wave UV; again, see Williams [2007] for more information). This was the case for the gemological UV lamps used in this study. Therefore, the fluorescence observed using most gemological lamps is a combination of fluorescence excited by several wavelengths and, in the case of long-wave UV, by the influence of light in the visible region (S. Elen, pers. comm., 2007). A stone that is believed to show "weak fluorescence" to short-wave UV may actually be responding to the long-wave component present in the lamp. It is not surprising, then, that the observed color of fluorescence taken with standard long- and short-wave UV lamps may not be directly analogous to the results presented here. The spectra recorded by the fluorescence spectrometer are activated by a narrow range of wavelengths that do not include radiation at other wavelengths and do not extend into the visible range.

While examining the DeYoung Red, we observed a very weak yellow fluorescence using a long-wave UV lamp, but we could not resolve a fluorescence spectrum with the CCD spectrometer. There could be several explanations for this discrepancy. The sensitivity of the instrument may have been too low to detect the yellow fluorescence, while the relatively large size of the DeYoung Red (5.03 ct) aided the visual observation of this luminescence. Alternatively, Shigley and Fritsch (1993) noticed a green luminescence when the diamond was excited at 425 nm. The observed yellow fluorescence when exposed to the long-wave UV lamp could be due to excitation outside the narrow band of UV radiation used in our spectroscopy experiments.

As mentioned above, the additive effect of fluorescence to the eye due to a gemstone's size is also a factor. The Portuguese diamond (figure 15) is famous for its strong blue fluorescence, which can be seen easily in ambient light. However, as the spectra in figure 15 show, the intensity of its fluorescence spectrum is not extraordinarily high relative to those of other diamonds. The combined effect of its large size (127.01 ct) with its fluorescence is what makes this diamond so notable.

In addition to the ambiguity of the excitation wavelength of UV lamps, the interpretation of fluorescence color can be difficult as well. Due to the contribution of subordinate peaks and the length of the tail of a fluorescing band, diamonds with fluorescence emissions of similar origin can yield fluorescence colors that are quite different. Figure 16 shows the effect of a subordinate peak in the diamond fluorescence spectra, and figure 17 shows the effect of a long spectral tail. As demonstrated by

Figure 15. The 127.01 ct very slightly yellow (G-to-I on the GIA color-grading scale) Portuguese diamond (left) is famous for its strong blue fluorescence (center). Yet its fluorescence spectrum (right) reveals that the intensity measured from a limited volume is comparable to that of smaller fancy-colored yellow diamonds that also show category 1 fluorescence. Photos by Chip Clark.

these examples, slight differences in peak positions and shapes may lead to considerable variation in the literature regarding reported fluorescence colors, even if the underlying causes of the luminescence are identical. Furthermore, gemologists could misinterpret the observed fluorescence of two diamonds that appear to fluoresce with similar colors as an indication that they have similar properties. For example, a comparison of observed fluorescence for diamond 1 in figure 16 against diamond 3 in figure 17 shows that both appear as shades of green. However, examination of the corresponding spectra indicates that the defects causing the observed fluorescence appear to be quite different.

Analysis of the Spectrometer. The absolute intensities of fluorescence measured in the spectra will, of course, depend on the UV radiation source. Within this study, we maintained a consistent measurement technique and geometry when using the CCD spectrometer, and we believe that the measured intensities are comparable between these diamonds. Our results were sufficiently consistent that we feel our spectroscopy system (i.e., figure 2; see box A for more information) allows semiquantitative intensity assignments based on the measured counts to replace the visual assessment descriptions that typically are used to describe diamond fluorescence, such as *weak*, *moderate*, and *strong*.

Implications for the Gemologist. Observed fluorescence is often included with the other properties of a diamond. However, the reliability of such data is called into question by the many ambiguities inherent in these observations, such as the viewer's estimation of intensity and color, the effect of the size of the sample, and the actual wavelengths of UV excitation. Here, we investigated the information provided by fluorescence spectroscopy on a wide variety of colored diamonds. Although there are large variations in the fluorescence colors reported for diamond (again, see, Fritsch and Waychunas, 1994), fluorescence spectroscopy was able to distill that variety into three main spectral patterns by discerning the contribution of subordinate peaks and long tails. Although this work was performed exclusively on colored diamonds, we are confident that valuable information could be gained on other gem materials as well.

As stated earlier, diamonds with fluorescence spectra that appear anomalous to the three main categories may be considered suspect. Additionally, the irradiated stones in table 1 indicate that samples with fluorescence spectra that appear similar to these three categories but do not conform to one of the bodycolor designations may be treated. However, with some colored diamonds, such as those with yellow-green bodycolors, fluorescence spectroscopy may not be a reliable indicator of treatment.

Fluorescence and phosphorescence spectra have a number of other potential applications as well. They could help explain unusual fluorescence and phosphorescence, such as the type IIb diamond with multiple colors of phosphorescence reported by Moe and Johnson (2007). Phosphorescence spectroscopy can distinguish between type Ia gray-to-blue diamonds and type IIb blue diamonds (see box B and Eaton-Magaña et al., 2008). In fact, the phosphorescence spectra of type IIb blue diamonds proved so distinctive of each diamond that the researchers termed it a "fingerprint" that could individually classify a type IIb diamond (again, see Eaton-Magaña et al., 2008).

Fluorescence spectroscopy can also help the gemologist distinguish between natural and synthetic diamonds. Martineau et al. (2004) correlated

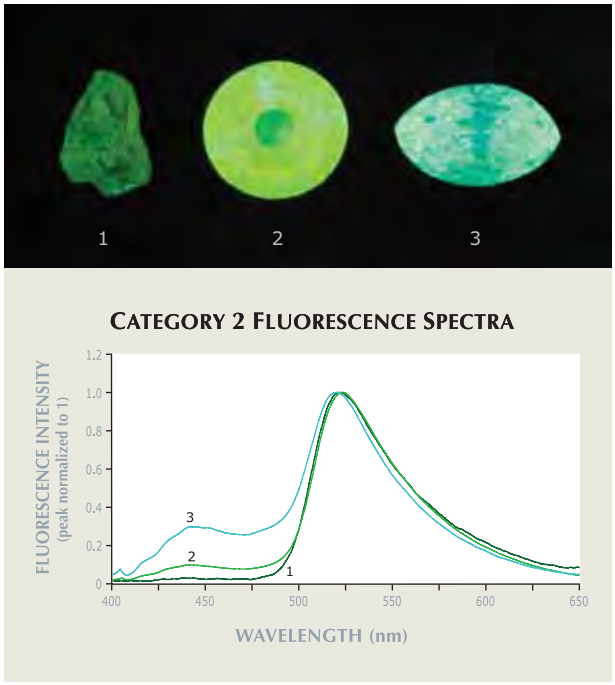

Figure 16. All of these diamonds (GIA 12172-5b [1], GIA 22020 [2], and GIA 21542 [3]) show category 2 fluorescence spectra, with a dominant peak at ~525 nm caused by the H3 defect. However, slight differences in peak shape and the presence of an N3-related subordinate peak centered at ~450 nm cause the observed fluorescence colors to appear different. The fluorescence photo was excited by narrow-band 365 nm radiation (also used to collect the spectra), and not a standard long-wave UV lamp. Photo by Shane Elen.

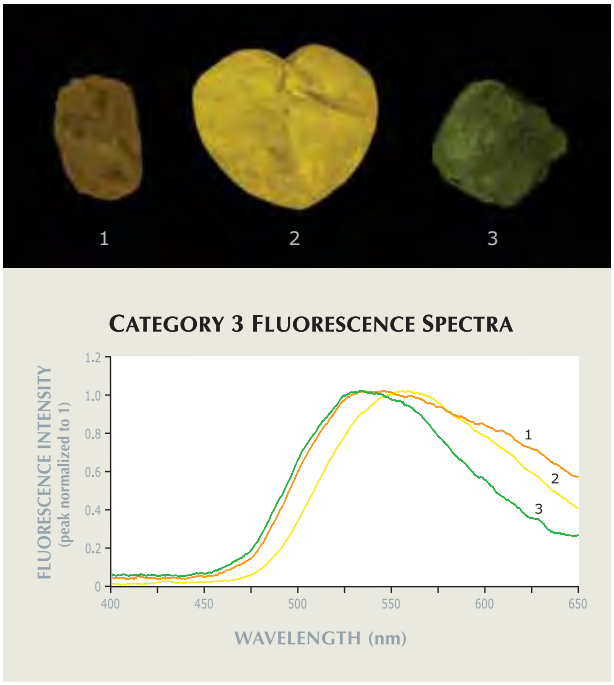

Figure 17. All of these diamonds (GIA 12172-8b [1], GIA 487988302 [2], and GIA 12172-8a [3]) show category 3 fluorescence spectra that are likely related to the 480 nm absorption band. Variations in peak position and shape cause the observed fluorescence colors to appear quite different. The fluorescence photo was excited by the same narrow-band 365 nm radiation that was used to collect the spectra. Photo by Shane Elen.

orange fluorescence observed in chemical vapor deposition (CVD) synthetic diamonds with the 575 and 637 nm lines seen in their photoluminescence spectra; Wang et al. (2005) made similar observations on treated pink-to-red diamonds. While visual assessment of fluorescence would be unable to reliably distinguish between the orange fluorescence sometimes observed in category 3 natural diamonds and the 575 nm–induced fluorescence observed in synthetic diamonds, treated-color diamonds, and some rare natural-color diamonds, spectroscopy could help make the distinction.

Other gemological testing equipment, such as the DiamondSure, looks for the presence of the N3 center in natural diamonds to help distinguish them from near-colorless synthetics (Welbourn et al., 1996). The N3-related center cannot be reliably confirmed by the mere observation of blue fluorescence; however, its presence in a fluorescence spectrum is a strong indicator that a diamond has a natural origin.

A laboratory might also offer more complete comparisons of long- and short-wave fluorescence (e.g., that the intensity of the short-wave fluorescence was 30% that of the long-wave fluorescence). This information would contribute to a more thorough characterization of the diamond for identification purposes.

While the equipment used in this study will not replace laser-excited spectrometers (such as FTIR or Raman) or higher-resolution spectrofluorometers used in gemological research laboratories, the affordability of the CCD spectrometer used in these tests makes it available to a greater number of gemologists. Its speed and ease of use make it possible to quickly and conveniently characterize large numbers of stones.

CONCLUSIONS

This work reports the fluorescence properties of 62 natural-color diamonds that span nearly the entire color spectrum observed in natural diamonds. For comparison, the spectra of 10 irradiated diamonds were also measured.

Due to limitations on the number of colors and kinds of diamonds used in this study, the fluores-

Figure 18. Fluorescence spectroscopy can help characterize important diamonds such as these 0.51–2.03 ct stones from the October 2007 Argyle tender. Highlights of the tender included the 1.74 ct Fancy purplish red oval, the 0.69 ct Fancy purplish red emerald cut, and the 0.77 ct Fancy Dark gray-violet shield shown here. Courtesy of Argyle Diamond; photo by Robert Weldon.

cence spectra reported here likely do not represent the entirety of possible fluorescence behaviors in natural or treated diamonds. For example, we did not test all known types of treated diamonds. Diamonds with different fluorescence spectra from those documented in this article could have additional color centers or combinations of centers. Nevertheless, this work illustrates the potential of this relatively inexpensive equipment, the mobile CCD spectrometer, for a more precise characterization of the fluorescence and phosphorescence properties of diamonds, especially important ones (figure 18). Our experience suggests that the attributes of this instrument make it suitable for rapidly characterizing the luminescence properties of large numbers of diamonds and other gems. Fluorescence spectra yield far more information than visual assessment alone, such as a semiquantitative assessment of intensity and the presence of subordinate peaks, and are much less ambiguous.

The vast majority of the fluorescence spectra fell into three major categories with respect to peak wavelengths and shapes. Only two of the 62 natural-color diamonds had peak positions other than those described in the three major categories. The fluorescence spectra were largely segregated by the diamonds' bodycolors. Category 1 fluorescence spectra were predominantly represented by pink, yellow, and fancy white natural-color diamonds; category 2 by natural diamonds in the yellow-green group or with brown bodycolors; and category 3 by natural diamonds with orange or gray-green (including chameleon) bodycolors or in the type Ia blue-gray group of natural diamonds. Evidence of an anomalous fluorescence spectrum may indicate that a stone needs to be submitted for additional testing.

ABOUT THE AUTHORS

Dr. Eaton-Magaña (sally.magana@gia.edu) was a postdoctoral fellow at the Naval Research Laboratory in Washington, DC, at the time of the original research. She is now technical editor of Gems & Gemology *at GIA in Carlsbad, California. Dr. Post is curator of the Gem and Mineral Collection of the National Museum of Natural History at the Smithsonian Institution in Washington, DC. Dr. Heaney is professor of geosciences at Penn State University in University Park, Pennsylvania. Dr. Walters, at the time of the original research, was director of Research and Development at Ocean Optics Inc. in Dunedin, Florida; he is now retired. Dr. Breeding is research scientist at the GIA Laboratory in Carlsbad, and Dr. Butler is head of the Gas/Surface Dynamics Section at the Naval Research Laboratory in Washington, DC.*

ACKNOWLEDGMENTS

The authors gratefully acknowledge the considerable contribution of Alan Bronstein and Harry Rodman for the loan of their Aurora collections. Thomas Moses, Dr. Wuyi Wang, and Kyaw Soe Moe, of the GIA Laboratory in New York, graciously loaned the DiamondView instrument, performed FTIR measurements, and collected color grading and origin-of-color information on some diamonds in the Aurora Butterfly collection. At the GIA Laboratory in Carlsbad, Shane Elen provided help and advice in operating the spectrofluorometer, and Karen Chadwick helped collect FTIR and UV-Vis-NIR data. Russell Feather helped with obtaining some of the data at the Smithsonian Institution. Financial support was provided by the Office of Naval Research and the Naval Research Laboratory. This research was partially funded by a National Research Council Fellowship Award to Dr. Eaton-Magaña.

REFERENCES

Anderson B.W. (1960) Luminescence of a large pink diamond. *Journal of Gemmology*, Vol. 7, No. 6, pp. 216–220.

Anderson B.W. (1962) Lines and line systems in the fluorescence spectra of diamonds. *Journal of Gemmology*, Vol. 8, No. 5, pp. 193–202.

Becquerel M.E. (1868) *Sources de Lumière: Ses Causes et Ses Effets* [*Sources of Light: Its Causes and Effects*]. Librairie de Firmin Didot Frères, Paris, 431 pp.

Bosshart G. (1999) Natural diamond colours and their causes. *The Singaporean Gemologist*, Vol. 6, No. 2, pp. 30–33.

Boyd S.R., Kiflawi I., Woods G.S. (1995) Infrared absorption by the B nitrogen aggregation in diamond. *Philosophical Magazine B*, Vol. 72, No. 3, pp. 351–361.

Collins A.T. (1980) Spectroscopic investigation of a canary yellow diamond. *Journal of Gemmology*, Vol. 17, No. 4, pp. 213–222.

Collins A.T. (1982a) A spectroscopic survey of naturally-occurring vacancy-related colour centers in diamond. *Journal of Physics D: Applied Physics*, Vol. 15, pp. 1431–1438.

Collins A.T. (1982b) Colour centres in diamond. *Journal of Gemmology*, Vol. 18, No. 1, pp. 37–75.

Collins A.T., Woods G.S. (1982) Cathodoluminescence from "giant" platelets, and of the 2.526 eV vibronic system, in type Ia diamonds. *Philosophical Magazine*, Vol. 45, No. 4, pp. 385–397.

Collins A.T., Kanda H., Kitawaki H. (2000) Colour changes produced in natural brown diamonds by high-pressure, high-temperature treatment. *Diamond and Related Materials*, Vol. 9, No. 2, pp. 113–122.

Davies G., Crossfield M.D. (1973) Luminescence quenching and zero-phonon line broadening associated with defect interactions in diamonds. *Journal of Physics C: Solid State Physics*, Vol. 6, pp. L104–L108.

Davies G., Crossfield M.D., Collins A.T. (1974) The role of defect interactions in reducing the decay time of H3 luminescence in diamond. *Journal of Physics C: Solid State Physics*, Vol. 7, pp. 1909–1917.

De Weerdt F., Van Royen J. (2001) Defects in coloured natural diamonds. *Diamond and Related Materials*, Vol. 10, No. 3/7, pp. 474–479.

Dyer H.B., Matthews I.G. (1958) The fluorescence of diamond. *Proceedings of the Royal Society of London: Series A, Mathematical and Physical Sciences*, Vol. 243, No. 1234, pp. 320–335.

Eaton-Magaña S., Post J.E., Walters R.A., Heaney P.J., Butler J.E. (2006a) Luminescence of colored natural diamonds. *Gems & Gemology*, Vol. 42, No. 3, pp. 131–132.

Eaton-Magaña S., Post J.E., Freitas J.A. Jr., Klein P.B., Walters R.A., Heaney P.J., Butler J.E. (2006b) Luminescence of the Hope Diamond and other blue diamonds. *Gems & Gemology*, Vol. 42, No. 3, pp. 95–96.

Eaton-Magaña S., Post J.E., Heaney P.J., Freitas J.A. Jr., Klein P.B., Walters R.A., Butler J.E. (2008) Using phosphorescence as a fingerprint for the Hope and other blue diamonds. *Geology*, Vol. 36, No. 1, pp. 83–86.

Fritsch E. (1998) The nature of color in diamonds. In G. Harlow, Ed., *The Nature of Diamonds*, Cambridge University Press, Cambridge, UK, pp. 23–47.

Fritsch E., Scarratt K. (1992) Natural-color nonconductive gray-to-blue diamonds. *Gems & Gemology*, Vol. 28, No. 1, pp. 35–42.

Fritsch E., Scarratt K. (1993) Gemmological properties of type Ia diamonds with an unusually high hydrogen content. *Journal of Gemmology*, Vol. 23, No. 8, pp. 451–460.

Fritsch E., Waychunas G.A. (1994) Gemstones. In M. Robbins, *Fluorescence*, Geoscience Press Inc., Phoenix, Arizona.

Fritsch E., Shigley J.E., Moses T., Rossman G.R., Zucker B., Balfour I. (1995) Examination of the twenty-two carat green chameleon diamond. In D. J. Content, Ed., *A Green Diamond: A Study of Chameleonism*, W. S. Maney & Son, Leeds, England, 42 pp.

Fryer C.W., Koivula J.I. (1986) An examination of four important gems. *Gems & Gemology*, Vol. 22, No. 2, pp. 99–102.

Hainschwang T., Simic D., Fritsch E., Deljanin B., Woodring S., Del Re N. (2005) A gemological study of a collection of chameleon diamonds. *Gems & Gemology*, Vol. 42, No. 1, pp. 20–35.

Hounsome L.S., Jones R., Martineau P.M., Fisher D., Shaw M.J., Briddon P.R., Öberg S. (2006) Origin of brown coloration in diamond. *Physical Review B*, Vol. 73, pp. 125203-1–125203-8.

Kiflawi I., Mayer A.E., Spear P.M., Van Wyk J.A., Woods G.S. (1994) Infrared absorption by the single nitrogen and A defect centres in diamond. *Philosophical Magazine B*, Vol. 69, No. 6, pp. 1141–1147.

King J.M., Shigley J.E., Gelb T.H., Guhin S.S., Hall M., Wang W. (2005) Characterization and grading of natural-color yellow diamonds. *Gems & Gemology*, Vol. 41, No. 2, pp. 88–115.

Martineau P.M., Lawson S.C., Taylor A.J., Quinn S.J., Evans D.J.F., Crowder M.J. (2004) Identification of synthetic diamond grown using chemical vapor deposition (CVD). *Gems & Gemology*, Vol. 40, No. 1, pp. 2–25.

Massi L., Fritsch E., Rossman G.R., Hainschwang T., Jobic S., Dessapt R. (2006) Chameleon diamonds: A proposed model to explain thermochromic and photochromic behaviors. *Gems & Gemology*, Vol. 42, No. 3, pp. 101–102.

Moe K.S., Johnson P. (2007) Lab Notes: Blue diamonds showing multiple colors of phosphorescence. *Gems & Gemology*, Vol. 43, No. 1, pp. 47–48.

Moses T.M., Reinitz I.M., Johnson M.L., King J.M., Shigley J.E. (1997) A contribution to understanding the effect of blue fluorescence on the appearance of diamonds. *Gems & Gemology*, Vol. 33, No. 4, pp. 244–259.

Robins L.H., Tjossem P.J.H., Smyth K.C., Barnes P.Y., Farabaugh E.N., Feldman A. (1991) Photoluminescence excitation by band-gap optical absorption in chemical vapor deposition diamond films. *Journal of Applied Physics*, Vol. 69, No. 2, pp. 3702–3708.

Rodman, Bronstein, and the Aurora Butterfly of Peace (2005) *JCK*, Vol. 176, No. 3, p. 44.

Shigley J.E., Fritsch E. (1993) A notable red-brown diamond. *Journal of Gemmology*, Vol. 23, No. 5, pp. 259–266.

Shigley J.E., Abbaschian R., Clarke C. (2002) Gemesis laboratory-created diamonds. *Gems & Gemology*, Vol. 38, No. 4, pp. 301–309.

Solotaroff I. (2003) Quest for color. *Modern Jeweler*, Vol. 102, No. 3, pp. 59–63, 94–95.

Titkov S.V., Solodova Y.P., Gorshkov A.I., Magazina L.O., Sivtsov A.V., Sedova E.A., Gasanov M.D., Samosorov G.G. (2006) Inclusions in white-gray diamonds of cubic habit from Siberia. *Gems & Gemology*, Vol. 42, No. 3, pp. 127–128.

Wang W., Smith C.P., Hall M.S., Breeding C.M., Moses T.M. (2005) Treated-color pink-to-red diamonds from Lucent Diamonds Inc. *Gems & Gemology*, Vol. 41, No. 1, pp. 6–19.

Watanabe K., Lawson S.C., Isoya J., Kanda H., Sato Y. (1997) Phosphorescence in high-pressure synthetic diamond. *Diamond and Related Materials*, Vol. 6, No. 1, pp. 99–106.

Welbourn C.M., Cooper M., Spear P.M. (1996) De Beers natural versus synthetic diamond verification instruments. *Gems & Gemology*, Vol. 32, No. 3, pp. 156–169.

Williams B. (2007) Technology update—Ultraviolet light. *Gem Market News*, Vol. 26, No. 1, pp. 8–11.

Zaitsev A.M. (2001) *Optical Properties of Diamond: A Data Handbook*. Springer-Verlag, Berlin, 502 pp.

AN EXAMINATION OF THE NAPOLEON DIAMOND NECKLACE

Eloïse Gaillou and Jeffrey E. Post

Napoléon Bonaparte gave an extraordinary diamond necklace to his empress, Marie-Louise, in 1811. Its intriguing history involves both royals and con artists (and one individual who was both), and it was ultimately donated to the Smithsonian Institution in 1962. Infrared absorption analysis of 101 stones in the necklace revealed that a high proportion of the larger diamonds are the relatively rare type IIa; most of the smaller stones are type IaAB. The luminescence behavior of the diamonds to ultraviolet exposure correlates with their diamond types.

Napoléon Bonaparte presented the diamonds now known as the Napoleon Necklace (figure 1) to his second wife, Marie-Louise of Austria, Empress of France, as a gift to celebrate the birth of their son, Napoléon François Joseph Charles, the King of Rome (later the Duke of Reichstadt), in 1811. The history of this jewel is well documented, and the brief summary presented here is based on an account by Bratter (1971) and unpublished research conducted in the National Archives of France by Marvin C. Ross. Mr. Ross was employed by American socialite Marjorie Merriweather Post, who donated the necklace to the Smithsonian Institution in 1962 (Post, 1997), and his notes are currently stored at the Hillwood Museum in Washington, DC (with copies at the Smithsonian).

The necklace was assembled in Paris by the firm of Nitot and Sons. Jeweler Ernst Paltscho (1811), who examined it at the time, estimated its value at 376,275 French francs. This was an enormous sum of money, approximately equal to the Empress's regular household budget for an entire year. Several portraits were subsequently painted of Marie-Louise wearing the necklace (e.g., figure 2).

When Napoléon was exiled to Saint Helena in 1815, Marie-Louise returned to Austria with her personal jewels, including the diamond necklace. After her death in 1847, the necklace passed to her cousin, Archduchess Sophie, who removed two diamonds from the necklace in order to shorten it and put them into earrings (the current whereabouts of these earrings is unknown). Following the Archduchess's death in 1872, the necklace was inherited by her three surviving sons, one of whom, Charles Louis, later acquired the interests of his two brothers. Charles Louis's third wife, Maria Theresa, inherited the Napoleon Necklace upon his death in 1914.

One of the more unusual episodes in the necklace's history took place in 1929, when Archduchess Maria Theresa sent the jewel to the United States to be sold. The agents she chose represented themselves as "Colonel Townsend," who had allegedly served in the British Secret Service, and his wife "Princess Baronti," a novelist (Nicolet, 1930; Bratter, 1971). These representations were false, and in fact the couple's true identities have never been con-

See end of article for About the Authors and Acknowledgments.
GEMS & GEMOLOGY, Vol. 43, No. 4, pp. 352–357.

Figure 1. The Napoleon Necklace, assembled in 1811, was presented by Napoléon Bonaparte to his second wife, Marie-Louise, to celebrate the birth of their son. It is composed of 234 diamonds weighing about 263 carats (width of the necklace as shown is about 20 cm), and is currently on exhibit at the National Museum of Natural History, Smithsonian Institution, in Washington, DC. Photo by Chip Clark.

firmed. Maria Theresa was seeking $450,000 for the necklace, but after the stock market crash in October of that year, the Townsends realized that a sale for this sum was impossible. They enlisted the assistance of Archduke Leopold of Hapsburg, Maria Theresa's grandnephew, to authenticate the necklace to prospective buyers and to provide credibility to the story that it was being offered at the bargain price of $100,000 because Maria Theresa was desperately in need of money. The Townsends negotiated deals to sell the necklace, first to New York jeweler Harry Winston and then to one Harry Berenson of Boston, but both backed out. David Michel, a New York diamond dealer, finally bought it for $60,000. The Townsends sent $7,270 to Maria Theresa and kept the balance of $52,730 to cover their "expenses related to the sale," which included a reported $20,000 for Leopold.

Prior to the sale, however, Maria Theresa had revoked the Townsends' authority to sell the necklace and sent an emissary to New York to retrieve the diamonds. The affair ultimately went to the courts. In the end, the necklace was returned to Maria Theresa and Leopold went to jail, while the Townsends fled the authorities and dropped out of sight.

In 1948, the Hapsburg family sold the necklace to Paul-Louis Weiller, a Paris industrialist and patron of the arts. Harry Winston acquired the necklace in 1960 and sold it to Marjorie Merriweather Post. In 1962, she gave the necklace in its original case (figure 3) to the Smithsonian Institution. The necklace is currently on exhibit in the Natural History Museum's National Gem and Mineral Collection Gallery.

The Napoleon Necklace contains 234 colorless to near-colorless diamonds set in silver and gold (again, see figure 1); the diamonds total approximately 263 carats, with the largest stone weighing about 10.4 ct. The piece consists of 28 old mine–cut diamonds, from which are suspended a fringe of nine pendeloques (five pear shapes—some with rounded points—alternating with four ovals) and 10 briolettes. Above each pear shape is mounted a small brilliant, while the four ovals are attached to motifs decorated with 23 smaller diamonds (figure 4, left). Each of the 10 briolette mountings is set with 12 rose-cut diamonds (figure 4, right).

In his description of the necklace, Paltscho (1811) detailed each stone by cut, weight, and price. The origins of the diamonds were not noted, but in 1811 the only significant diamond sources were India and Brazil. Paltscho does not describe the

Figure 2. This painting by Giovan Battista Borghesi depicts Marie-Louise wearing the diamond necklace while she was Duchess of Parma, after Napoléon's abdication in 1815. It currently resides in the Galleria Nazionale in Parma, Italy; courtesy of Scala/ Art Resource, New York.

quality of the stones, and, as far as is known, they have never been removed from their mountings.

Materials and Methods. We studied 101 of the 234 diamonds in the necklace: the 52 larger diamonds (~2.5–10.4 ct) and a selection of the others. We used a Meiji binocular microscope with attached polarizers to examine surface and near-surface features. We could not conduct a detailed study of the diamonds' interiors because the stones could not be removed from the historic and fragile mounting. We measured infrared spectra using a Bio-Rad Excalibur Series Fourier-transform infrared spectrometer (4 cm^{-1} resolution) fitted with a UMA-500 microscope. The microscope made it possible to direct the IR beam through the table and large culet of the old mine–cut diamonds. We observed the ultraviolet (UV) luminescence of all 234 diamonds using a Super Bright long- and short-wave UV lamp (365 and 254 nm respectively). UV luminescence descriptions for the 52 larger diamonds are given in a table available in the *G&G* Data Depository (www.gia.edu/gemsandgemology).

Results and Discussion. After almost two centuries, the necklace is in generally good condition. Several solder joints have been repaired, and a few of the larger diamonds show minor chips. There are obvious crystalline inclusions in some of the diamonds; for the most part, these appear to be sulfide crystals with associated disc-shaped tension halos (Richardson et al., 2004).

Luminescence reactions of the 52 larger diamonds to UV radiation (figure 5) fell into three groups. The six diamonds in the first group were inert to both long- and short-wave UV. The seven diamonds in the second group displayed pinkish orange fluorescence that was more intense to short-wave than long-wave. The strength of the short-wave UV luminescence ranged from weak to strong, depending on the diamond. No phosphorescence was observed from the diamonds in the second group. The third and largest group (39 diamonds)

Figure 3. Shown here is the original case for the Napoleon Necklace (21.8 cm in diameter), made in Paris by Gruel (see inset). It is also part of the Smithsonian National Gem Collection. Photos by Kenneth Larsen.

Figure 4. At left is a detail of one of the necklace's four oval pendeloques (1.5 cm; diamond no. 40 in the G&G Data Depository table), which is set with 23 smaller diamonds. The mountings for the briolettes (right, width 1 cm; diamond no. 37) are set with 12 rose cuts (some are very small and not visible in this photo). Photos by Chip Clark.

exhibited blue fluorescence that was stronger for long-wave (medium to very strong) than for short-wave (very weak to strong) UV. Diamonds in this group that showed strong fluorescence also exhibited strong whitish phosphorescence (again, see the table in the *G&G* Data Depository for complete descriptions).

The diamond types of the 52 larger diamonds, as determined from the IR spectra, are indicated in figure 5. Thirteen diamonds are type IIa (i.e., without nitrogen bands visible in their IR spectra; Fritsch and Scarratt, 1992); the remainder are type Ia diamonds with both A and B nitrogen aggregates (IaAB). These type Ia diamonds are similar to one another in that all contain small-to-moderate amounts of hydrogen, showed the Raman absorption line, and had (in most cases) high levels of platelets (e.g., figure 6, left). The absorption band at 1430 cm^{-1}, which is nitrogen

Figure 5. When the Napoleon Necklace is exposed to UV radiation (here, combined long- and short-wave UV), a variety of responses—pinkish orange, blue, or inert—can be observed. The diamond types, as determined by infrared spectroscopy, are labeled for the 52 larger stones; label colors correspond to the type of fluorescence: pink for pinkish orange, white for blue, and gray for inert. Photo by Chip Clark.

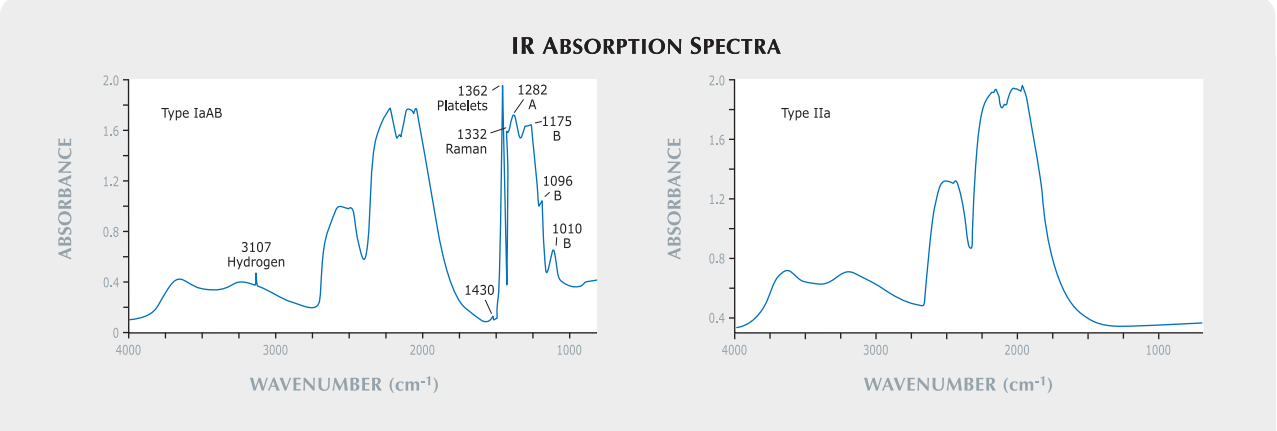

Figure 6. Typical infrared spectra of diamonds from the Napoleon Necklace are shown here for a type IaAB diamond (left, diamond no. 2), which shows the Raman line and absorption bands arising from the presence of A and B aggregates, platelets, and hydrogen; and for a type IIa diamond, which shows only the intrinsic absorption of diamond (right, diamond no. 37).

related (and correlates to N3 in type Ia diamonds; Zaitsev, 2001) was observed in the spectra of 19 of the 39 larger IaAB diamonds and in eight of the 49 smaller ones.

Comparison of luminescence behavior with diamond type reveals that type IIa diamonds were in the first and second fluorescence groups and showed either no fluorescence or pinkish orange fluorescence. The type Ia diamonds were in the third group of 39 stones that showed blue fluorescence. Interestingly, *all* of the larger type Ia diamonds in the necklace fluoresced (though very weakly in some cases), which is a significant departure from the overall average of 35% for colorless diamonds as reported by Moses et al. (1997).

It is also noteworthy that 13 of the 52 larger diamonds in the necklace are type IIa (again, see figure 5, and, e.g., figure 6, right); this includes seven of the nine large pendeloques, five of the old-mine cuts, and one of the briolettes. It appears that 200 years ago, as today, the finest large colorless diamonds were often type IIa (e.g., King and Shigley, 2003). Pinkish orange–fluorescing type IIa diamonds are commonly called *Golconda diamonds* (Scarratt, 1987; Fritsch, 1998), in reference to the historic trading area in India, a possible source for these stones. Golconda diamonds typically are described as having a faint-to-light pink color. However, no pink hue was evident in the type IIa diamonds in the Napoleon Necklace (as observed in the setting). This is consistent with observations on the larger (20.34 ct) diamond in the Marie Antoinette earrings (also in the Smithsonian National Gem Collection), which Fryer and Koivula (1986) described as colorless to near colorless (again, as observed in the setting) and is another type IIa diamond exhibiting pinkish orange fluorescence. (Note that Fryer and Koivula also reported blue fluorescence for this stone; however, our examination—conducted with the diamond unmounted—showed a pinkish orange reaction to short-wave UV.) The 34 ct Little Sancy, yet another historic colorless diamond, exhibits the same properties (E. Fritsch, pers. comm., 2007).

When examined between crossed polarizers, all the type IIa diamonds showed banded and cross-hatched extinction patterns with first-order interference colors of gray to blue. This feature, called "tatami graining," is typical of type IIa diamond (Smith et al., 2000).

Conclusion. Not only is the Napoleon Necklace a historic icon, but it also contains gemologically notable diamonds. Infrared spectroscopy indicated that 13 of the 52 larger diamonds are the relatively rare type IIa and are colorless to near colorless with good clarity, consistent with the jewel's imperial pedigree. Apparently, the standards used 200 years ago to select the finest diamonds are similar to those still used today. The necklace is equally spectacular under an ultraviolet lamp, and the diamonds' luminescence behavior correlates to their diamond type. Furthermore, it seems that colorless

or near-colorless type IIa diamonds showing a pinkish orange fluorescence are more common than previously thought. Indeed, those characteristics were usually associated with pink Golconda diamonds, but the diamonds examined here show no obvious bodycolor.

The Napoleon Necklace is one of the most spectacular jewelry pieces of its period. With this report, it joins other items in the Smithsonian's National Gem Collection for which gemological data have been preserved in the literature.

ABOUT THE AUTHORS

Dr. Gaillou (gailloue@si.edu) is a gemologist-geologist postdoctoral fellow, and Dr. Post is curator of the National Gem and Mineral Collection, both at the National Museum of Natural History, Smithsonian Institution, in Washington, DC.

ACKNOWLEDGMENTS

The authors appreciate the valuable assistance provided during this study by Russell Feather of the National Gem and Mineral Collection. We also gratefully acknowledge the reviewers for significant improvements. Dr. Gaillou is supported by grants from the JCK Industry Fund and from Apollo Diamond Inc.

REFERENCES

Bratter H. (1971) The Napoléon Necklace. *The Log of the Circumnavigators Club*, Vol. 1, pp. 5–16.

Fryer C.W., Koivula J.I. (1986) An examination of four important gems. *Gems & Gemology*, Vol. 22, No. 2, pp. 99–102.

Fritsch E. (1998) The nature of color in diamonds. In G. E. Harlow, Ed., *The Nature of Diamonds*, Cambridge University Press, Cambridge, UK, pp. 23–47.

Fritsch E., Scarratt K. (1992) Natural-color nonconductive gray-to-blue diamonds. *Gems & Gemology*, Vol. 28, No. 1, pp. 35–42.

King J.M., Shigley J.E. (2003) An important exhibition of seven rare gem diamonds. *Gems & Gemology*, Vol. 39, No. 2, pp. 136–143.

Moses T.M., Reinitz I.M., Johnson M.L., King J.M., Shigley J.E. (1997) A contribution to understanding the effect of blue fluorescence on the appearance of diamonds. *Gems & Gemology*, Vol. 33, No. 4, pp. 244–259.

Nicolet C.C. (1930) $400,000 necklace found; Crain to quiz Archduke. *New York Telegram*, March 1st.

Paltscho E. (1811) Détails des pierres au collier diamants. *National Archives of the French State*, file # 024I.

Post J. (1997) *The National Gem Collection*. Harry N. Abrams, New York, 144 pp.

Richardson S.H., Shirey S.B., Harris J.W. (2004) Episodic diamond genesis at Jwaneng, Botswana, and implications for Kaapvaal craton evolution. *Lithos*, Vol. 77, pp. 143–154.

Scarratt K. (1987) Notes from the Laboratory—10. *Journal of Gemmology*, Vol. 20, No. 6, pp. 356–361.

Smith C.P., Bosshart G., Ponahlo J., Hammer V.M.F., Klapper H., Schmetzer K. (2000) GE POL diamonds: Before and after. *Gems & Gemology*, Vol. 36, No. 3, pp. 192–215.

Zaitsev A.M. (2001) *Optical Properties of Diamond: A Data Handbook*. Springer-Verlag, Berlin, 502 pp.

Thank You Reviewers

GEMS & GEMOLOGY requires that all articles undergo a peer review process in which each manuscript is evaluated by at least three experts in the field. This process is vital to the accuracy and readability of the published article, but it is also time consuming for the reviewer. Because members of our Editorial Review Board cannot have expertise in every area, we sometimes call on other experts to share their intellect and insight. In addition to the members of our Editorial Review Board, we extend a heartfelt thanks to the following individuals who reviewed manuscripts for *G&G* in 2007.

Dr. John Angus
Dr. Brian Applegate
Dr. Christopher M. Breeding
Mr. Charles Carmona
Mr. Jean-Pierre Chalain
Mr. Martin Coeroli
Ms. Dona Dirlam
Mr. Makhmout Douman
Dr. David Fisher
Dr. Lee Groat
Dr. George Harlow
Dr. Jeff Harris
Mr. John King
Dr. Melissa Kirkley
Mr. John Koivula
Dr. Michael Krzemnicki
Ms. Gina Latendresse
Dr. David London
Dr. Phillip Martineau
Ms. Elise Misiorowski
Mr. Nicholas Paspaley
Mr. Carl Pearson
Dr. Benjamin Rondeau
Dr. Karl Schmetzer
Mr. Russell Shor
Ms. Elisabeth Strack
Dr. Wuyi Wang
Mr. Ray Zajicek
Dr. J. C. "Hanco" Zwaan

LAB NOTES 2007

EDITORS
Thomas M. Moses and
Shane F. McClure
GIA Laboratory

APATITE in SPESSARTINE

The science of gemology is a continuous and unlimited path of learning, with many side trails and stops along the way. One of the trails we like to explore are new inclusion-to-host relationships, because this information and the means used to gather it increase our knowledge and make us more effective laboratory gemologists.

Just such an opportunity arose when the Carlsbad lab was asked to identify a small group of assorted Sri Lankan gems. One of these gems was a bright orange 1.84 ct round mixed cut (figure 1) that proved to be spessartine. The garnet's refractive index was just below the limits of the refractometer at 1.80, and its visible spectrum showed strong manganese absorption. The presence of several dark blue-green rounded birefringent crystals (figure 2) sparked our curiosity, because we had never before encountered similar inclusions in a spessartine. Another interesting feature of these inclusions was that they, in turn, appeared to contain solid inclusions of their own.

Figure 1. Discovered in a group of Sri Lankan gems, this 1.84 ct bright orange spessartine contains very interesting dark blue-green inclusions.

We speculated that the blue-green inclusions might be apatite, since apatite crystals of similar color and condition have been observed in spinel and sapphire from Sri Lanka. This form of pre-analysis speculation is a way to stimulate thought and not allow the analytical apparatus to think for you. Since one of the inclusions had been polished through on the crown and exposed to the surface of the host garnet, it made an ideal target for Raman testing. The Raman spectra confirmed our suspicion, and as a bonus enabled us to identify an inclusion in the apatite as a carbonate, possibly calcite. We are not aware of any previous reports of such inclusions in spessartine from any locality, and thus believe this is a first observation.

Figure 2. Raman analysis proved that the blue-green inclusions were apatite, while the solids within the apatite crystals were identified as a carbonate. The apatite inclusion pictured here is 0.91 mm in longest dimension.

John I. Koivula and Alethea Inns

Editors' note: All items are written by staff members of the GIA Laboratory.

GEMS & GEMOLOGY, *Vol. 43, No. 4, pp. 358–365.*

DIAMOND

Atypical Photoluminescence Feature in a Colorless Type IIa

Type IIa diamonds typically contain almost no impurity-related defects. Any color present in most type IIa

stones is usually ascribed to extended defects, such as slip planes due to plastic deformation. While nitrogen is present in many type IIa diamonds, it is at such a low concentration that it is not detectable by mid-infrared spectroscopy. Often, however, nitrogen-related features (such as N-V centers and the H3 and H4 centers) are clearly resolved with photoluminescence (PL) spectroscopy, which shows that nitrogen is indeed present, even in aggregated forms.

Recently during routine testing of a 1.01 ct, E-color, pear-shaped type IIa diamond (figure 3) in the New York laboratory, we discovered the presence of a defect previously believed to occur only in certain type I diamonds. This defect is responsible for the so-called "480 nm band," which is typically seen in the absorption spectra of highly saturated orangy yellow to yellowish orange type I stones that also display medium-to-strong yellow fluorescence (see, e.g., Spring 2007 Lab Notes, pp. 49–50). Generally, these stones are a mixture of low- to medium-nitrogen type IaA and type Ib material; that is, the nitrogen is present as isolated single atoms and nearest-neighbor pairs (A. T. Collins et al., "Optical studies of vibronic bands in yellow luminescing diamonds," *Journal of Physics C*, Vol. 15, 1982, pp. 147–158). This feature is also found in the absorption spectra of chameleon diamonds. The exact structure and makeup of the 480 nm band defect is not known, but it has been suggested that it may be a complex defect containing nitrogen, hydrogen, and/or nickel (A. T. Collins, "Colour centres in diamond," *Journal of Gemmology*, Vol. 18, 1982, pp. 37–75).

The 480 nm band was not detected with absorption spectroscopy, since this stone was near colorless. The PL spectrum of the diamond at 488 nm excitation showed the distinct structure of the 480 nm band in luminescence, centered at ~700 nm (figure 4). The numerous phonon replicas visible between 600 and 700 nm indicate that this defect is strongly coupled to lattice vibrations. As expected, no zero-phonon line was detected for this system in luminescence. Note also that strong emission from the H3 defect at 503.1 nm was present in this spectrum. Multiple measurements at various locations around the stone showed that the 480 nm band defect was not homogeneously distributed.

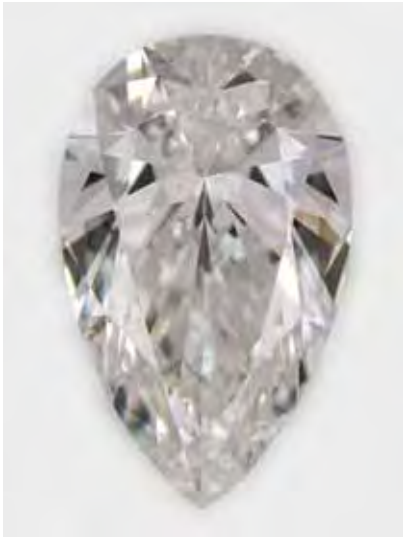

Figure 3. This 1.01 ct pear-shaped type IIa diamond shows photoluminescence due to the 480 nm band defect, which was previously thought to occur only in type I diamonds.

Visual examination of the diamond while it was exposed to long-wave UV radiation revealed a faint patch of orangy yellow fluorescence centered around a crystal inclusion; unfortunately, this inclusion was too deep within the stone to be identified by Raman analysis. PL spectra taken at 830 nm excitation at the same varied locations showed sharp doublet peaks at 883/884 nm (i.e., the 1.40 eV center), which are known to be related to a substitutional nickel impurity (figure 5; W. Wang et al., "Natural type Ia diamond with green-yellow color due to Ni-related defects," Fall 2007 *Gems & Gemology*, pp. 240–243).

Because the 480 nm band has previously been detected only in type I stones, we have theorized that the defect is likely nitrogen-related. The present findings do not disprove this speculation, since nitrogen is known to be present in type II material, although at very low concentrations.

Figure 4. The photoluminescence spectrum at 488 nm excitation shows the broad luminescence feature due to the 480 nm band defect, centered at about 700 nm. Also present are the H3 defect at 503.1 nm and its sideband, and a sharp peak at 575 nm due to the N-V center.

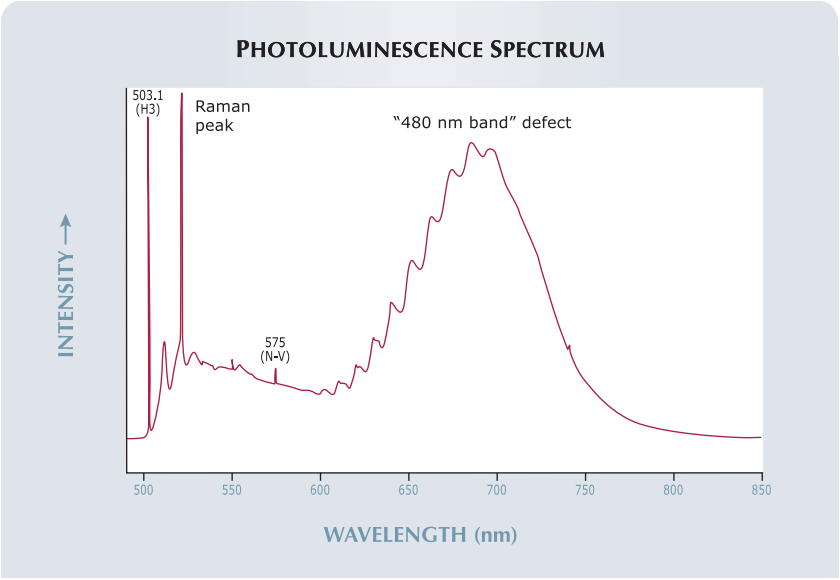

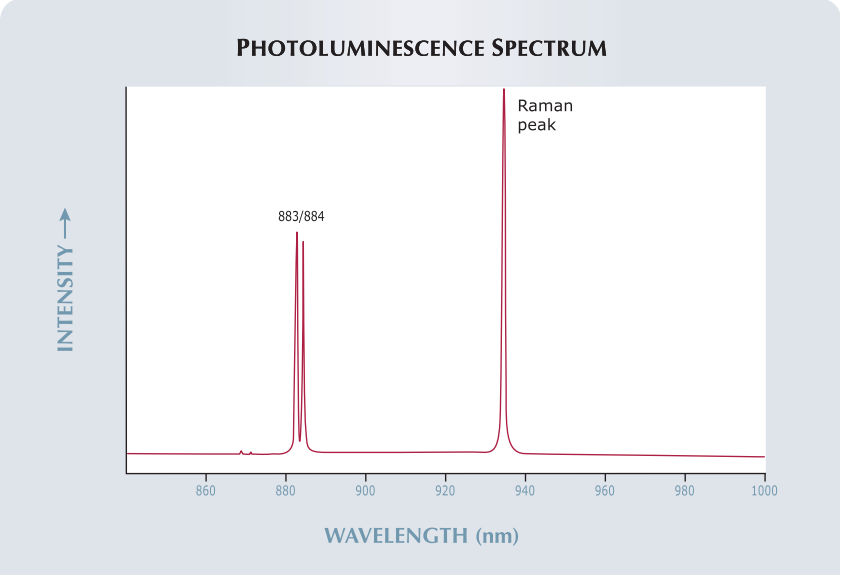

Figure 5. The photoluminescence spectrum at 830 nm excitation shows a doublet at 883/884 nm due to substitutional nickel.

Figure 6. This 1.01 ct diamond is distinguished by the presence of a reddish orange garnet crystal and bluish green omphacite crystals, visible at approximately the 10 o'clock position.

Rather, this example may indicate that the correlation between the 480 nm band and the presence of nitrogen is not very strong, or that the 480 nm band defect is related to nickel.

Jon Neal

Inclusions Fit for a Holiday Season

Mineral inclusions are very useful when identifying diamond, as well as in determining its origin of color and basic geology. Often, they are also the determining factor in setting the clarity grade. Unusual inclusion arrangements can be a pleasure to observe and can enhance interest in the stone when the internal feature resembles a heart or other familiar object. However, diamonds with euhedral crystals displaying vibrant color are exceedingly rare.

Recently, a grader in the New York lab observed just such features in a 1.01 ct, F-color, round brilliant diamond (figure 6) with well-formed bluish green and reddish orange crystal inclusions. In light of the upcoming holiday season, the grader fondly referred to the find as the "Christmas stone" due to its combination of colors. Although we have documented such eclogitic inclusions before (see, e.g., Spring 2002 Lab Notes, pp. 80–81; W. Wang et al., "Natural type Ia diamond with green-yellow color due to Ni-related defects," Fall 2007 *Gems & Gemology*, pp. 240–243), this inclusion scene was unusual because of the proximity of the crystals to each other and the vibrancy of their colors (figure 7). Also interesting was the discovery

Figure 7. With magnification, the vibrant colors of the garnet and omphacite crystals become more apparent. Note that the crystals are set apart by stress cracks. Magnified 100×.

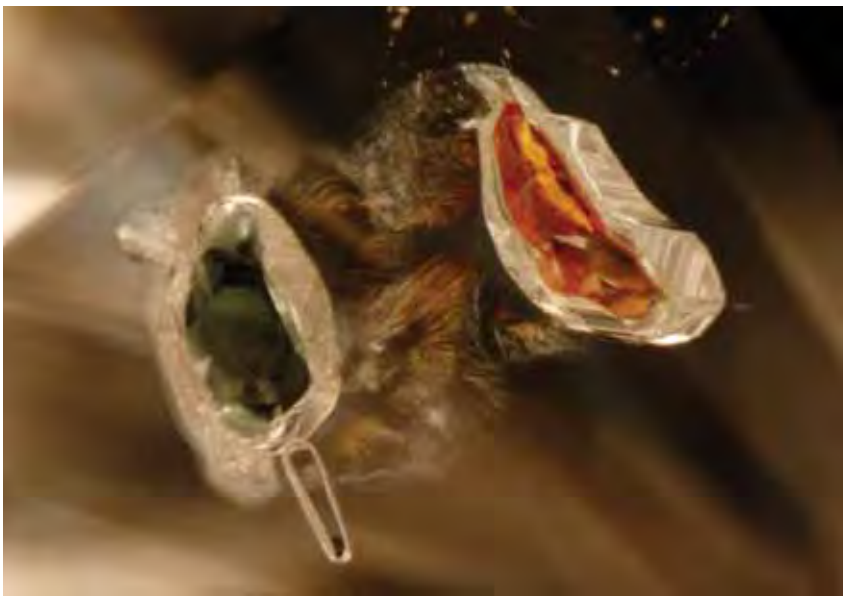

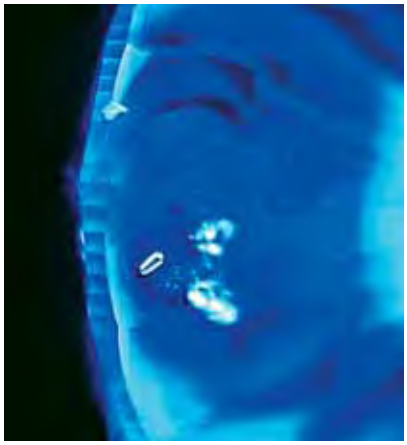

Figure 8. This DiamondView image shows that the crystals in figure 7 were trapped with a second omphacite crystal within a single octahedral growth sector.

that both crystals had formed within the same growth sector, as can be seen from the DiamondView image in figure 8, which distinctly illustrates an octahedral growth zone surrounding the inclusions. Using Raman analysis (830 nm laser), we identified the reddish orange crystal as almandine-rich garnet and the bluish green crystal as omphacite (a pyroxene).

These inclusions are an excellent example of well-formed syngenetic crystals (i.e., formed at the same time as the host) in diamond. In this case, they were also the features that led to an SI_2 clarity grade, a perhaps disappointing result given the diamond's unique beauty and character. GIA diamond graders view thousands of stones annually, and it is refreshing to see a grouping of inclusions that readily tell a story of the diamond's distinctive growth.

Bonny S. Alphonso, Jennifer Schan, and Paul Johnson

With Large Etch Channels Filled with Iron Sulfides

Etch channels have been found in both type I and II diamonds from almost every locality (see T. Lu et al., "Observation of etch channels in several natural diamonds," *Diamond and Related Materials*, Vol. 10, 2001, pp. 68–75). They occur in a variety of shapes, from nearly straight lines to irregular worm-like or branching patterns (see, e.g., Summer 2006 Lab Notes, p. 165). The New York laboratory recently encountered an interesting example of this feature, a 0.57 ct Fancy Deep brownish yellow round brilliant that had eye-visible etch channels with multiple branches that contained a dark brown material (figure 9).

Examination with a gemological microscope revealed intense brown radiation stains on the outer walls of the etch channels that locally penetrated into the adjacent diamond a short distance. Most of the channels had hexagonal openings (from 0.2 × 0.1 mm to 0.55 × 0.6 mm in diameter) at and just under the girdle (see figure 10). The main channel was partially polished out, so it was exposed from the girdle across the crown facets to the table, where it broke the surface of the table facet (again, see figure 10). Large cavities in this channel were possibly caused by the polishing process. The large opening in the table contained a transparent material that was completely surrounded by the dark brown material. Multiple channels branched out from this main channel, with a few isolated channels elsewhere in the diamond.

Figure 9. This 0.57 ct Fancy Deep brownish yellow diamond has several etch channels, which appear to contain a dark brown material.

DiamondView images showed green-fluorescing growth zones, while the materials in the etch channels fluoresced blue (figure 11). As can be seen in figure 11, the etch channels intersected different growth zones, which suggests they were formed epigenetically, after the diamond had completed its growth. Raman spectroscopy

Figure 10. Multiple etch channels in the 0.57 ct diamond branch from the main channel, which breaks the surface of the table facet (0.55 × 0.6 mm; left). At this opening, it can be seen that the channel contains a transparent material that is completely surrounded by a dark brown material, which is responsible for the perceived color. Part of the main channel was also exposed on the crown facets, and cavities can be seen on its surface. The etch channels show roughly hexagonal outlines where they reach the pavilion surface (right).

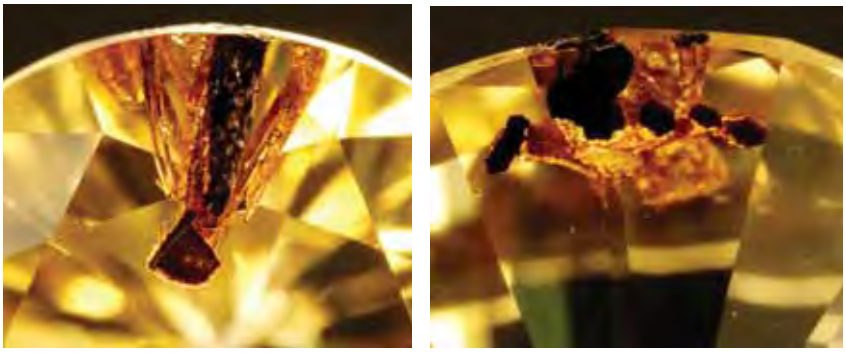

identified the dark brown material as predominantly pyrrhotite, a common iron sulfide inclusion in diamonds. At a few spots inside the pyrrhotite, pentlandite (a Ni-rich iron sulfide) was also identified. Raman spectroscopy identified the transparent material in the large opening in the table as diamond.

Filled etch channels have been reported previously; they may contain iron hydroxides, black host-rock materials, or serpentine (see, e.g., R. M. Davies et al., "Inclusions in diamonds from the K14 and K10 kimberlites, Buffalo Hills, Alberta, Canada: Diamond growth in a plume?" *Lithos*, Vol. 77, 2004, pp. 99–111). The unusual presence of pyrrhotite and pentlandite in these etch channels suggests that iron sulfide inclusions can be formed epigenetically, as well as syngenetically, in diamonds. It further suggests that Fe-Ni monosulfide solutions can be injected into a diamond even after post-growth etching.

Kyaw Soe Moe, Surjit Dillon, and Thomas Gelb

Figure 11. In this DiamondView image, the etch channels intersect different growth zones showing different intensities of green, while the dark brown material fluoresces blue. This image further suggests that the etch channels were created and the filling material (pyrrhotite and pentlandite) was deposited after the diamond was fully formed.

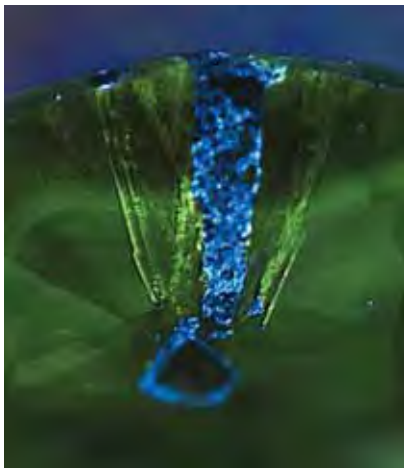

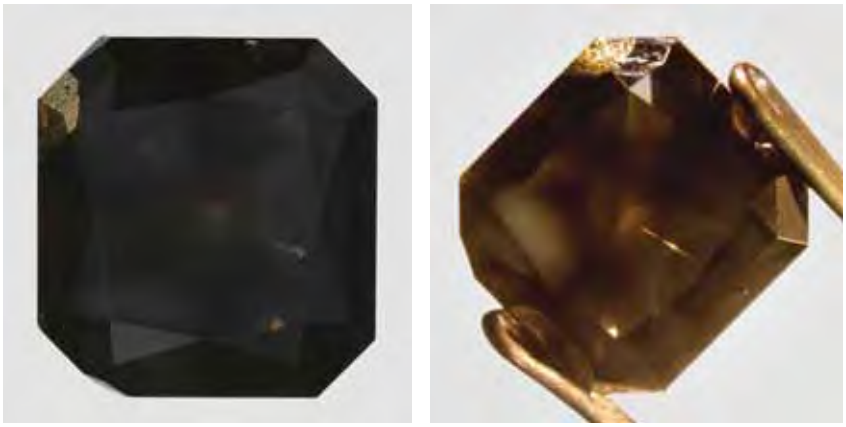

Figure 12. The 3.06 ct natural black diamond on the left, when viewed with strong transmitted light (right), shows an unusually long, straight etch channel as well as dark clouds of inclusions.

Natural Black DIAMOND with Oriented Etch Channel

Most "black" diamonds currently on the market are treated color, created either by heating or by exposure to intense radiation. Natural black diamonds suitable for jewelry use are not common. Recently, however, the New York laboratory examined an interesting natural-color black diamond that also had a well-developed and oriented etch channel.

This 3.06 ct diamond (figure 12) was color graded Fancy black. Infrared spectroscopy showed that it was type Ia with a relatively high concentration of hydrogen. The UV-Vis spectrum did not display any resolvable peaks due to the near-opacity of the stone. Energy-dispersive X-ray fluorescence (EDXRF) analysis indicated the presence of Fe and Ni, which have also been observed in black diamonds from Siberia (S. V. Titkov et al., "An investigation into the cause of color in natural black diamonds from Siberia," Fall 2003 *Gems & Gemology*, pp. 200–209). Infrared and photoluminescence spectroscopy did not reveal any evidence of treatment; the black color was undoubtedly caused by the presence of dark sectorial clouds that absorbed virtually all light.

The diamond's most notable feature was a well-developed etch channel that traversed almost half the stone from under the center of the table to one of the crown facets (figure 12, right), where it reached the surface with an approximately 10 µm wide near oval–shaped opening. DiamondView fluorescence imaging showed that the growth sectors were well aligned with respect to crystallographic symmetry and that the dark clouds generally correlated with the growth

Figure 13. The DiamondView fluorescence image of the stone in figure 12 reveals that the dark clouds correlate with cubic growth sectors and that the etch channel (visible in the lower right) is crystallographically aligned.

pattern (figure 13). It further indicated that the etch channel was perfectly aligned along the [111] direction. An additional frosty etch mark was present at one of the corners of the stone (again, see figure 12), but no other etch features were observed.

Not only does the testing of this stone prove that it is a natural-color black diamond, but the fluorescence imaging also confirms that etch-channel development follows growth zones and localized lattice defects, consistent with the earlier report by A. Nemirovskaya and W. Wang ("Diamond with unusual etch channel," Summer 2006 Lab Notes, p. 165).

Ren Lu and Wuyi Wang

Figure 15. This unusual diamond (approximately 12.0 × 6.7 × 3.5 mm) has been faceted in the shape of a fish.

The Pareidolia of Diamonds

Have you ever gazed up at the sky on a warm spring day and seen a human face in the clouds? Or a horse? Or another fanciful image? Now examine figure 14. What do you see? Some might see a feather with a crystal above it; others might see a person tossing a ball. *Pareidolia* is the term that psychologists use to describe the phenomenon in which the brain qualitatively assigns familiar shapes to random, abstract forms.

In seeming contrast, cutting diamonds is nominally a more quantitative process in which the manufacturer calculates the most profitable combination of clarity, cut, and weight retention. This, of course, is based on sober judgments regarding specific shapes with corresponding angles and proportions that result in an attractive diamond. That being said, there are exceptions to every rule, and not all diamonds are so straightforward in the decision process. Often creativity is needed to determine what shape will result in sufficient weight retention, good clarity, and an attractive appearance. And pareidolia may help that creativity. This is especially important in cases of oddly proportioned or otherwise "difficult" rough, which can be fashioned into truly fanciful shapes such as that in figure 15, which shows a 1.80 ct diamond cut in the shape of a fish.

Coincidentally, the New York laboratory recently encountered the oddly shaped 13.25 ct crystal in figure 16. Microscopic examination showed a number of graphitized inclusions and small crystals. The diamond was type IaB>A, as determined by infrared spectroscopy, and showed strong blue fluorescence to long-wave UV radiation and moderate yellow fluorescence to short-wave UV. While examining this crystal, several of the lab's graders

Figure 14. This diamond inclusion scene, composed of a feather and a crystal, reminds some observers of a person tossing a ball.

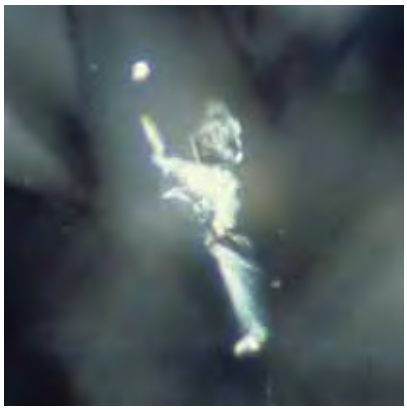

Figure 16. This large rough diamond (25.68 × 6.26 × 7.60 mm) also reminded some graders of a fish.

referred to it as "the fish" due to their perception of its shape. Those of us who had also seen the faceted fish felt they had an uncanny resemblance. This pareidolic perception is distinctive to each individual; so if the cutter also visualized this rough as a fish, perhaps he would create a finished stone similar to figure 15.

Joshua Sheby and Jason Darley

A Notable EMERALD Carving

Emerald has long been a popular carving material, and it is not unusual for carved emerald beads, tablets, and the like to be submitted to gemological laboratories such as GIA (see, e.g., Lab Notes—Fall 1981, pp. 161–162, and Winter 1994, pp. 264–265; Gem News International—Summer 2001, p. 145, and Fall 2002, pp. 262–263). It is unusual, however, to see an emerald carving the size of the 2,620.70 ct statue that Jeffery Bergman of Primagem submitted to the Bangkok laboratory for identification in November 2007 (figure 17).

The carving was of a standing Buddha, or *Baang Haarm Yaard* in Thai. It is said that the standing posture represents the Buddha's admonition to his family members to stop quarreling among themselves. This is also the Buddha image for those born on a Monday.

The size and shape of the medium-to-dark green statue made standard gemological testing difficult, so we used Raman spectroscopy to obtain a positive identification of the material as beryl. Microscopic examination revealed rectangular colorless crystals, brown crystals, two-phase inclusions, and partially healed fractures, proving the emerald was of natural origin. It also confirmed that the carving was fashioned from a single crystal.

Due to their growth conditions in nature and the recovery methods used by miners, most emeralds contain fractures. For this reason, it is common to apply oil to improve their apparent clarity, and such was the case with this Buddha. In fact, when we opened the plastic bag holding the item, the smell of cedarwood oil was obvious. Examination with a gemological microscope revealed a viscous liquid in fine crevices of the carving, providing clear evidence of oiling. Because the image was predominantly translucent to opaque with very few transparent areas, the normal clarity enhancement criteria used for GIA Emerald Reports was not applied to this piece.

The size and shape of the carving, as well as its having been fashioned from a single crystal, made this standing Buddha statue noteworthy.

Garry Du Toit

Figure 17. This standing Buddha (15.70 × 6.50 × 5.30 cm) was carved from a single emerald crystal.

Gold Coated ONYX

Recently, a client submitted the 10.45 mm (7.45 ct) round yellow metal bead in figure 18 to the Carlsbad laboratory for identification. While the lab makes every effort to avoid destructive methods in gemological testing, this client permitted us to polish a flat on the surface of the bead in order to study the material underneath (figure 19). The polished flat had RI values of 1.540–1.547, a granular structure, and a Fourier-transform infrared signal corresponding to chalcedony. Qualitative chemical analysis (by EDXRF spectroscopy) of the coating revealed that it was mainly gold with trace amounts of other elements. As a

Figure 18. This 10.45 mm yellow metal bead proved to be gold-coated black onyx.

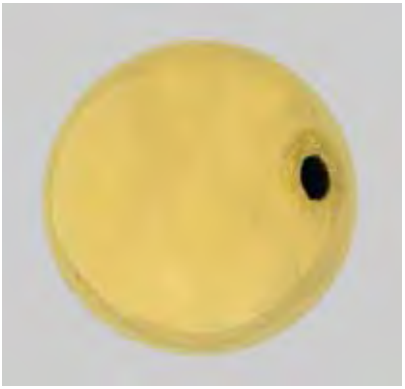

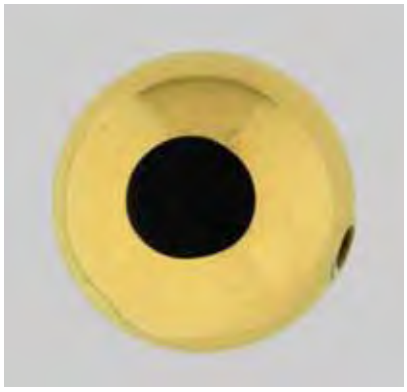

Figure 19. After the client allowed a flat to be polished on the bead, the black material underneath the gold was readily identified.

result, we issued a report stating "chalcedony, known in the trade as '*Black Onyx*,' with a metallic coating composed primarily of gold."

Over the years, the lab has received a few metal-coated articles for identification. Typically, this kind of material is extremely difficult, if not impossible, to identify using standard gemological methods.

Alethea Inns

SAPPHIRE with a Double Star

Recently, the New York laboratory received an unusual item for identification: a 3.78 ct light gray-blue oval sapphire cabochon showing not one but two separate well-formed stars when viewed under a single spot light (figure 20). Although we have seen corundum with superimposed double stars before (e.g., Fall 1993 Lab Notes, p. 212; Fall 1998 Lab Notes, p. 217), this is the first time we have documented two "side-by-side" stars in a single fashioned stone. In the previous cases, the overlapping stars were caused by lamellar twinning, with the rutile silk arranged in slightly different orientations from one layer to another.

In this cabochon, however, we noted that the two asteriated regions were separated by an irregular junction. Because of this irregularity, we concluded that the two silky areas were separate crystals with different orientations (i.e., they were not crystallographically related). The dual asterism was caused by the combination of the cabochon's curvature and the slightly different orientation of the two sectors.

In addition to a rich concentration of pristine epitaxial silk and arrowhead twins following partial hexagonal growth, unaltered "fingerprint" inclusions supported the conclusion that the stone had not been heat treated. Although the two differently oriented regions kept the two stars separate, the arms were well-formed, well centered, and sharp. This "double" cab was truly a beautiful variation on one of nature's more elegant phenomena.

David M. Kondo

Figure 20. This unusual double-star sapphire cabochon (10.75 × 7.00 × 4.20 mm) was likely fashioned from two intergrown crystals.

Impregnated Glass Imitation of TURQUOISE

Turquoise is commonly treated by impregnation with either wax or a polymer, such as oil, to improve durability and luster. The Carlsbad laboratory frequently receives impregnated turquoise for testing, as well as numerous dyed and/or impregnated turquoise imitations such as magnesite, howlite, and variscite, among others.

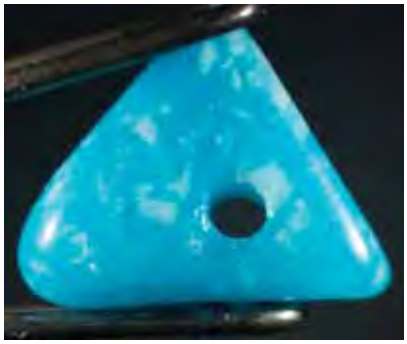

Figure 21. This 0.81 ct glass bead imitating turquoise also showed the presence of an oil filler.

Recently, the lab received the 0.81 ct triangular blue bead in figure 21 for identification. The sample was transparent to semitransparent, and magnification revealed spherical and elongated gas bubbles, flow lines, wave-like bands, and whitish granular crystal aggregates. The RI was 1.49 and the SG was 2.18, both of which are consistent for glass. Glass imitations (of all gem materials) are common. In this sample, however, the included crystals unexpectedly "sweated" when a thermal reaction tester was applied. FTIR spectroscopy revealed the presence of oil and typical glass peaks.

This is the first time we have come across a glass imitation for turquoise that also showed evidence of impregnation.

Alethea S. Inns

PHOTO CREDITS
Robert Weldon—1; John I. Koivula—2; Jian Xin (Jae) Liao—3, 6, 9, and 16; Jason Darley—7; Paul Johnson—8; Kyaw Soe Moe—10 and 11; Ren Lu—12 and 13; G. Robert Crowningshield—14; Unknown—15; Suchada Kittayachai-wattana—17; Robison McMurtry—18 and 19; Elizabeth Schrader—20; Alethea Inns—21.

EDITOR

Brendan M. Laurs (blaurs@gia.edu)

CONTRIBUTING EDITORS

Emmanuel Fritsch, *IMN, University of Nantes, France* (fritsch@cnrs-imn.fr)

Henry A. Hänni, *SSEF, Basel, Switzerland* (gemlab@ssef.ch)

Franck Notari, *GemTechLab, Geneva, Switzerland* (franck.notari@gemtechlab.ch)

Kenneth V. G. Scarratt, *GIA Research, Bangkok, Thailand* (ken.scarratt@gia.edu)

DIAMONDS

Colored diamonds break $1 million per carat with record auction prices. The fall 2007 auction season saw several colored diamonds achieve per-carat prices over $1 million. A 6.04 ct Fancy Vivid blue, internally flawless diamond (figure 1, left) set a new world-record per-carat auction price for a gemstone on October 8, when Sotheby's Hong Kong sold the stone for US$7.98 million—$1.32 million per carat. The seller was described by Sotheby's as a "private Asian client"; the buyer was London jeweler Alisa Moussaieff.

Several weeks later, another Fancy Vivid blue weighing 4.16 ct (figure 1, center) drew a winning bid of $4.73 million ($1.14 million per carat) at Sotheby's November 14 Geneva sale. The buyer of the pear-shaped diamond was London jeweler Laurence Graff. The following day, at Christie's Geneva auction, Graff paid $2.67 million ($1.18 million per carat) for a 2.26 ct Fancy purplish red diamond (figure 1, right), the highest price ever paid for a red diamond at auction.

Colorless diamonds saw near-record prices as well. Apparel magnate Georges Marciano paid $16.19 million for an 84.37 ct D-Flawless round brilliant (figure 2, left) at the Sotheby's auction in Geneva. He christened the stone the "Chloe Diamond," after his daughter. Sotheby's said the Chloe was the second most expensive diamond ever sold at public auction, the top spot belonging to the 100.1 ct Star of the Season purchased by Saudi jeweler Ahmed Fitaihi at a Sotheby's sale in 1995.

Graff completed a busy week by paying $10.4 million at a rough diamond tender sale in Antwerp for the 493 ct

Figure 1. Exceptional colored diamonds sold at auction in the fall of 2007 for record or near-record prices. The center stone in the ring on the left is a 6.04 ct Fancy Vivid blue diamond. The Fancy Vivid blue pear shape in the ring at center weighs 4.16 ct. At right, the 2.26 ct modified octagon–shaped diamond was graded Fancy purplish red. Photos courtesy of Sotheby's Hong Kong (left), Sotheby's (center), and Christie's Images (right).

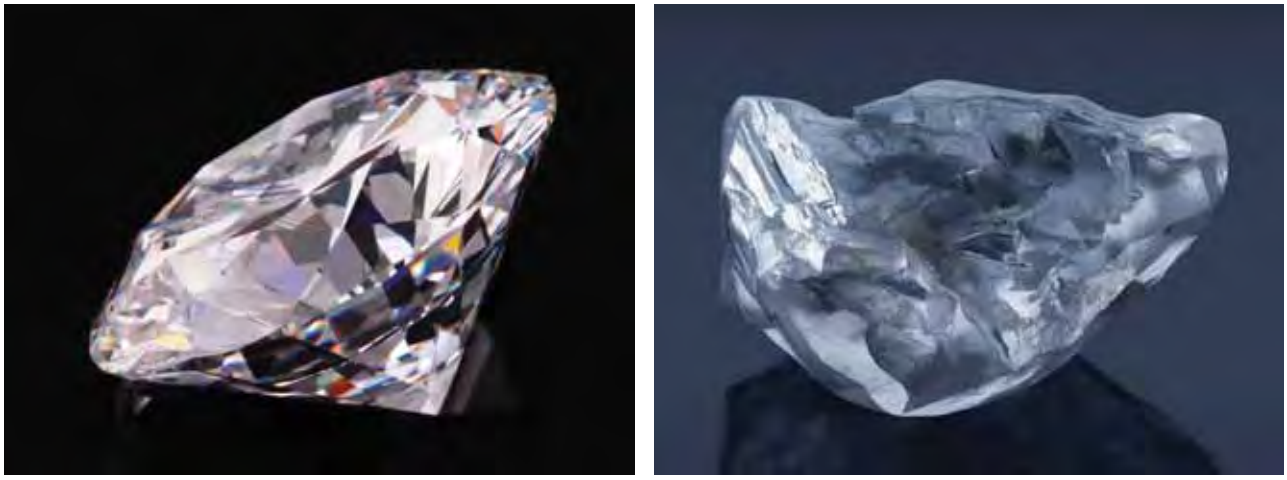

Figure 2. Two notable colorless diamonds also were sold recently. On the left is the 84.37 ct D-Flawless Chloe diamond; at right, the 493 ct Letšeng Legacy crystal was found earlier this year at the Letšeng mine in Lesotho. Photos courtesy of Sotheby's (left, by Donald B. Woodrow) and the Antwerp World Diamond Centre (right).

Letšeng Legacy (figure 2, right) found earlier this year in the Letšeng mine in Lesotho. Graff had also purchased the 603 ct Lesotho Promise, which was found at the same mine in 2006.

Russell Shor (rshor@gia.edu)
GIA, Carlsbad

Namibian diamond mining by Namdeb. In the Winter 1995 issue of *G&G* (pp. 228–255), A. J. A. (Bram) Janse's review of African diamond sources included a brief history of diamond mining in Namibia, from the discovery of diamonds in the coastal sands near Kolmanskop in 1908 to the formation of Namdeb Diamond Corp. in November 1994. Namdeb, created under Namibia's post-independence mining legislation as an equal partnership between De Beers Centenary and the national government, took over all the mining licenses and related rights of the De Beers subsidiary Consolidated Diamond Mines (CDM).

By all measures, diamond mining in Namibia has thrived under Namdeb. Today, the company is clearly the most important element of Namibia's economy, accounting for more than 10% of the country's gross domestic product and more than 40% of its export revenues. Diamond production has reached unprecedented levels, thanks in large part to offshore production by De Beers Marine Namibia, operating as an exclusive partner to Namdeb.

Editor's note: Interested contributors should send information and illustrations to Brendan Laurs at blaurs@gia.edu or GIA, The Robert Mouawad Campus, 5345 Armada Drive, Carlsbad, CA 92008. Original photos can be returned after consideration or publication.

GEMS & GEMOLOGY, Vol. 43, No. 4, pp. 366–391

The NamGem Diamond Manufacturing Co., created in 1998 as a wholly owned subsidiary of Namdeb, is the country's first diamond cutting operation. The factory is located in Okahandja, about 70 km north of Windhoek, and when it reaches full production it is expected to produce more than US$15 million worth of finished diamonds per year. The 2006 signing of the Namdeb Sales Agreement, negotiated between the government and De Beers, led to the creation of a new joint venture, the Namibia Diamond Trading Co. (NDTC), which will be responsible for sorting, valuing, and marketing diamonds. Together, Namdeb, De Beers Marine Namibia, NamGem, and NDTC employ more than 3,000 people, most of them Namibian citizens, making the group one of the country's largest employers.

Namdeb holds diamond mining licenses for six areas (figure 3). Except for the Atlantic 1 license, these are contained within the 26,000 km^2 *Sperrgebiet* (German for "forbidden area"), which was originally designated as such in 1908 to control access to the diamond-producing areas. In 2004, the Namibian government declared the *Sperrgebiet* a national park, and portions not being mined are open to visitors.

The world's greatest marine diamond deposits are located in Mining Area No. 1 (figure 4). These have been, and continue to be, the mainstay of Namdeb's production. The Plio-Pleistocene (1–5 million years [Ma] old) marine gravel deposits in Mining Area No. 1 extend almost continuously for 120 km along the coastline. Apart from the area at the mouth of the Orange River, the marine deposits lie unconformably on Late Proterozoic (650–500 Ma) bedrock of the Gariep Complex, where gullies act as trapsites that further promote diamond concentration. Onshore, the bulk of these placer deposits have been mined out, as production has been continuous since 1935. The intertidal and near-shore subtidal platform gravels, which also host significant diamond concentrations, are not accessible via conventional mining methods. A system designed to perform wet sampling in the

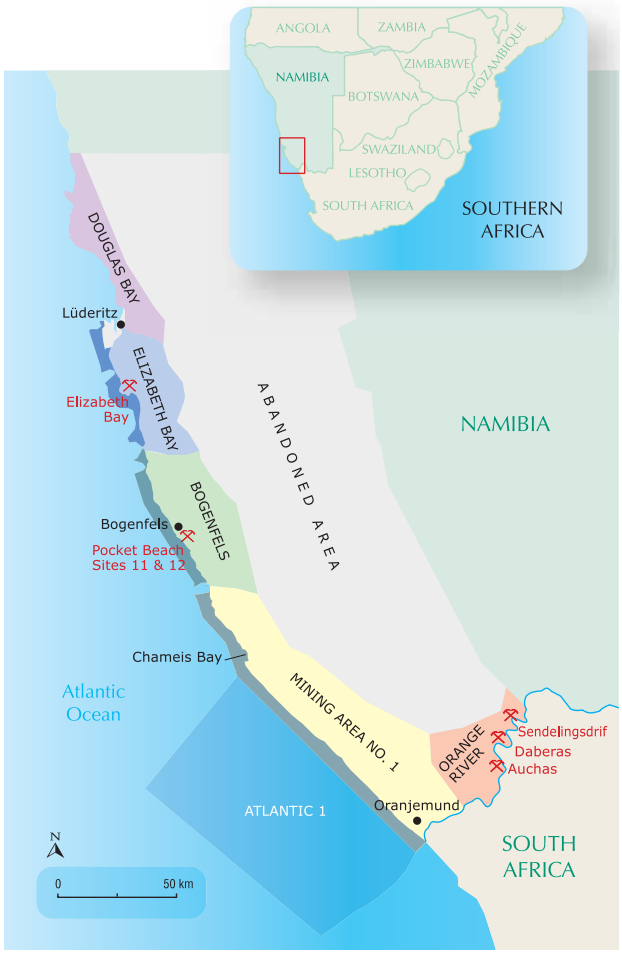

intertidal corridor is being tested. The "Jet Rig" is an eight-legged, self-elevating mobile platform with two jet-pump sampling tools and an onboard primary screening plant. It is hoped that the Jet Rig will be the prototype for an eventual mining system.

For more than two decades, Namdeb has been investigating the feasibility of mining "pocket beach" diamond deposits at Chameis Bay in Mining Area No. 1 north to Bogenfels. These gravel deposits (6,500–135,000 years old)

Figure 3. Diamonds are recovered from a variety of operations in southern Namibia. The Mining Area No. 1, Bogenfels, and Elizabeth Bay mining licenses extend from the Orange River in the south to the city of Lüderitz in the north, and from ~5.5 km offshore to 20–35 km inland. The Douglas Bay license extends from Lüderitz north to 26°S and from the low water mark of the Atlantic Ocean to approximately 15 km inland. The Orange River license extends along the river to about 50 km inland from the Mining Area No. 1 boundary. The Atlantic 1 license encompasses a portion of the middle shelf of the ocean, from the boundary of Mining Area No. 1 to about 65 km offshore. Except for the Atlantic 1 license, these areas are contained within the 26,000 km^2 Sperrgebiet.

Figure 4. Mining Area No. 1, Namibia's most important diamond-producing region, contains the richest marine deposits in the world. This aerial view is looking to the east from an area approximately over the beach. Photo by A. R. Kampf.

Figure 5. Elizabeth Bay is Namdeb's northernmost diamond mine in Namibia. The current operation is the third and most successful mine on this site since 1908. Photo by A. R. Kampf.

are confined to coastal embayments bounded by rocky headlands. The diamonds occur in thin, ribbon-shaped gravel bodies below the water table, deeply buried by dunes and marine sand. The geologic setting, coupled with the area's remoteness and lack of infrastructure, has presented significant challenges. Of 14 pocket beach sites identified, sites 11 and 12 are considered particularly promising because of the erosion and longshore transport of older gravels to favorable bedrock trapsites. Mining at these pocket beach sites is expected to create additional revenue at a time when production will decline at several of Namdeb's other land-based operations.

The northernmost gem in Namdeb's crown is the Elizabeth Bay mine (figure 5), situated about 25 km south of Lüderitz. It was in this area that the first Namibian diamonds were found in 1908, leading to the initial exploitation of the area by the Deutsche Kolonialgesellschaft für Südwestafrika (DKG) between 1911 and 1915. The second phase of mining, by CDM, lasted (with interruptions) from the early 1920s to 1948. The present Elizabeth Bay mine, opened in 1991, represents the third and most successful of the mining phases. The diamonds at Elizabeth Bay are found in ancient windblown (aeolian) sands that are significantly coarser than the desert sand. The diamonds recovered are small, averaging 0.1–0.3 ct, but the grades can be quite high. In the uppermost gray-colored grits, grades can reach 100 carats per hundred tonnes.

The lower Orange River was long considered barren of diamonds. It was not until the early 1960s that diamonds were found there and not until 1990 that the first mine, Auchas, went into production. Two principal types of diamond deposits flank the Orange River: The 17–19 Ma "Proto-Orange" terrace deposits more than 40 m above the river yield the bulk of the production, while the 2–5 Ma "Meso-Orange" deposits have only proved economic in localized areas. The Proto and Meso deposits both lie on eroded bedrock, where diamonds have been trapped in potholes and similar depressions. The Orange River deposits have relatively limited lifetimes. For example, after just 10 years of production, the Auchas mine ceased operations in 2000. Daberas (figure 6), which was started in 1999 and exploits the largest of the Proto-Orange deposits, is expected to have an 11-year life span. Sendelingsdrif, the second largest alluvial placer within Namdeb's license, is still in the sampling phase. The Orange River mines produce

Figure 6. The lower Orange River provides a minor but significant amount of Namibia's diamond production. The manager of the Orange River mines, Kakia Kakia, is shown here with a portion of the Daberas mine in the background. Photo by A. R. Kampf.

larger diamonds on average than those from the other Namdeb licenses. In 2005, the Orange River mines contributed 14.5% of Namdeb's total revenue and 7.3% of the total carats produced in Namibia.

With reduced production from onshore deposits, the offshore deposits clearly represent the future for Namdeb. In 1993, two decades of geologic research and prospecting in marine environments led to the initiation of successful mining operations in the Atlantic 1 license area. Since 2001, these have been conducted by the Windhoek-based De Beers Marine Namibia. Currently the company operates five mining vessels, four of which employ airlift drill technology and another that uses a track-mounted crawler. Mining is conducted up to 65 km from shore at depths ranging from 90 to 140 m. De Beers Marine Namibia also recently embarked on a near-shore pilot program that involves dredging diamondiferous material from the seabed and pumping it onshore for processing. Today, nearly half of Namibia's total annual diamond production is mined from the ocean, and this proportion is expected to increase in the years ahead.

Acknowledgments: Much of the information contained in this report was obtained on a Namdeb-sponsored visit to the area in October 2007. Special thanks are due to Chris Sivertsen, Namdeb general manager, and Kakia Kakia, manager of the Orange River mines, as well as to a host of Namdeb personnel who gave generously of their time, expertise, and hospitality.

Anthony R. Kampf (akampf@nhm.org)
Natural History Museum of Los Angeles County
Los Angeles, California

Figure 7. The emergence of a parasitic nematode from the abdomen of its host fly is well preserved in this Baltic amber. Photomicrograph by G. Poinar, magnified 35×; sample from the Poinar amber collection, maintained at Oregon State University (accession no. N-3-76).

COLORED STONES AND ORGANIC MATERIALS

Double jeopardy in amber. One of the wonderful aspects of amber preservation is that it fixes its victims so rapidly that various types of otherwise transient natural associations are often preserved. This includes a variety of parasitic associations, such as that seen in a 13 × 8 mm piece of Baltic amber from the Kaliningrad region of Russia (figure 7). About 40 million years ago—the age determined for Baltic amber by studying trace fossils (foraminifera) in the amber-bearing beds—a parasitic nematode belonging to the family Mermithidae was trapped while emerging from its host, a nonbiting midge belonging to the family Chironomidae. Midge-nematode associations have been reported previously in Baltic amber, but we believe this is the first to show the parasite and host still connected together.

In the normal life cycle of this nematode, a newly hatched worm lives on the bottom of a body of water until it encounters a fly larva. The nematode bores into the larva and remains there through the fly's adult stage, feeding on its nonvital tissues. When the nematode has finished growing, it emerges and searches for the nearest water source. However, when this fly landed on a drop of resin, the parasite exited through the host's body wall and found itself trapped in the resin as well. The midge made a valiant effort to escape from its parasite, as well as from the sticky trap. While it managed to pull away from the nematode, a coagulated strand of its blood still connected the two. In the final death stance, the fly appears to be pulling its parasite behind it.

From a biological point of view, it is astonishing to realize that the large nematode was coiled up in the abdomen of such a small fly. But a close examination of the midge's body cavity shows it to be empty, since all available protein and fat had been absorbed by the parasite. If the parasite had exited under normal circumstances (into a water source), it would have entered the mud, molted twice and searched for a mate. If it was a female, it would have deposited its eggs in the water and the hatching microscopic nematodes would have searched for another midge larva to start the cycle anew.

George Poinar (poinarg@science.oregonstate.edu)
Oregon State University, Corvallis

Brent Malgarin
Elegant Gems, Ltd.
Spokane, Washington

Inclusions in andradite from Namibia. At the 2007 Tucson gem shows, GIA received a donation from one of these contributors (CLJ) of several dozen crystal specimens of demantoid (the green variety of andradite that is colored by Cr and/or V) and eight cut stones that ranged from brownish red to yellowish green (0.10–5.51 ct; figure 8). These garnets were obtained from his Green Dragon mine,

Figure 8. These andradite samples (including the demantoid variety) were recently mined in Namibia, and contain needle-like inclusions. The cut stones weigh 0.10–5.51 ct (left), and the crystal is ~2 cm tall (right). Gift of Christopher L. Johnston, GIA Collection nos. 36713 (crystal), 36716 (brownish yellow cut stone), and 36741 (all the other cut stones); photos by Robert Weldon.

located approximately 12 km west of the Erongo Mountains and 28 km northeast of Klein Spitzkoppe in Namibia's Namib Desert. The andradite is hosted by a skarn-type deposit, where it forms euhedral-to-subhedral crystals that are fully enclosed within the calc-silicate units, as well as euhedral crystals in enrichment zones at the contacts between the calc-silicate units and various other rock types including granite, granodiorite, and schist. To date the largest concentration of andradite found at the mine measured approximately 1 m^3 and consisted of intergrown calcite and garnet.

Many of the andradites in the GIA donation were selected for their inclusions—some of which appeared quite similar to rutile needles. Since rutilated andradite/demantoid has not been documented previously, one of us (EAF) performed a detailed examination of the needle-like features in 50 samples (42 brownish green to yellowish green crystals and all eight faceted stones). The following gemological properties were collected on the brownish yellow, brownish yellowish green, and yellowish green cut stones (0.10–1.47 ct; figure 8): RI—over the limits of a standard refractometer; hydrostatic SG—3.83–3.85; Chelsea filter reaction—none; fluorescence—inert to long- and short-wave UV radiation; and a cutoff at 460 nm and a weak "chrome line" visible with the desk-model spectroscope. These properties are consistent with those previously reported for Namibian demantoid (see Fall 1997 Gem News, pp. 222–223; T. Lind et al., "New occurrence of demantoid in Namibia," *Australian Gemmologist*, Vol. 20, No. 2, 1998, pp. 75–79). Microscopic examination revealed the presence of long, fine "needles" (figure 9), curved fibers (figure 10), "fingerprints" composed of two-phase (liquid-gas) inclusions, and small crystals. The curved fibers appeared similar to the individual acicular inclusions that constitute "horsetail" inclusions found in demantoid from other localities. However, horsetails were not present in these samples, and they have not been previously documented in Namibian demantoid (M. Furuya, *Demantoid Garnet—The Legendary Gemstone Aroused from a Century of Sleep*, 2nd ed., Japan Germany Gemmological Laboratory, Yamanashi-ken, Japan, 2006, 31 pp.).

The properties of the five faceted brownish orange to brown-red andradites (1.19–5.51 ct; again, see figure 8) were the same as the other cut stones except for: hydrostatic SG—3.85–3.88, and a cutoff at 520 nm (reddish stones) or 460 nm (orangy stones) visible with the desk-model spectroscope. These properties are consistent with those previously reported for andradite in the Fall 1997 Gem News item cited above. Magnification revealed transparent angular growth zoning, "fingerprints" composed of two-phase (liquid-gas) inclusions, iridescence

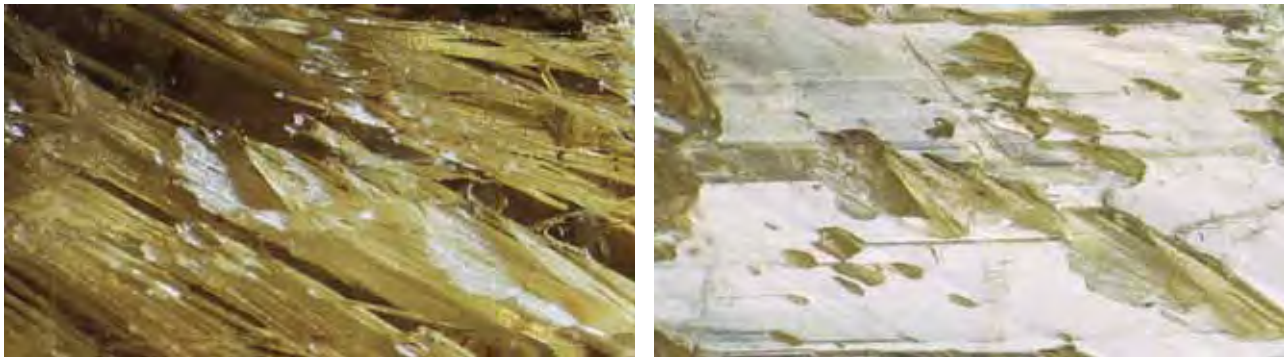

Figure 9. Long, fine "needles" in the demantoid samples (left) proved to be hollow tubes. Minute holes are seen in reflected light where they intersect the polished surface of this sample (right). Photomicrographs by J. I. Koivula; field of view 4.4 mm.

along growth planes (rainbow graining), and crystallographic trace lines (figure 11). Trace lines are internal representations of external crystal forms; such features are commonly seen as "phantoms" in crystals such as quartz, but trace lines also have been documented in pyralspite garnets (see E. J. Gübelin and J. I. Koivula, *Photoatlas of Inclusions in Gemstones*, Vol. 2, Opinio Publishers, Basel, Switzerland, 2005, pp. 22 and 446). The curved fibers and very fine needles noted in the demantoid samples tested were not seen in these brownish orange to brown-red andradites.

Surface-reaching needles in 12 rough and cut Namibian demantoid samples were tested by Raman analysis. Most of the features selected for analysis turned out to be empty holes when viewed with the microscope (again, see figure 9). However, the Raman spectra did indicate the presence of andradite, quartz (rough samples only), or diamond (cut samples only). The presence of quartz was not surprising, since it was found as an overgrowth on many of the crystals. The diamond apparently represents contamination from the faceting process.

With no clear information on the identity of the needles, we used a lap wheel to grind down portions of four of the demantoid crystals to expose their inclusions. Observation of the polished surfaces in reflected light showed minute openings or holes where the inclusions intersected the surface. In addition, we noted elongate surface channels in several places where the needles had been oriented parallel to the polished faces. This confirmed that the needles were actually hollow tubes, rather than mineral inclusions. Additional evidence for this conclusion was provided by powder X-ray diffraction (XRD) analysis of a demantoid crystal containing abundant needles by one of us (MG). The diffraction pattern showed only peaks corresponding to andradite, and no rutile or other minerals.

A demantoid pocket found in August 2007 contained some colorless fibrous crystal aggregates (figure 12), which

Figure 10. Curved fibers were present in two of the andradite samples shown in figure 8. Photomicrograph by E. A. Fritz; field of view 2.1 mm.

Figure 11. Rainbow graining and crystallographic trace lines are two of the features seen in the brownish orange to brown-red andradites. Photomicrograph by E. A. Fritz; field of view 4.8 mm.

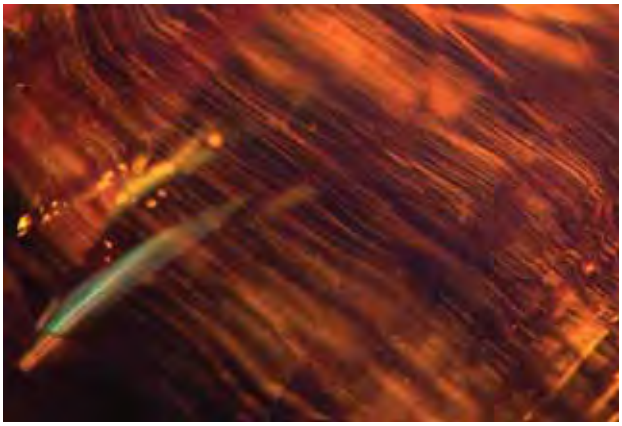

Figure 12. The fibrous crystals on this andradite specimen were identified as a mixture of calcite and asbestiform amphiboles. Photomicrograph by J. I. Koivula; field of view ~5.1 mm.

were identified as a mixture of calcite and asbestiform amphiboles (by MG) using a combination of XRD analysis and scanning electron microscopy. It is possible that needles of one or both of these minerals formed inclusions in the garnet that were subsequently etched away by late-stage hydrothermal fluids and/or weathering, leaving the empty channels documented in our samples.

Eric A. Fritz (eric.fritz@gia.edu) and John I. Koivula
GIA Laboratory, Carlsbad
Brendan M. Laurs
Mickey Gunter
University of Idaho, Moscow
Christopher L. Johnston
Green Dragon Mine, Namib Desert, Namibia

Andradite from Baluchistan, Pakistan. In recent years, some unusual gem materials have been found in Pakistan's Baluchistan region, such as quartz with petroleum inclusions (Spring 2004 Gem News International, pp. 79–81) and color-zoned axinite (Fall 2007 GNI, pp. 254–255). We were therefore curious to examine three unidentified faceted stones from Baluchistan that were loaned to GIA by Farooq Hashmi (Intimate Gems, Jamaica, New York). He obtained ~0.5 kg of the rough material in 2004 in Peshawar, Pakistan; the lot consisted of opaque dodecahedral crystals and gemmy broken pieces weighing 1–4 g.

Examination of the cut stones (0.65–0.99 ct; figure 13) showed the following properties: color—brownish yellow-orange to yellowish orange-brown; RI—over the limits of the standard gemological refractometer; hydrostatic SG—3.87–3.94; Chelsea filter reaction—none; fluorescence—inert to long- and short-wave UV radiation; and absorption to 500 nm visible with the desk-model spectroscope. These properties are consistent with those reported for andradite by C. M. Stockton and D. V. Manson ("A proposed new classification for gem-quality garnets" Winter 1985 *Gems & Gemology*, pp. 205–218). Microscopic examination revealed planes of one-, two-, and three-phase inclusions, as well as transparent angular graining.

Mr. Hashmi indicated that he has not seen any more of this andradite in the Peshawar market, although occasionally a similar "honey" colored garnet (grossular) has been produced from an area near the bastnäsite mines in the Peshawar region (H. Obodda and P. Leavens, "Zagi Mountain, Northwest Frontier Province, Pakistan," *Mineralogical Record*, Vol. 35, No. 3, 2004, pp. 205–220).

Eric A. Fritz and Brendan M. Laurs

Two axinite species from Tanzania. Axinite, $Ca_3Al_2BSi_4O_{15}(OH)$, is an uncommon biaxial gem material with a triclinic crystal habit. Much variation in the composition can occur, owing to the replacement of Ca by Fe, Mg, or Mn (W. A. Deer et al., *Rock-forming Minerals:*

Figure 13. These three gems (0.65–0.99 ct) from Baluchistan, Pakistan, proved to be andradite. Courtesy of Intimate Gems; faceted by Matt Dunkle (Aztec, New Mexico). Photo by Robert Weldon.

Figure 14. These three magnesio-axinites (0.20–0.42 ct) from Tanzania were characterized for this report. Courtesy of Rock Logic; photo by Robert Weldon.

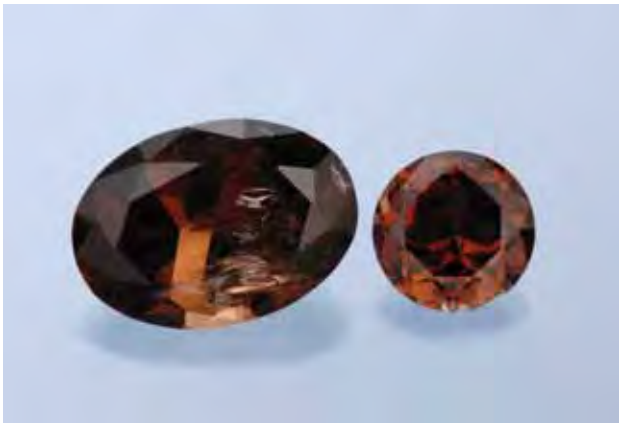

Figure 15. These ferro-axinites (1.30 and 4.40 ct) are also from Tanzania. Courtesy of Intimate Gems; photo by Robert Weldon.

Disilicates and Ring Silicates, 2nd ed., The Geological Society, London, Vol. 1B, 1997, pp. 603–623). Ferro-axinite is the species that is most commonly cut into gems (e.g., Fall 2007 Gem News International, pp. 254–255), while magnesio-axinite has been faceted only rarely (see Summer 2005 Lab Notes, pp. 170–171).

At the 2007 Tucson gem shows, Alexandra Woodmansee (Rock Logic, Glencoe, Minnesota) had some light bluish violet magnesio-axinite that was reportedly from the tanzanite mining area at Merelani, Tanzania. She initially obtained a faceted example (0.72 ct) of this magnesio-axinite in the mid-1980s. However, additional material did not become available until a small quantity of rough appeared at the 2006 Tucson shows. In Tanzania, the rough has been sold inadvertently as low-quality tanzanite, but it can be easily separated by its orangy pink UV fluorescence and subtle color shift (see below). From a total of 29 grams of rough, Ms. Woodmansee has cut about two dozen stones, typically weighing <1 ct, although a few larger included stones up to ~2 ct also were faceted.

Ms. Woodmansee loaned 11 faceted magnesio-axinites to GIA for examination, and we obtained gemological properties on three of them (0.20, 0.23, and 0.42 ct; figure 14). In daylight-equivalent illumination, they ranged from pale violet to pale grayish violetish blue with weak pleochroism in shades of light purple, yellow, and yellowish green. In incandescent light, all of the samples shifted to a more intense and uniform violet. The stones showed the following properties: RI—1.660–1.672; birefringence—0.012; hydrostatic SG—3.08–3.30; fluorescence—strong to very strong orangy pink to long-wave UV radiation, and medium orangy pink to short-wave UV; and an absorption line at 410 nm with a weak 580 nm cut-off seen with the desk-model spectroscope. These properties are comparable with those reported for a 0.78 ct transparent magnesio-axinite by E. A. Jobbins et al. ("Magnesioaxinite, a new mineral found as a blue gemstone from Tanzania," *Journal of Gemmology*, Vol. 14, 1975, pp. 368–375), who gave RIs of 1.656–1.668 (birefringence of 0.012) and an SG value of 3.18. Our variable SG values are probably due to the effect of the numerous fractures and inclusions in the stones we examined. Microscopic examination revealed fluid-filled "fingerprints" composed of thread-like and two-phase inclusions, thin fluid films with polygonal shapes, and numerous fractures and cavities with dark brown staining.

Tanzania is also the source of some very different axinite, which gem dealer Farooq Hashmi obtained in Arusha in 2006. It had a brown color that resembled zoisite before it is heat treated to tanzanite, and its trichroism could easily cause further confusion with zoisite. Although the material was offered as tanzanite, Mr. Hashmi suspected that it was axinite and therefore obtained only a small amount of the cobbed rough from which two stones were faceted (figure 15).

Mr. Hashmi loaned the two cut stones (1.30 and 4.40 ct) to GIA for examination, and we obtained the following properties: color—brown to reddish brown (showing no significant color shift in different light sources), with strong purple, yellow, and brownish orange pleochroism; RI—1.668–1.680; birefringence—0.012; hydrostatic SG—3.20; fluorescence—inert to both long- and short-wave UV radiation; and a weak 415 nm absorption line seen with the desk-model spectroscope. These properties are comparable to those reported for ferro-axinite by M. O'Donoghue (*Gems*, 6th ed., Butterworth-Heinemann, Oxford, UK, 2006, p. 386), except that publication listed somewhat higher RI and SG values, as well as additional absorption features at 444, 512, and 532 nm, with two broader bands at 466 and 492 nm. Microscopic examination revealed large fractures, "fingerprints" consisting of orderly parallel inclusions (figure 16), and thread-like or irregular fluid remnant inclusions (figure 17). There was also subtle straight and angular growth zoning in both stones.

Figure 16. The ferro-axinite contains "fingerprints" composed of orderly parallel inclusions. Photomicrograph by D. Beaton; field of view 4.8 mm.

Figure 17. Thread-like and irregular fluid inclusions are visible through the bezel of this ferro-axinite. Photomicrograph by D. Beaton; field of view 7.2 mm.

Electron-microprobe analyses (table 1) of one sample each of magnesio- and ferro-axinite showed similar compositions to those reported for these minerals by Jobbins et al. (1975) and Deer et al. (1997), except that the magnesio-axinite analyzed for this study contained somewhat more Mn (~2.0 vs. 0.4 wt.% MnO). The composition of the ferro-axinite closely resembled that of the material from Pakistan reported in the Fall 2007 GNI entry.

TABLE 1. Average electron-microprobe analyses of two axinites from Tanzania.[a]

Chemical composition	Magnesio-axinite 0.42 ct	Ferro-axinite 1.30 ct
Oxides (wt.%)		
SiO_2	43.84	42.97
B_2O_3 calc.	6.35	6.22
Al_2O_3	18.56	17.77
FeO	0.05	7.80
MnO	1.99	0.62
MgO	6.27	2.94
CaO	20.46	20.10
Na_2O	0.02	0.05
K_2O	0.02	0.04
H_2O calc.	1.64	1.61
Total	99.22	100.12
Ions per 16 (O,OH,F)		
Si	3.998	3.999
B calc.	1.000	1.000
Al	1.995	1.950
Fe^{2+}	0.004	0.607
Mn	0.154	0.049
Mg	0.852	0.408
Ca	1.999	2.005
Na	0.004	0.009
K	0.002	0.005
OH calc.	1.000	1.000

[a]*Average of five points per stone. Ti, Cr, V, Bi, Pb, Zn, and F were analyzed, but not detected.*

Hyejin Jang-Green (hjanggre@gia.edu)
and Donna Beaton
GIA Laboratory, New York

Brendan M. Laurs

William B. (Skip) Simmons and Alexander U. Falster
University of New Orleans, Louisiana

Baddeleyite from Mogok, Myanmar. Baddeleyite was first documented in faceted form in the Fall 2001 Lab Notes section (p. 212), as a 0.54 ct very dark greenish brown cushion cut that was represented as being from Sri Lanka. More recently, baddeleyite was recognized as a mineral associated with painite from Myanmar (unpublished data; see also Winter 2005 Gem News International, p. 356). Small quantities of baddeleyite from the Thurien-taung painite deposit in the western Mogok area have been faceted recently for gem collectors, according to Mark Smith (Thai Lanka Trading Ltd., Bangkok, Thailand). Mr. Smith reported that the rough baddeleyite is sometimes mixed in parcels of rutile, black amphibole, and schorl fragments, but it can be easily separated according to its higher specific gravity, as well as the distinctive bladed crystal shape and submetallic luster. The crystals are black (dark brown on a thin edge) and measure up to 2.5 cm long; some are intergrown with small red spinel crystals.

Since mid-2005, Mr. Smith has faceted nearly 100 pieces of the baddeleyite. The cutting yield is very low due to cracking and the thin bladed shape of the rough. Most of the stones were cut from broken crystals weighing 0.2–1 g. The shape of these pieces is most conducive to cutting flat rectangular stones. Most of the cut gems ranged from 0.2 to 3 ct, and a few weighed 5–6 ct. In addition, one exceptional faceted stone weighed 26.36 ct; it was cut from a broken piece of rough that was much larger than any other pieces Mr. Smith has seen.

Figure 18. These faceted stones (0.56–1.95 ct) are baddeleyite from the Thurien-taung painite deposit in Myanmar. Gift of Mark Smith, GIA Collection nos. 37141–37143; photo by Kevin Schumacher.

Mr. Smith donated three faceted stones (0.56–1.95 ct; figure 18) to GIA, and the following properties were determined: color—black, with no pleochroism; RI—over the limits of a standard gemological refractometer; hydrostatic SG—5.84–5.92; fluorescence—inert to long-wave UV radiation and very weak yellow-green to short-wave UV; and no spectrum visible with the desk-model spectroscope. These properties are consistent with those reported for baddeleyite in the Fall 2001 Lab Note, except that the Burmese stones were too opaque to view any color, pleochroism, or absorption spectrum. However, a reddish brown color was apparent with high-power fiber-optic illumination. Microscopic examination revealed numerous fractures, and small stringers of fine particles could be seen in the semitransparent edges of the stones.

The Burmese baddeleyite was produced as a byproduct of mining for painite, and Mr. Smith reported that it has become difficult to find rough baddeleyite in the Asian marketplace because of the decreased production of (and demand for) painite.

Editor's note: U.S. law covering import of Burmese gem materials was in the process of being reevaluated when this issue went to press. At the time GIA examined these stones, their import into the U.S. was permitted by existing law.

Eric A. Fritz and Brendan M. Laurs

Chrysocolla chalcedony from Iran/Armenia area. The majority of gem-quality chrysocolla chalcedony comes from Mexico and Arizona (e.g., Gem News, Spring 1992, pp. 59–60; Summer 1996, pp. 129–130). A new source reportedly was discovered recently in the border region between Iran and Armenia, according to Jack Lowell (Colorado Gem & Mineral Co., Tempe, Arizona). Mr. Lowell's supplier indicated that ~1,100 kg have been mined so far. Chalcedony has been previously reported from Iran (see Winter 2004 Gem News International, p. 337), but as adularescent material with a considerably paler blue color.

Mr. Lowell loaned two cabochons (8.86 and 3.17 ct) and a rough piece of the chalcedony to GIA for examination (figure 19). The following properties were obtained on the cabochons (with those for the larger cabochon given first here): color—green-blue and blue-green; diaphaneity—semitransparent to translucent; RI—1.54; hydrostatic SG—2.60 and 2.62; Chelsea filter reaction—none; fluorescence—inert to both long- and short-wave UV radiation. A 650 nm cutoff was observed with a desk-model spectroscope. Microscopic examination revealed spotty green

Figure 19. These samples of chrysocolla chalcedony came from a newly discovered source near the Iran/Armenia border. The cabochons weigh 8.86 and 3.17 ct, and the slab measures 5.5 × 3.7 cm. Courtesy of Jack Lowell; photo by Robert Weldon.

inclusions (chrysocolla particles). Raman analysis of both samples showed a close match to chalcedony spectra on file. Energy-dispersive X-ray fluorescence (EDXRF) spectroscopy of the two samples indicated major amounts of Si and Cu, and traces of Fe. Absorption spectroscopy showed typical features for chrysocolla chalcedony, with absorptions at 527–1176 nm (Cu^{2+}), 1370–1600 nm (total OH), and 1850–2120 nm (molecular water), and 2128–2355 nm (or 4700–4245 cm^{-1}; structurally bonded OH).

The Cu^{2+} band recorded from UV-Vis-NIR absorption spectroscopy can be used to determine the presence of dye (see A. Shen et al., "Identification of dyed chrysocolla chalcedony," Fall 2006 *Gems & Gemology*, p. 140), by calculating the ratio of the integrated intensity of the Cu^{2+} band compared to that of the structurally bonded OH band. The Shen et al. results showed a ratio between 0.5 and 3 for dyed chalcedony and between 7 and 44 for natural-color chrysocolla. The present samples had ratios of 15.7 and 7.4, establishing that they were not dyed.

Kevin G. Nagle (knagle@gia.edu)
GIA Laboratory, Carlsbad

Yellow-green clinohumite and yellow chondrodite from Tanzania. During a buying trip to Tanzania in 2006, gem dealer Farooq Hashmi obtained some brownish yellow and yellow-green rough from a few small parcels that were represented as tourmaline from a new deposit at Sumbawanga in west-central Tanzania. All of the rough consisted of broken pieces (figures 20 and 21), so it was not possible to determine if they originated from primary or secondary deposits. Most of the pieces weighed <1 g, and there was an approximately equal percentage of the two colors available in each parcel. The appearance and properties of the material were not typical of tourmaline normally found in Tanzania, so Mr. Hashmi loaned several rough and cut examples of each color for examination at GIA.

The following properties were recorded on three greenish yellow cut stones (figure 20): color—greenish yellow to yellow-green, with no obvious pleochroism; RI—n_α=1.620 and n_γ=1.648–1.649; birefringence—0.028–0.029; hydrostatic SG—3.21; Chelsea filter reaction—none; fluorescence—inert to long-wave UV radiation and very weak to weak yellow to short-wave UV; and a weak absorption band at 490 nm visible with the desk-model spectroscope. These properties are similar to those reported for clinohumite by M. O'Donoghue (*Gems*, 6th ed., Butterworth-Heinemann, Oxford, UK, 2006, p. 400), except that the colors were reported as yellow to orange or dark brown and the RI values were higher (n_α=1.623–1.702 and n_γ=1.651–1.728). Microscopic examination revealed clouds of fine needles and flat, ribbon-like fluid inclusions. Electron backscatter diffraction analysis showed that these needles were parallel to the b axis (i.e., the 4.7 Å unit cell direction). All three samples were moderately abraded and contained numerous fractures.

Figure 20. The greenish yellow to yellow-green color of this clinohumite from Tanzania (cut stones 0.90–1.81 ct) is quite unusual. Courtesy of Intimate Gems; photo by Robert Weldon.

The properties of three brownish yellow cut stones (figure 21) were: color—brownish yellow, with weak yellow to colorless pleochroism; RI—n_α=1.589–1.593 and n_γ=1.618–1.620; birefringence—0.027–0.029; hydrostatic SG—3.20–3.24; Chelsea filter reaction—none; fluorescence—inert to long-wave UV radiation and moderate yellow to short-wave UV; and no features visible with the desk-model spectroscope. These properties are consistent with those reported for chondrodite by O'Donoghue (2006, p. 399), except the colors reported in that publication were deep red and orange brown, and the RI values were slightly higher (n_α=1.592–1.643 and n_γ=1.621–1.636). Magnification revealed numerous abrasions, fractures,

Figure 21. These brownish yellow gems from Tanzania (cut stones 0.64–0.80 ct) were identified as chondrodite. Courtesy of Intimate Gems; photo by Robert Weldon.

screw dislocations, and planar fluid inclusions.

Electron-microprobe analyses were performed on the three cut clinohumites (15 analyses total) and on one faceted chondrodite (5 analyses), and all of the data points showed a homogenous composition within each mineral; average analyses are shown in table 1. In addition to the elements expected from the chemical formula, $(Mg,Fe^{2+})_9(SiO_4)_4(F,OH)_2$, the clinohumites contained traces of Ti, Al, and K. Much lower Fe was present than in the data for clinohumite reported by W. A. Deer et al. (*Rock-Forming Minerals—Orthosilicates*, Vol. 1A, 2nd ed., Longman, London, 2001, pp. 381–417). The relatively small amount of Fe is responsible for the low RI values; although fluorine-rich clinohumite may also show low RI values, these stones contained intermediate amounts of F. The chondrodite, $(Mg,Fe^{2+})_5(SiO_4)_2(F,OH)_2$, contained traces of Al, Mn, Ca, Na, K, and Ti; the last element was present in considerably lower amounts than the range shown by Deer et al. (2001).

TABLE 1. Average electron-microprobe analyses of clinohumite and chondrodite from Tanzania.[a]

Chemical composition	Clinohumite[b] 0.90 ct	Chrondrodite[c] 0.64 ct
Oxides (wt.%)		
SiO_2	37.57	33.50
TiO_2	0.42	nd
Al_2O_3	0.18	0.13
FeO	0.31	2.08
MnO	nd	0.11
MgO	58.39	56.00
CaO	nd	0.09
Na_2O	nd	0.02
K_2O	0.02	0.01
H_2O calc.	2.41	2.07
F	1.01	6.37
Subtotal	100.31	100.39
-O=F	0.43	2.68
Total	99.88	97.71
Ions per formula unit		
Si	3.908	1.975
Ti	0.033	nd
Al	0.022	0.009
Fe^{2+}	0.027	0.103
Mn	nd	0.005
Mg	9.056	4.921
Ca	nd	0.006
Na	nd	0.002
K	0.003	0.001
OH calc.	1.668	0.812
F	0.332	1.187

[a]*Abbreviation: nd = not detected. Cr, Bi, V, Pb, and Zn also were analyzed, but not detected.*

[b]*Ions were calculated using 18 (O,OH,F) per formula unit.*

[c]*Ions were calculated using 10 (O,OH,F) per formula unit. Similar chondrodite analyses where H_2O is analyzed typically have 1–2 wt.% H_2O, as well as additional O in the anion site. Thus, the water estimate here is probably somewhat high, since some O would be expected in the anion site. The slightly low total of the chondrodite analyses may reflect low F as a result of the standardization process.*

Vis-NIR spectroscopy of a polished piece of the rough clinohumite showed a broad peak centered at ~750 nm (figure 22)—quite unlike typical yellow-orange to orange clinohumite spectra, which are dominated by a peak at 435 nm related to Fe-Ti intervalence charge transfer (see K. Langer et al., "The crystal chemistry of the humite minerals: Fe^{2+}-Ti^{4+} charge transfer and structural allocation of Ti^{4+} in chondrodite and clinohumite," *European Journal of Mineralogy*, Vol. 14, No. 6, 2002, pp. 1027–1032). A weaker feature near 1040 nm is seen in most clinohumite spectra, including the Tanzanian specimen, but dominantly only in one orientation; absorption in this region is due to Fe^{2+} (Langer et al., 2002). Further research is necessary to fully characterize the origin of the unusual yellow-green color in this clinohumite.

Clinohumite and chondrodite were recently documented from Tanzania by the SSEF laboratory in Basel, Switzerland ("Uncommon minerals as gemstones from Tanzania," *SSEF Facette*, No. 14, 2007, p. 6). Similar "golden" yellow chondrodite is shown in that article (along with yellow-brown to brown, red, and near-colorless material), whereas the greenish yellow clinohumite

Figure 22. Polarized Vis-NIR absorption spectra of the clinohumite were obtained with a beam of light oriented nearly parallel to the a axis (i.e., the 13.84 Å unit cell direction). With this orientation, a spectrum (γ spectrum) nearly parallel to the Z indicatrix direction (b axis, or 4.7 Å unit cell direction) and a spectrum (~β spectrum) containing mostly the Y indicatrix direction, were obtained. A broad band centered at ~750 nm was recorded when the beam was polarized to obtain the ~β spectrum, and both spectra show an intense absorption in the 400 nm region. Sample thickness: 6.4 mm.

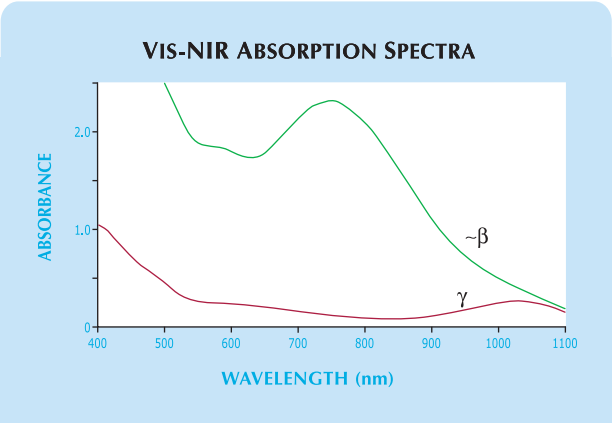

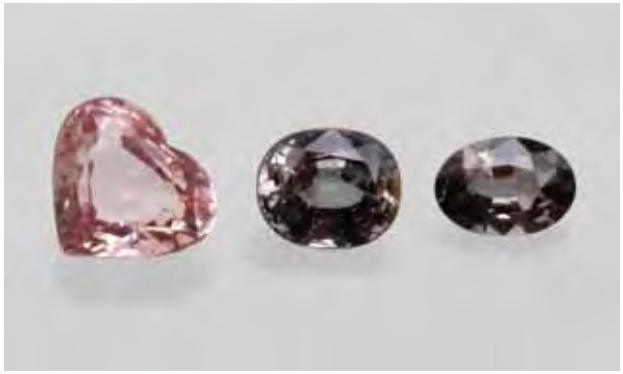

Figure 23. These samples of dumortierite (2.06, 1.18, and 0.61 ct) are from Tunduru, Tanzania. Photo by H. A. Hänni; © SSEF.

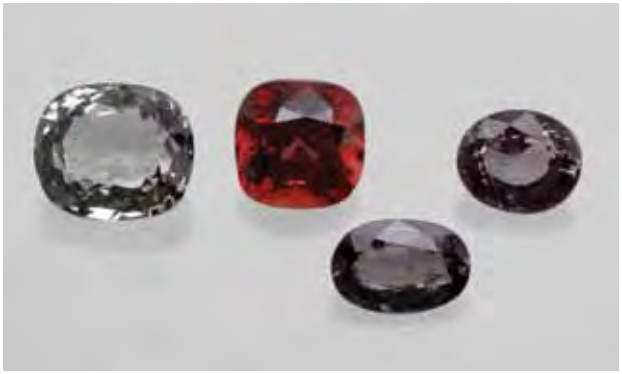

Figure 24. Tunduru is also the source of these sapphirine gems (2.14, 1.55, 0.67, and 0.93 ct). Photo by H. A. Hänni; © SSEF.

described here is quite different from the yellow-orange to orange stones shown in that report.

Eric A. Fritz and Christopher M. Breeding
GIA Laboratory, Carlsbad

George R. Rossman
California Institute of Technology
Pasadena, California

Brendan M. Laurs

William B. (Skip) Simmons and Alexander U. Falster

Transparent dumortierite and sapphirine from Tanzania. From time to time, the SSEF Swiss Gemmological Institute receives rough material for identification, often as parcels of pebbles, crystals, and fragments. Rough stone buyer Werner Spaltenstein, based in Chanthaburi, Thailand, is one source of such material, mainly from East Africa and Madagascar. In these lots, we have identified a number of uncommon and rare minerals. Here we report on two such transparent minerals found in gravels from Tunduru, Tanzania.

Dumortierite, an alumino-borosilicate, is best known as a polycrystalline blue ornamental stone, often mixed with quartz. The new material from Tunduru, however, was transparent and colored violetish gray and brownish pink. The three waterworn pebbles were identified by their SGs and Raman spectra; after faceting (figure 23), we obtained RI and birefringence values that were consistent with dumortierite. The following properties were recorded on the faceted stones: pleochroism—strong, light gray to red (pink stone); RI—n_α=1.679, n_γ=1.709; birefringence—0.030; SG—3.38–3.41; and UV fluorescence—inert to long-wave UV radiation and white to short-wave UV. The stones were nearly free of fluid or mineral inclusions. EDXRF analysis of all three samples showed major Al and Si, and traces of Ti and Ga in variable amounts (B cannot be detected by EDXRF); Ti is probably the chromophore of the pink stone.

Sapphirine, an aluminosilicate, is rarely transparent and is usually gray, green, or brownish violet. The samples from Tunduru consisted of four transparent waterworn pebbles ranging from gray to violet and red that came from parcels of rough spinel and sapphire. These samples were also identified by their SG and Raman spectra and, after faceting (figure 24), they yielded RI and birefringence values that were consistent with sapphirine. The following properties were obtained: pleochroism—strong, light pink to dark red (red stone); RI—n_α=1.701–1.704, n_γ=1.708–1.711; birefringence—0.007; SG—3.49–3.50; UV fluorescence—inert (gray-to-violet stones), and dull red to long-wave and weak orange to short-wave UV radiation (red stone). No inclusions were seen in any of the samples with a gemological microscope. EDXRF analysis of all the stones showed major amounts of Mg, Al, and Si, and traces of Fe, Ti, Cr, and Ga. Their color range is most probably due to variable amounts of Fe and Cr, the latter element being the main cause of color in the red stone.

Dumortierite and sapphirine are rare as faceted gemstones, and the occurrence of attractive pink dumortierite and red sapphirine was particularly surprising.

Henry A. Hänni

Brazilian blue opal, with cristobalite and quartz. At the 2007 Tucson gem shows, Si and Ann Frazier (El Cerrito, California) obtained two cabochons of a new Brazilian "opal" and loaned them to GIA for examination. One weighed 6.77 ct and was banded in light blue, white, light brown, and gray, while the other was a 6.84 ct light blue stone (figure 25).

We obtained the following properties on the cabochons: diaphaneity—translucent; spot RI—1.44 (blue portions), 1.54 (wide central light brown band), and 1.50 (darker brown area near the end of the cabochon). Hydrostatic SG was 2.25 for the blue cabochon and 2.53 for the banded specimen. Both stones were inert to long-wave UV radiation. The blue areas showed chalky very weak green-yellow fluorescence to short-wave UV, while the brown bands fluoresced weak-to-moderate green-yellow (brightest at the white transition zone to the blue area in the banded cabochon). No distinct absorption features were seen with a desk-model spectroscope.

Microscopic observation of the banded sample revealed that the narrow brown layer that transitioned to the light blue region contained pale brown transparent spherules

Figure 25. The blue portions of these two cabochons from Brazil (6.77 and 6.84 ct) appear to be a mixture of opal and cristobalite; the brown bands are quartz. Courtesy of Si and Ann Frazier; photo by Robert Weldon.

that were very small and densely packed. The darker brown band near the opposite end of the cabochon also contained these spherules (larger than the others) with milky white interstitial areas. Raman analysis of multiple areas of this band only gave spectral matches for quartz. The RI of 1.50 from this end of the banded cabochon could be due to the presence of both opal and quartz in this region (due to its amorphous nature, no Raman peaks would be expected for opal). The wide light brown band through the center of the cabochon contained no visible spherules or other structure, but it did have interstitial stubby white dendritic inclusions that suggested the location of grain boundaries. Raman analysis of this area also matched quartz, and the RI (1.54) of this region was consistent with quartz as well.

Microscopic examination of the blue areas of both cabochons revealed a milky nature, consistent with the scattering of light from submicroscopic particles. However, there were no visible inclusions in these areas other than a small surface fracture with brownish discoloration. The lower RI of these regions (1.44) is consistent with that of opal, and Raman analysis only yielded matches for cristobalite, a polymorph of quartz that is commonly found in opal. A high concentration of cristobalite (SG of 2.32–2.36) could explain the elevated SG (2.25) of the blue cabochon, since the SG of opal with lower RI values is typically closer to 2.0. *Gems & Gemology* previously reported on a cabochon that was a mixture of cristobalite and opal—a milky white specimen from Madagascar (see Winter 2004 Gem News International, pp. 339–340, for a more in-depth discussion of this type of material). Typically, we would expect a higher RI for a mixture of opal and cristobalite, to be consistent with the elevated SG value; however, both properties can be influenced by the amount of structural water—and additional minerals—present. Further study is necessary to better understand the relationship between these properties and the factors affecting them. The presence of the quartz bands (SG of 2.66) would explain the even higher SG (intermediate between opal and quartz) of the oval cabochon.

To explore the cause of the blue color in our samples, we performed EDXRF analysis. Together with traces of several other elements, minute amounts of Cu and Fe were found in the blue cabochon. A trace of Fe was also found in the banded cabochon, but no Cu was detected (this was probably due to the brown quartz band dominating the area that was analyzed). Although the minute traces of these common chromophores may be contributing to the blue color of this material, we could not confirm this.

Cheryl Y. Wentzell (cwentzell@gia.edu)
and Karen M. Chadwick
GIA Laboratory, Carlsbad

Otolith pendant. Fish ear bones, called otoliths (from the Greek *oto* [ear] and *lithos* [stone]), are complex polycrystalline structures composed of calcium carbonate and organic material. Most fish have three pairs of otoliths—sagittae, lapilli, and asterisci—that are located behind the

Figure 26. This unusual pendant is set with a baroque-shaped fish ear bone, or otolith (24.1 ct; 25 × 14 × 12 mm). Photo by B. Mocquet.

brain in the inner ear and contribute to their sense of equilibrium. Otoliths are scientifically important because they grow continuously until death, providing valuable information on the fish's age and environment (see, e.g., N. H. Halden, "Coloured fish ears: Cathodoluminescence as a guide to variation in aqueous environments," *Newsletter of the Mineralogical Association of Canada*, No. 64, 2001, pp. 1, 3–4). Otoliths also have a history of use in jewelry by native peoples (R. E. Martin et al., Eds., *Marine and Freshwater Products Handbook*, Technomic Publishing Co., Lancaster, PA, 2000).

One of these contributors (BM) had an otolith mounted into a pendant (figure 26). This baroque-shaped otolith is from a South American silver croaker (*Plagioscion squamosissimus*) that lived in the Orinoco River of Venezuela more than 60 years ago. The silver croaker can reach lengths of 80 cm; in Venezuela, it is known as *curvinata*, and its otoliths are used for amulets or good luck charms in the southern states of Amazonas and Bolívar.

The size of the otolith in this pendant (25 × 14 × 12 mm) suggests that it is probably a sagitta, the largest of the three types. The otolith was removed from the setting for gemological examination. SG and RI values (by the spot method) were approximately 2.82 and 1.54 (with "blink" birefringence), respectively. It had a greasy luster and was inert to long- and short-wave UV radiation. The Raman spectrum (obtained without a microscope) displayed aragonite peaks, as well as peaks for organic matter. Fish otoliths are mainly aragonitic, but they may also be composed of other carbonate polymorphs such as calcite and vaterite (R. W. Gauldie, "Polymorphic crystalline structures of fish otoliths," *Journal of Morphology*, Vol. 218, No. 1, 1993, pp. 1–28).

Stefanos Karampelas (steka@physics.auth.gr)
University of Thessaloniki, Greece;
Institut des Matériaux Jean Rouxel (IMN)
Université de Nantes, France

Blanca Mocquet
Centre de Recherches Gemmologiques
Jean-Pierre Chenet (CRG), Nantes, France

Emmanuel Fritsch

Goethite and hematite inclusions in quartz from Mina da Batalha, Brazil. Inclusions of native copper are well known in Paraíba tourmaline from Mina da Batalha (see, e.g., F. Brandstätter and G. Niedermayr, "Inclusions of native copper and tenorite in cuprian-elbaite tourmaline from Paraíba, Brazil," Fall 1994 *Gems & Gemology*, pp. 178–183). In June 2007, some pale amethyst and smoky quartz (e.g., figure 27) that contained copper-colored inclusions were recovered from a deeper level of this mine. Quartz containing Cu inclusions has not been documented previously from this locality, so Brian Cook (Nature's Geometry, Laguna Beach, California) donated two of the specimens to GIA to investigate this possibility.

Microscopic examination revealed scattered minute platy inclusions just beneath the surface of the amethyst crystals. These had a coppery metallic appearance in reflected light (figure 28, left), but in transmitted light they were dull red to earthy yellow and transparent to translucent (figure 28, right). This eliminated copper as a possibility. Also, unlike the copper inclusions seen in some tourmaline from this mine, these platelets were not oriented according to the crystallography of the host quartz, but instead appeared as randomly oriented inclusions on shallow prism and rhombohedral planes.

Figure 27. This quartz specimen (8.0 cm tall) from Mina da Batalha, Paraíba State, contains microscopic inclusions with a general appearance that is similar to the native copper platelets seen in some tourmaline from this famous locality. Gift of Brian Cook, GIA Collection no. 37354; photo by Robert Weldon.

The platelets' appearance in transmitted light is indicative of a common alteration pattern among a number of iron oxides and hydroxides. In this case, the platelets appeared to be composed of a mixture of hematite (red) and goethite (brownish yellow). EDXRF chemical analysis of one of the quartz samples where the inclusions were located close to the surface revealed traces of Fe, as expected for hematite and goethite, but no Cu was detected. The inclusions were too deep in the quartz to obtain a clear signal with the Raman microspectrometer, so a small amount of one sample was ground off to expose one of the

Figure 28. With reflected fiber-optic light (left), the platy inclusions in the Mina da Batalha amethyst have a coppery metallic appearance. In transmitted light (right), they are transparent to translucent and have a red to earthy brownish yellow color—consistent with goethite and hematite, rather than native copper. Photomicrographs by J. I. Koivula; field of view ~1.6 mm.

platelets on the surface; it was identified as one of the two suspected minerals, goethite.

Eric A. Fritz, John I. Koivula, and Brendan M. Laurs

Sinhalite from Myanmar. Sinhalite was first recognized as a new mineral (in faceted form) in 1952, after having been misidentified for decades, most commonly as "brown peridot." As early as 1912, a specimen of sinhalite at the British Museum that had originally been catalogued as chrysoberyl, and then "chrysolite," was flagged for "further examination" because its properties did not match any then-known minerals (B. W. Anderson, "Two new gemstones: Taaffeite and sinhalite," Summer 1952 *Gems & Gemology*, pp. 171–175). The name comes from the word *Sinhala*, the Sanskrit word for Ceylon (now Sri Lanka), which was at the time the only known locality. Gem-quality material has also been found in Mogok, Myanmar (C. J. Payne, "A crystal of sinhalite from Mogok, Burma," *Mineralogical Magazine*, Vol. 31, 1958, pp. 978–979; M. Gunawardene and M. S. Rupasinghe, "The Elahera gem field in central Sri Lanka," Summer 1986 *Gems & Gemology*, pp. 80–95). Although sinhalite has been known from Myanmar for decades, it has not become available in the gem market until fairly recently.

Figure 29. These attractive sinhalites (1.35–3.20 ct) are from Mogok, Myanmar. Courtesy of Bradley Payne; photo by Kevin Schumacher.

Bradley J. Payne (The Gem Trader, Grand Rapids, Michigan) recently loaned seven faceted sinhalites (1.35–3.20 ct; figure 29) from Mogok for examination at GIA. While Burmese sinhalite is not new, we welcomed the opportunity to examine several such gemstones at the same time. The following properties were obtained: color—pale yellow to pale brownish yellow; pleochroism—very weak pale yellow and pale brown; RI—n_α=1.666–1.668 and n_γ=1.704–1.706; birefringence—0.038; optic character—biaxial negative; hydrostatic SG—3.48–3.50; fluorescence—inert to both long- and short-wave UV radiation; and absorption lines visible with the desk-model spectroscope at 452, 463, 475, and 493 nm, as well as a broad band in the violet range (up to 435 nm). Microscopic examination revealed clouds, fluid inclusions, two-phase inclusions, and colorless graining. These results are comparable to reported properties for sinhalite (R. Webster, *Gems*, 5th ed., revised by P. G. Read, Butterworth-Heinemann, Oxford, UK, 1994, p. 373).

The brown coloration in sinhalite has been attributed to iron (Webster, 1994). EDXRF analysis of three of the seven stones confirmed that they did indeed contain significant levels of iron. Other trace elements detected were Cr, Mn, Ga, and Zn.

According to suppliers in Myanmar, the source of the Burmese sinhalite is Ohn Gaing (Ongaing) in northern Mogok. The most recent finds have occurred since 2005, and stones up to 16+ ct have reportedly been faceted (pers. comms., 2007: Mark Smith; Dudley Blauwet, Dudley Blauwet Gems, Louisville, Colorado). Mr. Smith indicated that the Burmese sinhalite is also notable for commonly occurring as well-formed crystals, unlike the material from Sri Lanka, which is typically found as water-worn pebbles. He also stated that the color of Burmese material is lighter and more yellow than the general range from Sri Lanka.

Editor's note: U.S. law covering import of Burmese gem materials was in the process of being reevaluated when this issue went to press. At the time GIA exam-

ined these stones, their import into the U.S. was permitted by existing law.

Karen Chadwick (karen.chadwick@gia.edu)
and Brendan M. Laurs

Field study of Cu-bearing tourmaline mines in Mozambique. In late August and early September 2007, these contributors visited Mozambique's Cu-bearing tourmaline deposits to obtain information on their location, geology, and mining. We were hosted by personnel from Mozambique Gems (Nampula, Mozambique), which owns the first claim that was staked in the area for this tourmaline in 2003.

The mining area for the Paraíba-type tourmaline is located near the eastern border of the Alto Ligonha pegmatite district, adjacent to the village of Mavuco in northeastern Mozambique. An area of approximately 3 km^2 has been mined for the Cu-bearing tourmaline, which is hosted exclusively by secondary deposits (paleoplacers) that are buried beneath as much as 5 m of lateritic material. The paleoplacers rest directly on top of weathered bedrock (e.g., biotite schist). Although nearby granitic pegmatites have been mined for aquamarine and quartz, they are not a source of Cu-bearing tourmaline. The extent to which gem tourmaline is distributed in the paleoplacers has not yet been established. In some places along the edges of the currently mined area, however, the diggers reported encountering only black tourmaline and no gem material, leading them to search elsewhere.

To date, most of the tourmaline mining in the Mavuco region has taken place in the area to the south and east of the Mozambique Gems claim by local diggers using simple hand methods (figure 30). The miners use picks and shovels to remove the overburden. Upon encountering the tourmaline-bearing horizon, they dig through the material with their picks to look for the gems. Although many stones are probably overlooked in the process, water for washing the soil is scarce or unavailable to the artisanal miners during most of the year, and the paleoplacers are infiltrated by clay so dry screening is not feasible.

At the time of our visit, Mozambique Gems was preparing for a major mechanized operation on their 300 ha mining concession. They had completed a comprehensive environmental impact report and performed systematic mapping and test pitting of their claim. The extent of the tourmaline-bearing horizon was being refined through additional test pitting with a backhoe, followed by wet-screening (figure 31) using water from a river adjacent to their claim. They were also constructing a washing plant that will be capable of processing 150–200 tonnes of material per day (figure 32). Mozambique Gems expects to complete the washing plant in early to mid-2008, at which time they will begin mining and simultaneous reclamation of the pits. In addition, the owners of other claims in the surrounding area have consolidated their claims and are making preparations for mechanized mining.

While in the regional capital of Nampula (about 90 km

Figure 30. Most of the production of Cu-bearing tourmaline from Mozambique has come from artisanal miners using simple hand tools. Photo by B. M. Laurs.

Figure 31. Material from test pits on the Mozambique Gems claim is first wet-screened and then hand picked for tourmaline. Photo by J. C. Zwaan.

Figure 32. Future mining for Cu-bearing tourmaline by Mozambique Gems will employ this washing plant. Photo by B. M. Laurs.

north of Mavuco), we purchased samples from a parcel of rough material that was reportedly mined from the Mavuco area. The parcel consisted of waterworn pebbles—all reportedly unheated—showing a range of colors and sizes. From the smaller pieces (e.g., figure 33), we obtained samples that were representative of the color range in that parcel. Subsequent laser ablation–inductively coupled plasma–mass spectrometry (LA-ICP-MS) analyses were done to chemically characterize the tourmaline, but the data showed that three of the 20 pebbles consisted of amethyst, light yellowish green fluorite, and light bluish green manufactured glass. A light green pebble that was obtained directly from one of the miners at the pits also was identified as fluorite. As with any gem mining area, the presence of imitations is of concern, regardless of whether they are unknowingly or intentionally offered to buyers. Separating out such imitations can be particularly challenging when dealing with multicolored parcels of waterworn rough.

Figure 33. A variety of colors is seen in this parcel of waterworn pebbles represented as unheated Cu-bearing tourmaline from Mozambique. Three of the samples obtained from this parcel proved to be imitations: an amethyst, a light yellowish green fluorite, and a light bluish green manufactured glass. Photo by J. C. Zwaan.

The future production of Cu-bearing tourmaline from Mozambique should be bolstered by the mechanized mining activities that are due to commence in the coming months. Additional information on this tourmaline will appear in an article being prepared for submission to *Gems & Gemology*.

Acknowledgments: We appreciate the helpful assistance of Moses Konate, Salifou Konate, Chirindza Henrique, and Daniel Trinchillo in facilitating our visit to the mining area.

Brendan M. Laurs

J. C. (Hanco) Zwaan
National Museum of Natural History
Leiden, The Netherlands

New Cu-bearing tourmaline from Nigeria. Copper-bearing (Paraíba-type) tourmaline is currently known from three countries: Brazil, Nigeria, and Mozambique. Within a given country, stones from different mines (in the case of Brazil and Nigeria) show variations in color and composition (e.g., A. Abduriyim et al., "'Paraíba'-type copper-bearing tourmaline from Brazil, Nigeria, and Mozambique: Chemical fingerprinting by LA-ICP-MS," Spring 2006 *Gems & Gemology*, pp. 4–21). However, most of the Nigerian stones we have examined at GIA were remarkably consistent in color (light blue to green) and trace-element composition (enriched in Pb).

In October 2007, Bill Barker (Barker & Co., Scottsdale, Arizona) informed these contributors about a new source of Cu-bearing tourmaline in Nigeria that has produced material with a wide range of saturated colors similar to those from the original source of Paraíba tourmaline at Mina da Batalha, Paraíba State, Brazil. These colors were quite different from those seen previously in Nigerian material. According to his supplier, the stones came from a different area than those that have been mined previously for this tourmaline. All of the rough material consisted of broken fragments, so it was not possible to determine whether they originated from a primary or secondary deposit. So far Mr. Barker has obtained approximately 100 g of rough, from which 24 stones have been faceted in weights ranging from 0.2 to 4 ct.

Mr. Barker loaned 12 of the faceted stones (0.31–1.04 ct; figure 34) to GIA for examination. They showed highly saturated violet to bluish violet (five stones), blue (two), bluish green (one), green (two), and purple (two) colors that we had not previously seen in Nigerian Cu-bearing tourmaline. Only the two blue stones and one of the bluish green samples were reported to have been possibly heat treated. The following properties were obtained on the 12 samples: RI—1.620–1.643; SG—3.01–3.12; and inert to both long- and

Figure 34. These 12 intensely colored Cu-bearing tourmalines (0.31–1.04 ct) were reportedly produced from a new locality in Nigeria. Courtesy of Barker & Co.; photo by Robert Weldon.

short-wave UV radiation. Microscopic examination revealed typical "trichites," growth tubes, and two-phase (liquid and gas) inclusions in nearly all samples.

EDXRF chemical analysis confirmed that the tourmalines contained significant concentrations of Cu, and LA-ICP-MS indicated Cu contents up to ~1.5 wt.%. Interestingly, most of these intensely colored tourmalines had relatively low Pb concentrations (<40 ppm). These new Nigerian stones show a strong resemblance to their Brazilian counterparts in both color and chemistry. They provide a good reminder of the difficulties associated with determining the country of origin for gems, given the almost inevitable discovery of new localities. Thorough characterization of gems as they are produced from new mines allows gemological laboratories to remain confident in their ability to determine their geographic origin.

Christopher M. Breeding (christopher.breeding@gia.edu) and Kimberly Rockwell
GIA Laboratory, Carlsbad

Brendan M. Laurs

SYNTHETICS AND SIMULANTS

New Tairus synthetic beryl simulating "Paraíba" tourmaline. The popularity of copper-bearing blue-to-green elbaite tourmaline, referred to as "Paraíba" in the trade, has increased remarkably in the last decade. This has led to a greater number of products intended to simulate it, such as apatite, glass, cubic zirconia, and beryl and topaz triplets. To this list we now add synthetic beryl.

At the September 2007 Bangkok Gem & Jewelry Fair, Tairus Created Gems (Novosibirsk, Russia) was selling a gem material they called "Synthetic Paraíba." A representative informed one of the authors (CG) that it was "Paraíba shade synthetic beryl," which Tairus had recently introduced into the market. The existence of a similar imitation from Tairus was mentioned by J. E. Shigley et al. ("An update on 'Paraíba' tourmaline from Brazil," Winter 2001 *Gems & Gemology*, pp. 260–276). At the Bangkok show, both crystals (~0.3–0.7 g) and cut specimens (~0.2–1 ct) of the bright greenish blue material were available. While only a minor amount of material was on display, we were told that any quantity could be made available upon ordering. Two samples (a 0.5 g crystal and a 0.42 ct oval cut; figure 35) were purchased for study and as reference material.

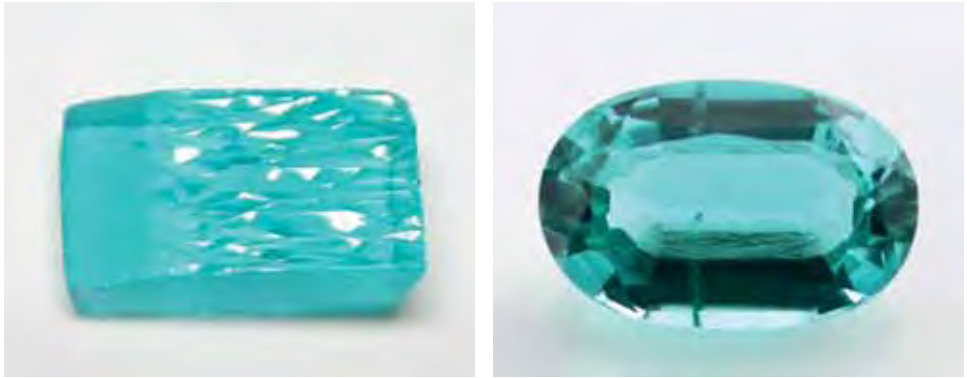

Figure 35. Tairus Created Gems represented this synthetic beryl crystal (0.5 g) and oval cut (0.42 ct) synthetic beryl as "Synthetic Paraíba," an imitation of the highly valued copper-colored tourmaline. The characteristic wavy surface of the crystal and the undulating chevron patterns in the faceted specimen indicate hydrothermal origin. Photos by C. Golecha.

Figure 36. Chevron growth patterns were obvious in the synthetic beryl with magnification. Photomicrograph by C. Golecha; magnified 35×.

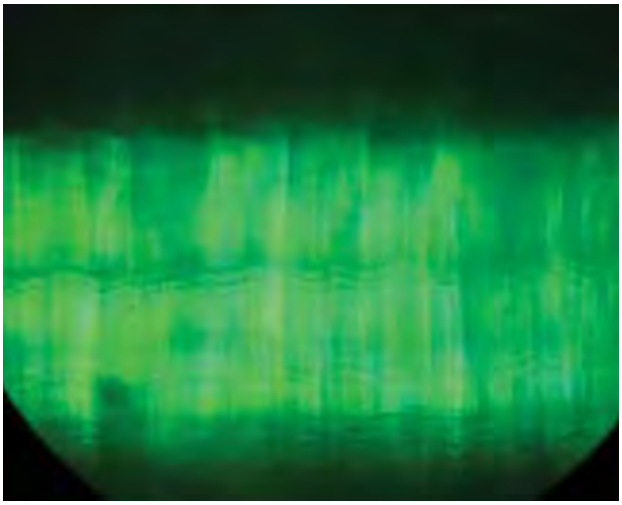

Figure 37. "Houndstooth" patterns were approximately 90° to the direction of the chevrons in the synthetic beryl. Photomicrograph by C. Golecha, immersion; magnified 25×.

The crystal was readily identifiable as a product of hydrothermal growth by the presence of wavy features on its surface (figure 35, left), similar to those seen on Tairus synthetic emeralds (K. Schmetzer et al., "A new type of Tairus hydrothermally-grown synthetic emerald, coloured by vanadium and copper," *Journal of Gemmology*, Vol. 30, No. 1/2, 2006, pp. 59–74). This pattern was expressed in the interior of both samples as (undulating) chevron features, some of which were visible even to the unaided eye (figure 35, right).

Both samples were greenish blue, with moderate light blue/greenish blue pleochroism. The faceted sample displayed a uniaxial optic figure, and it had refractive indices of 1.594–1.600. The hydrostatic SG of both samples was 2.75. These RI and SG values are much higher than those previously reported for synthetic aquamarine (e.g., K. Schmetzer, "Hydrothermally grown synthetic aquamarine manufactured in Novosibirsk, USSR," Fall 1990 *Gems & Gemology*, pp. 206–211; S. Smirnov et al., "New hydrothermal synthetic gemstones from Tairus, Novosibirsk, Russia," Fall 1999 *Gems & Gemology*, pp. 175–176). No absorption spectrum was visible in either sample with the desk-model spectroscope, and the samples were inert to long- and short-wave UV radiation.

Strong chevron growth patterns were the main features seen in both samples when examined with magnification (figure 36); these have been described as irregularly changing subgrain boundaries between subindividuals (Schmetzer, 1990). The crystal also exhibited a "houndstooth" pattern originating from planes parallel to the wavy surface (figure 37). This pattern is generally indicative of synthetic origin, though similar-appearing conical features have been reported in natural emerald (see Fall 2005 Gem News International, pp. 265–266).

Qualitative EDXRF chemical analysis revealed the presence of Al and Si, as expected for beryl. (Be cannot be detected by EDXRF spectroscopy.) Significant amounts of Fe and Cu were also detected. Fe is well known as the cause of color in aquamarine, while Cu has also been reported as the chromophore in synthetic blue beryl; (Schmetzer et al., 2006); the relatively high RI and SG values are possibly due to the presence of these impurities.

The FTIR absorption spectra of both samples exhibited a sharp peak at 5266 cm^{-1}, an absorption band ranging from 4000 to 3400 cm^{-1}, and general absorption below 2100 cm^{-1} (figure 38). The overall absorption pattern resembled the spectrum of natural emerald more than that of typical hydrothermal synthetic emeralds. However, the spectral pattern in the 2600–2100 cm^{-1} region revealed the difference (see also J. I. Koivula et al., "Gemological investiga-

Figure 38. The infrared absorption spectra of the Tairus synthetic beryl crystal and natural emerald are quite similar. However, the absence of a peak at 2358 cm^{-1} indicates synthetic origin.

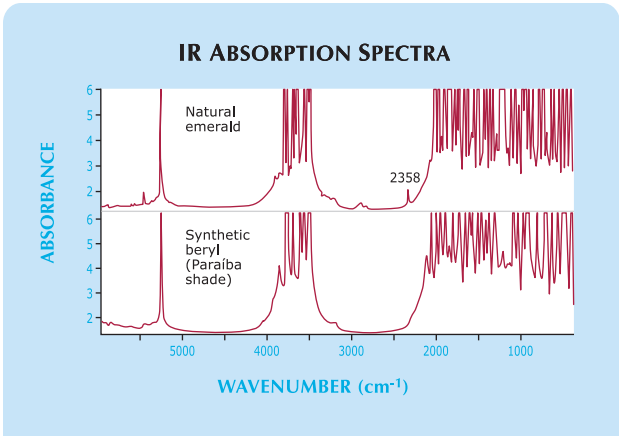

Figure 39. This 9.44 ct YAG was unusual due to its heavily included nature and its "reverse" color change: yellow in incandescent light (left) and sunlight, and orangy pink in daylight-equivalent fluorescent light (right). Photos by C. Golecha.

tion of a new type of Russian hydrothermal emerald," Spring 1996 *Gems & Gemology*, pp. 32–39).

Synthetic beryl has been known for decades, but the commercial availability of this particular color as a simulant for Paraíba tourmaline is a new development that is designed to capitalize on the popularity of this type of tourmaline.

Gagan Choudhary (gtl@gjepcindia.com)
and Chaman Golecha
Gem Testing Laboratory, Jaipur, India

An unusual YAG with a "reverse" color change. Yttrium aluminum garnet (YAG) is manufactured primarily for industrial purposes, with some "leftovers" used as a gem simulant. Though YAG was first produced commercially in colorless form, it has since been seen in numerous hues, such as green, yellow, pink, red, blue, and "lilac." Most YAGs are eye-clean, but a few included specimens have been reported (see, e.g., Winter 1993 Lab Notes, p. 284).

Recently, a 9.44 ct oval mixed cut gem was encountered at the Gem Testing Laboratory, Jaipur, India. Standard gemological testing identified it as YAG. In daylight the sample appeared yellow, with some tinges of orange, and it contained abundant eye-visible planes of inclusions (figure 39). The desk-model spectroscope revealed a series of strong lines and bands across the spectrum (i.e., a typical rare-earth spectrum). The sample fluoresced a reddish orange to UV radiation, stronger to short-wave than to long-wave.

With magnification, the YAG displayed a complex array of etch channel–like inclusions (figure 40), gas bubbles and tube-like inclusions (figure 41), and angular growth zoning (figure 42). The etch channel–like inclusions were highly reflective, and appeared either opaque or flux-like depending on the viewing direction and illumination. Some cloudy patches were also seen. We have not observed such inclusions in YAG in our laboratory, although somewhat similar features have been reported (see the Lab Note cited above). The presence of gas bubbles indicated that it was a product of Czochralski pulling and not a flux growth process; however, the possibility of production via the floating zone technique cannot be ruled out.

The sample became even more interesting when it was viewed with different types of illumination. In daylight-equivalent fluorescent light, it appeared orangy pink (again, see figure 39). However, when viewed in incandescent light, it appeared yellow (as in sunlight). As such, this YAG showed a "reverse" effect, since color-change stones generally appear pink or red in incandescent light. This type of color change has been referred to as *type 2*, and is commonly seen in manufactured glasses and, rarely, in some other gems (e.g., Y. Liu and B. A. Fry, "A colorimetric study of a tourmaline from Mozambique which shows a reverse alexandrite effect," *Journal of Gemmology*, Vol. 30, No. 3/4, 2006, pp. 201–206). Consistent with the YAG reported here, Liu and Fry (2006) indicated that type 2 stones show a color change between sunlight and daylight-equivalent fluorescent illumination, as well as between fluorescent and incandescent light, but not between sunlight and incandescent light. The cause of the type 2 color change in this YAG is not known.

Gagan Choudhary and Chaman Golecha

Figure 40. Although YAG is typically flawless, this sample contained abundant inclusions with the appearance of etch channels. These features were highly reflective in certain directions. Photomicrograph by C. Golecha, immersion in di-iodo-methane; magnified 20×.

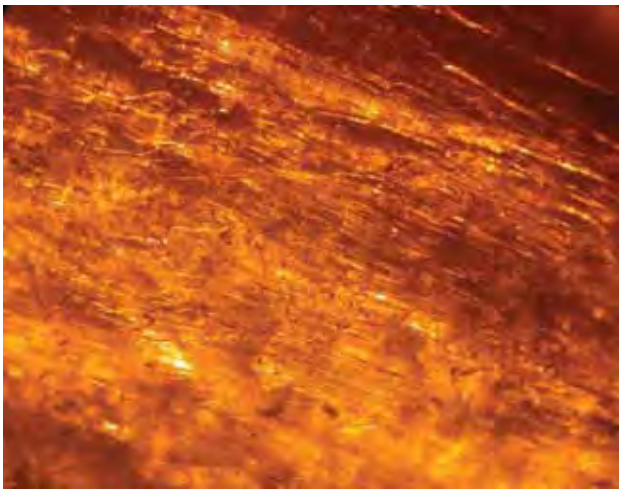

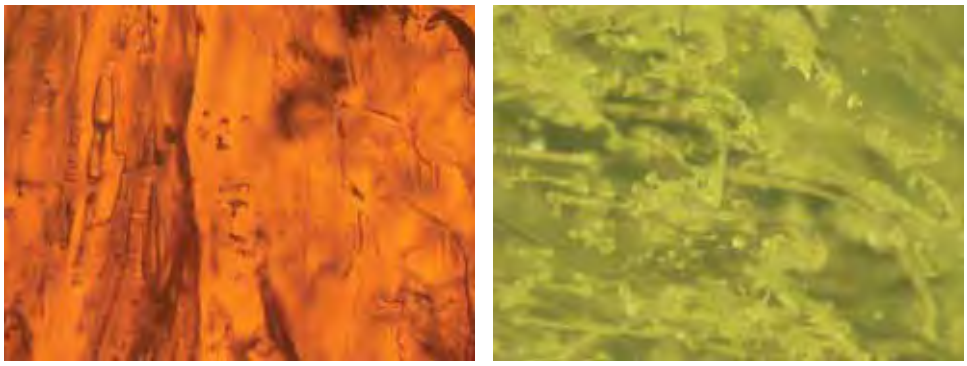

Figure 41. Numerous gas bubbles were present throughout the YAG, along with complex tube-like inclusions. Photomicrographs by C. Golecha; magnified 35× (left) and 30× (right).

CONFERENCE REPORTS

Geological Society of America 2007. The 119th Annual Meeting of the Geological Society of America was held October 28–31 at the Colorado Convention Center in Denver. This year's theme was Earth Sciences for Society and launched the International Year of Planet Earth. Nearly 7,000 geoscientists attended. Some presentations focused on gem topics, and a searchable database of all the conference abstracts is available on-line at http://gsa.confex.com/gsa/2007AM/finalprogram.

Dr. John-Paul Zonneveld (Geological Survey of Canada, Calgary) described the diamondiferous kimberlites of central Canada. The Fort à la Corne area contains unusually well-preserved examples of extrusive pyroclastic kimberlites. Volcanism occurred in this region during the Lower Cretaceous, approximately 100 million years ago (Ma), in coastal plain and shallow marine settings. Volcanically induced faulting caused elevation changes, allowing marine shale to cover and preserve these important diamond-bearing kimberlite deposits.

Dr. Monaliza C. Sirbescu and **James J. Student** (Central Michigan University, Mount Pleasant) explained the crystallization history of a granitic pegmatite dike (~2 m thick) in northeastern Wisconsin using microthermometry and conductive-cooling numerical modeling. High cooling rates in the outer zone exceeded the crystal nucleation rate and caused a temperature differential between the inner and outer zones. This undercooling caused rapid disequilibrium crystallization, and solidification was estimated at about 10 days. Similar crystallization times may be inferred for gem-bearing pegmatite dikes of comparable thickness.

Figure 42. Angular growth zoning, similar to that seen in some natural gems, was also present in the YAG. Photomicrograph by C. Golecha; magnified 30×.

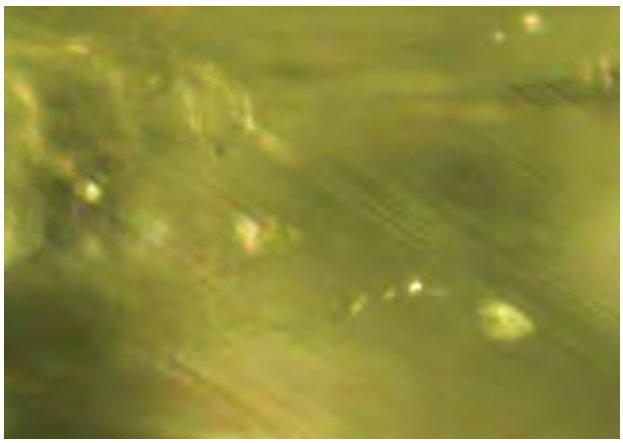

Laura Bergen (University of Manitoba, Canada) studied turquoise deposits in Nevada, California, Arizona, and New Mexico. The genesis of these deposits was influenced by tectonic, magmatic, and sedimentation events. This supports one hypothesis that turquoise formed by descending meteoric waters, a phenomenon known as supergene enrichment.

Dr. George Harlow (American Museum of Natural History, New York) gave two presentations on jadeitite (a rock composed of jadeite and other minerals) and related rocks from central Guatemala. The first described the sediment signatures of two adjacent serpentinite mélange belts along the Motagua fault zone, which suggested that the jadeitite originated "by precipitation from fluids coming off a subduction channel." The second looked at the geochronology of jadeitite-bearing high-pressure, low-temperature metamorphic blocks along the Motagua fault zone. Using regional geology and chronology data, the study concluded that tectonic blocks (including jadeitite) were metamorphosed during two tectonic events, one at ~130 Ma and the other at ~65 Ma.

Dr. Stephen Peters (U.S. Geological Survey, Denver, Colorado) spoke about the results of field studies to assess the non-fuel mineral resources of Afghanistan. There are known deposits of rubies, emeralds, tourmaline, and lapis lazuli; as-yet-undiscovered deposits of several commodities are likely. The full USGS report and supporting geologic studies are available at http://afghanistan.cr.usgs.gov.

Dr. Nancy McMillan (New Mexico State University, Las Cruces) presented a study on the use of laser-induced breakdown spectroscopy (LIBS) to rapidly identify carbonate and silicate minerals. Fifty-two minerals and their resultant spectra were analyzed; 95% of the minerals were correctly identified, with the other 5% misidentified as a mineral of similar composition from the same mineral family. The study suggests that LIBS may be useful in the future for the rapid identification of minerals in the field.

Dr. Denise Battles (University of Northern Colorado, Greeley) and **Dr. Jane Hudak** (Georgia Southern University, Statesboro) presented a proposal for a textbook on art and geology (with gemology as a key component), which would focus on the interdisciplinary relationship between the two. The textbook will fulfill a need for educational materials that support the concept of combined disciplines and will allow active learning with hands-on activities. The authors shared the first two chapters of the textbook prototype, one of which is richly illustrated with gems and includes a timeline showing jewelry through the ages.

Kathleen Dailey, Dona Dirlam, Cathy Jonathan, and Paula Rucinski (library@gia.edu)
GIA Library, Carlsbad

Goldschmidt 2007. The 17th Annual V. M. Goldschmidt Conference took place August 19–24 in Cologne, Germany, and featured a session titled "Applied geochemistry—from brines and rare-earth elements to diamonds" in honor of long-time *G&G* contributor Dr. Alfred A. Levinson. A portion of this session was devoted to the theme "Gem Mineralogy, Diamonds and Gemstones." There also were presentations of interest to gem scientists in other conference sessions. Abstracts are available via a searchable database at www.goldschmidt2007.org/abstracts.php.

Dr. H. Sommer (University of Botswana, Gaborone) described an ambitious new multidisciplinary endeavor—International Geological Correlation Programme Project 557, "Diamonds, Xenoliths and Kimberlites: A Window into the Earth's Interior"—that will study diamond formation and the effect of kimberlite ascent rate on diamond preservation during eruption.

Dr. S. Aulbach (University of Alberta, Edmonton, Canada) studied the isotopic composition (Re-Os) of syngenetic sulfide inclusions in diamonds from the Jagersfontein mine in South Africa. Several factors point toward diamond crystallization at multiple depths. In contrast to other eclogitic sulfide inclusion suites from the Kaapvaal craton, the absence of such suites of Archean age may relate to unique aspects of the Jagersfontein kimberlite (i.e., its transport and preservation of very deep diamonds, or its location on the edge of the craton).

Dr. R. S. Harmon (Army Research Office, Research Triangle Park, North Carolina) presented research conducted by **C. E. McManus** on the geographic origin determination of gem beryls with LIBS analysis. Considerable chemical variability was documented in beryls from just one locality in New Hampshire (Palemero No. 1 pegmatite), indicating the need for a large sample base to perform reliable origin identification.

Dr. T. Tsujimori (Okayama University, Tottori, Japan) presented **Dr. S. S. Sorensen's** work on the formation of jadeitite and related rocks in Guatemala. The unusual geochemical signature of meta-ultramafic rocks adjacent to the jadeitite bodies is apparently the result of interaction with metasomatic fluids that permeated along the contact between the jadeitite and host serpentinite.

Dr. D. E. Jacob (Johannes Gutenberg University, Mainz, Germany) examined the distribution and characteristics of vaterite (a polymorph of $CaCO_3$) in freshwater cultured pearls from a *Hyriopsis* mollusk. In high-quality pearls, vaterite formed relatively small areas (1–1.5 mm diameter) near their center. However, low-quality samples were in some cases comprised mostly of vaterite. Detailed examination of growth rings in the cultured pearls suggested that vaterite and aragonite grew simultaneously, and that vaterite may not have been an initial template for aragonite growth.

This contributor provided a genetic model for the formation of yellow gem tourmaline at the Canary mine in Zambia (see article in this issue of *Gems & Gemology*).

Brendan M. Laurs

The Madison Dialogue Ethical Jewelry Summit. The Madison Dialogue (www.madisondialogue.org) is a cross-sector initiative aimed at encouraging best practices in the gold, diamond, and other mineral industries by promoting communication and collaboration, sustainable economic development, and verifiable sources of responsibly mined materials. The initiative was launched at a meeting in New York (on Madison Avenue) in August 2006. On October 25–26, 2007, the Madison Dialogue Ethical Jewelry Summit took place at the World Bank headquarters in Washington, DC, to discuss ways to improve socioeconomic conditions for marginalized small-scale (artisanal) miners around the world. This meeting also sought to develop ethical standards for business conduct in source countries, with independent third-party verification systems. The overall goal was to lay the foundation for the manufacture of "ethical jewelry"—jewelry assembled in ways that meet environmental, social justice, and transparency standards along the supply chain from source countries to consuming nations.

Attendees included non-governmental organizations, such as Communities and Small Scale Mining (which hosted the forum), the Association for Responsible Mining, Earthworks, Partnership Africa Canada, Urth Solutions, Ethical Metalsmiths, and Fairtrade Labelling Organizations International. Among the mining (metal, diamond, and colored stone) concerns, gem dealers, and educational and jewelry trade organizations represented were the Council for Responsible Jewellery Practices, Jewelers of America, the De Beers Group, Rio Tinto, AngloGold Ashanti, Columbia Gem House, Nature's Geometry, Rapaport Group, the Gemological Institute of America, and Oro Verde. The jewelers and jewelry manufacturers contingent included representatives from Ben Bridge, Cartier, Tiffany & Co., Leber Jeweler, Cred Jewellery, greenKarat, Finesse Diamonds, and Sterling.

Although many of the participants had already undertaken a variety of ethical initiatives on their own, the Madison Dialogue was the first such forum for this cross-section of global players to openly share knowledge and discuss the issues of ethical jewelry. Participants agreed on

a mutual goal of building confidence for all players in the gem and metals supply chain. Discussions made it clear, however, that methods of accomplishing this goal might differ. As some differences are rooted in language or cultural realities, Madison Dialogue organizers included an initial session to discuss nomenclature and clear definitions for such terms as *fair trade*, *environmental and social responsibility*, *sustainability*, and *third-party assurance systems*.

At the close of the two-day summit, participants agreed to release the following declaration: "We believe there is an opportunity to make a difference in the lives and communities of artisanal/small-scale miners and other marginalized workers worldwide by developing and implementing robust standards for the production of ethical and fair trade metals, diamonds, gems, and jewelry. We also encourage governments, where needed, to develop policies and regulations that protect these miners, workers, and their communities." Participants also agreed to form working groups to address issues specific to the mining of metals, diamonds, and colored stones, as well as the development of standards and third-party assurance systems.

Robert Weldon (rweldon@gia.edu)
GIA Library, Carlsbad

ANNOUNCEMENTS

Visit *Gems & Gemology* in Tucson. Meet the editors and take advantage of special offers on subscriptions and back issues at the *G&G* booth in the publicly accessible Galleria section (middle floor) of the Tucson Convention Center during the AGTA show, February 6–11, 2007. GIA Education's traveling Extension classes will offer hands-on training with "Colored Stone Grading" (February 5–7), "Pearls" (February 8), and "Identifying Diamond Treatments" and "Identifying Ruby" (February 9). Several free seminars will also be offered by GIA staff February 10–11. To enroll, call 800-421-7250, ext. 4001. Outside the U.S. and Canada, call 760-603-4001. The GIA Alumni Association will host an auction and dance party at the Marriott University Park Hotel in Tucson on February 8, starting at 6:30 p.m. To reserve tickets, call 760-603-4204 or e-mail events@gia.edu.

Conferences

NAJA annual conference. The National Association of Jewelry Appraisers is holding its 29th annual Winter Educational Conference February 4–5, 2008, during the Tucson gem shows. Visit www.najaappraisers.com.

Hasselt Diamond Workshop. Held February 25–27, 2008 at Hasselt University, Diepenbeek–Hasselt, Belgium, this conference will cover a variety of diamond-related research subjects. Visit www.imo.uhasselt.be/SBDD2008.

PDAC 2008. The Prospectors and Developers Association of Canada convention will take place March 2–5 in Toronto. The technical session will include an update on the Canadian diamond industry (including progress at Snap Lake and Victor) and a review of current diamond prospecting in India. Visit www.pdac.ca/pdac/conv.

Bead Expo. The 2008 International Bead Expo will be held in Portland, Oregon, March 27–30. Over 60 workshops and educational lectures on bead jewelry design and manufacture are scheduled. Visit www.beadexpo.com.

BASELWORLD 2008. The BASELWORLD show will be held April 3–10 in Basel, Switzerland. During the show, *Gems & Gemology* editor-in-chief Alice Keller will be available at the GIA booth in Hall 2, Stand W23. Visit www.baselshow.com or call 800-922-7359.

35th Rochester Mineralogical Symposium. A variety of gem and mineral topics will be presented at this symposium, held April 10–13, 2008, in Rochester, New York. Visit www.rasny.org/MinSymposium/MineralSymp.htm.

Réunion des Sciences de la Terre. This earth science conference will be held April 21–24, 2008, in Nancy, France. The program will include a session on gems. Visit www.RST2008.u-nancy.fr.

Sinkankas garnet symposium. Garnet will be featured in the sixth annual John Sinkankas Memorial Symposium, held April 19, 2008 at GIA Carlsbad. A variety of experts will speak on garnet localities, inclusions, treatments, appraising, lapidary work, and literature at this all-day educational event. E-mail merksjade@cox.net.

CIM Conference and Exhibition. Held May 4–7, in Edmonton, Alberta, the 2008 meeting of the Canadian Institute of Mining, Metallurgy and Petroleum will feature a session on the geology of diamonds in Canada. Visit www.cim.org/edmonton2008.

Art2008. Held May 25–30 in Jerusalem, Israel, the *9th International Art Conference on Non-destructive Investigation and Analysis* will focus on items of cultural heritage, but will have implications for gem testing. Visit www.isas.co.il/art2008.

Quebec 2008: GAC-MAC-SEG-SGA. Held May 26–28 in Quebec City, Canada, this joint conference organized by the Geological Association of Canada, Mineralogical Association of Canada, Society of Economic Geologists, and the Society for Geology Applied to Mineral Deposits will include special sessions on "Diamonds: from Mantle to Jewellery" and "Challenges to a Genetic Model for Pegmatites," as well as a short course called "Rough Diamond Handling." Visit www.quebec2008.net.

NDNC-2008. The growth, processing, characterization,

properties, and applications of diamond and related materials will be covered at the 2nd International Conference on New Diamond and Nano Carbon, held May 26–29 in Taipei, Taiwan. Visit http://diamond.iams.sinica.edu.tw/NDNC2008.

ICAM 2008. Gems will be one of the subjects covered at the *9th International Congress for Applied Mineralogy* on September 8–10 in Brisbane, Australia. Visit www.icam2008.com.

2009 GIA Gemological Research Conference. The 2009 GRC will be held August 21–23, 2009 in San Diego, California. Further details will be made available as the date approaches. Visit http://grc2009.gia.edu or email grc2009@gia.edu.

Exhibits

Exhibits at the GIA Museum. Through February 29, 2008, "Reflections in Stone" will showcase famed gem carver Bernd Munsteiner's work during the period 1966–2003. On display in the Mikimoto Rotunda, the exhibit includes carved quartz, tourmaline, and beryl, ranging from pieces set in jewelry to large table-top sculptures. From May 21 through December 2008, "Facets of GIA" will showcase the various gemological services that GIA provides, including diamond grading, gem identification, education, and public outreach. As part of this exhibit, the Aurora Butterfly of Peace—a display comprised of 240 natural fancy-colored diamonds—will be featured through July 2008, courtesy of Alan Bronstein and Harry Rodman (see also the article on pp. 332–351 of this issue). Advance reservations are required; to schedule a tour, call 760-603-4116 or e-mail museum@gia.edu.

Gems! Colors of Light and Stone. The Michael Scott collection has returned to the Bowers Museum in Santa Ana, California, with an expanded display of rare colored stones, carvings, and sculptures. The exhibit will run until June 16, 2008. Visit www.bowers.org.

The Aurora Collection at The Vault. "The Vault," a new permanent collection of rare gemstones and mineral specimens, is now open at the Natural History Museum in London. Headlining the initial exhibit is the Aurora Collection, currently comprising 296 naturally colored diamonds (267.45 carats total weight) assembled by diamond collectors Alan Bronstein and Harry Rodman. Also on display is the 47.69 ct Star of Africa, which helped launch the 1869 diamond rush in South Africa, and the 1,385.95 ct Devonshire emerald crystal. Visit www.nhm.ac.uk/galleries.

BOOK REVIEWS

Jewels: A Secret History

By Victoria Finlay, 472 pp., illus., publ. by Ballantine Books, New York, 2006. US$25.95

What a wondrous jeweled travelogue Victoria Finlay has created! She takes the reader across the globe to learn the stories behind some of the world's most prized gem materials—from Kaliningrad's Amber Coast to Scotland's pearl-bearing rivers, a church built into an opal mine in Australia, and Cleopatra's legendary emerald mines. She even goes to Sri Lanka in an effort to learn more about a sapphire passed down in her family. Ms. Finlay relays her fascinating experiences meeting individuals in these far-flung locales, but with no sugar coating. She writes of the hardships of peridot mining on an Arizona reservation, of being warned of dishonestly sold synthetics, and of blood diamonds. As a reader, I greatly appreciated her candor and found the accounts of her experiences enthralling.

While this is not an all-encompassing work that will make the reader an expert on any of the chosen gems, it offers a thoughtful look at the role various gems have played in world history. Included are useful lists of birthstones, anniversary gems, a glossary of gem-related terms, and additional reading. If you are interested in the story of one woman's gem experiences around the globe, this is it!

JANA E. MIYAHARA-SMITH
Gemological Institute of America
Carlsbad, California

Fine Minerals of China: A Guide to Mineral Localities

By Guanghua Liu, 366 pp., illus., publ. by AAA Minerals AG, Switzerland, 2006. US$148.00

Not long ago, Chinese mineral specimens were curious rarities. A cinnabar crystal, even a meager one by today's standards, was something to boast about! Today, Chinese minerals are abundant on the market, and prices are relatively good. Although this is a great time to add them to your collection, there are still pitfalls to beware of. Because some localities have been vaguely or even deceptively reported, and many new sources and species are entering the market, there is definitely a need for a book that caters to the collector.

Most mineral collectors are not as interested in the scientific aspects as professional mineralogists are. Our concerns relate more to the sheer beauty and rarity of specimens, their acquisition, and pride of ownership. For instance, the comparative quality, characteristics, availability, and prices of the specimens are paramount. Also, the reliability of the localities given for the specimens and whether there are opportunities to visit the mines and personally collect material are important. *Fine Minerals of China*, written by experienced geologist and mineral dealer Guanghua Liu, addresses many of these concerns.

The book has three main parts. Part 1 presents a geologic overview, followed by brief sections on mineral deposits, mining history, mineral and rock collecting, and the mineral trade. Part 2 is a guide to localities, including 45 important sources of fine mineral specimens in 13 provinces. A brief look at each province is followed by locality descriptions that include location, mining history, accessibility, and major collectible minerals. There are photos of the localities as well as superb color photos of specimens. Part 3 is a compilation of data, with tables for Chinese deposits that have potential for collectible specimens, minerals first found in China, and meteorite finds. There are also indexes of mineral localities.

This book delivers much of what mineral collectors need most. Gemologists will enjoy the information on the many gem species China has to offer, though it should be noted that none of them are shown in fashioned form. There are many useful maps throughout, and the fine photos are helpful in determining if a specimen's characteristics are consistent with a particular locality. Using this book, I was able to verify or disprove the localities of many Chinese specimens in my collection, and to add details to the information in my catalog.

I liked the fact that the descriptions of the geology are not overly technical, but still give the big picture. Also useful were the history of the deposits and China's overall mining history. The pages devoted to mineral and rock collecting and the mineral trade are especially well suited for a collector's book.

In the introduction to Part 1, an

effort is made to explain that the translation from Chinese to English follows the Pinyin system, the official standard for romanizing Mandarin characters. A description of how some Pinyin pronunciations differ from the romanized versions is given. There is also a chart that compares the conventional spelling and Pinyin spelling of the provinces. Some common Chinese characters and their English translations also are included, such as *kuang* for mineral or mine and *shan* for mountain. This chart greatly helps those who cannot speak or read Chinese but want to pronounce the localities correctly and understand why other spellings are found on specimen labels.

On the minus side, a few of the figure captions seemed to be incorrect. One such technicality is the reporting of hiddenite, the green spodumene colored by chromium, as coming from one of the deposits. Is this true hiddenite or just green spodumene? And while the section on meteorites will be of interest to those who collect these interstellar specimens, there are no photos or any general discussion of them.

Overall, though, I highly recommend this book for collectors and anyone interested in fine minerals from China. I hope that additional volumes will be published as more fine minerals are discovered in this vast country.

MICHAEL EVANS
Gemological Institute of America
Carlsbad, California

The Jewelry Handbook: How to Select, Wear & Care for Jewelry

By Renée Newman, 177 pp., illus., publ. by International Jewelry Publications, Los Angeles, 2007. $19.95

The title suggests a consumer-oriented publication, and indeed this work lives up to those expectations. Ms. Newman's latest book informs and delights the end user of jewelry by explaining everything from why we use jewelry, to manufacturing methods, to what type of jewelry is best for which face shape. The 16 chapters are liberally illustrated with large color photos to help explain the different terms, cutting styles, textures, and techniques discussed. The first six chapters cover specifics of jewelry, gemstones, metals, and manufacturing; the balance of the book delves into selecting flattering necklaces, brooches, and rings, as well as many details about the care of jewelry. The basics are there as well as the unusual. Helpful and practical tips are given at the end of each topic, summing up the pros and cons. For example, silver is subject to consistent tarnishing but is the most affordable of all metals, whereas tungsten is, for the most part, hypoallergenic but cannot be sized.

I found the chapter on manufacturing methods to be the most helpful, because few laypeople have a good understanding of what is involved. This chapter focuses on four basic methods of making jewelry—casting, stamping, electroforming, and hand fabrication—with bullet points on the advantages and disadvantages of each. Included is an interesting discussion on *handmade* vis-à-vis *hand fabrication* and the potential for confusion with these terms. Newman counsels jewelers and salespeople to clearly "define what they mean when they use the term *handmade*" to customers.

This book is a great informational aid and sales tool for the counter person when addressing questions from potential buyers of fine jewelry. In addition, many of those in the trade could use it as their primer to fill in information not normally covered in standard classroom and jewelry show lectures.

The Jewelry Handbook is not all facts and data—the chapters on selecting rings, necklaces, bracelets, and brooches begin with a paragraph or two weaving in aspects of jewelry history, which helps put the item in context. This knowledge could easily become part of a sales conversation to entice customers to stay awhile at the counter!

GAIL BRETT LEVINE
National Association of Jewelry Appraisers
Rego Park, New York

The Pink Pearl: A Natural Treasure of the Caribbean

By Hubert Bari after the text by David Federman, 173 pp., illus., publ. by Skira Editore S.p.A. [www.rizzoliusa.com], Milan, Italy, 2007. US$58.00

Written with passion by respected industry journalist David Federman and adapted with the same love and care by Dr. Hubert Bari, a lecturer at the Muséum d'Histoire Naturelle de Paris and an inveterate collector of rare pearls, this book presents the "pink pearl"—or conch pearl—in a light that has never been seen before. This should not be surprising when one realizes the great names sitting behind the production: Susan Hendrickson, whom the book aptly describes as "the Venus of the Pink Pearls," and George Ruiz, the president of P. Lançon SA. This book is written for a broad audience, from the casual observer to the avid enthusiast. All will gain something from its informative text and sumptuous illustrations by, among others, photographers Christian Creutz, Tino Hammid, and John Koivula.

The book is divided into six main sections. The first, "Blue Seas and Pink Shells," provides the reader with a vivid description of the producing mollusk, *Strombus gigas*, otherwise known as the queen conch. Its lifespan, grazing habits, the growth of its extraordinary shell, and ancient and modern fishing techniques are all described in detail. Fishing for conch was once done primarily for the meat, originally a staple of the Caribbean diet and today a delicacy in several parts of the world; however, the text also describes conch diving as every-

thing from the idyllic shallow water escapades of a bygone era to the "gritty and dangerous" current situation in Honduras.

Interestingly, the pink pearl produced by *Strombus gigas* is considered a by-product of harvesting the meat. Indeed, the ownership of any pearls found is governed by the law of "finders keepers." Various recipes for the use of the meat, including conch salad, are scattered throughout the text and supported by excellent photography.

A particularly important section describes the concerns of the Convention on International Trade in Endangered Species (CITES), which has listed *Strombus gigas* in its Appendix II as a species that might face extinction unless its trade is strictly controlled. As the authors point out, it remains to be seen whether the CITES agreement exerts sufficient control over the fishing to ensure the long-term survival of this mollusk.

The section titled "An Extraordinary Pearl" contains some of the most incredible images of flame structures (those that produce the optical effect of *watered* or *moiré* silk) published to date and also reveals the array of potential colors for conch pearls. In addition, the section theorizes on the relationship between pearl color and the age of the harvested mollusk, outlines the reasons for pearl formation, and details their chemical composition. It decries as a knee-jerk reaction the long-held belief that non-nacreous pearls should be called "calcareous concretions." However, the section is disappointingly lacking in solid technical or scientific content. A revealing graphic of the microarchitecture of the shell of *Strombus gigas* compared with one of a nacreous mollusk would have better presented the reasons for the differences in toughness—the structure of *Strombus gigas* being far tougher—than the failed attempt that confuses hardness and toughness.

"From the Limelight to the Shadows" sets out in text and excellent photography the history of the conch pearl, primarily from 1850 to 1920—the bookends of its fashionable days. This section opens by describing the cameos carved from *Strombus gigas* shells prior to the popularity of conch pearls and then records some of the great historic supporters of these gems. The section rolls through such luminaries as Henry Philip Hope and J. P. Morgan and their connections with conch pearls, and touches on the World Fairs that exhibited great examples—particularly a Tiffany display at the Chicago World's Fair of 1893. The section goes on to describe the British royalty's love of these pearls, but impressively details Tiffany's passion for them through both text and archival images. The section ends with the authors speculating on the reasons for the conch pearl's decline at the outset of World War I.

"The Venus of the Pink Pearls: Sue Hendrickson" is an appropriately named section. Hendrickson is famous for so many extraordinary finds that she is often described as a female Indiana Jones—and quite rightly so. This section records her association with the conch pearl and how she set up her own "cartel," which today, with Georges Ruiz as her partner, controls some 60% of the market. Similarly, the next section, "The Rarest of all Pearls," speaks to the fascination some of the industry's key players have for these natural pearls. Championed by jewelers Fred Leighton in the United States, Mikimoto in Japan, Boghossian in Switzerland, Jeremy Morris in London, and Gianmaria Buccellati and Roberto Cuso in Milan, the conch pearl is experiencing a new era of popularity, one attested to by Tiffany's unveiling of a 26-piece collection in 2004.

The last section, "La Vie en Rose," consists of mouth-watering image after image of some of the finest conch pearl jewelry ever conceived. There is no question that this text achieves all it sets out to do and gives the widest possible audience an opportunity to enjoy this fascinating gem.

KENNETH SCARRATT
GIA Research (Thailand)
Bangkok

OTHER BOOKS RECEIVED

Opal: The Phenomenal Gemstone. *By J. Clifford, P. Clifford, A. Frazier, S. Frazier, B. P. Gaber, C. J. Gaber, G. Neumeier, and G. Staebler, Eds., transl. by G. Neumeier, 108 pp., illus., publ. by Lithographie LLC, East Hampton, CN, 2007, US$40.00.* Like the other issues in this series, this volume is an English translation of previously published work from the German-language *extraLapis* series (in this case, *No. 10, Opal: Das edelste Feuer des Mineralreichs*, 1999), updated with new information.

After a general overview of the subject, including opal history and the cause of opal's play-of-color, there is a comprehensive review of the major Australian localities. The geology, gemology, mining, and history of each locality are discussed, accompanied by high-quality photos of top specimens. Rare varieties such as hydrophane and opalized fossils and dinosaur bones are also covered. Following the Australian section is a review of other localities, particularly Mexico but also Brazil and the United States, likewise illustrated with numerous specimen photographs.

The issue includes a guide for buying and caring for opal and a glossary of opal terminology. It concludes with brief sections on opal lapidary arts and synthetic and imitation opal.

TWO

Namibia, 2nd Ed. *By L. von Bezing, R. Bode, and S. Jahn, 856 pp., illus., publ. by Bode Verlag [www.bodeverlag.de], Haltern, Germany, 2007, US$158.00.* This oversized and encyclopedic text, published for the first time in English with this edition, reviews the history and production of Namibia's vast mineral wealth. Detailed reviews of all significant localities are included, with an extensive section on Tsumeb. All known minerals discovered in Namibia are described in detail. The work is well illustrated with many high-quality color photographs.

TWO

GEMOLOGICAL ABSTRACTS

COLORED STONES AND ORGANIC MATERIALS

Amber's botanical origins revealed. J. A. Santiago-Blay [blayj@si.edu] and J. B. Lambert, *American Scientist*, Vol. 95, No. 2, 2007, pp. 150–157.

The study of plant exudates (i.e., the liquids they secrete) can help separate amber from its many modern imitations. The resin that turns into amber differs from other common exudates such as gums, gum resins, latexes, and kinos. Based on a five-carbon molecule called isoprene, the resin forms cross bonds and polymer structures over time under elevated pressure and temperature, thereby becoming amber.

The senior author collected numerous resin samples from around the world, and characterized them with nuclear magnetic resonance spectroscopy. The resins had chemical signatures that were often distinct from one plant family to another. The study of exudates could shed light on amber, not only to discriminate real from fake, but also to distinguish the botanical origins of this gem material. *DMK*

Cherry amber, real or fake? M. C. Pedersen [info@maggiecp.com], *Organic Gems*, No. 1, 2006, www.maggiecp.co.uk/free_organic_gems-magazine/cherry_amber.html.

Material called *cherry amber* is commonly found in antique shops and online auctions. This article reviews current knowledge about the material and its identity. The only true red amber is mined in Myanmar, and it is very rarely observed in transparent specimens. Burmese amber—commonly called *burmite* in the trade—is more often brownish yellow, yellow with reddish brown streaks, brown, or brownish red. Baltic amber never occurs naturally in red, nor does it appear red in

This section is designed to provide as complete a record as practical of the recent literature on gems and gemology. Articles are selected for abstracting solely at the discretion of the section editors and their abstractors, and space limitations may require that we include only those articles that we feel will be of greatest interest to our readership.

Requests for reprints of articles abstracted must be addressed to the author or publisher of the original material.

The abstractor of each article is identified by his or her initials at the end of each abstract. Guest abstractors are identified by their full names. Opinions expressed in an abstract belong to the abstractor and in no way reflect the position of Gems & Gemology *or GIA.*

transmitted light (as can amber from Mexico or Borneo). The surface of Baltic amber naturally oxidizes and darkens over time (as seen in ancient artifacts, some that date back to the Stone Age); it can appear orange or orangy brown but is usually opaque. This process can be duplicated by treating Baltic amber in various ways, and most of the material on the market today has been processed in some fashion.

Cherry amber is created by heating finished pieces of amber in an autoclave, which results in a clarified and darkened appearance (the latter can be removed by repolishing). Some plastics can resemble cherry amber.

JEC

The origin of color in "fire" obsidian. C. Ma [chi@gps.caltech.edu], G. R. Rossman, and J. A. Miller, *Canadian Mineralogist*, Vol. 45, 2007, pp. 551–557.

Obsidian from Glass Buttes, Oregon, was investigated using field-emission scanning electron microscopy, X-ray energy-dispersive spectroscopy, electron backscatter diffraction, and optical spectroscopy methods. The name *fire obsidian* refers to the vibrant colors seen when light reflects off thin layers (300–700 nm) within the material that contain nanometric crystals of magnetite. The magnetite crystals give these layers a higher refractive index (from 1.496 to 1.519) than that of the host glass (1.481). The combination of layer thickness and difference in refractive index causes thin-film optical interference, which gives rise to the brilliant colors. *EAF*

Production of akoya pearls from the southwest coast of India. V. Kripa, K. S. Mohamed [ksmohamed@vsnl.com], K. K. Appukuttan, and T. S. Velayudhan, *Aquaculture*, Vol. 262, 2007, pp. 347–354.

In India, the pearl oyster *Pinctada fucata* typically yields cultured pearls 3–5 mm in diameter. The southwest coast of India was chosen to study the feasibility of increasing their diameter to 6–8 mm. This study also examined the mortality and nuclei retention of implanted oysters, rates of nacre production, nacre thickness, and the quality of cultured pearls harvested. The effects of water clarity and temperature were also studied.

A total of 706 oysters were implanted and stocked in cages for 317 days. Of these, 311 oysters were implanted with 5 mm nuclei and 395 received 6 mm nuclei. At the end of the study, the mortality rate was roughly 50%, with a slightly higher rate for the 6 mm nuclei. Nacre deposition rates were 4.0 ± 1.0 µm per day for 5 mm nuclei, and 3.0 ± 1.0 µm per day for 6 mm nuclei. Nacre deposition was faster in warm water, but higher-quality nacre was deposited in colder water. Of the 131 cultured pearls obtained, 27.6% were A-grade, 31.3% B-grade, 19.8% C-grade, 7.6% baroque, and 13.7% unusable. Greater amounts of suspended solids in the water correlated to higher mortality rates. This study showed that relatively thick nacre could be produced within 10 months, as opposed to the 16–24 months required for pearls grown in Japanese waters. *EAF*

Spectroscopic characterization of Mn-rich tourmalines. B. J. Reddy, R. L. Frost [r.frost@qut.edu.au], W. N. Martens, D. L. Wain, and J. T. Kloprogge, *Vibrational Spectroscopy*, Vol. 44, No. 1, 2007, pp. 42–49.

Spectroscopic analyses were performed on powdered samples of two Mn-bearing tourmalines (one green and one pink) from Minas Gerais, Brazil. Visible spectra of both samples revealed increasing absorption below 400 nm. Spectral bands at about 295, 345, and 365 nm in the pink sample were due to Mn^{2+}; an additional broad band at about 520 nm was due to Mn^{3+}. The spectrum of the green sample displayed broad bands at about 320 nm due to Mn^{2+} and at about 715 nm due to Fe^{2+}-Fe^{3+} intervalence charge transfer. Near-infrared spectral bands at 10240 and 8000 cm^{-1} provided evidence of Fe^{2+}. Mid-infrared spectra displayed four OH-stretching bands between 3800 and 3200 cm^{-1} that indicated a mixed occupancy of OH in the Y and Z octahedral sites of the tourmaline structure. No quantitative chemical analyses for Mn were performed. *JES*

DIAMONDS

An integrated model of kimberlite ascent and eruption. L. Wilson and J. W. Head III [james_head@brown.edu], *Nature*, Vol. 447, 2007, pp. 53–57.

Diatremes are carrot-shaped bodies that form the upper portions of deep magmatic intrusions of kimberlite rock. These complex features are important sources of diamonds. A new six-stage model of ascent and eruption is put forth to explain the complex and contradictory characteristics of kimberlites and diatremes.

Stage 1 involves the propagation of a dike from an area of the mantle lying within the diamond stability field (~250 km and 8 GPa). Rapid dike propagation minimizes the thermodynamic problems associated with transporting diamonds from the mantle to the surface. The pressure release associated with the rise in the magma facilitates the segregation of a CO_2-rich fluid in the upper regions of the dike, and increasing pressure from the escaping gas creates a layer of magmatic foam. Stage 2 is marked by dike ascent and wall fracturing. As the dike nears the surface, country rock is torn from the walls to become xenoliths, which are incorporated into the underlying foam. During stage 3, the dike tip breaks the surface, vents CO_2, and implodes the walls. Upward velocity increases from 20 m/sec for the rising dike to between 300 and 600 m/sec for the exploding gas. The velocity of the exploding material depends on the size of magmatic fragments expelled during the eruption. Meanwhile, the erosive forces associated with rising magma and the fracturing of wall rock combine to create the carrot shape that is typical of kimberlite pipes.

Stage 4 is a depressurization wave that propagates down through the magmatic foam. This wave disrupts the foam, releasing more gas, which in turn creates more foam. In stage 5, gas expansion creates an upward fluidization wave, causing sorting of the brecciated diatreme zone and the fractured county rock. This process continues until either the pressure is relieved or the temperature decreases, solidifying the magma. At this point the eruption ceases, locking any unerupted material into the carrot-shaped diatreme. Stage 6 is the formation of the volcanic cone from the collapse of the eruptive plume and the settling of debris. This cone is often quickly eroded due to its unconsolidated nature. It is thought that the entire eruption terminates within tens of minutes of onset. *EAF*

Naturally formed epitaxial diamond crystals in rubies. G.-S. Park [sg8144.park@samsung.com], S. C. Bae, S. Granick, J.-H. Lee, S.-D. Bae, T. Kim, and J. M. Zuo, *Diamond and Related Materials*, Vol. 16, 2007, pp. 397–400.

This article documents a rare discovery of natural epitaxial diamond crystals in a Vietnamese ruby. Formed as needle-like inclusions with several other minerals, these diamond crystals were characterized using a variety of analytical techniques. The diamond inclusions showed a distinct relationship to the orientation of the ruby substrate (i.e., epitaxy), suggesting they formed after ruby crystallization.

The inclusions were identified as diamond with electron energy-loss spectroscopy, selected area electron diffraction, and confocal Raman spectroscopy. Trapezoidal in cross section, the diamond crystals were 0.6–1.4 mm long and 3–10 μm wide, and exhibited a straight interface with the ruby host. Transmission electron microscopy showed the needles were composite in nature, with several other mineral phases present, including titanium oxide (TiO_{1+x}), aluminum oxide (AlO_x), iron oxide (Fe_2O_3), and Fe-Cr-Ni-F oxide.

The composite nature of the needles suggests that they crystallized from trapped fluids and were not the result of exsolution. Based on a report that Vietnamese rubies crystallized from CO_2-rich fluids, the authors speculate that this CO_2 was the source of carbon for the diamond inclusions. As Fe and Ni are known to be catalysts for diamond growth and Cr is a carbon solvent, it is believed the presence of these elements facilitated the unusual growth of diamond as inclusions in the ruby. *DMK*

The new diamond hunters. P. Barta, *Wall Street Journal*, May 12–13, 2007, pp. B1–B2.

As the De Beers Group pulls back from its traditional control over much of the world's diamond mining and exploration, smaller firms are filling the gap. This article describes how junior exploration companies have moved into Botswana, already the world's largest diamond producer by value, to explore heretofore neglected areas of the country. Some companies have employed zeppelins instead of heavier-than-air aircraft to survey potential sites because the airships offer a slower, smoother ride that allows more precise measurements. The article reports that while there may be a shortage of rough diamonds as new consumer markets increase demand, diamond exploration and mining remain risky because very few kimberlite deposits result in an economic mine. *RS*

The peculiarities of natural plastically deformed diamond crystals from "Internatsionalnaya" pipe (Yakutia). G. M. Rylov [ryl@uiggm.nsc.ru], E. N. Fedorova, A. M. Logvinova, N. P. Pokhilenko, G. N. Kulipanov, and N. V. Sobolev, *Nuclear Instruments and Methods in Physics Research A*, Vol. 575, No. 1/2, 2007, pp. 152–154.

Using Laue synchrotron radiation and infrared spectroscopy, the authors evaluated 40 Siberian diamond crystals in the following color groups: brown (I), smoky gray (II), purplish pink with a brown or gray modifier (III), and purplish pink (IV). Since these diamonds receive much of their color from plastic deformation, analysis of the spots in the Laue diffraction patterns can help gauge the effects of crystal distortion associated with plastic deformation. In addition to analyzing the placement of each spot, the authors also examined its appearance. The brown and smoky gray diamonds (I and II) had very elongated Laue spots, which indicated significant plastic deformation. These diamonds also showed a greater intensity of "amber centers" (located at 4170 and 4065 cm^{-1}) than those of group III, but no "amber centers" were observed in the group IV crystals. The Laue spots in purplish pink diamonds (III and IV) showed near-parallel striations due to polygonization. Sometimes, dislocation motion can cause horizontal rows of dislocations to be rearranged to form vertical walls. The resulting polygonized fragments have a more perfect crystal structure. *SE-M*

Thermochromic and photochromic behaviour of "chameleon" diamonds. E. Fritsch, L. Massi [laurent.massi@cnrs-imn.fr], G. R. Rossman, T. Hainschwang, S. Jobic, and R. Dessapt, *Diamond and Related Materials*, Vol. 16, No. 2, 2007, pp. 401–408.

"Chameleon" diamonds display a reversible change in color from grayish green to yellow when they are gently heated (thermochromism), or kept in the dark for an extended period of time (photochromism). In this study, 45 chameleon diamonds were investigated by several spectroscopic techniques. Heating to 125–135°C for approximately one minute resulted in a yellow color; the diamonds returned to grayish green within several minutes of the heat source being removed. Yellow coloration could also be produced by placing the diamonds in a darkened environment for a number of hours; the grayish green color returned within

approximately one minute of exposure to light.

Infrared spectra showed that the samples were type Ia diamonds with predominantly A nitrogen aggregates, as well as moderate-to-high amounts of hydrogen and a small component of type Ib nitrogen. Absorption spectra exhibited increasing absorption toward the ultraviolet and broad bands centered at about 480 and 800 nm; the yellow color was accompanied by a decrease in intensity of the latter band. The diamonds displayed turbid yellow fluorescence to both long- and short-wave UV radiation (with greater intensity for the former). They also had persistent phosphorescence. Based on the premise that yellow is the stable color and grayish green is the metastable color, the authors propose an electronic model to explain the color-change behavior and other features of these unusual diamonds. *JES*

GEM LOCALITIES

Amethyst geodes in the basaltic flow from Triz quarry at Ametista do Sul (Rio Grande do Sul, Brazil): Magmatic source of silica for the amethyst crystallizations. D. Proust [dominique.proust@univ-poitiers.fr] and C. Fontaine, *Geological Magazine*, Vol. 144, No. 4, 2007, pp. 731–739.

Amethyst-filled geodes are widely encountered in basalt flows in southern Brazil, Uruguay, and Argentina. Geodes in tholeiitic basalts from the Triz quarry at Ametista do Sul show well-layered infillings with, from the outside in, celadonite, chalcedony, fine-grained quartz, and—finally—large amethyst crystals. Primary fluid inclusions indicate a range of amethyst crystallization temperatures (152–238°C). The geodes occur in the massive, fracture-free upper portion of the flow and are surrounded by an alteration halo in the basalt, the thickness of which depends on the geode radius. Geochemical analysis indicates that sufficient silica was released from the alteration halo to produce the amethyst and other minerals in the geodes without the need for an additional source. The amethyst is of volcanic origin, having crystallized from hydrothermal fluids generated within the basalt. These residual fluids migrated from the surrounding basalt into the open cavities as a result of a pressure gradient, leaving an alteration halo. As these fluids cooled, they formed the minerals that partially filled the cavities. *JES*

Australian sapphires and rubies. F. L. Sutherland [l.sutherland@uws.edu.au] and G. B. Webb, *Rocks & Minerals*, Vol. 82, No. 2, 2007, pp. 116–125.

The authors present a clear, nontechnical overview of Australia's sapphire and ruby deposits. Topics include statistics on famous stones (e.g., the Martin Luther King Jr., a 3,294 ct carved sapphire from Queensland), a review of localities (including non-gem and ornamental occurrences), mining techniques, geologic origin, crystal features, and future prospects for the industry in Australia.

Australia's gem corundum was transported to the surface as xenocrysts in basalt from the upper mantle/lower crust. The corundum formed by different mechanisms at various times. For example, both magmatic and metamorphic deposits have been differentiated using gallium as a key trace element—magmatic corundum has a higher Ga content—while other stones may have a metasomatic or intermediate composition. Zircon fission-track dating has shown that Australian sapphires have a wide age range (e.g., 3 Ma for Lava Plains and up to 400 Ma for Tumbarumba).

Of particular geologic interest is a discussion of the upper Kings Plains Creek in New England, north of Inverell and Glen Innes. At the Strathdarr deposit, narrow buried channels of eroded Oligocene age (~36 Ma) basaltic rocks yielded an average sapphire grade of 1,500 carats/m^3 (up to an impressive 25,000 carats/m^3) in gravel beds <1–6 m thick. These basal channels were linked to lahars (volcanic mud flows) that were produced by occasional catastrophic collapses of maars (rimmed craters, often with water-filled lakes). In effect, the sapphires underwent a double concentration and winnowing process, through the effects of surface water within the maars and subsequent lahar deposition, resulting in the outstanding concentrations at Kings Plains Creek.

The authors note that only two of the 13 named 100+ ct sapphires from Queensland have been found since 1982, suggesting a maturing resource. However, they correctly point out that many Australian sapphires have been marketed under different origins after passing through foreign cutting and distribution markets. Both heat treatment and gem tourism offer revenue prospects for Australian producers, though good heat treatment results are quoted as being sporadic.

KAM

Les gisements de corindons gemmes de Madagascar [The gem corundum deposits of Madagascar]. G. Giuliani, D. Ohnenstetter, A. F. M. Rakotondrazafy, A. E. Fallick, S. Rakotosamizanany, A. Andriamamonjy, T. Ralantoarison, M. Razanatseheno, C. Dunaigre, and D. Schwarz, *Revue de Gemmologie*, No. 159, 2007, pp. 14–28 [in French with English abstract].

While A. Lacroix's *Minéralogie de Madagascar* (1922) lists only a few corundum occurrences, many new deposits have been discovered since then and have made Madagascar a major producer of gem corundum. The authors compiled a survey of the country's known corundum localities. The primary deposits can be subdivided into magmatic and metamorphic types, the latter including two new variations of gem corundum formation within shear zones. The secondary deposits are classified according to both basaltic and sedimentary environments. By far the most important sedimentary deposit is the mining district at Ilakaka. The article is illustrated with sam-

ples of corundum from various sources as well as a map of deposits. *RT*

Le Nigeria. Source de pierres de couleur [Nigeria. Source of colored stones]. J.-C. Michelou, *Revue de Gemmologie*, No. 159, 2007, pp. 30–41 [in French with English abstract].

The author studied Nigerian gem deposits during two visits in 2006. Nigeria produces sapphire and ruby, but it is mainly known for emerald, green beryl, aquamarine, tourmaline (of various colors), topaz, and spessartine. All reportedly show good potential for the future. At present, however, almost all deposits are exploited on a small scale. The production is irregular, and most is purchased by dealers from neighboring states; exports usually occur outside of official channels. Apart from informal gem sales at Ibadan and Jos, there are few marketing structures. Gemological knowledge and education are almost nonexistent, and there is little or no local cutting industry. However, initiatives supported by the World Bank are underway to map the country geologically, mechanize mining, and establish gemological education and cutting facilities. *RT*

Persistence pays off—again: Mining for emeralds in Hiddenite, Alexander County, North Carolina. R. B. Cook, *Rocks & Minerals*, Vol. 82, No. 2, 2007, pp. 149–150.

This article provides a brief update on notable emerald finds at the Ellis and Rist mine properties near Hiddenite, North Carolina. Jamie Hill of North American Emerald Mines Inc. is pictured with several impressive 2006 discoveries from his operation, including a diverging pair of 25-cm-long crystals (118.2 g) of medium green color, and two fine dark green crystals weighing 28.7 and 30 g. Also pictured is a 13-cm-long, 372.4 g terminated emerald crystal in a matrix of dolomite and muscovite crystals, discovered in 2003. This specimen was subsequently purchased by the Houston Museum of Natural Science. Hill's operation has yielded ~1,300 g of emerald crystals in the 2–20 g range, though the time required to obtain this total is not made clear. An emerald discovered in 1998 was later cut into two stones weighing 18.8 and 7.8 ct, named the Carolina Queen and Carolina Prince, respectively. *KAM*

The pink topaz–bearing calcite, quartz, and white mica veins from Ghundao Hill (North West Frontier Province, Pakistan): K/Ar age, stable isotope and REE data. G. Morteani [gmorteani@gmx.de] and A. Voropaev, *Mineralogy and Petrology*, Vol. 89, No. 1/2, 2007, pp. 31–44.

Orange-yellow to red gem-quality topaz is found in calcite, quartz, and white mica veins that crosscut limestones at Ghundao Hill near Katlang in northern Pakistan. The topaz is characterized by low amounts of V, Cr, Fe, and F, and relatively high hydroxyl contents. K/Ar age determination on the white mica gave an Eocene age of 43.2 Ma. Geochemical data indicate that these topaz-bearing veins formed at temperatures of about 240°C from metamorphic fluids. The fluids resulted from a period of widespread regional metamorphism associated with the collision of the Indian and Asian continental plates that began about 55 Ma. Circulation of these fluids mobilized elements from the country rocks that were needed to form the vein minerals. There is no evidence that the topaz crystallized from pegmatitic or pneumatolitic granite-related fluids. *JES*

INSTRUMENTS AND TECHNIQUES

TMA and SEM characterization of the thermal dehydration of Australian sedimentary opal. A. Smallwood, P. S. Thomas [paul.thomas@uts.edu.au], A. S. Ray, and P. Šimon, *Journal of Thermal Analysis and Calorimetry*, Vol. 88, No. 1, 2007, pp. 185–188.

The dehydration of Coober Pedy sedimentary white opal displaying play-of-color was investigated using thermal mechanical analysis. Various samples were heated to 200°C, 400°C, 600°C, 800°C, and 980°C, and then cooled back to room temperature. The samples were then etched with hydrofluoric acid vapor and coated with platinum for micro-structural analysis with a scanning electron microscope. The opals experienced expansion up to 210°C and then underwent contraction due to dehydroxylation and formation of silicon-oxygen-silicon bridges. This process resulted in a more dense silica network. While not pursued here, thermal methods studying the dehydration of opal have successfully differentiated opal from the Andamooka, Coober Pedy, and Lightning Ridge deposits. *EAF*

JEWELRY RETAILING

The king of bling. S. Adams, *Forbes*, Aug. 13, 2007, pp. 85–89.

Laurence Graff is a London jeweler specializing in top-end fancy-color diamonds and very large, high-quality colorless stones. This article traces Graff's rise from apprentice in London's Hatton Garden jewelry district to owner of one of the most prestigious shops on New Bond Street. Fueled by a rapid increase in the number of extremely affluent individuals around the world, Graff built his reputation by acquiring and selling high-profile large diamonds to which he could link his name. One example detailed in this article is his recent purchase of the 603 ct Lesotho Promise diamond for $12.4 million, which Graff estimates will realize US$25–30 million after cutting. Graff's sales have rocketed from $90 million in 2000 to $400 million in 2006. In addition, his acquisition of a majority stake in the South African diamond firm Safdico has insured a steady supply

of stones for his jewelry workshops in London. Today, Graff claims the world's highest average transaction price for any jeweler, an astounding $400,000, and includes among his clientele such celebrities as soccer player David Beckham, TV host Oprah Winfrey, entrepreneur Donald Trump, and actress Elizabeth Taylor. His largest single sale was a multi-colored diamond necklace, created from 267 carats of various shaped diamonds for an Asian client, which he sold for $30 million in 2006. *RS*

SYNTHETICS AND SIMULANTS

Dependence of limited growth rate of high-quality gem diamond on growth conditions. Y. Tian, H.-A. Ma, S.-S. Li, H.-Y. Xiao, Y.-F. Zhang, G.-F. Huang, L.-Q. Ma, and X.-P. Jia, *Chinese Physics Letters*, Vol. 24, No. 7, 2007, pp. 2115–2117.

The authors introduce the concept of "limited growth rate of diamond," the maximum growth rate at which high-quality synthetic diamond can be created. Several crystals were grown using the temperature gradient method under high-pressure, high-temperature conditions (5.5 GPa and 1240–1280°C for 3–8 hours). Pure graphite was used as the source of carbon, the alloy $Ni_{70}Mn_{25}Co_5$ was used as the solvent/catalyst, and 0.5 mm diamond crystals were used as seeds, with the {100} face as the growth surface. The authors explored the impact of temperature and time on growth rate, and evaluated the synthetic diamond crystals for inclusions and voids using optical microscopy. For a period of three hours, the limited growth rates were 1.5 mg/hour for 1240°C, 0.9 mg/hour for 1260°C, and 0.5 mg/hour for 1280°C. When they increased the time to eight hours, the limited growth rates increased to 2.9 mg/hour at 1240°C, and 2.0 mg/hour at 1260°C (the rate at 1280°C was not reported). These results can be explained by the fact that the area available to absorb the carbon increases at longer growth times. *JS-S*

MISCELLANEOUS

Diversification, design, strategic planning and new product development: A jewellery industry knowledge transfer partnership. G. Penfold, *Design Journal*, Vol. 10, No. 1, 2007, pp. 3–11.

Jewelry manufacturers centered in Birmingham, England, face all the competitive challenges of their counterparts in other mature sectors, as well as competition from Asian manufacturers and an insular operating style that makes change and innovation difficult. The article surveys a government-sponsored program between a medium-sized jewelry manufacturer and an institution of higher education—called Knowledge Transfer Partnership—to help the firm respond to a changing market.

The jewelry manufacturer traditionally produced an array of rings, pendants, and earrings in 9K gold without great attention to design or image. Using a consultant from the University of Central England, the company embarked on a two-year program to revamp their jewelry line. The key objectives were to move up-market into 18K gold and platinum, and to develop an image of contemporary-designed jewelry that differentiated its products from competitors. Working with the consultant, the firm embarked on a design line created by a newly hired in-house designer and ultimately increased market share and world recognition of its products by winning high-profile design competitions. *RS*

End of the blood diamond syndrome? N. Ford, *African Business*, October 2007, pp. 80–82.

Liberia, under its new president Ellen Johnson-Sirleaf, is moving to reestablish a legitimate diamond industry by permitting citizens to apply for mining and trading licenses. Such activities were suspended during the reign of previous ruler Charles Taylor, who is now on trial for war crimes related to the conflict in neighboring Sierra Leone during the 1990s. Although there has never been a full survey of the nation's potential diamond resources, Liberia has opened an official diamond certification office to insure all diamond exports conform to the Kimberley Process.

However, there remain many challenges to an open, transparent diamond industry in Liberia because the country is still unstable, with a huge wealth disparity between the business elite and the remainder of the population. While Johnson-Sirleaf has expressed a commitment to reform Liberia's economic and political institutions, there is no indication how her government will distribute the nation's mineral wealth. *RS*

The Tagil school of masters. L. Pavlenko, *Platinum*, No. 22, 2006, pp. 60–61 [in Russian].

Jewelry manufacturing in Russia's Ural Mountains dates back to the 18th century. One well-known deposit of iron, copper, and malachite, called Mednorudyansk, is located near the town of Nizhny Tagil. This mine has supplied malachite for many lapidary factories and museums around the world. It is fitting, therefore, that the Ural School of Applied Arts was founded in Nizhny Tagil. At this school, specialists are trained in faceting, engraving, minting, casting, and other manufacturing processes. Students benefit from exposure to high-quality gem materials, old masterpieces, and the local landscape (for inspiration). They also take part in excursions to the famous Ural deposits of emerald, aquamarine, topaz, rhodonite, and jasper, and maintain their own collections of rocks and minerals. Among the faculty are well-known local masters as well as invited experts. The carvings and jewels created by Tagil students have been displayed at numerous mineral shows and exhibitions of folk art. Many others are preserved in the Museum of Decorative and Applied Arts in Ekaterinburg. *BMS*

Volume 43 Index 2007

Numbers 1–4

SUBJECT INDEX

This index gives the first author (in parentheses), issue, and inclusive pages of the article in which the subject occurs for all feature articles, Notes & New Techniques, and Rapid Communications that appeared in Volume 43 of *Gems & Gemology*. For the Gem News International (GNI), Lab Notes (LN), Letters (Let), and Last Page (LP) sections, inclusive pages are given for the item. The Author Index (p. 408) provides the full title and coauthors (if any) of the articles cited.

C

D

E

Q

R

S

T

U

V

W

X

Y

Z

AUTHOR INDEX

This index lists, in alphabetical order, the authors of all feature articles, Notes & New Techniques, and Rapid Communications that appeared in the four issues of Volume 43 of *Gems & Gemology,* together with the full title and inclusive page numbers of each article and the issue (in parentheses). Full citation is given under the first author only, with reference made from coauthors.